Airport Asphalt Pavement Technology Program

Balanced Mix Design: Evaluation of Cracking Tests for Airfield Pavements

Final Report

August 2026

Credit: AAPTP

Airport Asphalt Pavement Technology Program

PREPARED BY:

University of Illinois at Urbana-Champaign
Imad L. Al-Qadi
Akash Bajaj
John Lambros
Namith Gangidi

University of New Hampshire
Eshan Dave
Jo Sias
Shubham Modi

Arizona State University
Hasan Ozer
Samuel Castro Brockman
Awais Zahid

The Heritage Research Group
Bill Pine

Applied Research Associates
Dario Batioja-Alvarez
Hasan Kazmee
Scott Murell

The Airport Asphalt Pavement Technology Program (AAPTP) is a cooperative agreement effort between the **National Asphalt Pavement Association** (NAPA) and the **Federal Aviation Administration** (FAA) to advance asphalt pavements and pavement materials. The AAPTP promotes solutions for asphalt pavement design, construction, and materials deemed important to airfield reliability, efficiency, and safety. The program leverages NAPA's unique technology implementation capabilities with assistance from the FAA and industry to advance deployment and adoption of innovative asphalt material technologies.

Acknowledgments

The authors would like to acknowledge the support of Richard Willis, NAPA Vice President for Engineering, Research, & Technology, and Brett Williams, NAPA Senior Director for Engineering and Technical Services, along with project panel members, including Navneet Garg, Brandon Brever, Sadie Casillas, Alfredo Castro, Chuck Mills, Tim Peffer, and Kelly Senger, for providing critical feedback, overseeing the project, and reviewing project deliverables. The airport sample collection was facilitated by Thomas Bennert (EWR and TEB), Robbie Robinson (TPA), Dylan Stutters (RTS), Frank Rancadore (SFO), Fred Cole (ORD and ORAP), Tim Bannon (CMI), and Mallie Hare (MCI). Their help is greatly appreciated. The authors also acknowledge the help of the Illinois Center for Transportation research engineers and students throughout the project.


Credit: AAPTP

Table of Contents

List of Figures

List of Tables

List of Acronyms and Abbreviations

AAPTP	Airport Asphalt Pavement Technology Program
AASHTO	American Association of State Highway and Transportation Officials
APA	Asphalt Pavement Analyzer
ASTM	ASTM International
AV	Air voids
BMD	Balanced Mix Design
Caltrans	California Department of Transportation
CDCT	Cyclic Disk-shaped Compact Tension
CMI	University of Illinois–Willard Airport
CMOD	Crack mouth opening displacement
COV	Coefficient of variation
CT	Cracking tolerance
CZ	Cohesive zone
DCT	Disk-shaped Compact Tension
DI	DONUT Index
DIC	Digital image correlation
DONUT	Disc with O-Notch for Uniaxial Testing
DOT	Department of Transportation
ESAL	Equivalent single axle load
EWR	Newark Liberty International Airport
FAA	Federal Aviation Administration
FBF	Flexural beam fatigue
FC	Field cores
FE	Finite element
FHWA	Federal Highway Administration
FI	Flexibility Index
FPZ	Fracture process zone
FST	Fracture strain tolerance
HMA	Hot mix asphalt
HWTT	Hamburg Wheel-Tracking Test
IDEAL-RT	IDEAL Shear Rutting Test
IDOT	Illinois Department of Transportation
I-FIT	Illinois Flexibility Index Test
JMF	Job mix formula
LaDOTD	Louisiana Department of Transportation and Development
LCI	Low-temperature Cracking Index
LEFM	Linear elastic fracture mechanics
LLD	Load-line displacement
LMLC	Laboratory-mixed, laboratory-compacted

LTA	Long-term aging
LTPP	Long-Term Pavement Performance
LTRC	Louisiana Transportation Research Center
LVDT	Linear variable differential transformer
LWT	Loaded Wheel Tester
MCI	Kansas City International Airport
ME	Mechanistic-empirical
NAPA	National Asphalt Pavement Association
NAPMRC	National Airport Pavement and Materials Research Center
NFE	Normalized fracture energy
NLFM	Nonlinear fracture mechanics
NMAS	Nominal maximum aggregate size
NPIAS	National Plan of Integrated Airport Systems
OBC	Optimum binder content
OGFC	Open-graded friction course
ORAP	Chicago O'Hare International Airport's reclaimed asphalt pavement mixture
ORD	Chicago O'Hare International Airport
OT	Overlay Test
PEMD	Performance Engineered Mixture Design
PFE	Pre-peak fracture energy
PG	Performance grade
PGH	High-temperature performance grade
PGL	Low-temperature performance grade
PMLC	Plant-mixed, laboratory-compacted
PRS	Performance-related specifications
PWL	Percentage within limits
QA/QC	Quality assurance/quality control
RAP	Reclaimed asphalt pavement
RAS	Recycled asphalt shingles
RDCI	Rate-Dependent Cracking Index
RHMA-G	Rubberized Hot Mix Asphalt-Gap Graded
RSST	Repeated simple shear tests
RTS	Reno Stead Airport
SCB	Semi-Circular Bend
SFO	San Francisco International Airport
SHRP	Strategic Highway Research Program
SLT-SCB	Simplified Low-Temperature Semi-Circular Bend
SMA	Stone matrix asphalt
SMF	Sacramento International Airport
STA	Short-term aging
S-VECD	Simplified viscoelastic continuum damage

TEB	Teterboro Airport
TPA	Tampa International Airport
TxDOT	Texas Department of Transportation
VDOT	Virginia Department of Transportation
VECD	Visco-elastic continuum damage
VFA	Voids filled with asphalt
VMA	Voids in mineral aggregate
WLF	Williams–Landel–Ferry
WMA	Warm mix asphalt
XCM	Cross-combination mixture

Executive Summary

Performance-based asphalt mixture design is gaining widespread adoption for highway pavements due to limitations of the volumetric approach in addressing potential increases in vehicle torque and evolving material components. Airports face similar challenges, including increasing gear loads and tire pressures. The objective of this research was to develop and recommend practical, scientifically robust test protocols to characterize and predict asphalt mixture cracking potential. The resulting test methods, specimen requirements, and provisional acceptance thresholds were prepared for consideration by the Federal Aviation Administration (FAA) and for possible inclusion in FAA Advisory Circular 150/5370-10H, *Standards for Specifying Construction of Airports,* Part 6—Flexible Pavements, for both laboratory mixture design and production quality assurance/quality control.

A broad set of aggregates, binders, plant-loose mixes, and field cores (FC) were sampled from major airports across the United States. Diverse climates and construction practices were considered to ensure field applicability of the final recommended protocols. Protocol development included laboratory-mixed, laboratory-compacted (LMLC) and plant-mixed, laboratory-compacted (PMLC) specimen testing. Results were validated using FC from airfield pavements.

Cracking was evaluated in two performance domains: (i) low-temperature cracking, where crack initiation is dominant, and (ii) service-temperature cracking, where propagation and post-peak behavior are critical. Simplicity and ease of implementation in a balanced mix design framework, while being scientifically grounded, were the guiding principles for this work. Since specimen preparation and aging influence asphalt mixture laboratory-measured cracking potential, standardized specimen fabrication and testing protocols were developed.

Simplified Low-Temperature Semi-Circular Bend (SLT-SCB) is a modification of the existing low-temperature SCB test. It was introduced in this study and is recommended to characterize cracking potential at low temperatures. The SLT-SCB test, readily available for implementation in regions with known susceptibility to low-temperature cracking, can capture and discriminate between mixtures with differing cracking potential using the Low-temperature Cracking Index (LCI). The LCI, which characterizes crack initiation, is the ratio of pre-peak fracture energy to loading stiffness. An LCI threshold of 15 is recommended for asphalt mixes.

At service temperature, the Illinois Flexibility Index Test (I-FIT) and the Cracking Tolerance (CT) Index test were used to characterize the asphalt mixture cracking potential. I-FIT, a fracture-based test, was able to discern mixtures with known field cracking, and CT, a strength-based test, was shown to be less reliable. The standard notch in I-FIT was able to concentrate stresses and direct cracking, while the stress distribution in CT was impacted

by aggregate structure and localized yielding beneath the loading strip. A Flexibility Index threshold of 7 is recommended for short-term aged specimens; a corresponding CT threshold could not be identified.

To retain the use of a disc-shaped CT specimen, which is a practical geometry for testing, a two-step modification to the CT was developed. A central core and thicker loading strips were proposed to create a cored Brazil or Disc with O-Notch for Uniaxial Testing (DONUT) protocol. The proposed test is fracture-based and discriminates between mixtures with varying cracking potential. An associated DONUT Index (DI) was introduced using the ratio of fracture energy to the secant slope after the peak in the load-displacement curve, which may be considered a crack speed proxy. DI successfully distinguished between asphalt mixtures with different levels of cracking potential and was validated using FC from FAA test lanes at the National Airport Pavement and Materials Research Center. A DI threshold of 6 is recommended for screening asphalt mixtures using short-term aged specimens.

Three cracking potential tests have been recommended, and their associated protocols were introduced: one is a low-temperature crack initiation test, while the other two are for crack propagation at service temperature.

Chapter 1. Introduction

Background

The aviation sector has experienced significant growth in recent years and has become a major contributor to the travel and cargo transportation industry (IATA, 2025). Robust and reliable infrastructure is essential to support current airfield operations and the growth of the aviation sector. Air transport accounts for 4.4 billion passenger takeoffs and 61.4 million tons of freight, representing 35 percent of world trade by value, carried annually (ATAG, 2024). In the United States alone, approximately 850 million passengers and 9.3 million tons of freight were transported by airlines in 2024 (BTS, 2024).

Approximately 3,300 airports (68 percent of existing public-use airports) in the United States are included in the National Plan of Integrated Airport Systems (NPIAS), which is currently maintained by the Federal Aviation Administration (FAA, 2024). This network includes commercial service, reliever, and general aviation airports, comprising 5,175 runways that support 101 million aircraft operations annually.

To ensure high resilience, aircraft safety, operational efficiency, and passenger comfort, the FAA plans to spend $22.5 billion (33.3 percent) from the NPIAS budget on rehabilitation and reconstruction between 2025 and 2029 (FAA, 2024). The FAA aims to maintain at least 93 percent of paved runways above fair condition. The latest survey noted that 79 percent of runways are in good condition, 19 percent are in fair condition, and 2 percent are in poor condition (BTS, 2022).

Approximately 75 percent of runways in the NPIAS are paved with asphalt mixtures due to lower construction cost, ease of rehabilitation, and smooth surface characteristics (NAPA, 2023). FAA Advisory Circular (AC) 150/5370-10H, *Standards for Specifying Construction of Airports,* includes specifications for materials and methods used for airport construction, ranging from sitework to pavements and lighting installation (FAA, 2018).

Asphalt mixtures are designed in accordance with AC 150/5370-10H, Part 6—Flexible Pavements. Part 6 includes specifications for P-401 asphalt mixtures used for surface courses on pavements subject to aircraft loadings of gross weights greater than 13,600 kg (30,000 lb). P-403 asphalt mixtures are used for base and/or leveling courses in flexible pavements or surface courses subject to aircraft loadings of gross weights less than or equal to 13,600 kg (30,000 lb). Where a fuel-resistant surface is required (e.g., refueling stations at the apron or hangar), P-404 asphalt mixtures are used.

Asphalt mixes, under Part 6 specifications, may be designed using either the Marshall method (ASTM D6926) or the Superpave Gyratory method (ASTM D6925). The specifications include component material tests for coarse and fine aggregates, performance grade (PG) selection for asphalt binder, and mixture requirements for aggregate gradation bands. Asphalt mixture volumetrics (air voids [AV] and percent voids in mineral aggregate [VMA]), tensile strength ratio, and rutting potential tests are also a part of current specifications. Rutting potential is measured using either an Asphalt Pavement Analyzer or a Hamburg wheel-tracking test. AV measurements in the mat and at the joint are used for tolerance limits in quality assurance and quality control (QA/QC) for asphalt mixtures during and after construction.

Cracking is a major distress that affects asphalt pavements in the United States (Monismith & Deacon, 1969; Harvey et al., 1995). Cracking occurs as an energy release mechanism, resulting in surface fractures caused by temperature fluctuations or traffic-induced stresses in asphalt pavements. It leads to a reduction in asphalt mixture durability, infiltration of deleterious materials, loss of load-bearing capacity, and possible creation of foreign object debris, thereby reducing the service life of asphalt paving materials.

Volumetric properties have been used as an indicator for asphalt pavement performance (Kennedy et al., 1994). However, the relationship between volumetrics and field performance is complex and was never intended to serve as the sole indicator of a high-quality asphalt mixture. The initial Strategic Highway Research Program (SHRP) research included some performance testing, but it was never adopted due to the perceived testing complexity, equipment requirements, and associated cost (Bennert, 2021).

However, with the growing emphasis on sustainability, enhanced performance, and innovation in asphalt material components, many highway agencies are adopting performance-based testing to address major distresses in the United States, such as rutting and cracking. Volumetrics alone may not be used to ensure the resilience of asphalt mixes, especially as the use of recycled materials and new technologies (e.g., warm-mix asphalt and stone-mastic asphalt) has increased (Alvarez et al., 2024; Epps Martin et al., 2020; Prowell et al., 2009).

In addition, the complex gear configurations of many aircraft types, relatively high aircraft gross weights, and increasing tire inflation pressures make the use of volumetrics as a performance indicator insufficient for airfield pavements. Hence, the Balanced Mix Design (BMD) philosophy has recently been considered for airports after its successful implementation in highways.

BMD has gained significant traction recently to predict potential asphalt mixture performance. This methodology involves the use of mechanical testing in addition to volumetric properties. Mechanical tests have been used as part of Marshall and Hveem mixture design methods. However, the current BMD approach was developed by Zhou and colleagues and was shown to provide better predictions of asphalt mixture potential performance than mixture volumetrics alone (Zhou et al., 2006).

BMD methodologies highlight the importance of performance-based testing. Current FAA specifications primarily address rutting potential; therefore, this research builds on guidance needed for performance-based evaluation of asphalt mixture cracking potential.

Objective and Scope

The objective of this research study was to develop a set of protocols to characterize the cracking potential of asphalt mixtures for incorporation into the next iteration of AC 150/5370-10, Part 6. To achieve the study objective, an experimental testing program was developed. It consisted of commonly used tests reported in the literature and adopted by various State and Federal agencies, as well as development and modification of selected tests to characterize cracking potential effectively. The protocols include test standards, test specimen requirements, and acceptance threshold criteria for both mixture design and production control stages. The recommended protocols include the following:

- **Selection of Fundamental and Practical Tests**: Testing methodologies were established to measure fundamental properties linked to asphalt mixture performance while being rapid, cost-effective, and easy to implement in QA/QC procedures. The selected tests require minimal training and equipment.
- **Extensive Lab Testing**: As part of the project, specimens tested included plant-mixed, laboratory-compacted (PMLC); laboratory-mixed, laboratory-compacted (LMLC); and in-service field cores (FC) from a diverse range of asphalt mixture designs. The mixture designs were selected from various airports to ensure a wide representation of mixture type, aggregate gradation and lithology, asphalt binder type and content, climatic region, and traffic conditions.
- **Evaluation of Mixture Design Parameters**: The effects of variables such as asphalt binder content, AV, and other factors on asphalt mixture cracking potential were analyzed. Thresholds were developed based on representative conditions of in-service airfield pavements to ensure field applicability. The proposed acceptance thresholds accounted for in-service cracking, including thermal and fatigue-related cracking, and differentiated between crack initiation and propagation susceptibilities.
- **Validation of Protocols Using Real-World Data**: The developed protocols and thresholds were validated with pavement performance data from multiple sources. Asphalt pavement materials were collected from recent construction projects at major airports, as well as from the National Airport Pavement and Materials Research Center (NAPMRC) at the FAA William J. Hughes Technical Center for Advanced Aerospace in Atlantic City, NJ.

Report Organization

The research study investigated cracking mechanisms in asphalt mixtures across three major domains: fatigue cracking parameters, low-temperature cracking parameters, and strength and fracture parameters. This report outlines the materials and methodology employed, as well as the results obtained using an initial testing suite to characterize cracking. It recommends testing protocols for consideration in a future FAA AC, so that asphalt mixture cracking potential can be incorporated into airfield BMD.

Chapter 2 summarizes an extensive current state of knowledge on the fundamentals of asphalt mixture cracking and application of BMD philosophy in the context of asphalt pavements. The full literature review is available in Appendix A.

Chapter 3 details the materials, test specimen protocols, and experimental methods utilized during the study. Information about aging and reheating protocols for lab and plant mixtures that could be used by contractors for BMD is detailed in the chapter.

Chapter 4 describes the development and testing performed for low-temperature cracking susceptibility in asphalt mixes. Results from Disk-shaped Compact Tension (DCT) and a newly developed Simplified Low-Temperature Semi-Circular Bend (SLT-SCB) test are presented, along with mixture parameters that significantly affect low-temperature cracking. The importance of crack initiation is discussed for low-temperature cracking.

Chapter 5 explores the strength and fracture properties that have been shown to relate to field cracking in asphalt pavements. Results from the Cracking Tolerance (CT) Index test and Illinois Flexibility Index Test (I-FIT) are discussed. Simple modifications are suggested for the CT Index test to convert CT from a strength test to a fracture/toughness test. The new cored Brazil disc or "DONUT" test is also presented. The chapter also examines crack propagation along with the factors influencing it.

Chapter 6 summarizes the key findings of the study and provides recommendations for cracking potential testing protocols for inclusion in the FAA AC.

Chapter 2. Summary of the Current State of Knowledge on Asphalt Mixture Cracking

This chapter provides a synthesis of the literature review performed for this project, covering the philosophy of BMD and its increasing use for highways and airfields, as well as fundamental and applied research on fracture in materials in general and asphalt mixtures in particular. The insights formed the basis for the experimental framework and analysis presented in this study. An extensive review of the current state of the art and practice is presented in Appendix A.

BMD for Asphalt

BMD is an asphalt mixture design approach that integrates performance tests into the design process. The Federal Highway Administration (FHWA) BMD Task Force defined BMD as "asphalt mix design using performance tests on appropriately conditioned specimens that address multiple modes of distress, taking into consideration mix aging, traffic, climate, and location within the pavement structure." BMD aims to achieve an optimal balance between rutting and cracking potential, often through performance tests. The broader goal is to determine the ideal combination of binder, aggregate, and other components to meet performance test criteria—typically rutting and cracking tests—based on traffic level, climate, and pavement structure (West et al., 2018).

The concept of a "performance pendulum" is often used to illustrate the adjustments of asphalt mixture to shift performance between cracking and rutting, emphasizing the need to find an optimal balance (Buchanan, 2016). Additionally, performance interaction diagrams are frequently employed to visualize the cracking and rutting potential of asphalt mixtures after selecting preferred tests for characterization (Zhou et al., 2014; Al-Qadi et al., 2015; Ali et al., 2019; Jichkar, 2021).

BMD is implemented through various approaches that integrate volumetric mixture design with performance tests. FHWA outlines four distinct BMD approaches, each offering varying levels of flexibility and innovation:

- **Approach A**—This method adheres to traditional volumetric criteria, followed by performance verification. It is the most conservative approach, prioritizing standard parameters while allowing limited innovation.
- **Approach B**—This approach starts with a volumetric design but permits minor adjustments to optimize performance. It strikes a balance between volumetric compliance and performance test outcomes, offering slightly more flexibility than Approach A.

- **Approach C**—In this method, some volumetric requirements are relaxed to focus on performance-driven optimization. Adjustments may involve modifying the initial binder content or altering mixture component properties.
- **Approach D**—This is the most flexible and least conservative approach, where volumetric parameters are minimized in favor of performance-driven optimization. It allows the highest level of innovation in mixture design.

These approaches provide distinct levels of adaptability, enabling State agencies and transportation departments to select a method best suited to their specific climate conditions, traffic volumes, and pavement distress concerns. FHWA incorporates these approaches into its performance engineered mixture design framework. According to a recent survey conducted by the National Center for Asphalt Technology for the National Asphalt Pavement Association (NAPA), several States have adopted BMD in their pavement design processes (Yin & West, 2021). Various approaches were used based on climate, traffic volumes, and specific pavement distress potential.

Application of BMD to Airfield Asphalt Mixtures

BMD is widely used for highway pavements and is now gaining attention for its potential application to airfield asphalt mixes. Airfield pavements are distinguished from highway pavements by loading conditions, particularly from large aircraft exerting concentrated loads, which accelerate pavement distress. Rutting is a critical concern due to the narrow, concentrated wheel paths of aircraft, which can cause severe deformation over time. While rutting potential is usually prioritized, sufficient endurance against thermal, fatigue, and aging cracks is essential.

Despite its potential, BMD has rarely been implemented in airfield projects. For the Phase 3 expansion of Delhi International Airport in India, performance-based mixture design was used to balance asphalt mixture stiffness at high temperatures with binder workability during extended delivery times (Tipnis et al., 2023). Three job mix formulas (JMF) were designed using the Marshall mix design method, and their performance was evaluated through Hamburg wheel tracking (rutting potential), CT Index test (cracking potential), and tensile strength ratio (moisture susceptibility). Field inspections confirmed that the designed surface was performing well after 2 years.

BMD was also applied recently for selection of a highly polymer-modified asphalt mixture for runway rehabilitation at a Brazilian airport (Marcela et al., 2025). Two mixture designs were initially created via the Marshall design method and iteratively refined based on laboratory performance tests for fatigue and rutting along with FlexPAVE software. The tests showed that highly polymer-modified asphalt mixtures may reduce cracking potential for the wearing surface compared to a standard polymer-modified asphalt mixture.

Airfield pavement design requires additional considerations beyond highways, including binder grade bumping, optimized aggregate gradations, foreign object debris resistance, and specific pavement structures. However, current BMD guidelines focus primarily on highway applications versus airfields. To bridge this gap, this study was part of a larger initiative that aims to develop BMD guidelines specifically for airfield pavements. In this study, the focus was on cracking potential evaluation to enhance durability and long-term performance of airfield asphalt pavements. The following sections describe the mechanisms of cracking in asphalt mixtures and highlight several influential studies that informed this research.

Mechanisms of Fracture in Materials

Cracks occur when a material fails under applied stress, leading to separation and the formation of new surfaces to release stored energy. Traditionally, cracking susceptibility was evaluated using a strength-based approach, assuming failure when external loading exceeded the material's predefined strength. However, this method fails to explain structural failures occurring at stress levels below the material's strength.

Fracture mechanics introduced crack geometry as a critical factor, recognizing its direct influence on stress distribution. Inglis (1913) demonstrated that the presence of cracks produced amplified stresses in their vicinity, explaining material failure at lower stresses than their nominal strength. The assumption of crack tip autonomy (Williams, 1957), which neglects far-field boundary effects, led to the introduction of fracture toughness. Irwin formalized the concept of stress amplification near cracks as the stress intensity factor, establishing that fracture occurs when it exceeds the material's fracture toughness (Irwin, 1957).

Simultaneously, Griffith (1921) developed an energy-based approach, recognizing cracking as an energy release mechanism. He defined the energy release rate as the dissipated energy per unit fracture surface and proposed that fracture initiates when the rate exceeds a critical material threshold. These stress- and energy-based approaches were unified under linear elastic fracture mechanics (LEFM) through the assumptions of small-scale yielding and crack tip autonomy. LEFM principles were later extended by Paris and Erdogan (1963), who established a power-law relationship between crack growth rate and the stress intensity factor using experimental data. For viscoelastic materials under small strains, Schapery (1975) developed the correspondence principle to adapt LEFM principles.

While LEFM provides a reasonable approximation for bulk material behavior, it leads to stress singularities at the crack tip that lack physical meaning. These singularities manifest as a nonlinear region near the crack tip, involving plasticity, microcracking, and other dissipative mechanisms. The Dugdale-Barenblatt model addressed this nonlinear behavior using a cohesive zone approach (Dugdale, 1960; Barenblatt, 1962), later formalized as the Fracture Process Zone or FPZ (Anderson, 2017).

To account for nonlinearities, nonlinear fracture mechanics was developed. When the FPZ is small relative to the crack length, the material's behavior can be approximated using LEFM. Rice (1968) introduced the J-integral parameter as an energy-based analog to the energy release rate in LEFM, quantifying energy dissipation per unit crack area. Although the J-integral parameter has been applied for ductile and quasi-brittle materials (Hillerborg et al., 1976), its practical utility remains limited due to the complexity of its calculation.

Cracking in Asphalt Mixtures

Early attempts to characterize cracking in asphalt pavements involved relating measured strains in asphalt mixture slabs under repeated loading to stiffness degradation until failure (Monismith et al., 1961; Pell, 1962). While these empirical approaches provided some insights, their limited applicability led to the adoption of fracture mechanics for characterizing cracking.

LEFM was first applied to asphalt mixtures in the 1970s (Ramsamooj, 1970; Majidzadeh et al., 1971; Van Dijk & Visser, 1977) to describe crack growth. The fatigue life of asphalt mixture specimens was divided into three stages: Region I – crack initiation, Region II – crack propagation, and Region III – failure. Paris' law was used to model crack growth in Region II (Jacobs et al., 1996), but it did not account for asphalt binder's viscoelastic behavior. Researchers at Texas A&M applied Schapery's correspondence principle to asphalt mixtures with some success, though it was found to be unreliable for low asphalt content mixtures (Germann & Lytton, 1979). Dissipated energy approaches were also developed to define failure in asphalt mixture fatigue testing and validated with field performance data (Ghuzlan & Carpenter, 2000).

Crack initiation occurs when the tensile stresses exceed the asphalt mix's tensile strength and continued loading leads to propagation through the asphalt pavement layer. In asphalt pavements, crack growth is influenced by inelastic deformation, aggregate interlock, and viscoelastic dissipation of the binder matrix. These mechanisms give rise to the FPZ, necessitating the use of nonlinear fracture mechanics for both experimental (Mobasher et al., 1997) and numerical modeling aspects (Jenq & Perng, 1991). The use of fracture energy has demonstrated reasonable success in assessing the cracking characteristics of asphalt mixtures in the field (Zhang et al., 2001; Roque et al., 2004).

Cracking in asphalt pavements is generally classified as load-related or non-load-related. Fatigue cracking is the most common load-related distress, caused by repeated tensile and shear stresses due to traffic loading. In thin pavements, tensile stresses develop at the bottom due to bending from wheel loads (Huang, 1993). In thicker pavements, tires induce both surface tensile stresses (Roque et al., 2010) and near-surface shear stresses (Wang & Al-Qadi, 2010), with tire acceleration, deceleration, and cornering significantly increasing the likelihood of near-surface cracking. Fatigue cracking is more prevalent on highways, where frequent loading cycles dominate, than on airfields, which experience fewer load repetitions.

Thermal cracking in asphalt pavements results from temperature-induced tensile stresses combined with reduced stress relaxation capacity at low temperatures (Marasteanu et al., 2012). It occurs through two distinct mechanisms: (i) Low-temperature cracking occurs when temperature drops, causing contraction-induced tensile stresses that exceed the asphalt mix's tensile strength (Roque et al., 1995); and (ii) thermal fatigue cracking results from cyclic thermal stresses due to daily temperature variations, leading to localized damage accumulation and eventual crack formation. This type of transverse cracking is most common in regions with moderate climates and high diurnal temperature variations (Lytton et al., 1983). Al-Qadi et al. (2005) emphasized the role of viscoelastic properties and layer interface conditions in predicting thermal fatigue responses.

Reflective cracking occurs when movement at underlying concrete joints (or severely cracked asphalt pavement) propagates through an asphalt overlay. This movement, caused by temperature fluctuations and/or traffic loading, generates localized stresses in the asphalt overlay. Interlayer bonding plays a major role in reflective cracking.

Laboratory Characterization of Cracking

The cracking potential of asphalt mixture is evaluated using both monotonic and fatigue fracture experiments, typically conducted under load-line displacement (LLD) or crack mouth opening displacement (CMOD) control. These fracture tests provide valuable insights into asphalt mix's fracture development by assessing indexed performance metrics, fracture and recovery energy parameters, crack growth rates, and fatigue life. A review was conducted to identify cracking tests suitable for common asphalt mixture designs within a BMD framework, and a summary is presented in Table 1.

Table 1. Summary of Laboratory Cracking Tests

Test Name	Test Standard	Loading Condition	Mode of Loading	Notched/ Unnotched[1]	Specimen Geometry[2]	Test Temperature[3]	Test Parameter
DCT	ASTM D7313	Monotonic	CMOD controlled	N	D: 150 mm (6") T: 50 mm (2") ND: 62.5 mm (2.5")	PGL + 10 °C (18 °F)	• Fracture energy (G_f) • Fracture strain tolerance (FST)
SCB	AASHTO T 394	Monotonic	CMOD controlled	N	D: 150 mm (6") T: 24.7 mm (1") ND: 15 mm (0.6")	PGL + 10 °C (18 °F)	• Fracture energy (G_f) • Fracture toughness (K_{IC}) • Stiffness (S)
IDT	AASHTO T 322	Monotonic	LLD controlled for strength	UN	D: 150 mm (6") T: 38 to 50 mm (1.5–2")	−30 °C (−22 °F) to 10 °C (50 °F)	• Tensile strength • Creep compliance
I-FIT	AASHTO T 393	Monotonic	LLD controlled	N	D: 150 mm (6") T: 50 mm (2") ND: 15 mm (0.6")	25 °C (77 °F)	• Fracture energy (G_f) • Post-peak slope (m) • Flexibility Index (FI)
LTRC SCB	ASTM D8044	Monotonic	CMOD controlled	N	D: 150 mm (6") T: 57 mm (2.25") ND: 15 mm (0.6")	(PGH + PGL)/2 + 4 °C (7 °F)	• Critical strain energy release rate (J_c)
CT Index	ASTM D8225	Monotonic	LLD controlled	UN	D: 150 mm (6") T: 62 mm (2.5")	(PGH + PGL)/2 + 4 °C (7 °F)	• Cracking Tolerance Index (CT Index)
DTCF	AASHTO T 400	Cyclic	Displacement controlled	UN	D: 150 mm (6") T: 62 mm (2.5")	5 °C (41 °F) to 25 °C (77 °F)	• Damage characteristic curve (D^R and S_{app})
Texas Overlay Test	Tex-248-F (Revised)	Cyclic	Displacement controlled	UN	L: 150 mm (6") W: 75 mm (3") T: 37.5 mm (1")	25 °C (77 °F)	• Number of cycles to failure • Paris law crack growth parameters
Flexural Bending Beam Test	AASHTO T 321	Cyclic	Strain controlled (usually)	UN	L: 380 mm (15") W: 50 mm (2") T: 63 mm (2.5")	20 °C (68 °F)	• Number of cycles to failure • Dissipated energy

[1]N – notched, UN – unnotched
[2]D – diameter, W – width, T – thickness, ND – notch depth
[3]PGL = low-temperature PG, PGH = high-temperature PG
IDT = Indirect Tensile Strength Test; LTRC = Louisiana Transportation Research Center; DTCF = Direct Tension Cyclic Fatigue Test.

Chapter 3. Research Methodology

This chapter outlines the research methodology used to evaluate the cracking potential of selected asphalt mixes. The methodology was developed based on an extensive literature review and discussions between the research team, other subject matter experts, and the project panel. The experimental program was designed to assess material behavior at both the component and mixture levels. Mixture-level testing included PMLC and LMLC specimens, along with FC extracted from existing pavement sections.

Material Sampling

The asphalt mixes, component materials, and FC were sampled from ongoing airport construction and rehabilitation projects across the United States between 2022 and 2024, as shown in Figure 1. The selection process aimed to capture a representative range of asphalt mixtures used in airfield pavements. The research team coordinated with the companion project investigating rutting protocols for BMD in airfield pavements to ensure thorough data collection.

The following locations were used for sampling:

- **Plant mix**: Newark Liberty International Airport (EWR), Teterboro Airport (TEB), Tampa International Airport (TPA), Reno Stead Airport (RTS), Sacramento International Airport (SMF), San Francisco International Airport (SFO), and Chicago O'Hare International Airport (ORD).
- **Aggregates and asphalt binder**: Newark Liberty International Airport (EWR), Teterboro Airport (TEB), Tampa International Airport (TPA), Reno Stead Airport (RTS), San Francisco International Airport (SFO), and Chicago O'Hare International Airport (ORD).
- **Field cores**: University of Illinois–Willard Airport (CMI), Kansas City International Airport (MCI), and the National Airport Pavement and Materials Research Center (NAPMRC).

The research team obtained two different mixtures from Chicago O'Hare International Airport, labeled ORD and ORAP. ORAP is a P-405 City of Chicago aviation mixture that includes 25-percent reclaimed asphalt pavement (RAP) and is used as a base course at Chicago O'Hare Airport. FC obtained from the University of Illinois–Willard Airport consisted of three different mixes, which were placed in 2004, 2012, and 2024 and labeled S1, S2, and S3, respectively. Also, six different asphalt pavement FC were obtained from Test Cycle 2 at NAPMRC, labeled FAA L1, FAA L2, FAA L3, FAA L4, FAA L5, and FAA L6.

Source: AAPTP

Figure 1. Geographic Location of Sampled Asphalt Mixes and FC

The research team identified climate, aggregate lithology and gradation, binder PG, recycled material, maximum aircraft gross weight, and mixture design types as attributes that would impact the cracking potential of asphalt mixes. Mixtures designed by the Marshall method and Superpave Gyratory method were considered in the testing plan to incorporate variations related to mixture design method as allowed by FAA AC 150/5370-10H. The selected projects' mixture design formulas also provided variations in important volumetric attributes such as AV and VMA. Table 2 summarizes the main mixture design differences of the sampled asphalt mixes.

FC were used to validate the developed test protocols. The oldest cores (2004) were sampled from CMI before it underwent reconstruction in 2024. CMI cores were extracted from pavement sections constructed in 2004 (S1), 2012 (S2), and 2024 (S3). Cores from the 2024 construction cycle consisted of two lifts: the surface course with no RAP (S3) and the base course with 20-percent RAP (S3 RAP). Asphalt pavement cores were extracted and tested from the new taxiway configuration at CMI in 2025. Cores were obtained from six test lanes from the NAPMRC that underwent accelerated loading, details of which can be found elsewhere (Alvarez et al., 2024). The JMF for the test lanes and sampled asphalt mixtures can be found in Appendix B. Test lanes L3 and L4 exhibited cracking after the accelerated loading, while the other lanes showed no cracking.

Table 2. Properties of Sampled Airfield Mixes

Airport	EWR	TEB	TPA	RTS	SMF	SFO	ORD	ORAP
Thickness	200 mm (8.0")	75 mm (3.0")	50 mm (2.0")	88 mm (3.5")	100 mm (4.0")	100 mm (4")	125 mm (5.0")	400 mm (15.5")
Mix Type	P-401 Surface	P-401 Surface	P-404 Surface	P-401 Surface	P-401 Surface	P-401 Surface	P-401 Surface	P-405 Base
Location	Taxiway	Runway	Hangar	Taxiway	Apron	Runway	Taxiway	Taxiway
Air Traffic	≥100,000 lb	<100,000 lb	≥100,000 lb	≥100,000 lb	≥100,000 lb	≥100,000 lb	≥100,000 lb	≥100,000 lb
Climate	Wet-Freeze	Wet-Freeze	Wet-Non freeze	Dry-Freeze	Dry-Non freeze	Dry-Non freeze	Wet-Freeze	Wet-Freeze
PG Value	PG 82-22	PG 64-22	PG 82-22	PG 64-28	PG 76-22	PG 76-22	PG 76-28	PG 76-22
Asphalt Binder %	4.49%	5.03%	6.80%	5.70%	5.70%	5.50%	6.20%	5.02%
Aggregate Lithology	Granite	Granite	Granite	Shale (or Mudstone)	Alluvium Deposit	Granite	Limestone	Limestone
Gradation Type	19 mm (3/4") FAA Grad-1	12.5 mm (1/2") FAA Grad-2	9.5 mm (3/8") FAA Grad-3	12.5 mm (1/2") FAA Grad-2	12.5 mm (1/2") FAA Grad-2	19 mm (3/4") FAA Grad-1	12.5 mm (1/2") FAA Grad-2	19 mm (3/4") (non-FAA)
Design Type	Marshall (75 blow)	Marshall (75 blow)	Marshall (50 blow)	Marshall (75 blow)	Superpave (75 gyr)	Marshall (75 blow)	Superpave (75 gyr)	Superpave (90 gyr)

Experimental Matrix

Cracking characterization of asphalt mixtures is typically performed using either monotonic or cyclic loading. While cyclic (fatigue) loading better simulates real-world conditions, it is resource-intensive, requiring significant time, cost, and expertise for execution and analysis. Due to these limitations, monotonic tests are often preferred in BMD methodologies and have been widely adopted by various agencies due to their simplicity and ease of implementation (Yin & West, 2021). These tests are classified into two categories based on temperature conditions: low-temperature and service-temperature testing. Given the viscoelastic nature of asphalt mixes, temperature plays a crucial role in determining potential material performance.

The experimental characterization of cracking was conducted in two key domains:

- Low-temperature cracking assessed using the DCT test and the new SLT-SCB test that was developed as part of this study (discussed in Chapter 4).
- Service-temperature strength and fracture evaluated using the CT Index test and the I-FIT (detailed in Chapter 5). A modified CT Index test, called DONUT, was also developed as another fracture metric.

The selection of these tests was based on their ability to capture the primary cracking mechanisms observed in airfield asphalt pavements under different environmental and loading conditions. In addition, the dynamic modulus test and the Texas Overlay Test were performed on the eight sampled mixtures using PMLC specimens. The results are presented in Appendix C.

Asphalt Mixture Testing Protocols and Specifications

The specimen fabrication and testing protocols for this project were developed in coordination with the research team investigating rutting protocols for airfield asphalt pavements (Hajj et al., 2025). This collaboration ensured consistency in specimen preparation and field-representative testing conditions for rutting and cracking, the two pillars of BMD. All test specimens were obtained from a typical compacted Superpave gyratory specimen measuring 180 mm (7 inches) in height and 150 mm (6 inches) in diameter. The specimens were sawed from the middle of the gyratory specimen due to high AV concentration near the edges.

Lab Design of Mixes

Aggregates, asphalt binder, and additives were obtained—along with the plant mix—from seven airfield projects. The components were used to design asphalt mixtures so that the cracking potential of PMLC specimens could be directly compared to that of LMLC specimens. The controlled laboratory setting was expected to reduce variability in the test results. Additionally, the lab-mix designs were modified to isolate the impacts of factors such as binder type, binder content, and aggregate gradation on cracking potential within each of the three specified test domains.

For each asphalt mix, the stockpiled aggregates were fractionated into individual standard sieve sizes ranging from 19 mm (3/4 inch) to 75 µm (#200 sieve) and then batched until a consistent gradation was achieved for each batch. The aggregates sampled from the RTS airport were pre-treated with lime (i.e., coated with lime as specified in the JMF). Furthermore, the stockpiles labeled “1/2 inch” and “3/8 inch” were received as a mixed batch. Thus, this combined stockpile was assumed to represent the aggregate gradation of the combined individual stockpiles.

To ensure that the LMLC specimens were representative of the JMF, the team implemented two checks on the lab batch aggregate gradation. First, the differences between the JMF values and the lab-batched values for each mixture were constrained to lie within the FAA tolerances permitted during construction, as specified in the AC. Second, a tolerance of 0.3 percent was chosen for the difference in VMA values to ensure that the volumetric properties of the LMLC specimens closely matched those of the PMLC specimens. The design details for the LMLC specimens can be found in Appendix D.

In addition to LMLC, the project created cross-combination LMLC (XCM) designs to quantify the impact of binder grade on asphalt mixture cracking potential. The XCMs were designed using the same aggregate skeleton design, but different binders were used. The binders were from other asphalt mixtures for varying PG values. Aggregate gradation designs of TPA and SFO were used along with various binder grades sampled for this project.

Specimen AV

In highway pavement testing, specimens are typically prepared with 7 percent AV to simulate field density. However, FAA specifications require lower design AV for airfield asphalt mixes. To determine representative AV levels for testing, the research team analyzed approximately 1,000 data points from P-401 mixtures and 140 from P-404 mixes, shown in Figure 2. Statistical analysis revealed that 5 percent AV for P-401 and 3 percent AV for P-404 best represented in-field density conditions for airfield pavements (Bajaj & Al-Qadi, 2026; Elias et al., 2024; Modi et al., 2026). Given the significant influence of AV on cracking potential (Barry, 2016), additional testing was conducted at higher AV levels (7 percent for P-401 and 5 percent for P-404) to assess their impact on cracking potential.

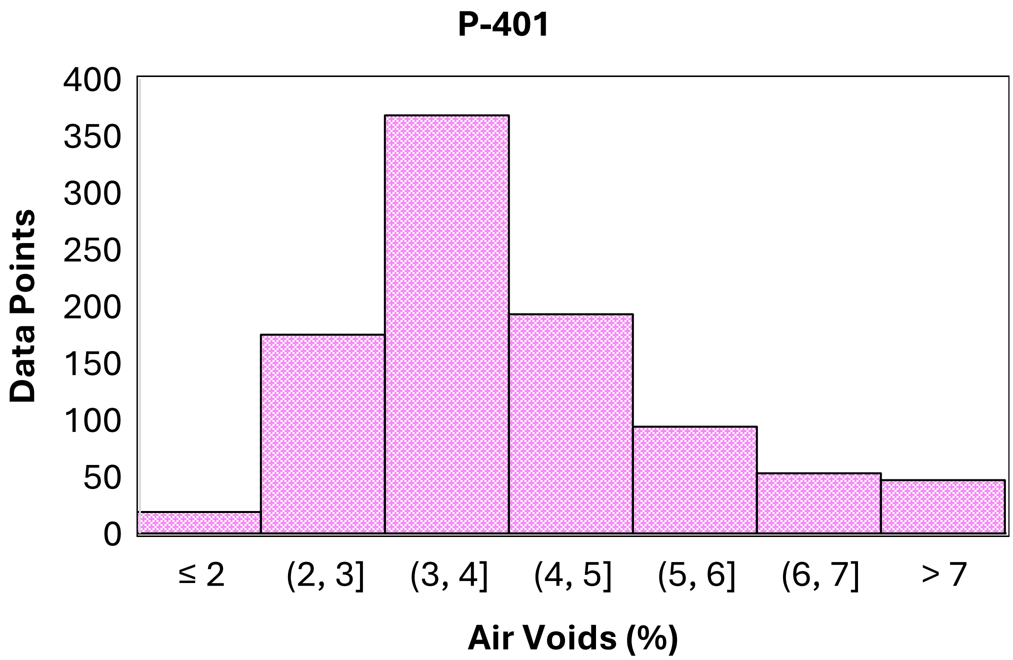

(a)

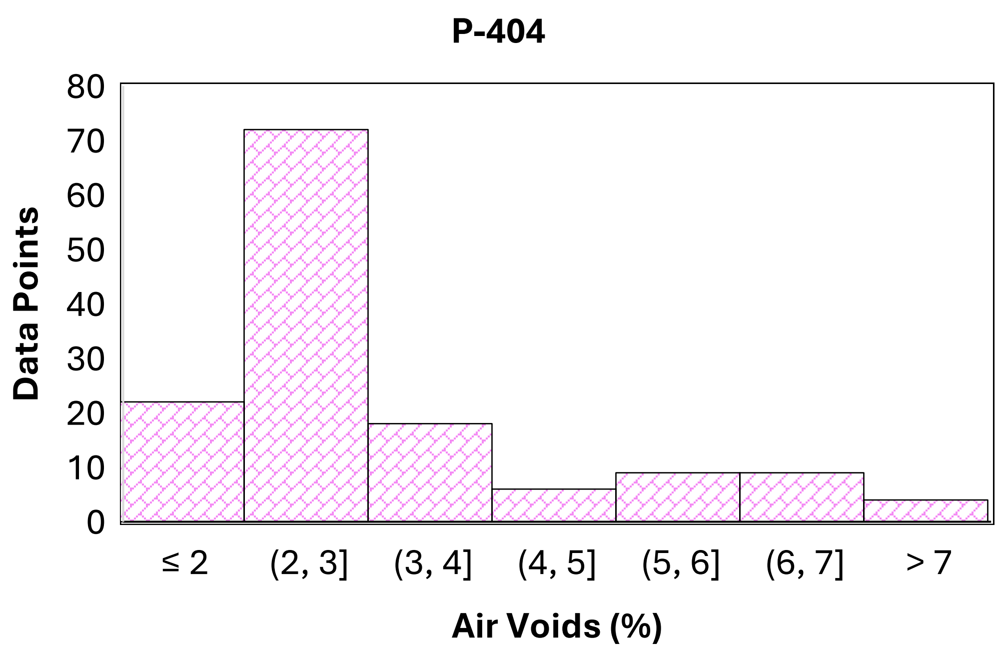

(b)

Source: AAPTP

Figure 2. Lab and In-Field AV Data for (a) P-401 and (b) P-404 Mix Designs

Reheating and Splitting of Plant Mix

The research team obtained plant mixture samples in 20 L (5 gal) metal buckets from various airport projects. Because these mixtures had already undergone short-term aging (STA) during production, the reheating protocol was designed to minimize additional aging effects while ensuring uniform sample preparation. To fabricate gyratory specimens of 180 mm (7 inches) in height and 150 mm (6 inches) in diameter, the following reheating procedure was followed:

- At least two buckets of plant mixture were simultaneously heated in a draft oven at the specified compaction temperature for 1.5 hr with lids removed.
- The mixture was then transferred into large metal pans and returned to the draft oven for an additional 1-hr heating cycle to ensure uniform temperature distribution.
- After heating, the mixture was reduced to the required compaction weight in accordance with American Association of State Highway and Transportation Officials (AASHTO) R47 procedures, ensuring uniform particle distribution.
- The weighted mixture was returned to the oven until it reached the contractor-specified compaction temperature, with periodic stirring every 30 min to maintain uniform heating.
- Once the target compaction temperature was achieved, the mixture was placed into a gyratory mold and compacted to fabricate asphalt mixture gyratory specimens.

Short-Term Aging of Laboratory Mix

The LMLC specimens were fabricated in a controlled environment and provided less variability than specimens compacted from the PMLC mixture. The aggregates and asphalt binder were heated to the suggested mixing temperature as provided by the contractor to achieve desired viscosity. After the temperature was reached, the components were mixed in the lab with a pre-heated rotating drum and mechanical mixing arm for 90–120 s before being transferred to pans and kept in a draft oven for 2 hr at the suggested compaction temperature, with stirring after 1 hr in the oven. This STA procedure was used to mimic aging during production that the loose field mixture would have undergone.

Long-Term Aging of Laboratory and Field Mix

To assess the impact of aging on cracking potential, selected specimens underwent long-term aging (LTA) at 95 °C (203 °F) for 3 days, following the protocol established by Al-Qadi et al. (2019). This LTA procedure was chosen due to its practicality and established relevance for asphalt mixes. The research team considered changing the duration of aging based on geographic location, as suggested by Kim et al. (2017), but decided against it for two reasons: (i) A uniform protocol could help screen out mixtures whose cracking potential is highly affected by aging; and (ii) mixtures from Florida would need to be aged in the oven for 10–15 days to reach the level of in-field aging observed in the State, hence, the protocol would be rendered impractical for application by contractors in such locations.

Chapter 4. Low-Temperature Cracking

At low temperatures, asphalt mixture exhibits predominantly brittle elastic behavior, resulting in an increase in its apparent strength. External stresses exceeding this strength often lead to low-temperature cracking (Li & Marasteanu, 2004). Therefore, material resistance to crack initiation is of critical significance because the brittle, elastically dominant nature of the material does not allow controlled crack growth once a crack begins to propagate. This typically results in the instantaneous release of energy during the propagation stage, making it challenging to measure or use within a practical testing framework, such as BMD. In addition, the fracture energy of the material (its ability to absorb and dissipate energy to resist fracture) is also an important parameter in evaluating its low-temperature performance.

Several laboratory tests have been developed and adapted for asphalt mixes to characterize their low-temperature performance. Among them, the DCT and the Low-Temperature SCB tests are the most commonly used. Both tests utilize notched asphalt mixture specimens to localize crack initiation and are considered in this study. The following sections present the implementation and findings of these tests.

Disk-Shaped Compact Tension Test

The DCT test was conducted in accordance with ASTM D7313, using a servo-hydraulic universal testing machine load frame with a sealed, temperature-controlled chamber. A 150-mm (6-inch) diameter, 180-mm (7-inch) tall gyratory specimen was sawed to obtain 50-mm (2-inch) thick disks. One edge of the disk was shaved to create a flat surface for installing the CMOD gauge. Additionally, 25-mm (1-inch) diameter holes were cored for the loading rods, and a 62.5-mm (2.5-inch) long notch was introduced at the center. The test temperature was set to 10 °C (18 °F) above the low-temperature PG (PGL) of the asphalt binder.

Specimens were placed inside the temperature-controlled chamber along with a dummy asphalt mixture specimen, equipped with a thermometer to monitor specimen temperature. Testing commenced once the specimen temperature stabilized within ±1 °C (2 °F) of the desired testing temperature. Upon stabilization, the two loading rods were moved apart until a seating load of approximately 0.2 kN (45 lb) was achieved to ensure proper contact between the specimen and loading rods. The specimen was then pulled apart at a constant CMOD rate of 1 mm/min (0.04 inch/min) until the measured load dropped to 0.1 kN (22.5 lb). The DCT specimen, test setup, and a typical load-CMOD curve are shown in Figure 3.

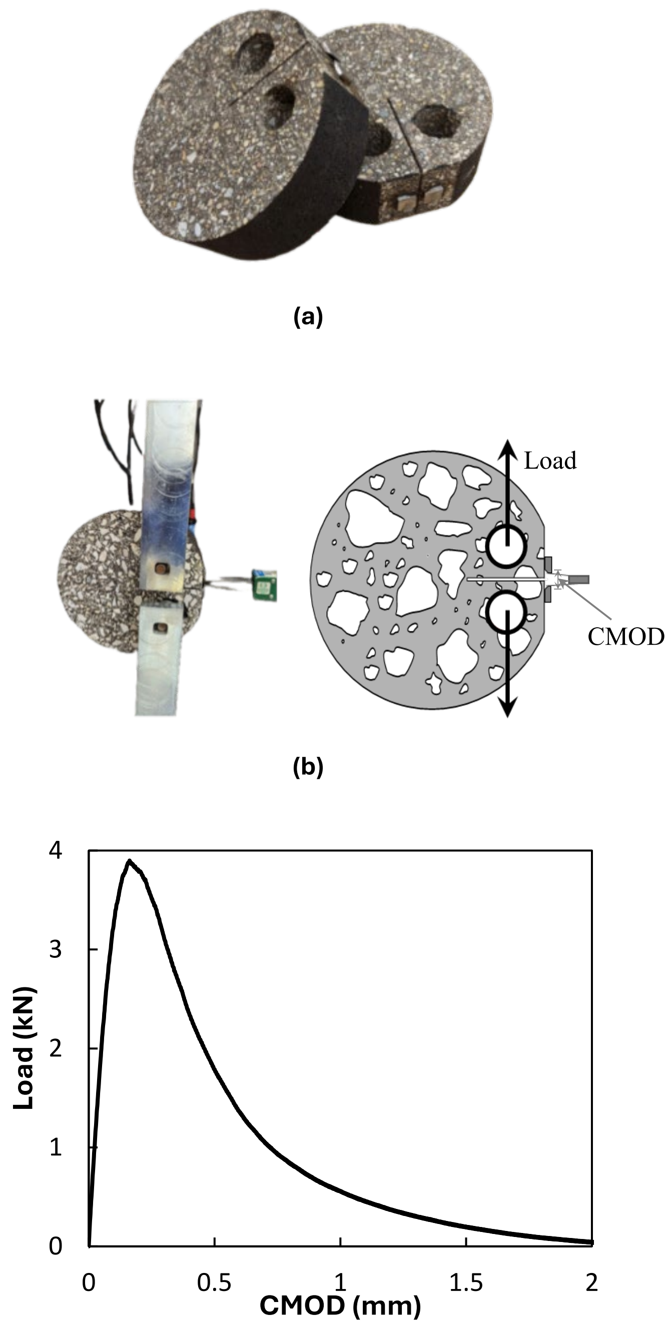

Source: AAPTP

Figure 3. DCT Test (a) Specimens, (b) Setup, and (c) Load-CMOD Plot

The work of fracture was determined as the area under the load–CMOD curve for each specimen. Fracture energy, expressed in J/m^2, was calculated by dividing the work of fracture by the ligament area (i.e., the product of the ligament length and the specimen thickness prior to testing). A higher fracture energy indicates greater cracking tolerance of asphalt mixes.

The PMLC specimens were tested at 3 percent AV for TPA and 5 percent AV for the other specimens to represent field conditions. Specimens from RTS, ORD, and ORAP mixtures were tested at −18 °C (0 °F), while the remaining mixes were tested at −12 °C (10 °F). The test results are shown in Figure 4, in which the error bars denote one standard deviation of the mean fracture energy from replicate tests.

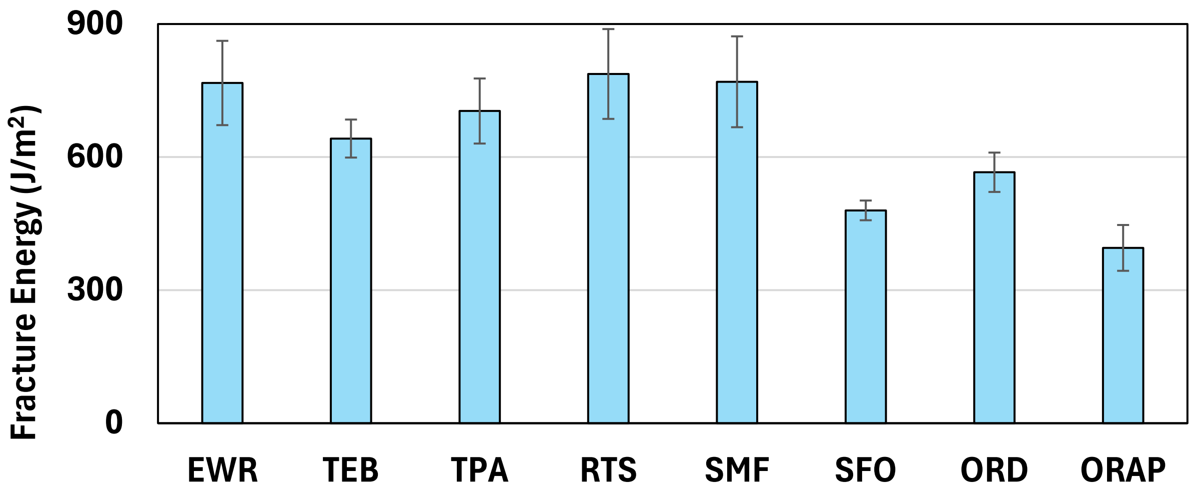

Source: AAPTP

Figure 4. DCT Test Results from PMLC Specimens

The effects of both AV and testing temperature on fracture energy have been documented in the literature (Marasteanu et al., 2012) and were validated for airfield asphalt mixtures in this project. Three selected mixtures (EWR, TEB, and TPA) were tested at two AV levels: field-representative AV (5 percent for P-401 and 3 percent for P-404) and a higher AV level (7 percent for P-401 and 5 percent for P-404), as defined in the previous chapter. As shown in Figure 5, fracture energy generally decreased with increasing AV. However, the influence of a 2-percentage-point change in AV was minimal for most mixes, except in the case of TEB—which may be attributed to variability in plant mixture sampling.

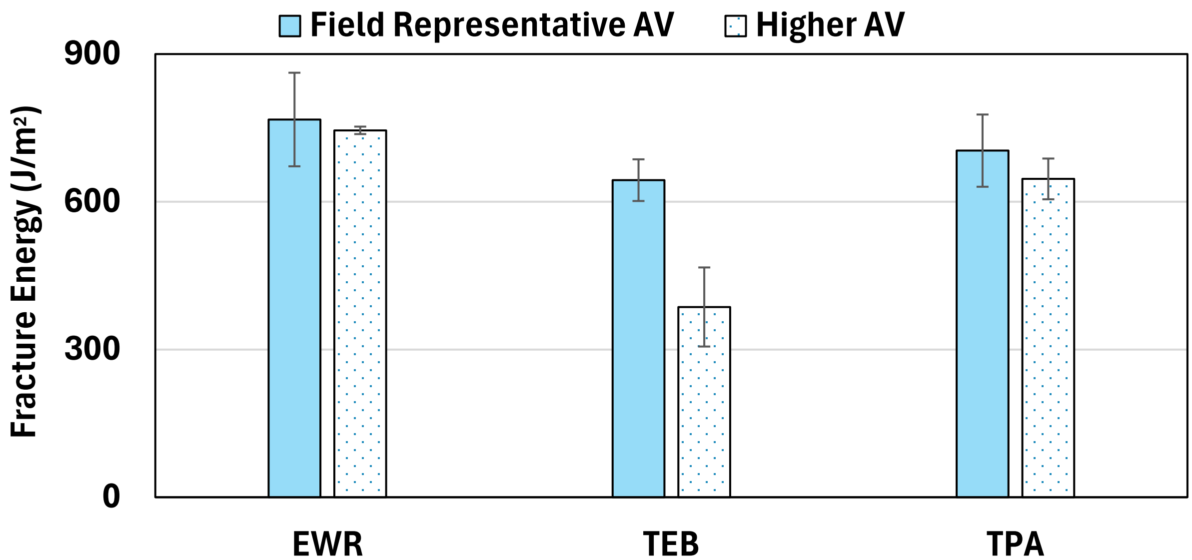

Source: AAPTP

Figure 5. Effect of AV on DCT Fracture Energy

Testing temperature was also varied for two selected mixtures (ORD and ORAP), with the resulting fracture energy plotted in Figure 6. A decrease in fracture energy was observed as the test temperature decreased. This behavior is attributed to increased brittleness and a corresponding reduction in the material's ability to deform and absorb energy before fracturing.

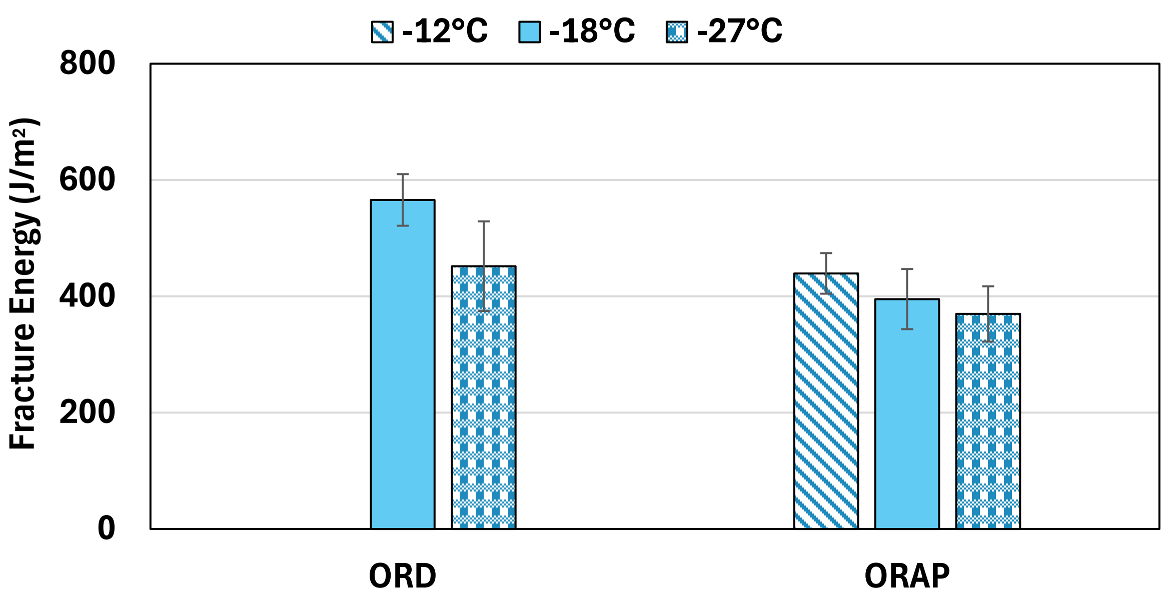

Source: AAPTP

Figure 6. Effect of Testing Temperature on DCT Fracture Energy

Preliminary testing on PMLC specimens revealed that the DCT test had a limited ability to differentiate the cracking potential among various asphalt mixes. Mixtures exhibiting distinct load–CMOD curves can yield similar fracture energy values and fail to capture the nuances of the loading/unloading behavior, a finding that has been reported in the literature (Buttlar et al., 2015; Haslett et al., 2022). Consequently, further DCT testing was not pursued.

Simplified Low-Temperature Semi-Circular Bend Test

AASHTO T 394 details the protocols developed for the low-temperature SCB test. However, the research team, with input from the panel, modified these protocols to characterize low-temperature cracking in a more practical way to facilitate field implementation. Accordingly, the SLT-SCB test was developed. Because crack initiation is the dominant mechanism dictating low-temperature cracking potential (see Chapter 3), three major modifications were implemented for this study:

- **Specimen geometry:** The thickness of the SCB test specimen was increased from 24.7 mm (1 inch) to 50 mm (2 inches). This change was made to create a standard specimen geometry that could be used across multiple test domains and to better accommodate 19-mm mixes commonly used in airfield pavements.
- **Loading:** The original loading rate of 0.03 mm/min using a CMOD gauge was replaced with a faster rate of 0.15 mm/min using LLD. This increased rate reduced testing time from 1 to 2 hr to approximately 5 min, thereby minimizing creep effects and making the test more suitable for a BMD protocol.
- **Testing temperature:** While AASHTO suggests determining the low-temperature SCB testing temperature based on the binder's PGL, discrepancies between the binder PG and the actual lowest pavement temperature at a project location can unfairly penalize or reward an asphalt mixture. Therefore, the research team recommended using the field temperature at the project location to set the SLT-SCB testing temperature.

The modified SLT-SCB specimen, test setup, and a typical load-LLD curve are shown in Figure 7.

(a)

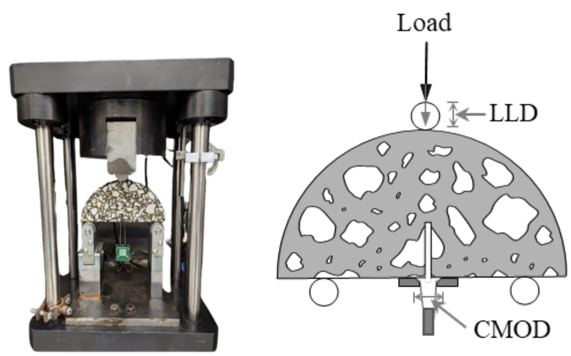

(b)

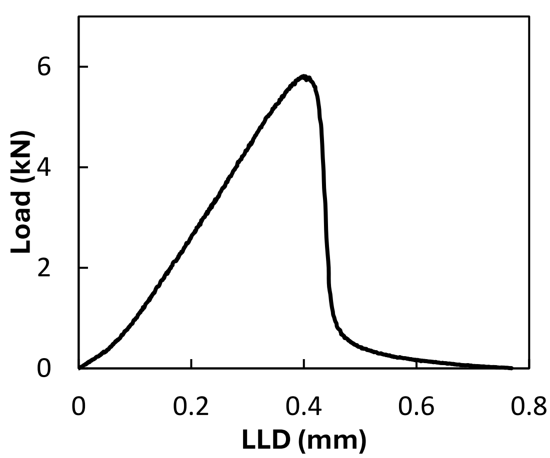

(c)

Source: AAPTP

Figure 7. SLT-SCB Test (a) Specimen, (b) Setup, and (c) Load-LLD Plot

Selection of Loading Rate

As a viscoelastic material, the fracture behavior of asphalt mixture depends on the loading rate (Al-Qadi et al., 2015), with a higher loading rate resulting in a more elastic response. Because elastic behavior is dominant when characterizing low-temperature cracking, increasing the loading rate is justified to better capture cracking potential. The SLT-SCB protocol focuses on the loading portion of the curve, so the selected rate was chosen to ensure a smooth loading response from all tested asphalt mixture specimens. Furthermore, the study aimed to eliminate the dependence on CMOD gauge clips to enhance compatibility with commercial testing machines and ensure simplicity.

Previous research (Dave & Behnia, 2018; Son et al., 2019) on SCB geometry utilized a CMOD opening rate of 0.7 mm/min (0.03 inch/min) to mimic fracture properties obtained using a 1 mm/min (0.04 inch/min) CMOD rate in DCT geometry. CMOD gauges were attached to PMLC specimens of EWR, TEB, and a 4.75 mm (0.19 inch) nominal maximum aggregate size (NMAS) highway asphalt mixture (RR). Tests were conducted at various LLD loading rates to match the 0.7 mm/min (0.03 inch/min) CMOD opening rate. The loading rate required to match the CMOD rate was found to be dependent on the NMAS: 0.19 mm/min (0.0075 inch/min) for EWR, 0.21 mm/min (0.0083 inch/min) for TEB, and 0.23 mm/min (0.0091 inch/min) for RR. Additional tests evaluated the effect of slight variations in these rates on fracture energy (see Appendix E). Ultimately, an LLD loading rate of 0.15 mm/min (0.006 inch/min) was selected to minimize the possibility of dynamic brittle failure. All subsequent testing was performed in LLD control at a rate of 0.15 mm/min (0.006 inch/min).

Development of New Parameter

A typical load-LLD plot obtained using the modified SLT-SCB protocol is shown in Figure 8(a). The plot can be divided into two regions: (i) the pre-peak load region and (ii) the post-peak load region. The curve exhibits a steep drop after the peak load, which is attributed to the highly elastic nature of the specimen and the rapid energy release once crack initiation occurred. This behavior is consistent with the fact that most of the energy supplied to the specimen—measured as the area under the load-LLD curve—occurs in the pre-peak region. Figure 8(b) shows the progression of the corresponding CMOD for the test. A sudden increase in CMOD is noted around the time of peak load, validating the assumption that crack initiation starts around peak load. Given that under low testing temperatures and high loading rates the material behaves in the glassy domain, the energy supplied up to the peak load can be approximated as strain energy (i.e., the energy stored in an elastic body under loading) and termed pre-peak fracture energy (PFE).

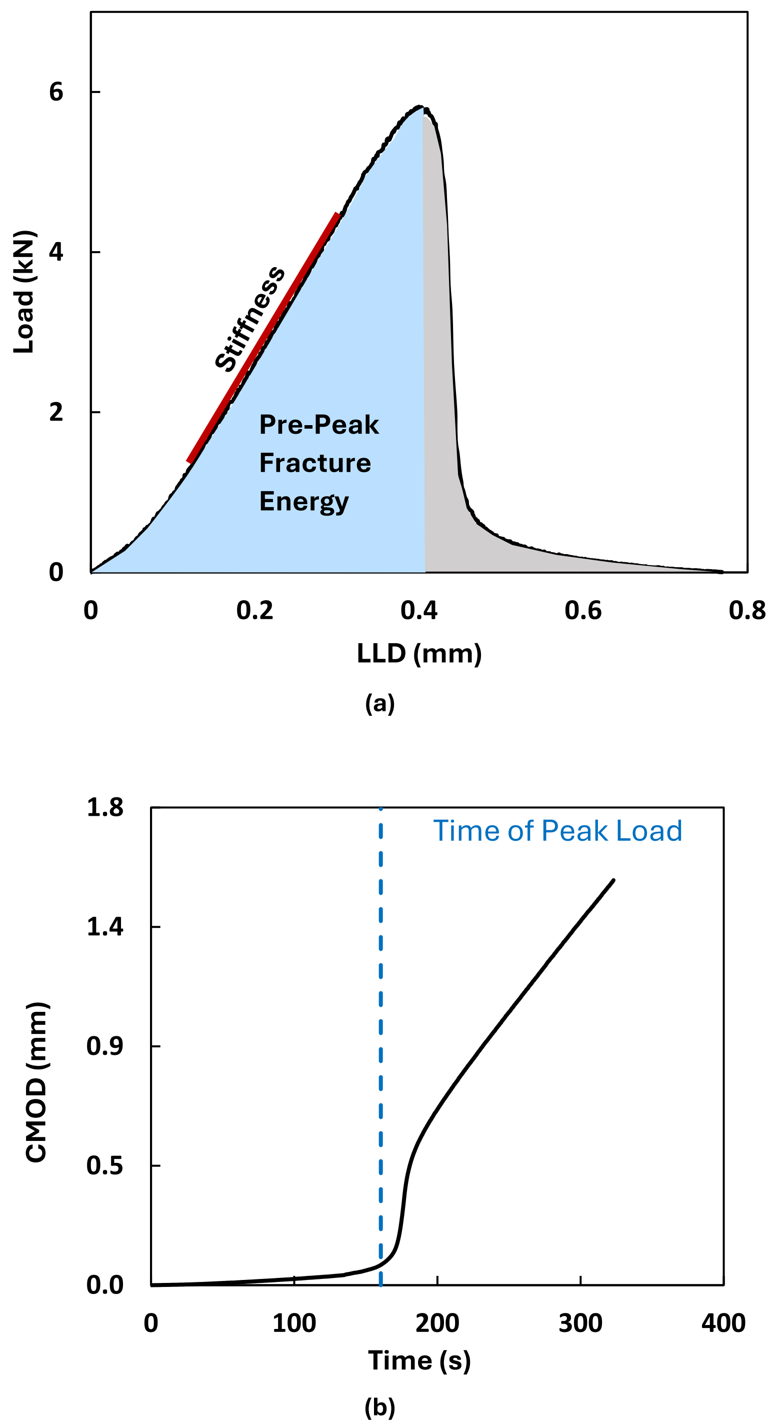

Source: AAPTP

Figure 8. Typical (a) Load-LLD and (b) CMOD-Time Plot for the SLT-SCB Test

In conjunction with PFE, the loading characteristics of the curve are also considered by inclusion of stiffness, shown by the thicker red line segment in Figure 8(a). This loading stiffness was obtained from the linear elastic portion of the load-LLD curve using a sliding window near the midpoint of the curve and a chi-square penalty term (α). This approach was used to reduce the influence of nonlinear behavior near the bounds of the loading portion and focus on the most stable and consistent region. A window length of 15 percent and α=0.05 were selected after optimization, details for which can be found in Appendix E. The resulting stiffness demonstrated good consistency, resulting in lower standard deviation for replicates of various asphalt mixes.

A novel index called Low-temperature Cracking Index (LCI) was developed to assess the cracking potential of asphalt mixtures at low temperatures. LCI was defined as the ratio of PFE to stiffness (S) from the SLT-SCB test as shown in the following equation:

$$\text{Low-temperature Cracking Index, LCI} = \text{PFE}/S$$

where PFE is in J/m^2 and loading stiffness, S, is in kN/mm, calculated using a 15-percent window length and α=0.05.

A higher LCI of an asphalt mixture indicates either greater energy required for crack initiation or lower stiffness, which implies an increased strain tolerance before fracture of materials with similar fracture energies. Therefore, a higher LCI reflects greater tolerance for low-temperature cracking.

Impact of Binder Grade and Content

The effect of binder properties on PFE, stiffness, and LCI was investigated using the XCM specimens. XCM specimens with TPA aggregate gradations were created with PG 64-28, PG 64-22, PG 76-28, and PG 76-22 binders. The specimens were tested at three temperatures: PGL+10 °C and ± 6 °C (one PG difference) on either side to verify the glassy-to-viscoelastic transition of fracture response. The load-LLD plots of XCM at different temperatures are shown in Figure 9. When tested at one grade warmer than PGL+10 °C, all XCM specimens showed a viscoelastic response by an increased fracture energy. Testing at PGL+10 °C and below, the load-LLD curves showed only marginal changes and collapsed into tight bands, indicating the onset of glassy (elastic brittle) behavior with lowering of temperature. This is further seen in the PFE values shown in Figure 10, validating its use as an indicator of fracture at low temperatures.

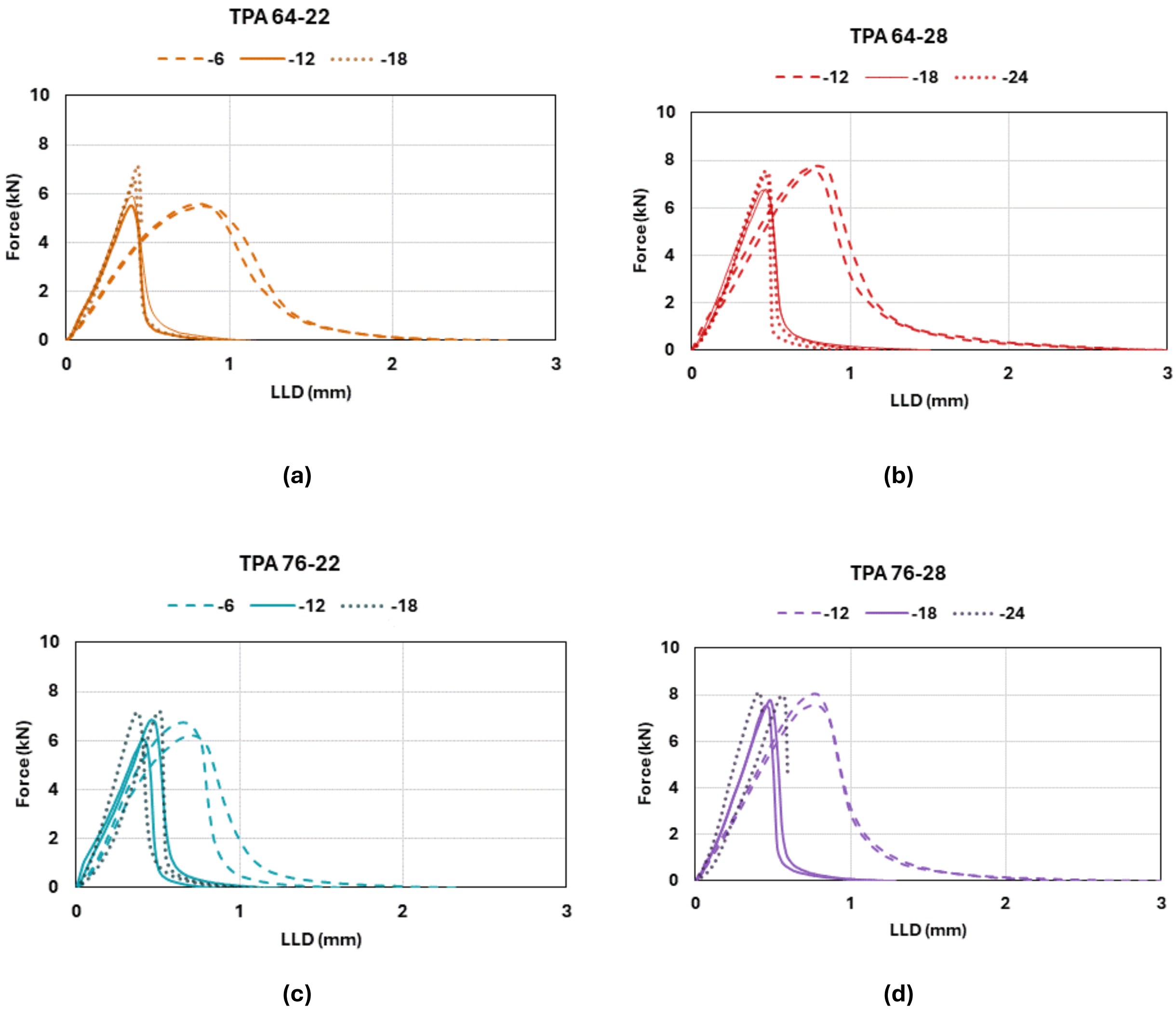

Source: AAPTP

Figure 9. Effect of Test Temperature on TPA XCMs with (a) PG 64-22, (b) PG 64-28, (c) PG 76-22, and (d) PG 76-28 Binders Tested at PGL+10 °C and ±6 °C (one PG difference on both sides)

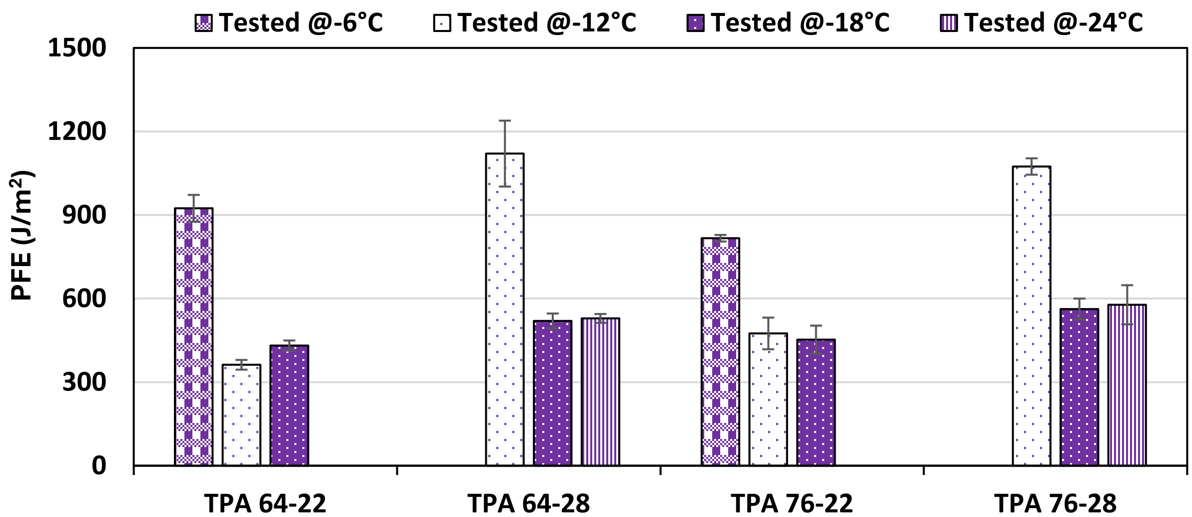

Source: AAPTP

Figure 10. Effect of Test Temperature and Binder Grade on PFE for TPA XCMs

Binders used in XCM specimens were characterized in terms of their shear stress relaxation modulus, G(t=60s), and corresponding time-dependent slope, m_r (t=60s). Lower G(t) values and steeper m_r(t) at 60 s are indicative of a binder being less prone to accumulating thermal stress and more able to dissipate the stress rapidly; hence, lower thermal cracking potential (Farrar et al., 2015). The loading stiffness (S) from mixture testing is plotted against G(t) and m_r(t) results from binder testing in Figure 11.

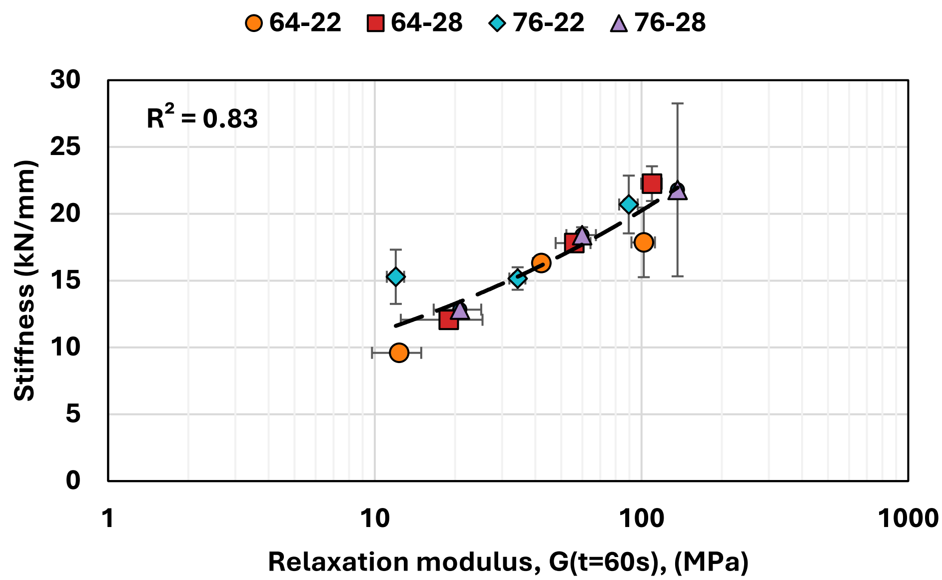

(a)

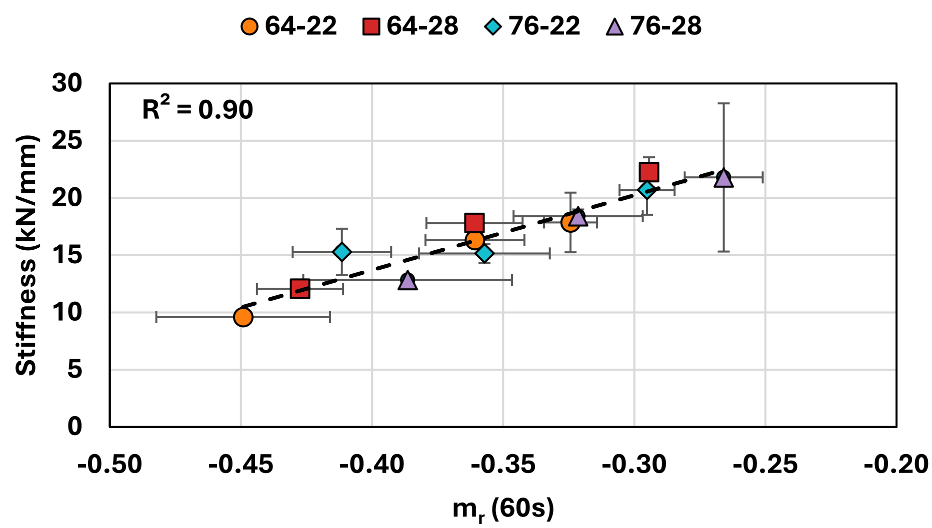

(b)

Source: AAPTP

Figure 11. Relationship of Mix Loading Stiffness with (a) G(t=60s) and (b) m_r(t=60s) for Binders at Three Test Temperatures

An increase in stiffness was observed with increasing G(t) and decreasing (less negative) m_r values, indicating a strong correlation between asphalt mixture specimen stiffness and binder rheology at low temperatures. A power-law fit with R^2=0.83 for stiffness and G(t) and a linear fit with R^2=0.90 for stiffness and m_r were observed. This corroborates the benefit of stiffness when assessing low temperature cracking potential of asphalt mixes, validating the use of LCI.

Lastly, the effect of binder content variability on LCI was tested at ±0.5 percent from the optimum binder content (OBC), as stated in the JMF for the TPA mixture. "O-," "O," and "O+" labels were used to denote OBC −0.5 percent, OBC, and OBC +0.5 percent, respectively. Specimens for all three binder contents were tested at −12 °C and −18 °C only, with the results presented in Figure 12.

Minor binder content adjustments had limited impact on LCI in most cases. An increase in LCI with an increase in binder content was observed in cases of PGL −28 binder being tested at −12 °C, attributed to a transition from glassy to viscoelastic response. Binder volume has little impact on crack initiation under near-brittle conditions, as seen in the literature (Li et al., 2008). However, at warmer temperatures, when the response has a larger viscous component, the energy dissipation due to excess binder leads to an increase in PFE and a lowering of stiffness, resulting in lower cracking potential.

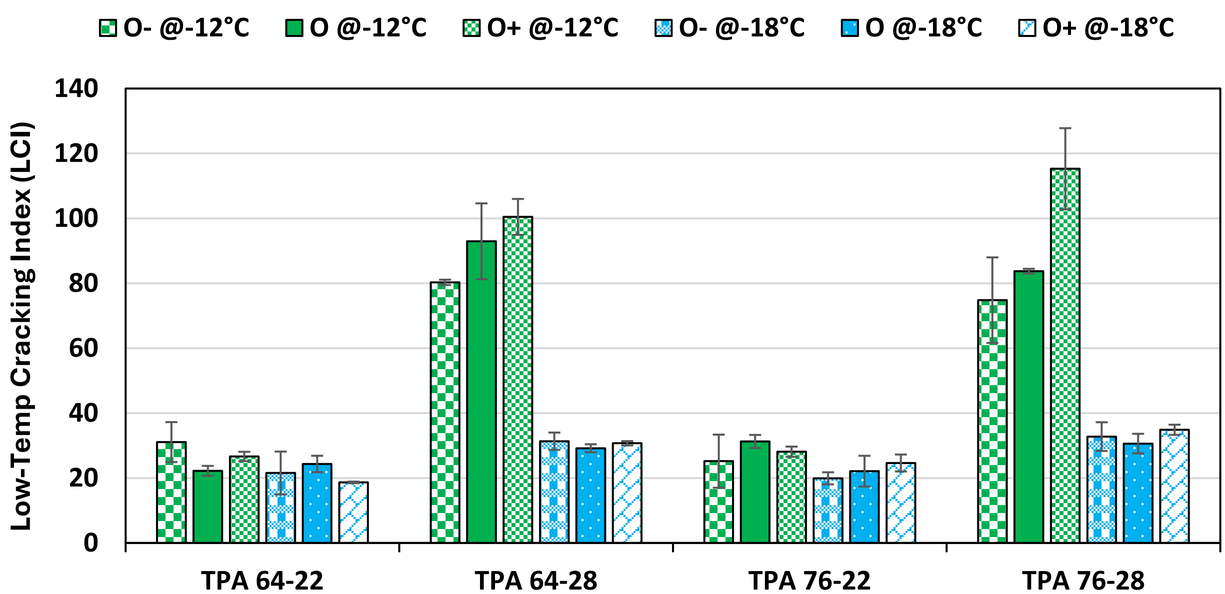

Source: AAPTP

Figure 12. Effect of Binder Content Variability at −12 °C and −18 °C on LCI for XCMs

Selection of Testing Temperature

The testing temperature recommended in this study is based on local in-field environment rather than the asphalt binder's PGL. This approach was adopted because the viscoelastic nature of asphalt mixture makes its properties highly dependent on temperature. The lowest pavement temperature was obtained from the Long-Term Pavement Performance (LTPP) InfoPave website at both 50- and 98-percent reliability for the sampled plant mixture locations (see Table 3 along with the binders' PGL values).

Table 3. Sampled Mixtures with the Lowest Pavement Temperature and Binder PGL

Sampled Location	Lowest Annual Pavement Temperature, 50% (°C)	Lowest Annual Pavement Temperature, 98% (°C)	PGL (°C)
EWR	−16.0	−22.6	−22
TEB	−17.0	−23.7	−22
TPA	1.70	−3.7	−22
RTS	−17.0	−23.6	−28
SMF	−3.3	−8.1	−22
SFO	1.2	−3.7	−22
ORD	−27.9	−36.8	−28
ORAP	−27.9	−36.8	−22

LCI values for two asphalt mixes—RTS and ORD—were compared at 98- and 50-percent lowest annual pavement temperature reliability, as shown in Figure 13. A consistent decrease in LCI with lowering of testing temperature was seen for both field-representative and high-AV specimens. The decline results from an increased glassy response of asphalt mixtures with lowering of temperature, reflecting reduced PFE and an increased stiffness at lower temperatures. This underscores the importance of testing asphalt mixtures at an appropriate temperature reflecting the local environment for realistic assessment of their low-temperature cracking potential.

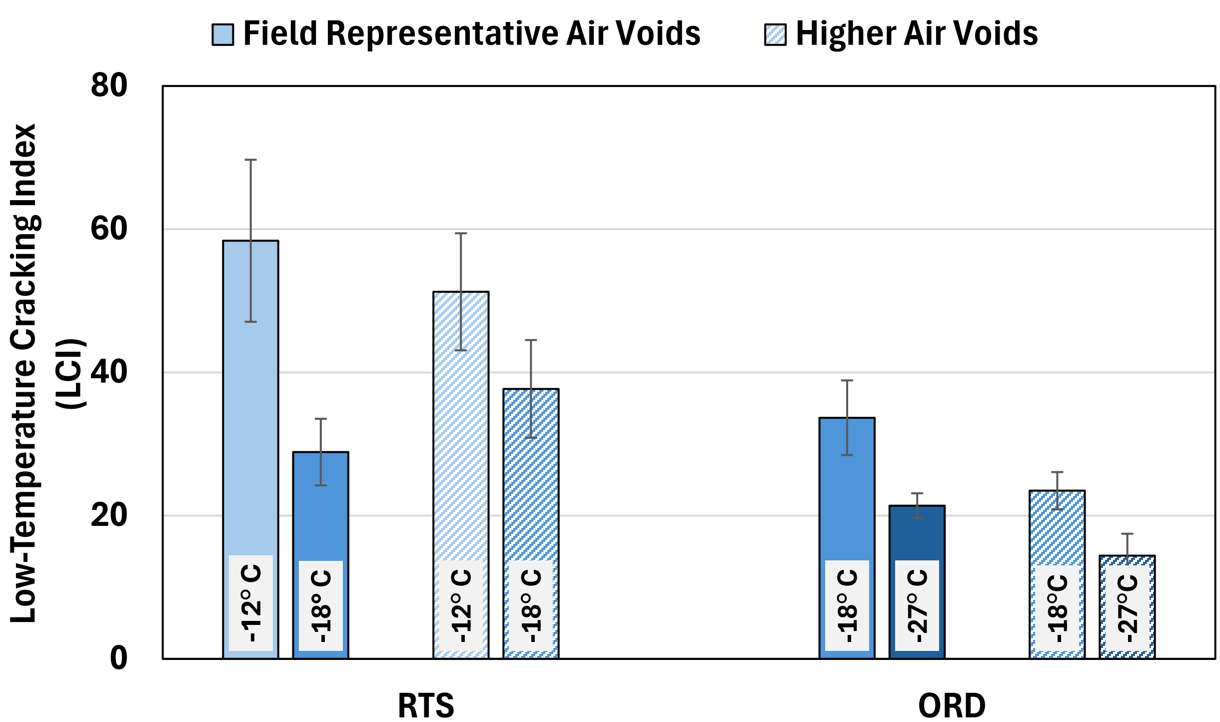

Source: AAPTP

Figure 13. Effect of Temperature on LCI Values

A testing temperature equal to the lowest pavement temperature at 50-percent reliability plus an additional 10 °C (18 °F) was chosen for the SLT-SCB test protocol. This shift was selected to mimic adjustments used in other low-temperature tests, thereby making the test more practical and efficient. Temperatures corresponding to 98-percent reliability represent extreme cases that may not be achievable with commercially available equipment and make the test impractical for BMD application.

Furthermore, an upper limit of −12 °C (10 °F) was established, requiring that the test temperature not exceed −12 °C. This constraint prevents creep effects and ensures assumptions of small-scale yielding for LEFM application for the test. In addition, FAA specifications require binders to have a PGL of at least −22 °C (−8 °F), based on historical binder performance, aligning with the proposed upper limit of test temperature.

Results and Discussion

The results of seven LMLC specimens tested at field-representative and higher AV for STA and LTA are shown in Figure 14. ORD and ORAP were tested at −18 °C, while the others were tested at −12 °C in accordance with the aforementioned test temperature selection. Higher variability in EWR was attributed to the large NMAS aggregate skeleton of the mix, while ORAP's scatter likely reflected the 25-percent RAP content. The highest LCI values were observed for RTS (tested at −12 °C) and ORD (tested at −18 °C), both mixtures using a PGL −28 binder. The comparatively low PGL value for RTS and ORD during the test would lead to the presence of viscous dissipation, and therefore energy dissipation ability, leading to high PFE and low stiffness. This underscores the impact of proper binder grade selection, especially for low-temperature cracking.

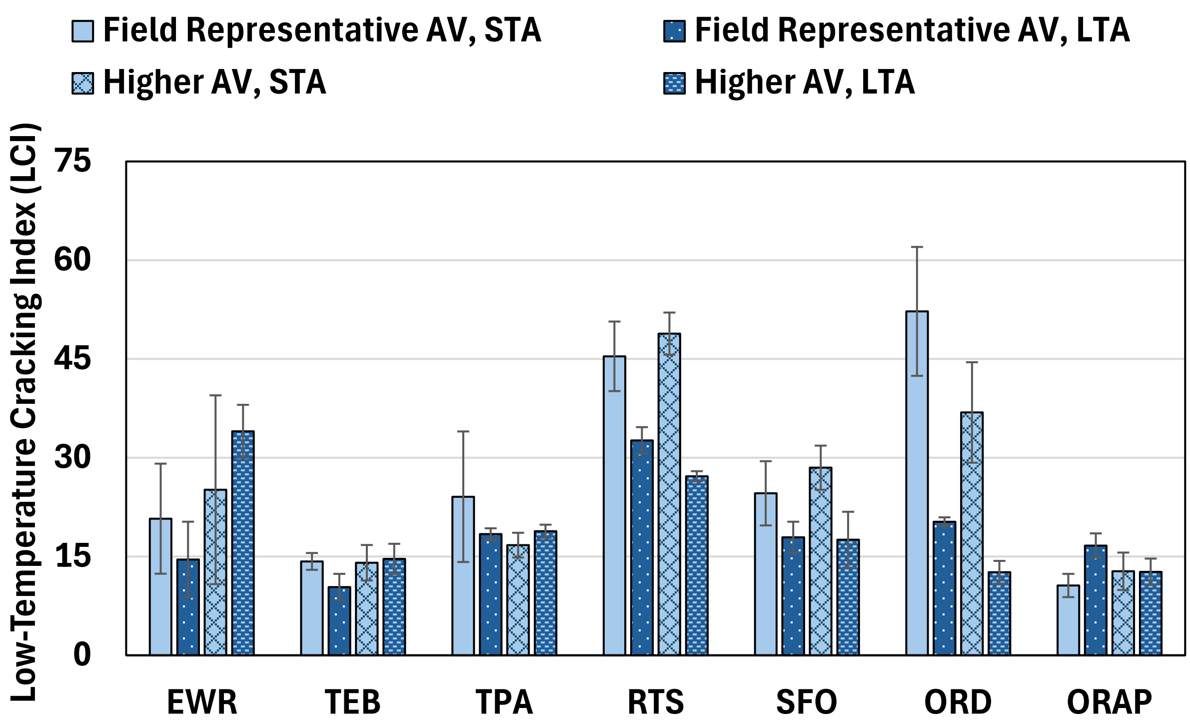

Source: AAPTP

Figure 14. LCI Values for LMLC Mixes at Various AV and Aging Levels

Mixes with higher AV showed statistically similar or slightly lower LCI values when compared with field-representative AV mixtures. The impact of AV on PFE or stiffness for either STA or LTA specimens was minimal, and other studies have demonstrated a similar limited impact of AV on low-temperature cracking (Li et al., 2008).

The SLT-SCB test is designed to evaluate crack initiation potential, which is the driving mechanism at low-temperature conditions where asphalt mixture behaves as a near-brittle elastic material. A marginal increase in AV in this case would have little or no influence on crack initiation mechanics in the asphalt mixture specimen. Crack propagation, especially in the viscoelastic domain, is influenced by AV increase to a greater degree and is discussed later in this report.

LTA for RTS and ORD led to a pronounced drop in LCI values for both field-representative and high-AV specimens. The drop was driven by a decrease in PFE due to a shift toward glassier and more brittle behavior post-aging, reducing the energy dissipation ability and strain tolerance of asphalt mixture before fracture. The stiffness increased after LTA for most mixes, which is typically associated with oxidative hardening and maltene loss (Petersen & Harnsberger, 1998). Overall, LCI values either decreased or remained unchanged after aging, consistent with expected trends for cracking potential at low temperatures.

LCI values were compared for LMLC and PMLC specimens at STA (field-representative AV and high-AV) and LTA (field-representative AV) to assess the robustness of the LCI parameter. The results show good agreement between PMLC and LMLC values, as illustrated in Figure 15. Higher differences were seen between RTS and ORD mixtures for PMLC versus LMLC. As seen previously, PGL −28 mixtures showed greater specimen variability even at low temperature. Further investigation indicated the ORD plant-loose mixture was likely overheated and not representative of the JMF, leading to excessive aging and a low PMLC LCI value. The RTS mixture was designed with PG 64-28 and tested at −12 °C (10 °F) in SLT-SCB. Therefore, the asphalt mixture retained some viscoelastic energy dissipation potential, and small differences in aging or relaxation capacity can significantly affect the observed fracture response.

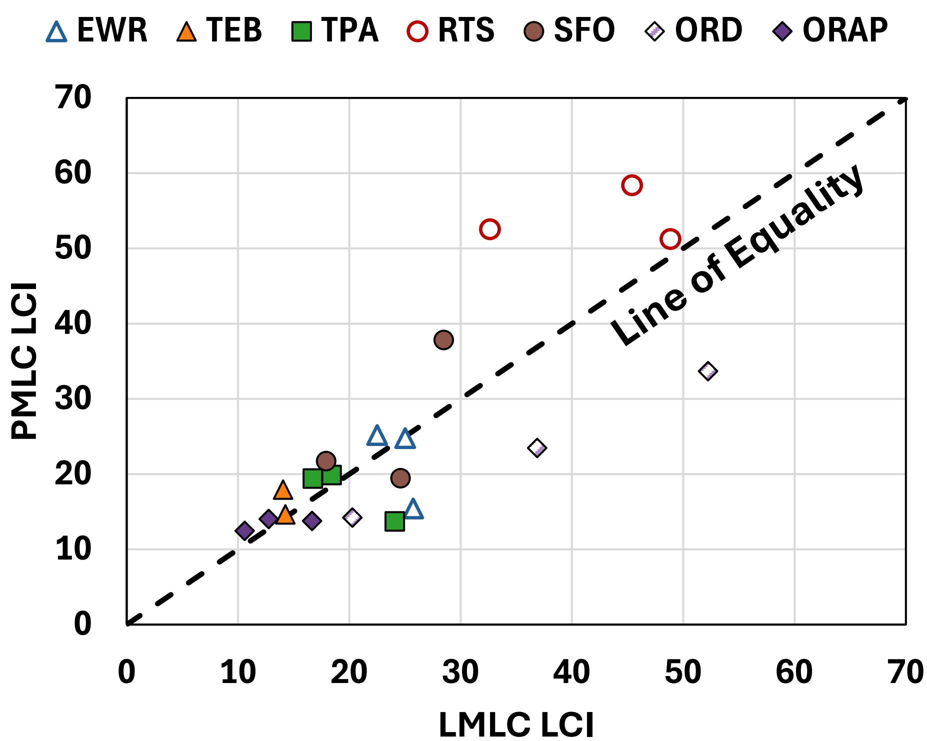

Source: AAPTP

Figure 15. LCI Values for LMLC and PMLC Mixes at Various AV and Aging Levels

LCI values from FC specimens are shown in Figure 16. The specimens from FAA test lanes were tested at −12 °C (10 °F), specimens from CMI were tested at −14 °C (7 °F), and specimens from MCI were tested at −18 °C (0 °F), in accordance with the aforementioned temperature-selection protocol. As expected, the LCI value of FC was lower than those of PMLC and LMLC specimens due to in-field aging. Accelerated loading of FAA test lanes led to cracking in Lanes 3 and 4 only. The cracks were believed to have initiated below the pavement surface during loading and propagated to the surface after the first winter cycle

(Alvarez et al., 2024). This increase in L3 and L4 cracking susceptibility can be seen in the lower values of LCI for the respective pavement mixtures. Greater variability of LCI for L6 was attributed to the presence of 4-percent latex and 20-percent RAP.

The two pavement sections from CMI (2004 and 2012) exhibited low LCI values, consistent with an increase in cracking potential for asphalt mixtures with aging. Before the recent reconstruction in 2024, both sections were noted to have medium-severity cracking, including longitudinal, transverse, alligator, and block types (Illinois DOT, n.d.). The MCI section, rehabilitated in 2022, showed a comparatively higher LCI value even when tested at −18 °C (0 °F), reflecting its satisfactory performance.

The two mixtures from the newly paved sections at CMI exhibited low LCI values after testing, and the load-LLD curves showed a high loading stiffness and early fracture. The cracking potential for the two mixes, characterized at service temperature (shown in Chapter 5), showed excellent resistance to cracking by both I-FIT and CT Index tests. The two paved mixtures were designed using a PG 70-22 binder, while the lowest annual temperature with 50-percent reliability, used for selection of testing temperature for SLT-SCB, was noted as −24 °C (−11 °F). In addition, the Airfield Asphalt Binder Selection Tool recently developed by the Airport Asphalt Pavement Technology Program also suggested the use of a PGL −28 binder (AAPTP, 2004). The LCI results suggest the use of an improper binder grade for the asphalt mixes, leading to tested specimens in a glassy, brittle state.

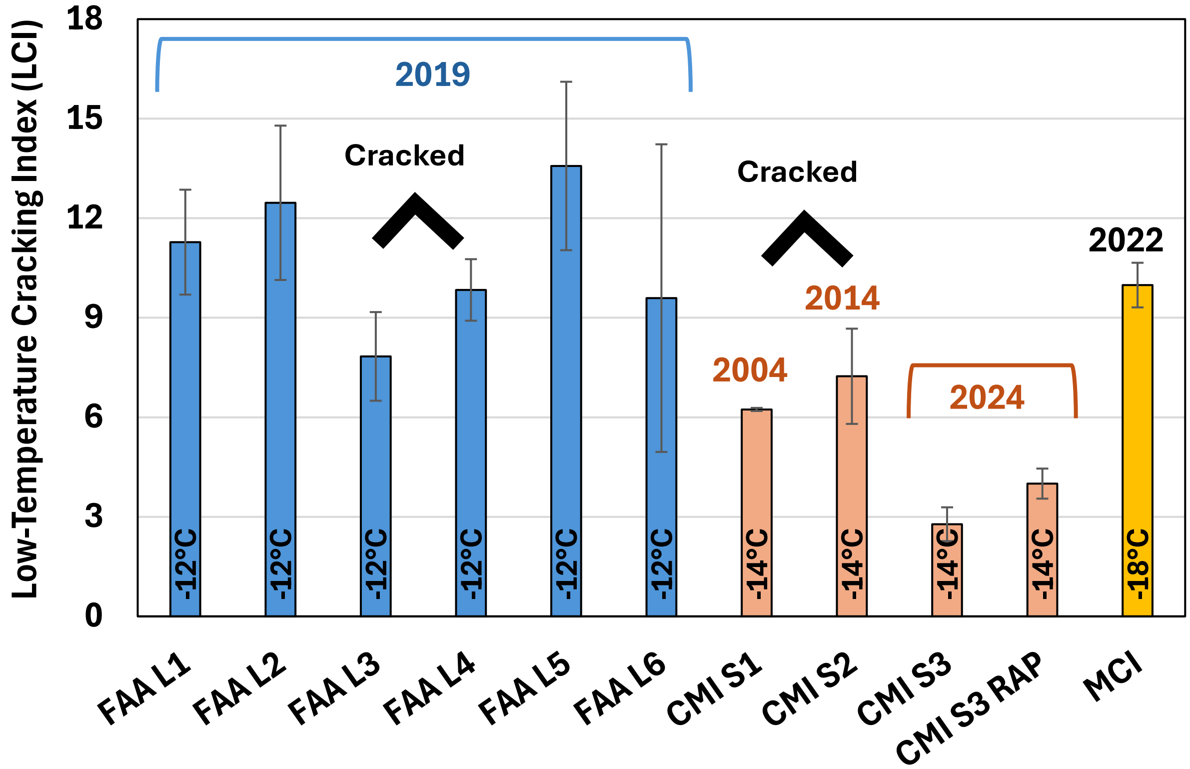

Source: AAPTP

Figure 16. LCI Values of Field Core Specimens

Overall, LCI value from the SLT-SCB test was able to discriminate asphalt mixtures with higher low-temperature cracking potential. An LCI threshold of 15 is recommended for LMLC specimens at field-representative AV, as shown in Figure 17. The threshold was selected to be used during design and QA processes; the LMLC and PMLC LCI values are statistically similar.

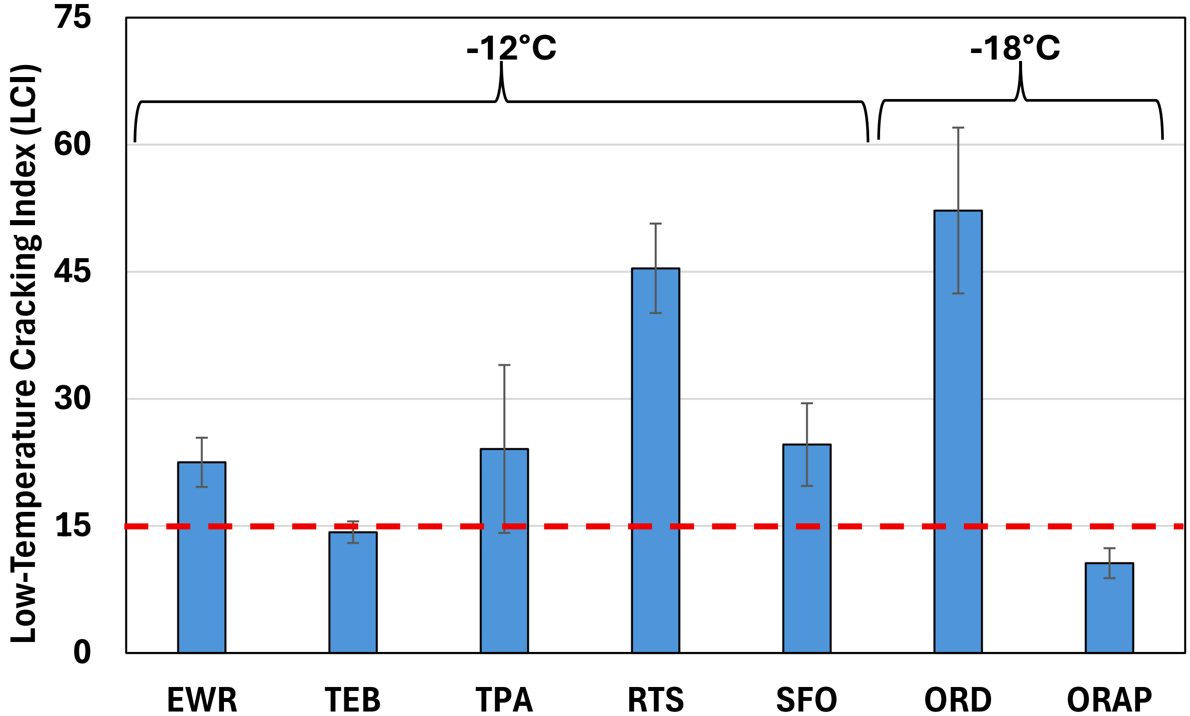

Source: AAPTP

Figure 17. Threshold for LCI for LMLC Specimens at Field-Representative AV

Summary

In summary, the project developed and validated the SLT-SCB. The study recommends changes to the original AASHTO T 394 specification to make it more adaptable for a BMD framework while retaining the use of fundamental material properties and comparing the cracking potential of asphalt mixtures. The major differences in the SLT-SCB and AASHTO T 394 are listed in Table 4. The modifications ensured that the test parameters measured crack initiation potential, which is a major mechanism of cracking at low temperatures.

The test results are used to calculate stiffness from the elastic portion of the loading curve and PFE. These two parameters are used to compute LCI. LCI comprises both the energy required for crack initiation and the resistance to deformation. The PGL played an important role in dictating the low-temperature cracking potential of asphalt mixtures.

Increasing test temperature from the PGL+10 °C would increase PFE due to load response moving from a glassy brittle to a viscoelastic region. The loading stiffness showed strong correlation with binder shear relaxation modulus and its slope. Minor changes in binder content and AV produced no significant changes in LCI if the test was done near the glassy region.

Table 4. Comparison of the SLT-SCB Protocol with AASHTO T 394

Test Aspect	AASHTO T 394	SLT-SCB Protocol
Control Type	CMOD	LLD
Loading Rate (mm/min)	0.003 (CMOD-controlled)	0.15 (LLD-controlled)
Specimen Thickness (mm)	24.7	50
Test Temperature Selection	Based on binder PGL	Based on a geographic location (LTPPBind tool)
Test Duration	~ 1 hr	~ 5 min

LCI was shown to be a robust parameter that can be used for both LMLC and PMLC specimens, effectively assessing the low-temperature cracking potential of the sampled asphalt mixtures. The ability of the LCI parameter to discern mixtures with high cracking potential at low temperatures was validated using FC from 10 different mixtures. An LCI threshold of 15 is suggested for asphalt mixtures placed in regions with known susceptibility to low-temperature cracking. However, further validation of the LCI threshold using additional mixtures is needed. Additional details for development of SLT-SCB can be found in Appendix E and elsewhere (Bajaj, Modi, et al., 2026; Modi et al., 2026).

Chapter 5. Service-Temperature Cracking

Due to the viscoelastic nature of asphalt binder, its inherent strength at service temperature is relatively low and, therefore, crack initiation may occur more readily. However, this may lead to greater potential for energy dissipation during loading, making crack propagation the dominant factor in determining pavement service life. The cracking potential at service temperature is traditionally measured using either a strength-based or a fracture-based test. For a BMD framework, having a simple monotonic loading test ensures practicality and ease of implementation for contractors and agencies.

Two of the most commonly used service-temperature cracking potential tests across the country are the I-FIT and the CT Index test (or Indirect Tensile Asphalt Cracking Test [IDEAL-CT]). While I-FIT has been shown to be fracture-based, CT is more of a strength-based test. The following sections detail the characterization of I-FIT and CT, concluding with recommended modifications to CT to make it a fracture-based test.

Illinois Flexibility Index Test

The I-FIT was performed in accordance with AASHTO T 393 protocols. A 50-mm (2-inch) thick disk was fabricated from a typical gyratory specimen and then cut into a semi-circular shape. A 15-mm (0.6-inch) long notch was introduced at the center of each specimen. The specimens were conditioned at 25 °C (77 °F) and then placed in the servo-hydraulic universal testing machine frame. A seating load of 0.1 kN (22.5 lb) was applied to ensure proper contact between the specimen and the loading fixture before testing. Thereafter, the specimen was loaded under LLD control at a rate of 50 mm/min (2 inches/min) until the measured load dropped to 0.1 kN (22.5 lb), at which point the test was terminated. The I-FIT specimen, test setup, and a typical load-LLD curve are shown in Figure 18.

(a)

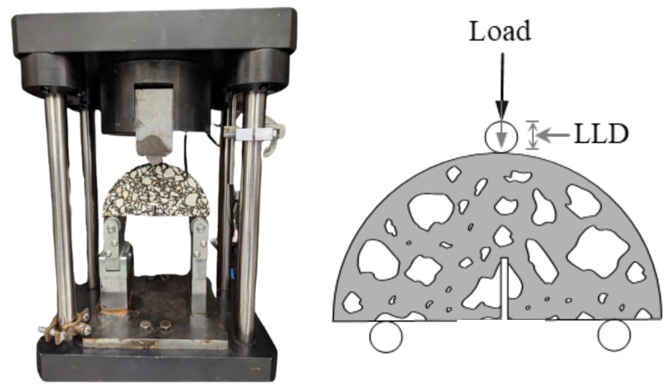

(b)

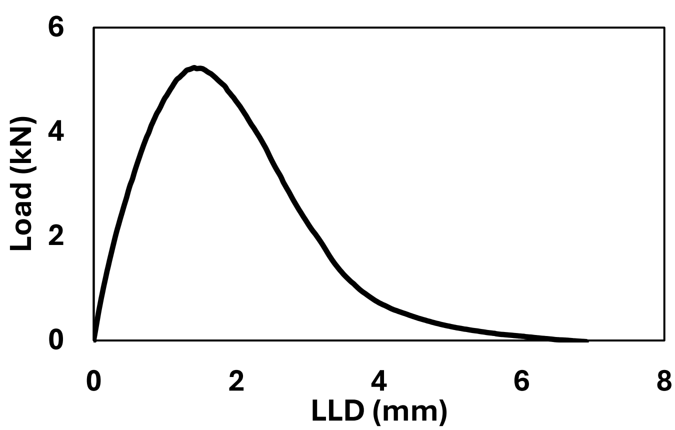

(c)

Source: AAPTP

Figure 18. I-FIT (a) Specimen, (b) Setup, and (c) Load-LLD Plot

The measured load versus LLD data were plotted and used to determine both the fracture energy and the post-peak slope. These parameters were then employed to calculate the Flexibility Index (FI) for each specimen. Higher FI values have been correlated with lower cracking potential for asphalt mixtures.

Asymmetrical Shear Loading

The I-FIT protocol specifies a centrally located notch to ensure pure Mode-I cracking. However, because airfield asphalt pavements regularly experience mixed-mode tension and shear stresses during operation, the research team investigated a simplified procedure to induce mixed-mode loading for assessing cracking potential. A 20-mm (0.8-inch) offset notch was evaluated using the same I-FIT protocol on PMLC specimens, as shown in Figure 19. The slight asymmetry introduced by the displaced notch was considered a potential means to induce shear stress during cracking.

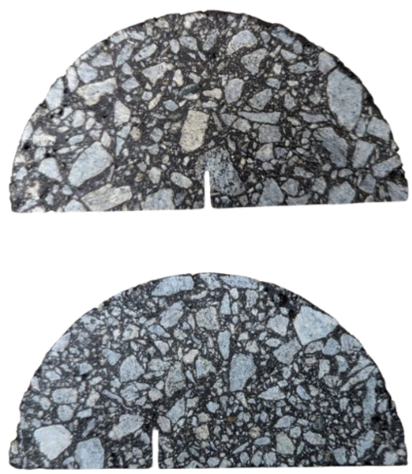

Source: AAPTP

Figure 19. I-FIT Specimen for Centered vs Offset Notch

In comparing the centered and displaced notch configurations, only fracture energy was considered for two reasons: (i) it was assumed that the displaced notch would affect only crack initiation while the crack-opening mechanism remained consistent and (ii) post-peak behavior is dependent on both specimen and notch geometry, hence, comparing the slopes for different notch configurations would not directly reflect differences in cracking potential.

As shown in Figure 20, the fracture energies for the two notch geometries exhibited minimal differences at room temperature. The error bars denote one standard deviation of fracture energy. The variability observed between most cases was within the range of variability among replicates of a given mixture. Moreover, the FPZ exhibited a similar shape around both notches, indicating that any changes in stress distribution at the notch tip due to displacement were masked by the effects of aggregate distribution and binder dissipation. Consequently, the displaced notch configuration was deemed unsuitable for mixed-mode testing and was not pursued further.

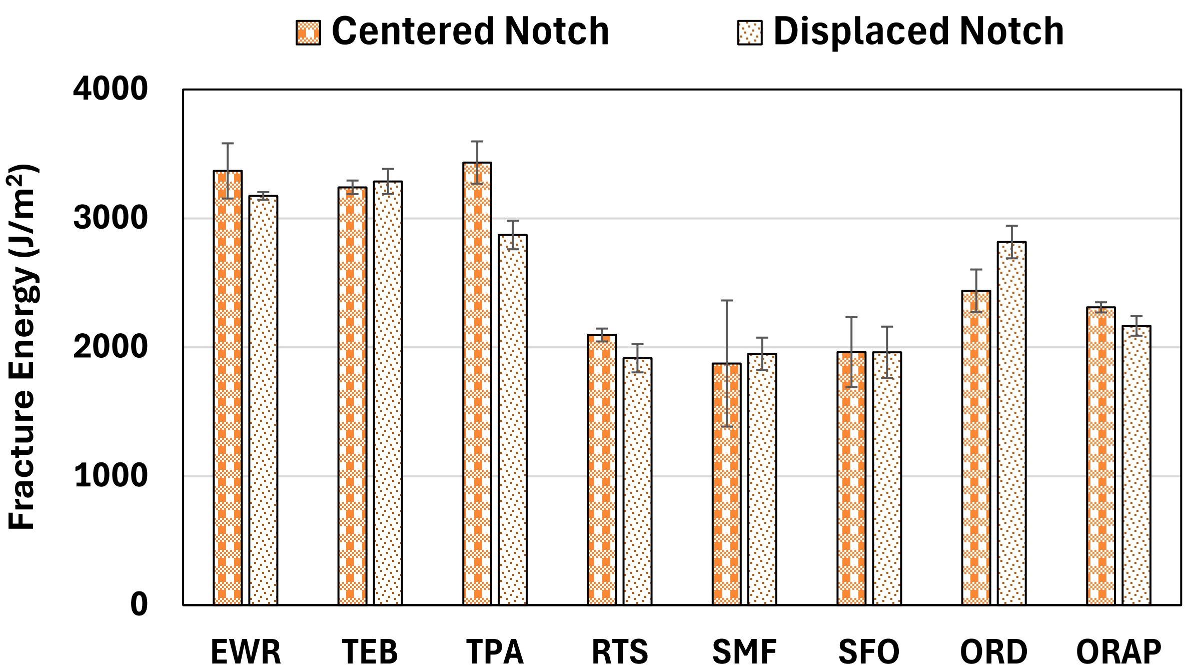

Source: AAPTP

Figure 20. Fracture Energy Results from Centered vs Displaced Notched PMLC Specimens

Results and Discussion

I-FIT results for PMLC specimens are presented in Figure 21. Testing was performed for two levels of AV: field representative (5 percent for P-401 and 3 percent for P-404) and higher (7 percent for P-401 and 5 percent for P-404). Additionally, LTA specimens were tested for field-representative AV PMLC samples. The lowest FI values were observed for SMF, EWR, and ORAP. The higher cracking potential for these mixtures was consistent with fatigue test results from the Texas Overlay Test (Appendix C). The EWR mixture was designed with a low binder content (4.49 percent) and correspondingly displayed a low FI value. ORAP was the only sampled mixture with 25-percent RAP and therefore a lower FI value was anticipated.

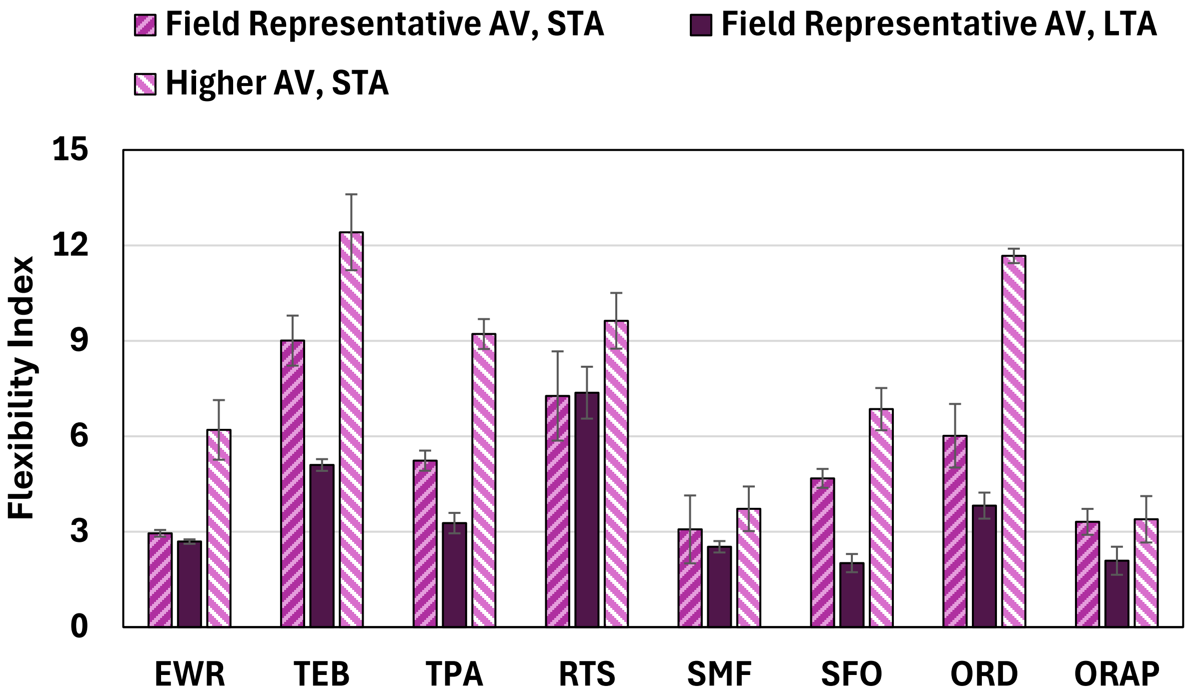

Source: AAPTP

Figure 21. I-FIT Results from PMLC Specimens

Similar tests at multiple AV and aging levels were performed for LMLC specimens, as shown in Figure 22. The largest difference between PMLC and LMLC occurred in the ORD mix, with FI values increasing from 6 to 20 for field-representative AV and 12 to 46 for higher AV specimens. Extraction and gradation did not show any significant difference in gradation between PMLC and LMLC, and the drop in FI is attributed to plant-loose mixture that was believed to have been overheated before sampling. Differences between PMLC and LMLC were also seen for low-temperature testing (chapter 4) and for CT Index testing in the subsequent section.

As expected, FI values decreased after LTA. An increase in AV was associated with higher FI values—a trend both observed in this study and noted in the literature for up to 10 percent AV. Airfield mixtures were designed for high strength and stability values, with all sampled specimens having a strength around or exceeding 550 kPa (80 psi). In addition, the cracking potential was influenced by the post-peak slope, an indicator of the crack speed and crack propagation potential. This slight skew toward high-strength mixtures is considered an artifact of having strict rutting potential controls for mixture designs with no protocols to assess the corresponding cracking susceptibility to date.

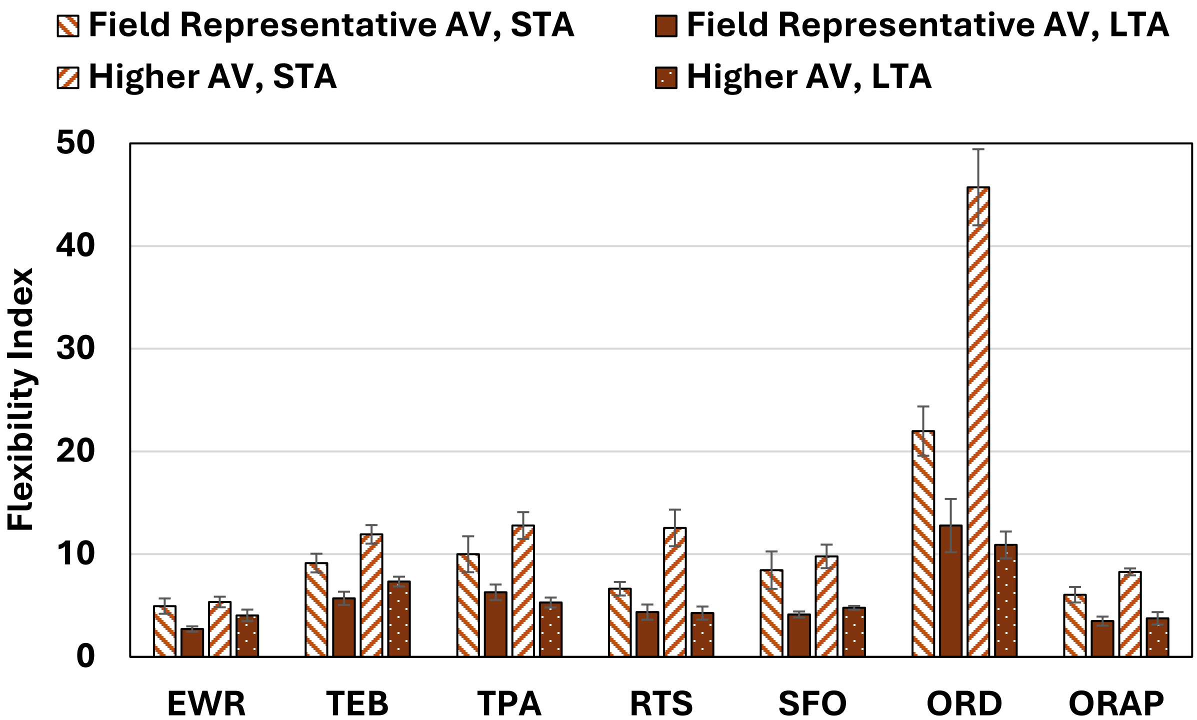

Source: AAPTP

Figure 22. I-FIT Results from LMLC Specimens

Threshold values were established using LTA LMLC and FC specimens. I-FIT was performed on top-lifts from collected FC, and the results are shown in Figure 23. The test successfully distinguished between test lanes that exhibited cracking and those with lower cracking potential. CMI section 1—placed in 2004—displayed a low FI value due to field aging and increased brittleness of the asphalt mixture. In contrast, the MCI core exhibited a high FI value, likely reflecting the recent construction of the section. An LTA threshold of FI=4 distinguished mixtures with higher cracking potential and the FC sections that exhibited cracking in the field.

Based on the LMLC FI values, LTA produced an approximate 40-percent reduction in FI. Using an LTA threshold of FI=4, a corresponding STA threshold of FI=7 is recommended for airfield mixtures. Figure 24 presents the STA LMLC FI values along with the proposed threshold of FI=7, which clearly identified the high cracking-potential mixtures (EWR and ORAP). The proposed STA and LTA thresholds are also consistent with thresholds adopted by the Illinois Department of Transportation for highway asphalt mixtures (STA FI=8; LTA FI=5) (Al-Qadi et al., 2017). Because highway performance testing is conducted at 7 percent AV—higher than recommended for airfields—a lower FI threshold for airfield mixtures is expected. The LTA protocol is intended for quality control during the design and is recommended primarily for screening and additive selection.

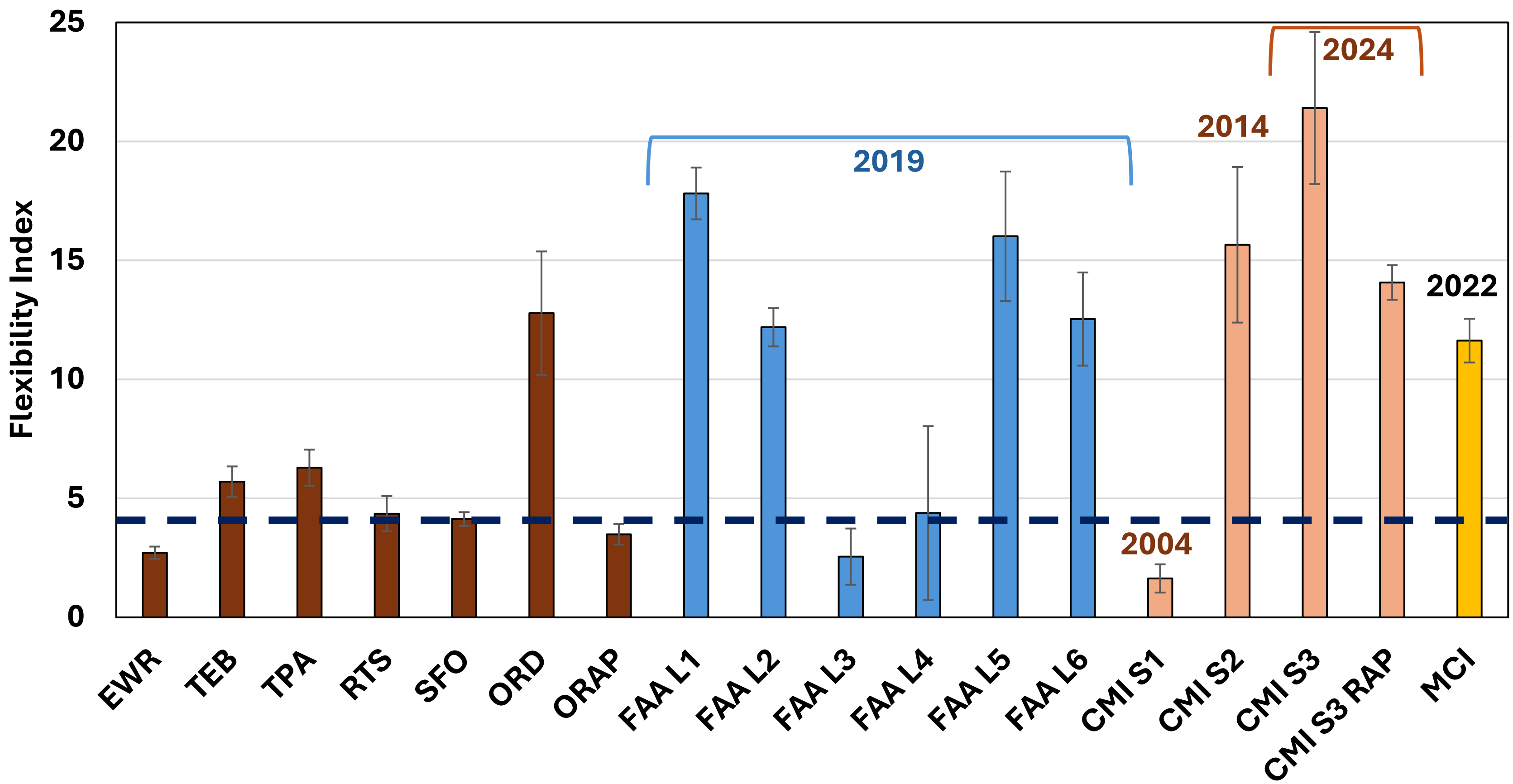

Source: AAPTP

Figure 23. FI Threshold for LTA LMLC and FC Specimens at Field-Representative AV

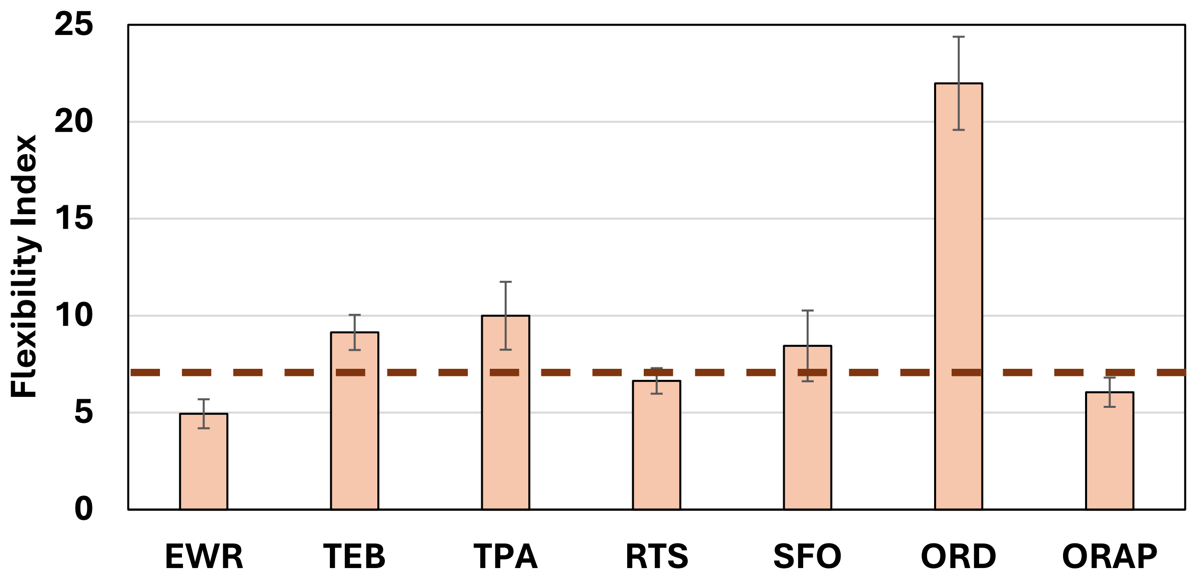

Source: AAPTP

Figure 24. FI Threshold for STA LMLC Specimens at Field-Representative AV

Cracking Tolerance Index Test

The CT Index test was performed in accordance with the protocols detailed in ASTM D8225. A 62-mm (2.5-inch) thick specimen was conditioned at 25 °C (77 °F) for 2 hr and then loaded in a servo-hydraulic universal testing machine load frame. The specimen was preloaded until a seating load of 0.1 kN (22.5 lb) was achieved. Subsequently, testing was conducted under LLD control at a rate of 50 mm/min (2 inches/min) until the measured load dropped to 0.1 kN (22.5 lb). The CT specimen, test setup, and a typical load-LLD curve are shown in Figure 25.

(a)

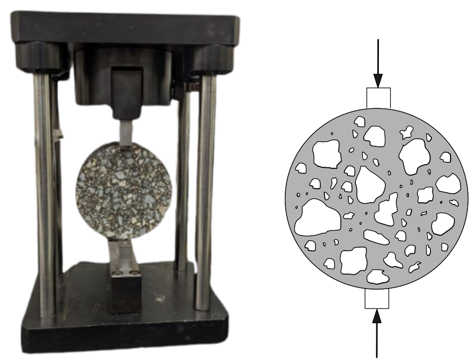

(b)

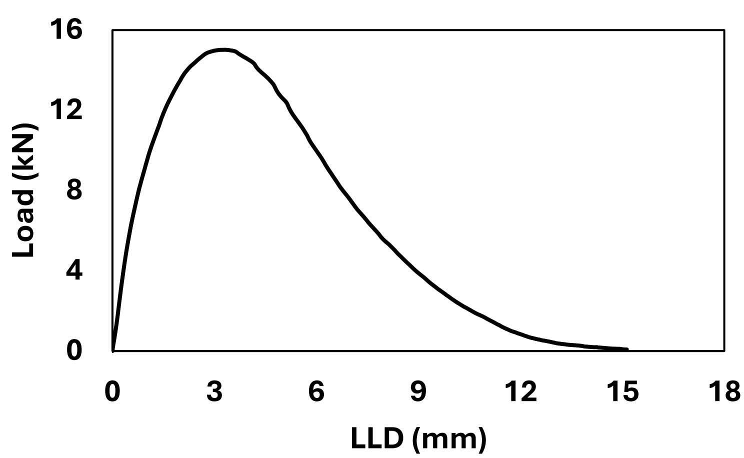

(c)

Source: AAPTP

Figure 25. CT Index Test (a) Specimen, (b) Setup, and (c) Load-LLD Plot

The measured load-LLD graph was used to determine the failure energy, the slope, and the displacement at the 75-percent drop point from peak load. These parameters, together with the specimen dimensions, were used to calculate the CT Index. A higher CT Index indicates lower cracking potential in asphalt mixtures.

Compacted vs Sawed Specimens

One of the benefits often attributed to the CT is its simple specimen-fabrication protocol, with no need for sawing or notching. Most highway agencies that have adopted CT specify that contractors mold the 62-mm (2.5-inch) disk directly at the recommended 7 percent AV. The research team evaluated the effect of using directly compacted CT disks versus specimens obtained by sawing for selected PMLC mixtures at 5 and 7 percent AV; the results are shown in Figure 26.

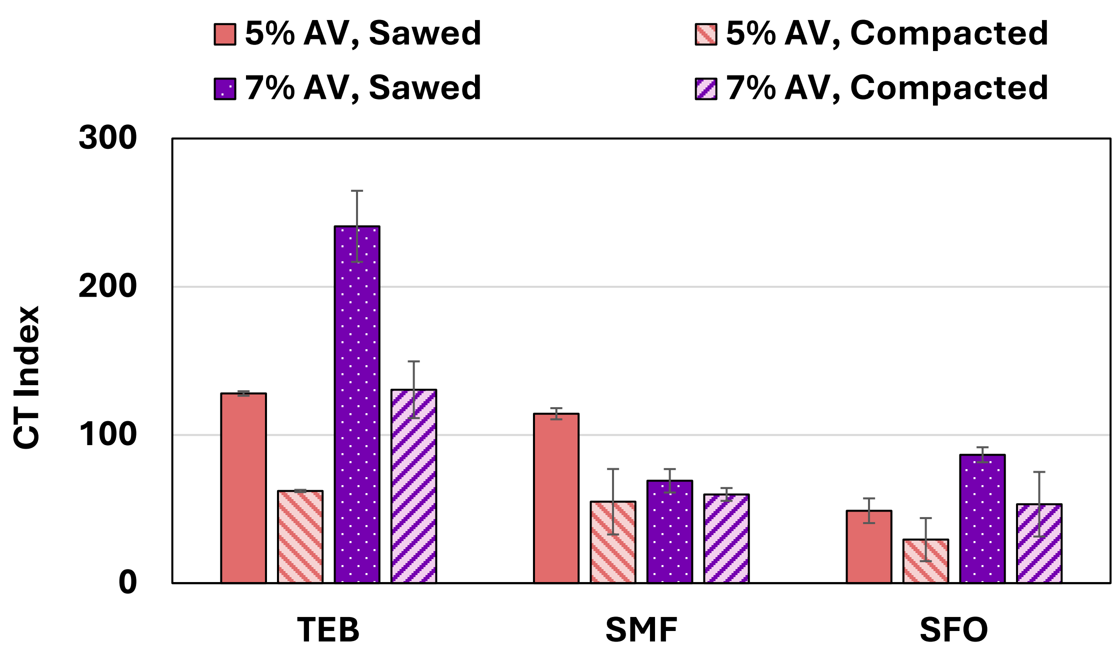

Source: AAPTP

Figure 26. CT Index Test Results for Sawed vs Directly Compacted PMLC Specimens

The CT Index for directly compacted specimens at both AV levels was nearly half that of specimens obtained by sawing from a 180-mm (7-inch) gyratory specimen. The higher number of gyrations—associated with the disk reaching a locking point—was apparent for all mixes, particularly at 5 percent AV. The relatively high gyration levels were believed to cause breakdown of the aggregate skeleton in airfield mixes, which are designed for tight packing and high strength. In addition, high gyration levels may increase microdamage in the binder matrix, thereby increasing the measured cracking potential of asphalt mixtures in cracking tests.

To validate the hypothesis that high gyration levels caused aggregate breakage, LMLC specimens for EWR and RTS were batched and mixed. Two specimens were compacted for each mixture and then extracted for aggregate recovery. EWR specimens required approximately 98 gyrations, whereas RTS required approximately 318 gyrations. Sieve analysis was performed on the batched aggregates prior to mixing and on the extracted aggregates after recovery. The results, illustrated in Figure 27, show evidence of aggregate breakdown, with an increased proportion observed in the smaller sieve sizes. Subsequent CT Index testing therefore used sawed specimens. The directly compacted specimens were not considered any further.

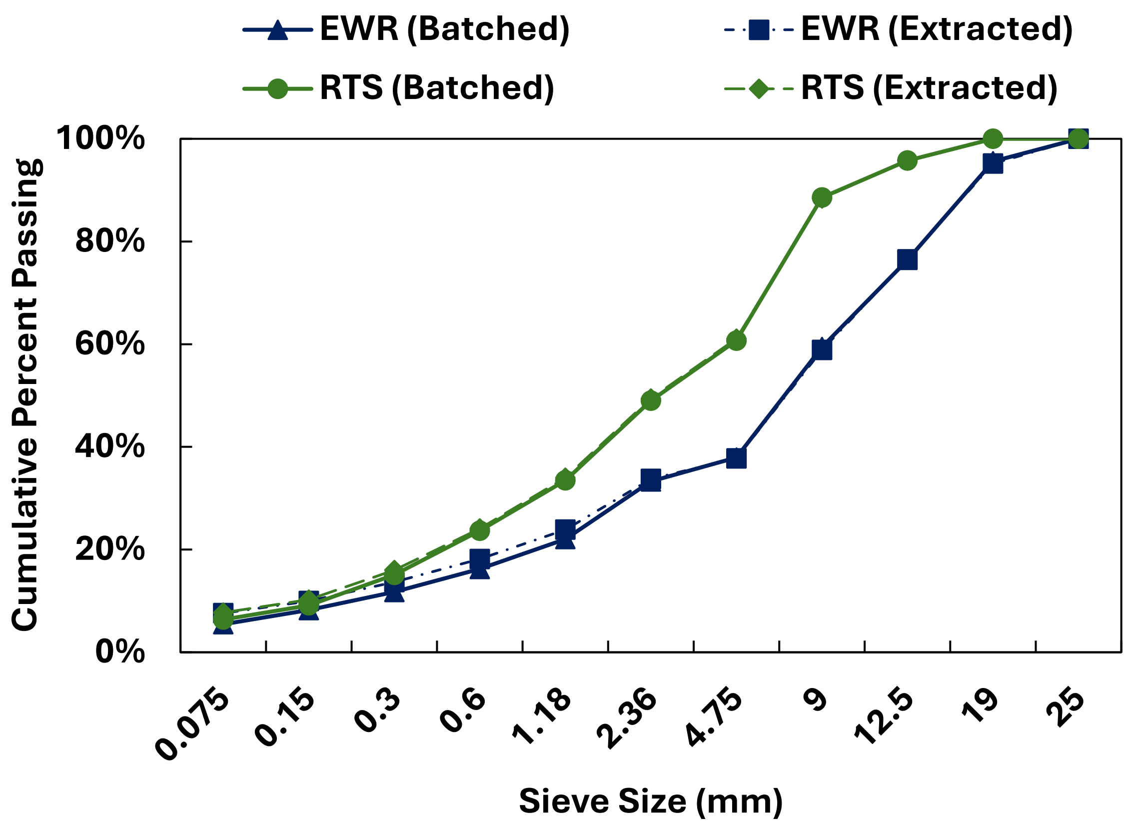

Source: AAPTP

Figure 27. Comparison of Disk-Compacted Aggregate Gradation Before and After Compaction for LMLC Mixes

Results and Discussion

PMLC specimens from the eight sampled asphalt mixtures were tested at both field-representative AV (3 percent for TPA and 5 percent for the rest) and higher AV (5 percent for TPA and 7 percent for the rest). Testing was also performed after LTA for mixtures at field-representative AV levels. Test results are presented in Figure 28.

PMLC mixtures with an NMAS of 19 mm (3/4 inch), namely ORAP, EWR, and SFO, had the lowest CT Index values. The CT Index values increased with increasing design VMA for the PMLC. EWR and SMF mixtures have been shown to be more susceptible to cracking in the fatigue domain (see Appendix C), where the loading conditions are more representative of field. The low CT Index value for ORAP could be attributed to the use of 25-percent RAP in the mixture production. CT Index values increased for all PMLC with increasing AV, except for SMF. The increase was more pronounced for mixtures with granitic aggregates (77–112 percent) as compared to mixtures with much softer limestone or shale aggregates (26–39 percent). These observations suggest that the aggregate skeleton influences the CT Index values significantly.

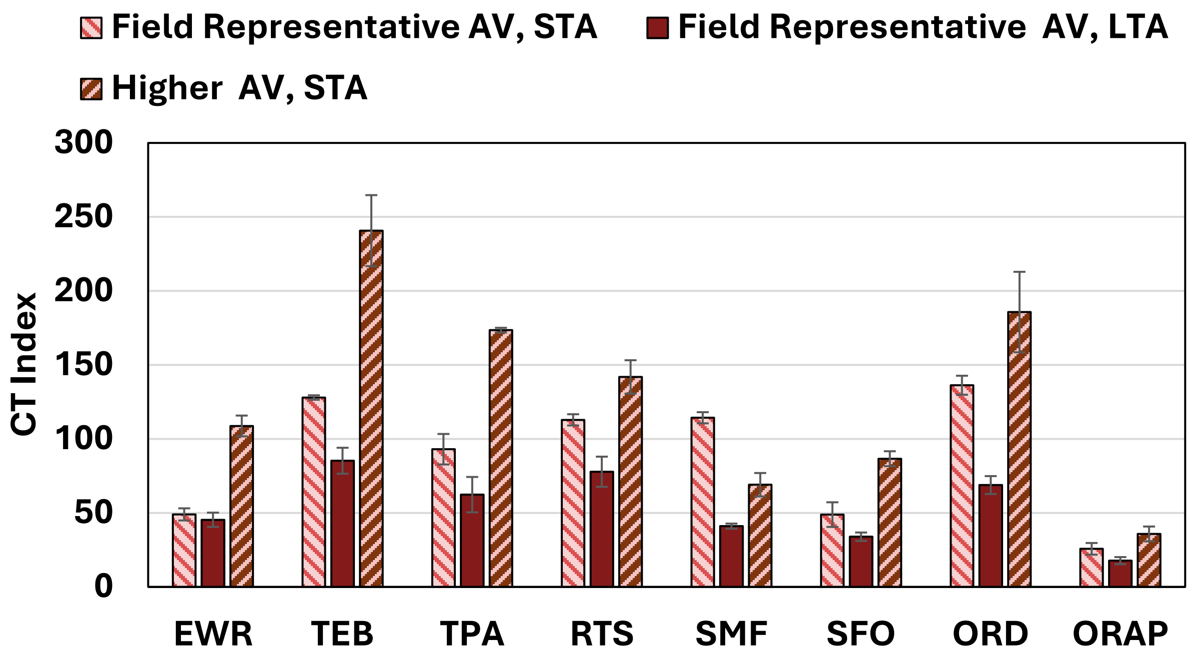

Source: AAPTP

Figure 28. CT Index Test Results for PMLC Mixes

Test results for LMLC specimens for STA at field-representative AV levels were compared with PMLC specimens in Figure 29. For I-FIT, as would be expected, the PMLC specimens had statistically similar or slightly lower FI values compared to LMLC specimens. The only exception was ORD, as explained above. For CT, the trend was not clear, with some mixtures having higher CT Index values for PMLC than LMLC.

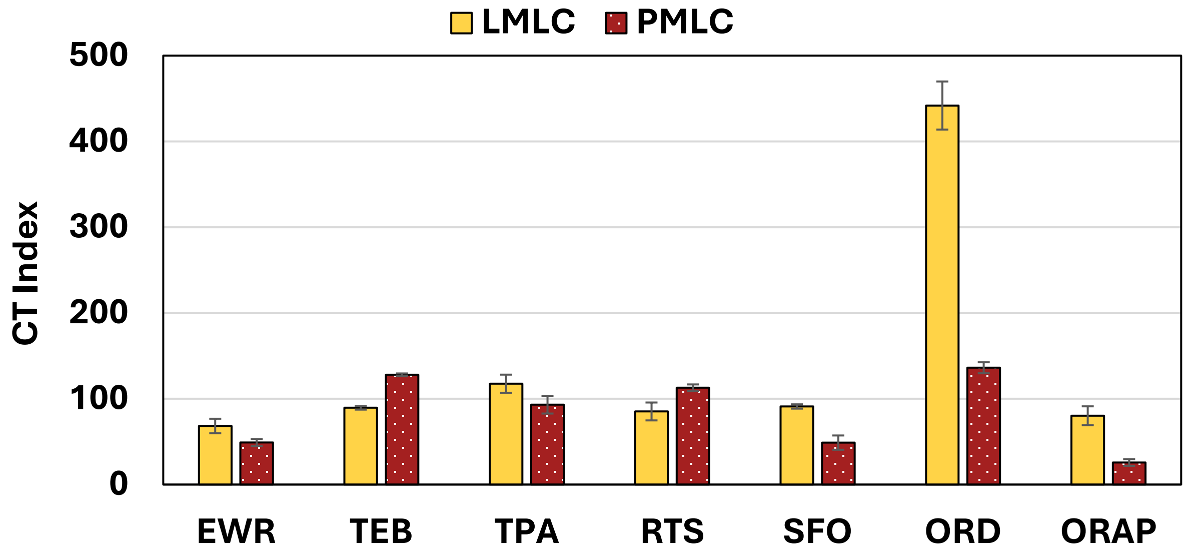

Source: AAPTP

Figure 29. CT Index Test Results for LMLC vs PMLC Mixes

The CT Index results for FC, along with LTA PMLC specimens, are plotted in Figure 30. Cores collected from CMI S1, CMI S2, and MCI did not have sufficient 62-mm (2.5-inch) thickness to be tested. Test results were able to identify test lane 3 as being susceptible to cracking, however, test lane 4, which also exhibited cracking after the accelerated loading, had a similar CT Index as other lanes that performed well. Additionally, the difference between the CT Index values for the PMLC and the FAA test lanes makes the use of a threshold value impossible. Therefore, it was determined the CT Index test was unsuitable for differentiating cracking potential among mixtures.

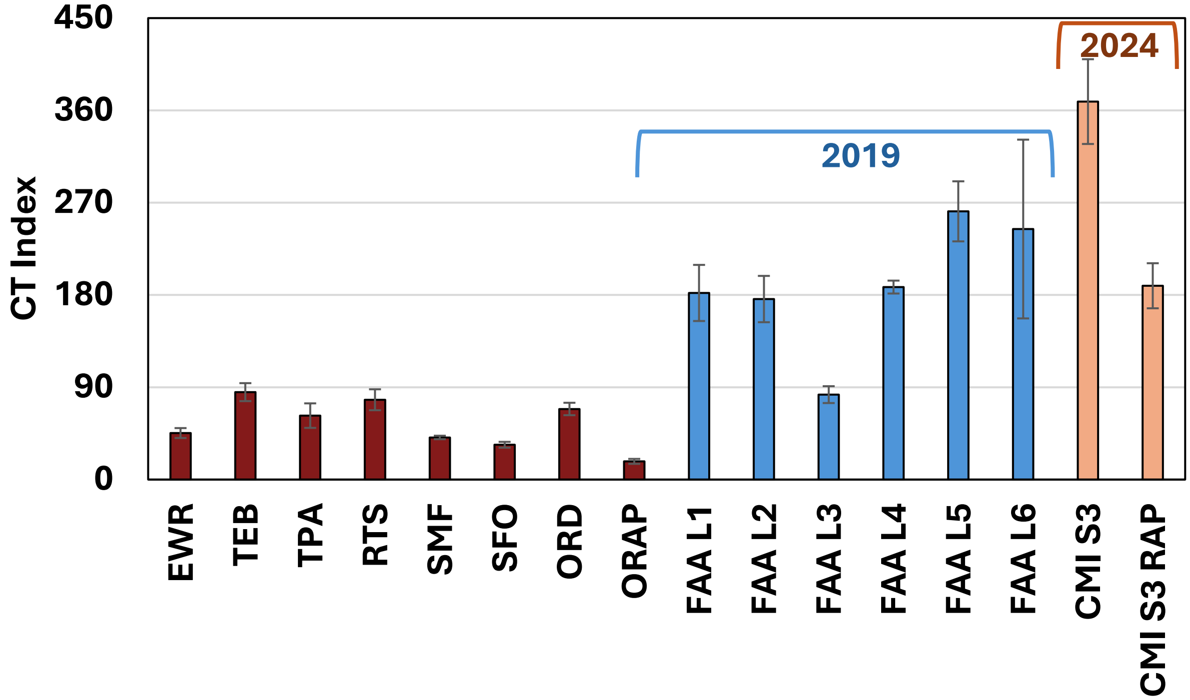

Source: AAPTP

Figure 30. CT Index Test Results from LTA PMLC and FC

Cored Brazil Disc Test or DONUT

The CT Index test was adapted from the low-temperature indirect tensile test (AASHTO T 322, 2007), in which the diametrical compressive loading induces high tensile stresses near the center core of the specimen when the material response is predominantly brittle-elastic. When testing is performed in a visco-elastoplastic regime, representative of asphalt pavement at service temperature, the cracking mechanism shifts from primarily tensile cracking at the center core of the specimen to a complex stress state influenced by localized inelastic deformation.

Additionally, the tested specimens exhibited significant plastic deformation and bulk energy dissipation during loading. As observed by Al-Qadi et al. (2022), this response suggests that the measured energy input cannot be solely attributed to crack formation and propagation. Digital image correlation indicated pronounced compressive strains beneath the loading strip, consistent with local yielding. Crack initiation subsequently occurred due to tensile separation developing near the specimen perimeter rather than as the intended dominant crack initiating at the center.

The research team, with input from the panel, recommended updating the current CT Index test to address these limitations and make the response more fracture dominated, while maintaining its simplicity and cost efficiency. A two-step modification to the test protocols is recommended:

1. Core a central, circular hole in the asphalt mixture specimen using a 25.5-mm (1-inch) core drill.
2. Increase the loading-strip thickness from 20 mm (0.79 inch) to 30 mm (1.18 inches).

Analytical solutions for circular holes in elastic materials were developed by Kirsch (1898). These solutions highlight tensile stress concentration around the core in the direction of loading. Figure 31 compares crack initiation in the conventional CT Index test and the modified cored Brazil disc using digital image correlation (DIC). In the cored Brazil disc, named the Disc with O-Notch for Uniaxial Testing (DONUT), crack initiation occurred at the cored hole rather than beneath the loading edges, as is typically observed in the CT Index test. Four symmetrical crack fronts were observed to develop during crack initiation.

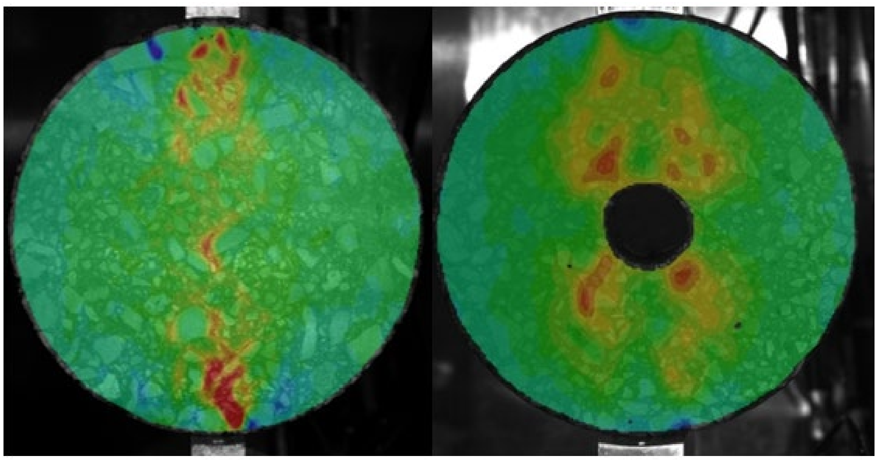

Source: AAPTP

Figure 31. DIC Images of Crack Initiation for the CT Index (Left) and the DONUT (Right) Tests

Load-LLD curves obtained from the DONUT test for LMLC specimens are shown in Figure 32. Four replicates of each asphalt mixture were tested, and repeatability was relatively high compared to those determined from CT and I-FIT. This improved repeatability is attributed to the use of a circular hole in the middle of the specimen instead of a sharp notch. Combined with the longer ligament length, this geometry promotes more consistent cracking behavior among replicates. In addition, unlike a sharp notch, a circular hole does not predefine a single crack initiation location or crack path. With reduced stress concentration, crack initiation is more gradual in the test specimen and can deviate around aggregate if present at the crack-initiation location. This provides greater freedom for the aggregate skeleton and local heterogeneity to govern where damage localizes and cracking initiates.

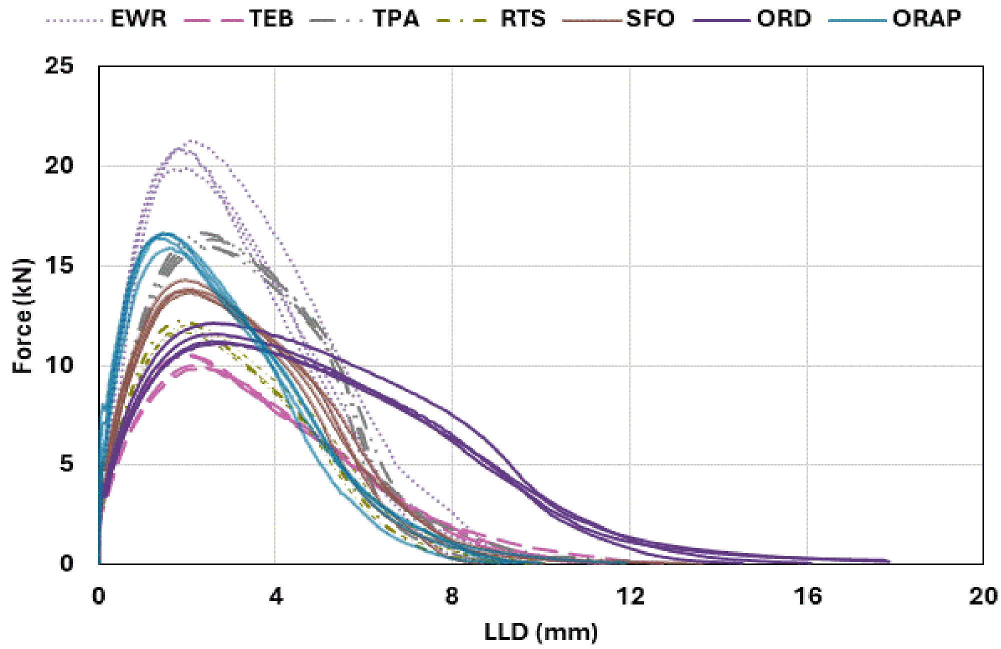

Source: AAPTP

Figure 32. Load-LLD Curves from DONUT for LMLC Specimens

Test Fracture Characteristics

The area under the load-LLD curve is the work of fracture. Fracture energy (G_f) is calculated by dividing the work of fracture by the crack ligament area. PMLC specimens for select asphalt mixture designs were tested at thicknesses of 50 mm, 62 mm, and 75 mm using this geometry. The selected values were chosen due to the commonly used geometry in laboratory testing of asphalt mixtures. The results, shown in Figure 33, indicate that G_f was essentially independent of specimen thickness over the range evaluated, supporting its use as a fundamental mixture property for this test configuration.

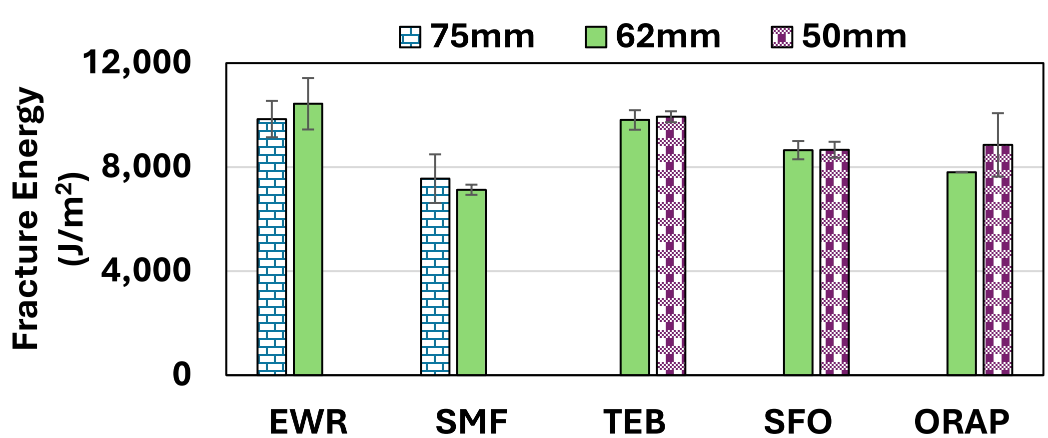

Source: AAPTP

Figure 33. Fracture Energy Values for PMLC Specimens of Multiple Thicknesses

Earlier research has shown that G_f is not sufficient to characterize cracking potential (Al-Qadi et al., 2015) because it reflects both peak load and post-peak ductility. Therefore, a crack propagation term is needed to normalize the energy component and improve the sensitivity to brittle, fast-propagating cracking behavior. The post-peak slope, m, from I-FIT was developed as a crack speed proxy (Ozer et al., 2016). However, the post-peak slope in I-FIT is mathematically complex, and the change in crack propagation rate may not be as clear in the DONUT test.

LMLC specimens were tested at multiple AV levels and aging conditions, and several metrics derived from the load–LLD response were compared with the post-peak slope obtained from the corresponding I-FIT results. The secant slope is defined as the slope between the peak load and the post-peak load at 75 percent of the peak value, S_{75}. This parameter exhibited the strongest correlation with the I-FIT post-peak slope, as shown in Figure 34.

A DONUT index (DI) was developed using G_f and S_{75} as shown below.

$$DI = \frac{G_f}{|S_{75}|} \times A$$

The value of the correction factor (A) was chosen as 0.001 to scale the index down to the same range as that of FI. More information regarding the development of the DONUT can be found in Bajaj et al. (2026).

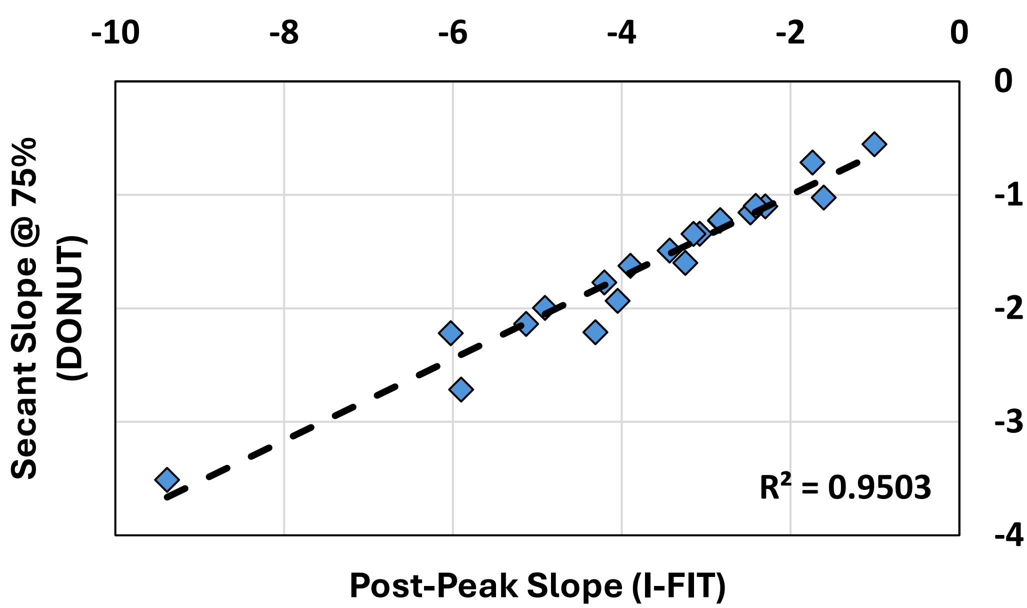

Source: AAPTP

Figure 34. Secant Slope from DONUT vs Post-Peak Slope from I-FIT

Results and Discussion

The influence of asphalt binder type and binder content on the proposed cracking potential index was evaluated. For the binder type study, XCM specimens were fabricated using the SFO aggregate gradation with different binder types. The DI values for the XCM specimens are shown in Figure 35. The lowest DI values were observed for the 64-22 binder (the only unmodified binder) and the 70-10 binder, which has been shown to have high cracking potential in the field. In general, DI increased with polymer modification; however, binders with softeners and relatively low PGL exhibited the highest DI values. Both the 64-28 and 76-28 binders are softener-modified and, therefore, exhibit lower susceptibility to cracking.

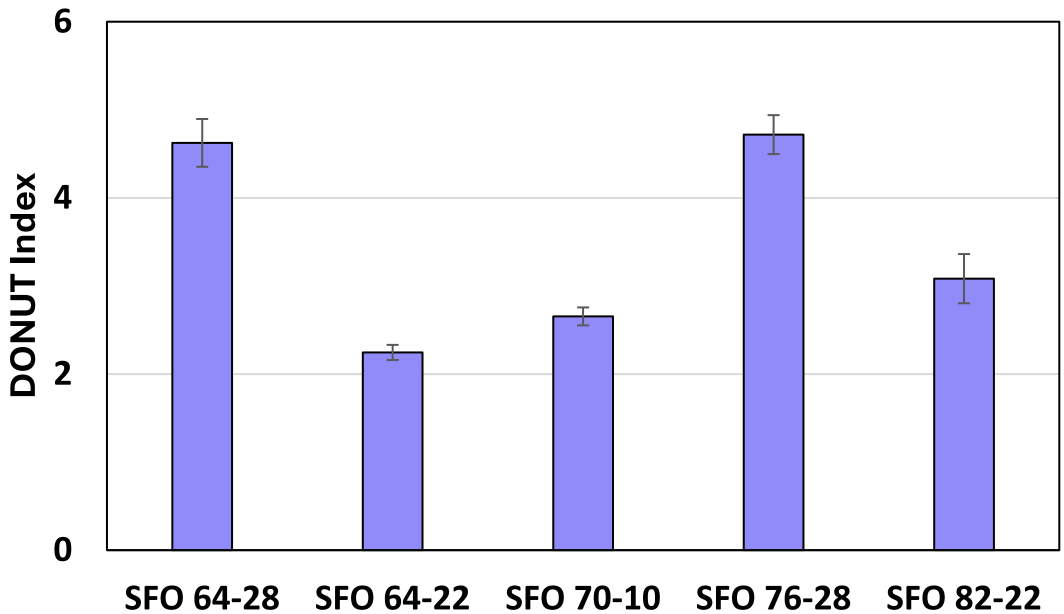

Source: AAPTP

Figure 35. DI Values of XCM Specimens for Different Binder Types

The effect of binder content was evaluated for a ductile mixture (ORD) and a brittle mixture (ORAP). LMLC specimens were prepared at the OBC, as well as at OBC ±0.5 percent and ±1.0 percent. This evaluation was conducted to confirm that DI is sensitive to binder-content variability that may occur during paving. Figure 36 illustrates that DI is highly sensitive to binder content. As expected, DI reduced as binder content decreased.

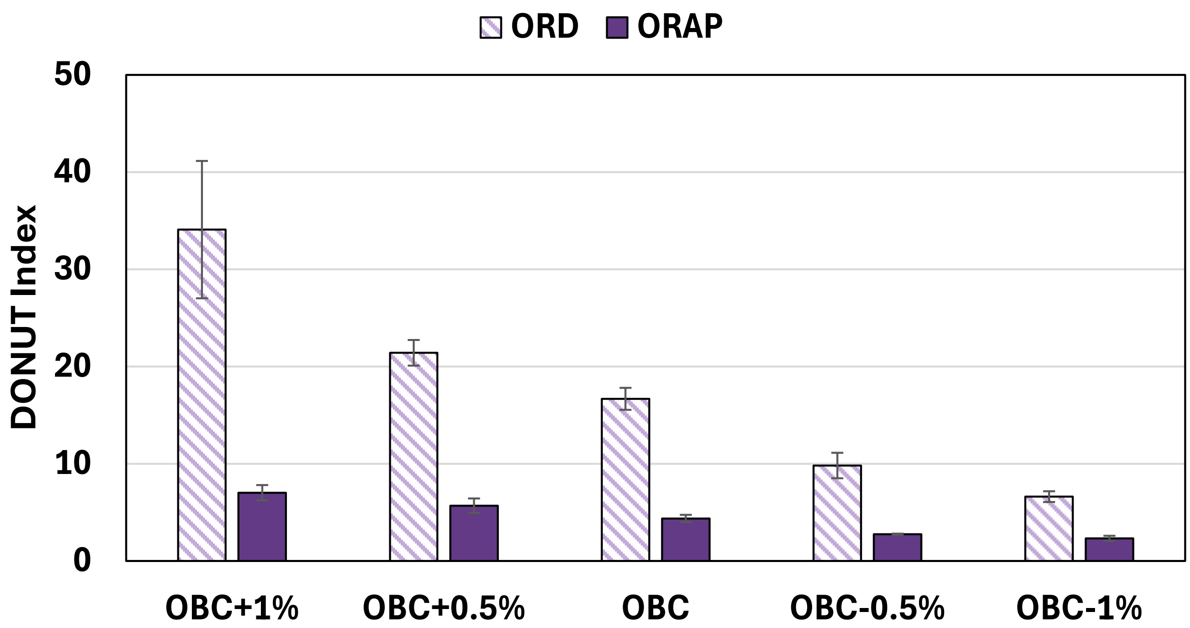

Source: AAPTP

Figure 36. DI Values for LMLC Specimens at Various Binder Content

The LMLC specimens were tested for sampled mixtures at multiple AV levels and aging conditions, with the results shown in Figure 37. As expected, DI increased with an increase in AV for most mixtures and decreased with aging of specimens.

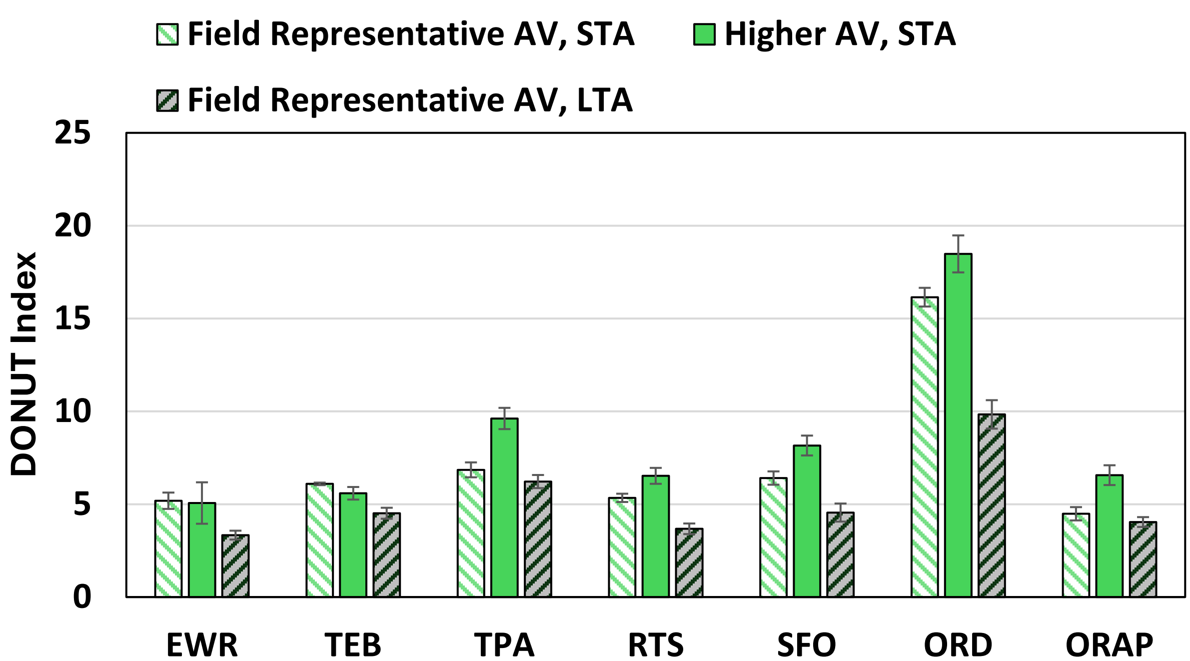

Source: AAPTP

Figure 37. DI Values for LMLC Specimens

The correlation between DI from the DONUT and FI from the I-FIT is presented in Figure 38. The values followed a linear trend except for one outlier with an FI value of 48. After removing the outlier, a linear trendline with an R^2 of 0.87 was obtained, indicating strong correlation between FI and DI values.

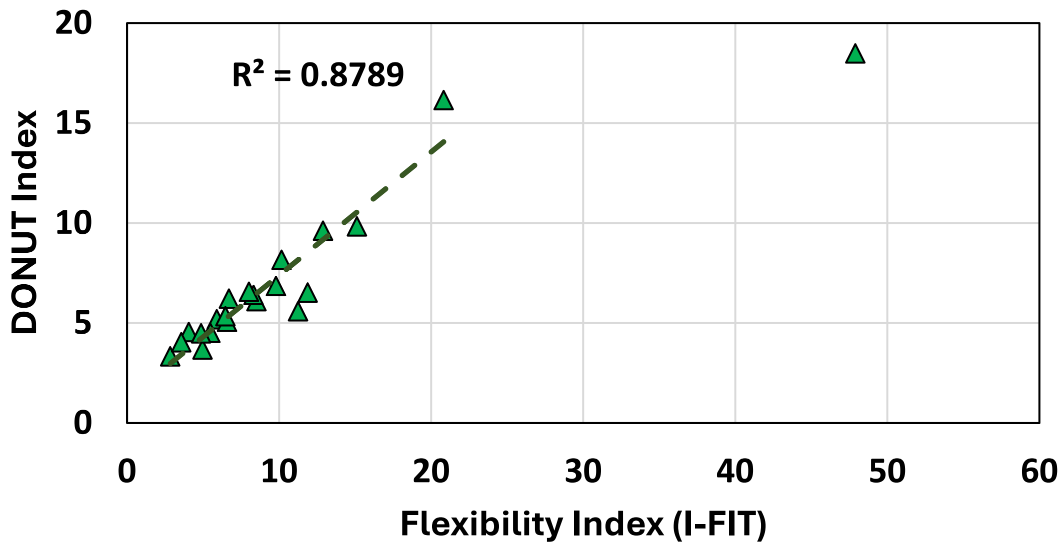

Source: AAPTP

Figure 38. DI vs FI Value for LMLC Specimens

Final validation of the DONUT was done using the FAA test lane FC. DI results for the six test lanes are shown in Figure 39. The DI successfully distinguished the two test lanes, lane 3 and 4, which exhibited cracking after accelerated pavement testing loading.

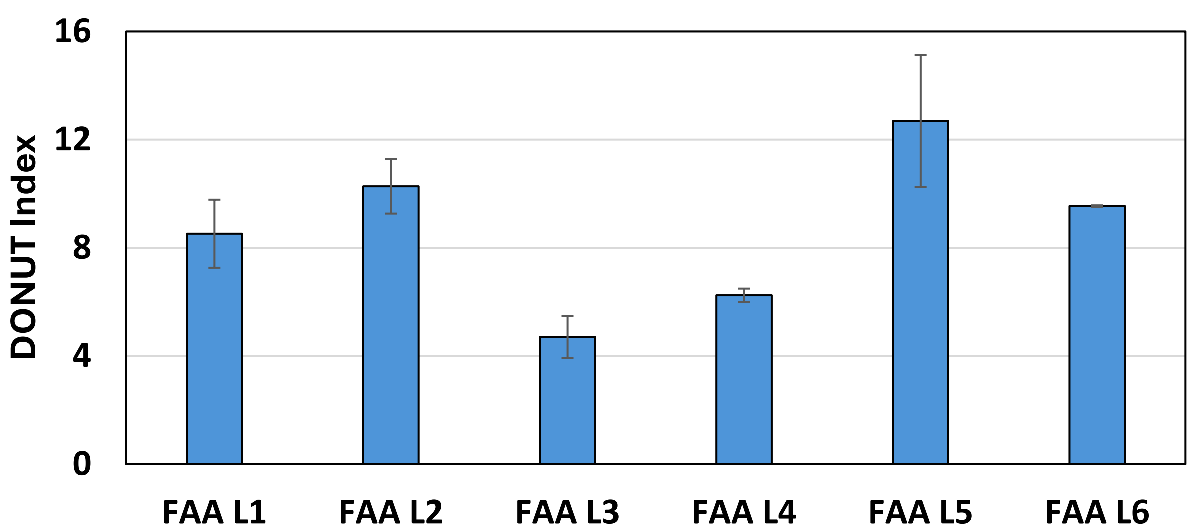

Source: AAPTP

Figure 39. DI Values for FAA Test Lane FC

In general, the results validate the use of DI as an index for asphalt mixture cracking potential at service temperature. A threshold of DI=6 is proposed for LMLC specimens at field-representative AV as shown in Figure 40. EWR and ORAP showed the lowest values, and their high cracking potential was observed in other tests.

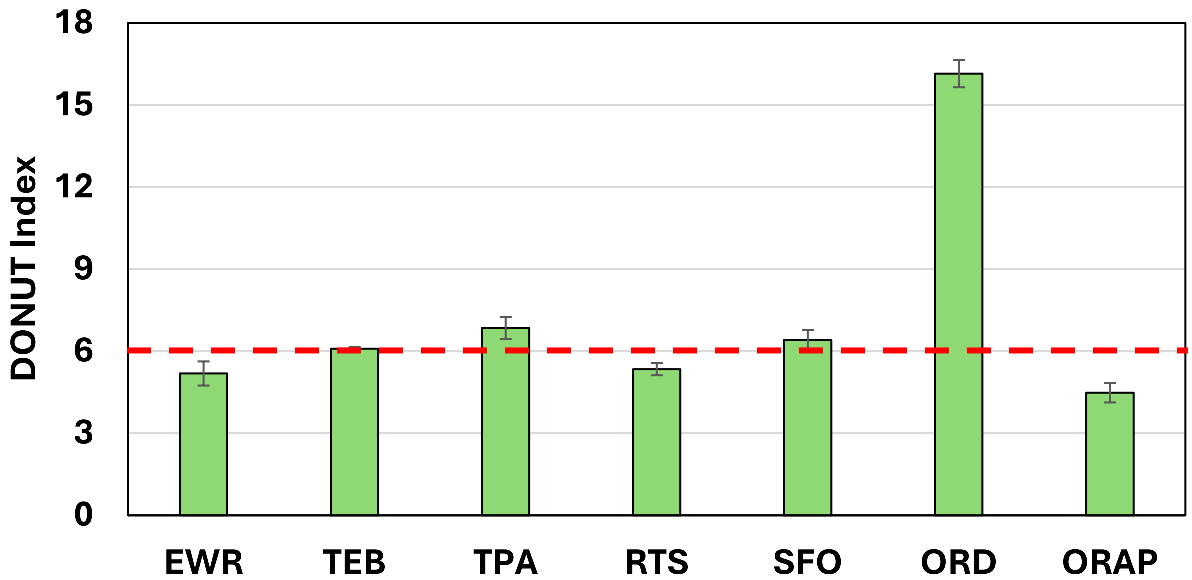

Source: AAPTP

Figure 40. DI Threshold for LMLC Specimens at Field-Representative AV

Summary

This project used I-FIT, a fracture-based test, and CT Index, a strength-based test, to evaluate the cracking potential of sampled asphalt mixtures. I-FIT employs an indirect bending mechanism to induce cracking. The introduction of a notch directs the stress distribution toward the notch tip, resulting in a localized stress concentration that facilitates crack initiation and subsequent propagation. The measured FI primarily characterizes crack propagation, as it is significantly influenced by the post-peak slope behavior. Meanwhile, the CT Index test is an indirect tension test that was developed to result in tension at the core center of a specimen when loaded. However, as the load increases, stress within the specimen is primarily distributed through the aggregate skeleton. The modulus mismatch between the stiff aggregates and the more compliant asphalt binder results in localized stress concentrations around the aggregates and beneath the loading strip because of an undirected cracking path.

Test results from FC with known performance have demonstrated that I-FIT correlates well with actual in-field cracking behavior. However, the CT Index test failed to detect the higher cracking potential observed in FAA test lane 4 and for the SMF mixture. A threshold of FI=7 was proposed for specimens at field-representative AV levels. Because the CT Index test benefits from a simple specimen fabrication process, as used by highway agencies, a simple two-step modification to existing protocols is recommended to transform the test from strength-based to fracture-based. A central core in the disc specimen, along with thicker loading strips, allowed stresses to concentrate near the middle of the specimen. The new test is called DONUT.

The DONUT geometry lends itself to a highly repeatable test, making it ideal for asphalt mixture design as well as QA/QC. The fracture energy obtained was normalized with the secant slope, which was shown to correlate strongly with the post-peak slope from I-FIT. A DI was developed as a simple metric to assess cracking potential. The metric was tested for different binder types and contents and validated with FC with known performance. A DI threshold is proposed.

Using softer or more compliant binders enhances resistance to crack propagation when the aggregate skeleton remains unchanged. AVs act as energy-release centers and can blunt the crack tip, slowing down crack growth. Hence, an increase in AV, up to a certain limit, would further increase binder matrix compliance, thereby increasing the FI and DI.

Chapter 6. Conclusions and Recommendations

Summary

The interest in using performance-based airfield asphalt mixture design has been gaining traction in recent years due to multiple factors: (i) the use of novel material components, (ii) increasing gear loads and tire pressure, and (iii) high torque and complex gear configurations. In addition, the limitations of the traditional volumetrics approach necessitate the exploration of adapting mechanistic performance metrics to correlate asphalt mixture parameters with potential field performance.

This study was conducted to investigate asphalt cracking behavior and recommend fundamental and practical performance-based protocols to predict the cracking potential of airfield asphalt mixes. The outcome of this study, including cracking test protocols, is recommended for inclusion in FAA AC 150/5370-10, Part 6—Flexible Pavements for both laboratory asphalt mixture design and QA/QC stages.

In this study, a broad set of materials were sampled from across the United States to ensure field applicability across various climates, binder sources and types, aggregate gradations and lithologies, asphalt mixture design, and construction practices. Aggregates, binder, and loose plant mixtures were obtained from seven major airports (EWR, TEB, TPA, RTS, SMF, SFO, and ORD) and FC were obtained from two additional airports (MCI, CMI), along with FC with known field performance from the NAPMRC test lanes. In addition to testing FC, tests were performed on PMLC and LMLC specimens.

The asphalt mixture cracking potential was assessed in two key domains: (i) low-temperature cracking potential, where crack initiation is considered critical, and (ii) service-temperature cracking potential, which is dominated by crack propagation. Current test protocols were explored for use, with consideration given to specimen geometry, loading mode, test temperature, and scientific basis, among other factors. Development of new tests and/or modification of existing test standards were considered. Emphasis was placed on tests that balance fundamental mechanics with practicality and ease of implementation for construction projects.

For low temperatures, the study evaluated the existing DCT and low temperature SCB tests. The SCB test was modified to develop the SLT-SCB test. The SLT-SCB protocol is practical and easy to incorporate in a BMD framework, while maintaining its ability to discern asphalt mixtures based on their low-temperature cracking potential. LCI, a new parameter, was introduced and successfully evaluated for robustness.

For service temperature, the study compared a fracture-based approach, I-FIT, to a commonly used strength-based approach, the CT Index test. The notched geometry in I-FIT was observed to direct stress concentration and resulted in most of the applied loading being directed toward fracture. The FI, using the specimen fracture energy and crack speed rate, correlates well with known field performance. In contrast, the CT Index test was observed to be less reliable in distinguishing between asphalt mixtures. Due to the absence of a notch or a pre-crack in the specimen geometry, significant energy goes toward plastic deformation.

A practical, fracture-mechanics-based test was developed: the cored Brazil disc or DONUT. A two-step modification to the existing CT Index test was proposed: insert a hole in the center of the disk and increase the thickness of the loading strip. These modifications allowed applied stresses to be concentrated and promoted controlled fracture behavior while enhancing test repeatability. The test parameter, DI, which correlated well with FI, was able to discern between mixtures based on their cracking potential.

Major Findings

Standardization of specimen fabrication protocols is necessary to enable fair comparison of cracking potential among asphalt mixture designs. Factors such as AV, oven aging, and compaction method can significantly influence cracking behavior.

- Testing of P-401/403 asphalt mixtures at 5 percent AV, and of P-404 asphalt mixtures at 3 percent AV, is recommended to better reflect in-field compaction densities for airfield pavements.
- For test specimens, it is recommended that fabrication be done by sawing 160-mm gyratory specimens, or 180-mm specimens for 19-mm (0.75-inch) NMAS coarse-graded asphalt mixes. The gyratory specimen size ensures removal of end faces, which have been shown to possess higher AV than the remaining specimen. Compaction to 62-mm (2.5-inch) thick discs resulted in significant aggregate breakage and reduced cracking index values and is, therefore, not recommended.
- Test thresholds were developed for short-term aging (STA), which consisted of heating loose mixtures in a forced-draft oven at compaction temperature for 2 hr. A long-term aging (LTA) protocol—conditioning specimens at 95 °C for 3 days—was suggested as a screening tool for long-term potential performance.

SLT-SCB test, a modification of LT-SCB, was developed and validated for use within a BMD framework for airfield mixtures. The protocol specifies monotonic loading of a standard 50-mm (2-inch) thick SCB specimen at 0.15 mm/min (0.006 inch/min) until test termination. The resulting LLD curve is used to calculate the LCI parameter.

- The SLT-SCB protocol replaces the use of external crack-mouth opening displacement gauges with LLD to control the loading rate. The lowest pavement temperature at 50-percent reliability, obtained from the LTPP InfoPave website, is recommended for determining the testing temperature instead of binder PGL, thereby avoiding penalization of softer binders. Test duration was reduced from approximately 1 hr to about 5 min. Because the LCI uses only the pre-peak region of

the response, test termination can be advanced to 25 percent of peak load for further time savings.
- LCI was defined as the ratio of PFE (J/m^2) to loading stiffness (kN/mm). PFE correlated with the energy required for crack initiation, while loading stiffness correlated with the strain tolerance of the asphalt binder.
- LCI was shown to be a robust parameter applicable to both LMLC and PMLC specimens. Its ability to distinguish mixtures with higher cracking potential was validated using XCM designs and FC. Based on the dataset, an LCI acceptance threshold of 15 is recommended for asphalt mixture designs in regions susceptible to low-temperature cracking.

The study concluded that **I-FIT correlated well with observed field cracking behavior** and demonstrated superior capability for differentiating asphalt mixtures based on service-temperature cracking potential.

- Due to the inherent mode mixity associated with testing viscoelastic, heterogeneous asphalt mixes at service temperatures, no significant shear loading was achieved through notch displacement in the I-FIT protocol.
- The fracture-based I-FIT approach was better aligned with service-temperature cracking behavior than the traditional strength-based CT approach. Introduction of a notch in I-FIT simulated realistic fracture and crack-propagation mechanisms through the binder matrix.
- An FI threshold of 7 is recommended for STA specimens tested at field-representative AV. A threshold of 4 is recommended for LTA specimens.

A **fracture-dominated cored Brazil disc (DONUT) test** was developed based on a two-step modification of the conventional CT Index test.

- Direct compaction of CT specimens led to aggregate breakage and degradation of the load-carrying skeleton. CT Index values from compacted specimens were approximately half of those obtained from specimens sawed from typical gyratory specimens.
- CT loading was distributed through the aggregate skeleton, reducing sensitivity to fracture differences among mixtures. In addition, a significant portion of the energy goes to plasticity due to the absence of a pre-crack or a notch. Hence, a corresponding CT threshold could not be identified.
- A central, circular hole was cored into the 62-mm (2.5-inch) thick CT specimen using a 25.5-mm (1-inch) core barrel. This size was selected due to availability, low cost, and its diameter exceeding NMAS to function as a stress concentrator. Additionally, loading strip thickness increased from 20 mm to 30 mm to reduce localized yielding beneath the strips. These modifications resulted in more regularized fracture behavior during testing.

- The applied energy was shown to be independent of specimen thickness, indicating a significant portion of the energy is consumed by fracture, which is a material property. The secant slope at 75 percent of peak load correlated well with the post-peak slope from I-FIT, a crack-speed metric. A new DI was developed using fracture energy and secant slope.
- DI demonstrated better ability to distinguish cracking potential in LMLC and PMLC specimens than CT. The DI was further validated using FAA FC and cores from other airports. A DI threshold of 6 is proposed for sawed DONUT specimens tested at field-representative AV.

Implementation Plan

It is recommended that the SLT-SCB and DONUT/I-FIT tests be adopted for predicting cracking potential at low temperatures and service temperatures, respectively. Evaluation by professional laboratories is recommended to validate the tests' capacity, repeatability, and acceptance thresholds.

Integration of the findings from this research study and the companion study on rutting potential of asphalt mixtures is suggested to allow the development of a holistic BMD protocol for airfield asphalt mixtures. A follow-up implementation phase is recommended to include a pilot project where asphalt mixes are designed, produced, and tested under the proposed revised FAA P401-403 specifications. The pilot project can either be constructed at a commercial airport or at the NAPMRC or similar accelerated loading facility.

As part of this pilot project, asphalt mixture designs will be developed using the recommended test protocols and threshold for cracking and rutting potential. If the pilot project is constructed at an accelerated pavement testing site, asphalt mixture design should be developed with differing rutting and cracking potential to monitor their long-term performance and further calibrate the recommended threshold values. The influence of various parameters such as binder type, aggregate gradation, and polymer modification on in-field cracking and rutting can be studied.

This pilot project will establish key production parameters, such as test frequency, sampling practices, and mixture adjustments and variability, while also identifying practical challenges associated with implementation of BMD protocols, including turnaround time. The pilot project will further clarify mix-design modifications to ensure they meet the proposed thresholds for cracking and rutting potential.

The follow-up phase will (i) validate the proposed revisions to the FAA advisory circular for inclusion of thresholds for cracking and rutting potential of asphalt mixes, (ii) quantify test and production challenges and variability for implementation of BMD for airfields, (iii) provide asphalt mixture designers with practical and more fundamental understanding of the influence of each mixture design component on field performance, and (iv) strengthen the relationship between cracking/rutting indices and measured airfield performance for greater confidence.

References

AAPTP. (2004). Airfield Asphalt Binder Selection Tool. Airport Asphalt Pavement Technology Program. https://www.airfieldasphaltbinder.org/

AASHTO R 47. (2023). *Standard Practice of Reducing Asphalt Mixtures to Testing Size*. American Association of State Highway and Transportation Officials.

AASHTO T 321. (2022). *Standard Method of Test for Determining the Fatigue Life of Compacted Asphalt Mixtures Subjected to Repeated Flexural Bending*. American Association of State Highway and Transportation Officials.

AASHTO T 322. (2007). *Standard Method of Test for Determining the Creep Compliance and Strength of Hot Mix Asphalt (HMA) Using the Indirect Tensile Test Device*. American Association of State Highway and Transportation Officials.

AASHTO T 393. (2021). *Standard Method of Test for Determining the Fracture Potential of Asphalt Mixtures Using Illinois Flexibility Index Test (I-FIT)*. American Association of State Highway and Transportation Officials.

AASHTO T 394. (2021). *Standard Method of Test for Determining the Fracture Energy of Asphalt Mixtures Using the Semicircular Bend Geometry (SCB)*. American Association of State Highway and Transportation Officials.

AASHTO T 400. (2022). *Standard Method of Test for Determining the Damage Characteristic Curve and Failure Criterion Using the Asphalt Mixture Performance Tester (AMPT) Cyclic Fatigue Test*. American Association of State Highway and Transportation Officials.

Ali, U. M., Hernandez, J., Al-Qadi, I., & Ozer, H. (2019). Three-Dimensional Balanced Mix Design for Asphalt Concrete. *Airfield and Highway Pavements 2019*, 178–188. https://doi.org/10.1061/9780784482452.018

Al-Qadi, I. L., Hassan, M. M., & Elseifi, M. A. (2005). Field and Theoretical Evaluation of Thermal Fatigue Cracking in Flexible Pavements. *Transportation Research Record*, *1919*(1), 87–95. https://doi.org/10.1177/0361198105191900110

Al-Qadi, I. L., Lippert, D., Wu, S., Ozer, H., Renshaw, G., Said, I., Espinoza Luque, A., Safi, F., Murphy, T., Butt, A., Gundapuneni, S., Trepanier, J., & Vespa, J. (2017). *Utilizing Lab Tests to Predict Asphalt Concrete Overlay Performance* (FHWA-ICT-17-020). Illinois Center for Transportation. https://doi.org/10.36501/0197-9191/17-026

Al-Qadi, I. L., Ozer, H., Lambros, J., Khatib, A. E., Singhvi, P., Khan, T., Rivera-Perez, J., & Doll, B. (2015). *Testing Protocols to Ensure Performance of High Asphalt Binder Replacement Mixes Using RAP and RAS* (FHWA-ICT-15-017). Illinois Center for Transportation.

Al-Qadi, I. L., Ozer, H., Zhu, Z., Singhvi, P., Mohamed Ali, U., Sawalha, M., Espinoza Luque, A. F., Garcia Mainieri, J. J., & Zehr, T. (2019). *Development of Long-Term Aging Protocol for Implementation of the Illinois Flexibility Index Test (I-FIT)* (FHWA-ICT-19-009). Illinois Center for Transportation. https://doi.org/10.36501/0197-9191/19-012

Al-Qadi, I. L., Said, I. M., Ali, U. M., & Kaddo, J. R. (2022). Cracking Prediction of Asphalt Concrete Using Fracture and Strength Tests. *International Journal of Pavement Engineering*, *23*(10), 3333–3345. https://doi.org/10.1080/10298436.2021.1892108

Alvarez, D. B., Kazmee, H., & Garg, N. (2024). Laboratory and Field Performance Evaluation of Cracking of Airfield Warm Mix Asphalt with Reclaimed Asphalt Pavement at the National Airport Pavement and Materials Research Center. *Transportation Research Record: Journal of the Transportation Research Board*, *2678*(11), 530–546. https://doi.org/10.1177/03611981241242071

Anderson, T. L. (2017). *Fracture Mechanics: Fundamentals and Applications, Fourth Edition* (4th ed.). CRC Press. https://doi.org/10.1201/9781315370293

ASTM D6925. (2023). *Standard Test Method for Preparation and Determination of the Relative Density of Asphalt Mix Specimens by Means of the Superpave Gyratory Compactor*. ASTM International.

ASTM D6926. (2020). *Standard Practice for Preparation of Asphalt Mixture Specimens Using Marshall Apparatus*. ASTM International.

ASTM D7313. (2020). *Standard Test Method for Determining Fracture Energy of Asphalt Mixtures Using the Disk-Shaped Compact Tension Geometry*. ASTM International.

ASTM D8044. (2016). *Standard Test Method for Evaluation of Asphalt Mixture Cracking Resistance using the Semi-Circular Bend Test (SCB) at Intermediate Temperatures*. ASTM International.

ASTM D8225. (2019). *Standard Test Method for Determination of Cracking Tolerance Index of Asphalt Mixture Using the Indirect Tensile Cracking Test at Intermediate Temperature*. ASTM International.

ATAG. (2024). Aviation Benefits Beyond Borders. Air Transport Action Group. https://atag.org/facts-figures

Bajaj, A., & Al-Qadi, I. L. (2026). Performance Characterization of Airfield Asphalt Concrete for Service Temperature Cracking. In: M. Pasetto, E. Pasquini, A. Cannone Falchetto, G. Giacomello, & A. Baliello (Eds.), *Proceedings of the 2nd RILEM International Symposium on Bituminous Materials (ISBM 2026)* (pp. 330–336). Springer Nature Switzerland. https://doi.org/10.1007/978-3-032-30655-5_49

Bajaj, A., Al-Qadi, I. L., & Lambros, J. (2026). A Novel Fracture-Inspired Cored Brazil Disc Test to Characterize Cracking Potential for Asphalt Concrete. *International Journal of Pavement Engineering*, *27*(1). https://doi.org/10.1080/10298436.2026.2670562

Bajaj, A., Modi, S. H., Al-Qadi, I. L., Dave, E. V., Lambros, J., & Sias, J. E. (2026). Lab and Field Validation of Simplified Low-Temperature SCB Test for Airfield Asphalt Mixtures. *Journal of Transportation Engineering, Part B: Pavements, In Production*.

Barenblatt, G. I. (1962). The Mathematical Theory of Equilibrium Cracks in Brittle Fracture. *Advances in Applied Mechanics*, *7*, 55–129. https://doi.org/10.1016/S0065-2156(08)70121-2

Barry, M. K. (2016). *An Analysis of Impact Factors on the Illinois Flexibility Index Test* [Master's thesis, University of Illinois at Urbana-Champaign]. https://hdl.handle.net/2142/95565

Bennert, T. (2021). *Performance Evaluation of Asphalt Mixtures Statewide* (NYSDOT C-19-03). Center for Advanced Infrastructure and Transportation (CAIT), Rutgers University. https://rosap.ntl.bts.gov/view/dot/57049

BTS. (2022). U.S. Airport Runway Pavement Conditions. Bureau of Transportation Statistics. https://www.bts.gov/content/us-airport-runway-pavement-conditions

BTS. (2024). TranStats. Bureau of Transportation Statistics. https://www.transtats.bts.gov/

Buchanan, S. (2016, September 20). *Balanced Mix Design (BMD) for Asphalt Mixtures*. SHRP2 Peer to Peer Exchange 2016. AASHTO Strategic Highway Research Program 2. https://shrp2.transportation.org/documents/presentations/10_Buchanan_SHRP2BalancedMixDesignforAsphaltMixtures.pdf

Buttlar, W. G., Na Chiangmai, C., Al-Qadi, I. L., Murphy, T. R., & Pine, W. J. (2015). *Designing, Producing, and Constructing Fine-Graded Hot Mix Asphalt on Illinois Roadways* (FHWA-ICT-15-009). Illinois Center for Transportation. https://rosap.ntl.bts.gov/view/dot/28816

Dave, E. V., & Behnia, B. (2018). Cohesive Zone Fracture Modelling of Asphalt Pavements with Applications to Design of High-Performance Asphalt Overlays. *International Journal of Pavement Engineering*, *19*(3), 319–337. https://doi.org/10.1080/10298436.2017.1353393

Dugdale, D. S. (1960). Yielding of Steel Sheets Containing Slits. *Journal of the Mechanics and Physics of Solids*, *8*(2), 100–104. https://doi.org/10.1016/0022-5096(60)90013-2

Elias, N. G., Hajj, E. Y., Hand, A. J. T., Zhou, F., Bennert, T., Decker, C., & Patel, H. (2024). Developing Representative Test Specimen Conditions for Rutting Mechanical Test Methods of Airfield Pavements. *Transportation Research Record*, *2679*(1), 1127–1143. https://doi.org/10.1177/03611981231225638

Epps Martin, A., Kaseer, F., Arámbula-Mercado, E., Bajaj, A., Cucalon, L. G., Yin, F., Chowdhury, A., Epps, J., Glover, C., Hajj, E. Y., Morian, N., Daniel, J. S., Oshone, M., Rahbar-Rastegar, R., Ogbo, C., & King, G. (2020). *Evaluating the Effects of Recycling Agents on Asphalt Mixtures with High RAS and RAP Binder Ratios* (NCHRP Research Report 927). The National Academies Press. https://doi.org/10.17226/25749

FAA. (2018). *Standard Specifications for Construction of Airports, Advisory Circular 150/5370-10H*. Federal Aviation Administration.

FAA. (2024). *National Plan of Integrated Airport Systems (NPIAS) 2025–2029*. Federal Aviation Administration. https://www.faa.gov/sites/faa.gov/files/airports/planning_capacity/npias/current/ARP-NPIAS-2025-2029-Narrative.pdf

Farrar, M., Sui, C., Salmans, S., & Qin, Q. (2015). *Determining the Low-Temperature Rheological Properties of Asphalt Binder Using a Dynamic Shear Rheometer (DSR)* (Nos. DTFH61-07-D-00005). Western Research Institute.

Germann, F. P., & Lytton, R. L. (1979). *Methodology for Predicting the Reflection Cracking Life of Asphalt Concrete Overlays* (FHWA/TX-79/09+207-5). Texas Transportation Institute. https://trid.trb.org/view/142495

Ghuzlan, K. A., & Carpenter, S. H. (2000). Energy-Derived, Damage-Based Failure Criterion for Fatigue Testing. *Transportation Research Record*, *1723*(1), 141–149. https://doi.org/10.3141/1723-18

Griffith, A. A. (1921). The Phenomena of Rupture and Flow in Solids. *Philosophical Transactions of the Royal Society of London. Series A, Containing Papers of a Mathematical or Physical Character*, *221*, 163–198. https://www.jstor.org/stable/91192

Hajj, E. Y., Elias, N. G., Khanal, B., Alrajhi, A., Hand, A., Bennert, T., Zhou, F., Epps, J., Chan, K. M., Decker, C. S., Patel, H., & Duval, J. (2025). *Balanced Mix Design: Rutting Performance Tests*. Airport Asphalt Pavement Technology Program (AAPTP). https://www.asphaltpavement.org/uploads/documents/ERT%20Related/AAPT_Program/Final_Report_BMD_508.pdf

Harvey, J. T., Deacon, J. A., Tsai, B.-W., & Monismith, C. L. (1995). *Fatigue Performance of Asphalt Concrete Mixes and Its Relationship to Asphalt Concrete Pavement Performance in California* (RTA-65W485-2). University of California, Berkeley. https://ucprc.ucdavis.edu/pdf/Fatigue%20Performance%20of%20AC.pdf

Haslett, K. E., Sias, J. E., & Dave, E. V. (2022). Assessment of Asphalt Mixture Disk-Shaped Compact Tension Test Indexes for Reflective Cracking Performance. *Journal of Testing and Evaluation*, *50*(2), 755–769. https://doi.org/10.1520/JTE20210196

Hillerborg, A., Modéer, M., & Petersson, P.-E. (1976). Analysis of Crack Formation and Crack Growth in Concrete by Means of Fracture Mechanics and Finite Elements. *Cement and Concrete Research*, 6(6), 773–781. https://doi.org/10.1016/0008-8846(76)90007-7

Huang, Y. H. (1993). *Pavement Analysis and Design*. Prentice Hall.

IATA. (2025). Industry Statistics. International Air Transport Association. https://www.iata.org/en/iata-repository/pressroom/fact-sheets/industry-statistics/

Illinois DOT. (n.d.). *Illinois 2022–2025 IDEA — Airport Details*. Illinois Department of Transportation. Retrieved https://idea.appliedpavement.com/hosting/illinois/airport-details/airport-details.html

Inglis, C. E. (1913). Stresses in a Plate Due to the Presence of Cracks and Sharp Corners. *Transactions of the Institute of Naval Architects*, *55*, 219–241.

Irwin, G. R. (1957). Analysis of Stresses and Strains Near the End of a Crack Traversing a Plate. *Journal of Applied Mechanics*, *24*(3), 361–364. https://doi.org/10.1115/1.4011547

Jacobs, M., Hopman, P. C., & Molenaar, A. A. A. (1996). Application of Fracture Mechanics Principles to Analyze Cracking in Asphalt Concrete. *Journal of the Association of Asphalt Paving Technologists*, *65*, 1–39. https://trid.trb.org/view/487700

Jenq, Y.-S., & Perng, J.-D. (1991). Analysis of Crack Propagation in Asphalt Concrete Using Cohesive Crack Model. *Transportation Research Record*, (1317), 90–99. https://trid.trb.org/view/365394

Jichkar, P. D. (2021). *Implementation of HMA Design Tool to Develop Balanced Mix Design Based on Gradation Parameters* [Master's thesis, University of Texas at El Paso]. https://scholarworks.utep.edu/open_etd/3278/

Kennedy, T. W., Huber, G. A., Harrigan, E. T., Cominsky, R. J., Hughes, C. S., Von Quintus, H., & Moulthrop, J. S. (1994). *Superior Performing Asphalt Pavements (Superpave): The Product of the SHRP Asphalt Research Program*. https://onlinepubs.trb.org/onlinepubs/shrp/SHRP-A-410.pdf

Kim, Y. R., Castorena, C., Elwardany, M., Rad, F. Y., Underwood, S., Gundha, A., Gudipudi, P., Farrar, M. J., & Glaser, R. R. (2017). *Long-Term Aging of Asphalt Mixtures for Performance Testing and Prediction* (NCHRP Research Report 871; p. 24959). National Academies of Sciences, Engineering, and Medicine. https://doi.org/10.17226/24959

Kirsch, E. G. (1898). Die Theorie der Elastizität und die Bedürfnisse der Festigkeitslehre. *Zeitshrift Des Vereines Deutscher Ingenieure*, (42), 797–807.

Li, X., Braham, A. F., Marasteanu, M. O., Buttlar, W. G., & Williams, R. C. (2008). Effect of Factors Affecting Fracture Energy of Asphalt Concrete at Low Temperature. *Road*

Materials and Pavement Design, *9*(sup1), 397–416. https://doi.org/10.1080/14680629.2008.9690176

Li, X., & Marasteanu, M. (2004). Evaluation of the Low Temperature Fracture Resistance of Asphalt Mixtures Using the Semi Circular Bend Test. *Journal of the Association of Asphalt Paving Technologists*, *73*, 401–426. https://trid.trb.org/view/749998

Lytton, R. L., Shanmugham, U., & Garrett, B. D. (1983). *Design of Asphalt Pavements for Thermal Fatigue Cracking* (FHWA/TX-83/06+284-4). Texas Transportation Institute, Texas A&M University. https://static.tti.tamu.edu/tti.tamu.edu/documents/284-4.pdf

Majidzadeh, K., Kauffmann, E. M., & Ramsamooj, D. V. (1971). Application of Fracture Mechanics in the Analysis of Pavement Fatigue. *In Association of Asphalt Paving Technologists Proceedings*, *40*, 227–246. https://trid.trb.org/view/103438

Marasteanu, M., Buttlar, W., Bahia, H., Williams, C., Moon, K. H., Teshale, E. Z., Falchetto, A. C., Turos, M., Dave, E., Paulino, G., Ahmed, S., Leon, S., Braham, A., Behnia, B., Tabatabaee, H., Velasquez, R., Arshadi, A., Puchalski, S., Mangiafico, S., … Kvasnak, A. (2012). *Investigation of Low Temperature Cracking in Asphalt Pavements National Pooled Fund Study – Phase II* (Report MN/RC 2012-23). Minnesota Department of Transportation. http://conservancy.umn.edu/handle/11299/135177

Marcela, A., Regis, C., Silvio, S., Victoria, R., Douglas, M., Gesley, F., Diogenes, S., Gracieli, C., Luciano, S., & Lelio, B. (2025). The Use of Balanced Mix Design Process with High Polymer Modified Asphalt: A Case Study at a Brazilian Airport. *Airfield and Highway Pavements 2025*, 187–200. https://doi.org/10.1061/9780784486214.017

Mobasher, B., Mamlouk, M. S., & Lin, H.-M. (1997). Evaluation of Crack Propagation Properties of Asphalt Mixtures. *Journal of Transportation Engineering*, *123*(5), 405–413. https://doi.org/10.1061/(ASCE)0733-947X(1997)123:5(405)

Modi, S. H., Bajaj, A., Dave, E. V., Sias, J. E., Al-Qadi, I. L., Lambros, J., & Tormos, S. (2026). Development of a Simplified Low-Temperature SCB Test Protocol to Characterise Cracking Potential of Airfield Mixtures. *International Journal of Pavement Engineering*, *27*(1), 2698794. https://doi.org/10.1080/10298436.2026.2698794

Monismith, C. L., & Deacon, J. A. (1969). Fatigue of Asphalt Paving Mixtures. *Transportation Engineering Journal of ASCE*, *95*(2), 317–346. https://doi.org/10.1061/TPEJAN.0000023

Monismith, C. L., Secor, K. E., & Blackmer, E. W. (1961). Asphalt Mixture Behavior in Repeated Flexure. *In Association of Asphalt Paving Technologists Proceedings*, *30*, 188–222. https://trid.trb.org/view/728292

NAPA. (2023). *The Asphalt Pavement Industry: Fast Facts*. National Asphalt Pavement Association.

https://www.asphaltpavement.org/uploads/documents/GovAffairs/NAPA_Asphalt_Pavement_Fast_Facts_2023.pdf

Ozer, H., Al-Qadi, I. L., Lambros, J., El-Khatib, A., Singhvi, P., & Doll, B. (2016). Development of the Fracture-Based Flexibility Index for Asphalt Concrete Cracking Potential Using Modified Semi-Circle Bending Test Parameters. *Construction and Building Materials*, *115*, 390–401. https://doi.org/10.1016/j.conbuildmat.2016.03.144

Paris, P., & Erdogan, F. (1963). A Critical Analysis of Crack Propagation Laws. *Journal of Basic Engineering*, *85*(4), 528–533. https://doi.org/10.1115/1.3656900

Pell, P. S. (1962). Fatigue Characteristics of Bitumen and Bituminous Mixes. *International Conference on the Structural Design of Asphalt Pavements*, *203*(1), 43–58. https://trid.trb.org/View/717074

Petersen, J. C., & Harnsberger, P. M. (1998). Asphalt Aging: Dual Oxidation Mechanism and Its Interrelationships with Asphalt Composition and Oxidative Age Hardening. *Transportation Research Record: Journal of the Transportation Research Board*, *1638*(1), 47–55. https://doi.org/10.3141/1638-06

Prowell, B. D., Watson, D. E., Hurley, G. C., & Brown, E. R. (2009). *Evaluation of Stone Matrix Asphalt (SMA) for Airfield Pavements* (Final Report AAPTP 04-04). National Center for Asphalt Technology at Auburn University.

Ramsamooj, D. V. (1970). *Analysis and Design of the Flexibility of Pavements*. [Doctoral dissertation, The Ohio State University]. https://www.proquest.com/dissertations-theses/analysis-design-flexibility-pavements/docview/302444857/se-2

Rice, J. R. (1968). A Path Independent Integral and the Approximate Analysis of Strain Concentration by Notches and Cracks. *Journal of Applied Mechanics*, *35*(2), 379–386. https://doi.org/10.1115/1.3601206

Roque, R., Birgisson, B., Drakos, C., & Dietrich, B. (2004). Development and Field Evaluation of Energy-Based Criteria for Top-Down Cracking Performance of Hot Mix Asphalt. *Journal of the Association of Asphalt Paving Technologists*, *73*, 229–260. https://trid.trb.org/view/749993

Roque, R., Hiltunen, D. H., Buttlar, W. G., & Farwana, T. (1995). *Development of the SHRP Superpave Mixture Specification Test Method to Control Thermal Cracking Performance of Pavements*. https://doi.org/10.1520/STP15562S

Roque, R., Zou, J., Kim, Y. R., Baek, C., Thirunavukkarasu, S., Underwood, B. S., & Guddati, M. N. (2010). *Top-Down Cracking of Hot-Mix Asphalt Layers: Models for Initiation and Propagation* (p. 22935). Transportation Research Board. https://doi.org/10.17226/22935

Schapery, R. A. (1975). A Theory of Crack Initiation and Growth in Viscoelastic Media. *International Journal of Fracture*, *11*(1), 141–159. https://doi.org/10.1007/BF00034721

Son, S., Said, I. M., & Al-Qadi, I. L. (2019). Fracture Properties of Asphalt Concrete Under Various Displacement Conditions and Temperatures. *Construction and Building Materials*, *222*, 332–341. https://doi.org/10.1016/j.conbuildmat.2019.06.161

Texas DOT. (2022). *Test Procedure for the Overlay Test. Tex-248-F (Revised)*. Texas Department of Transportation.

Tipnis, M., Kataware, A. V., Chowdary, K., Gupta, A., & Das, S. K. (2023). Case Study—Delhi International Airport Phase 3 Expansion Performance Based Mix Design for Bituminous Surface Course. *Airfield and Highway Pavements 2023*, 213–228. https://doi.org/10.1061/9780784484913.020

Van Dijk, W., & Visser, W. (1977). Energy Approach to Fatigue for Pavement Design. *In Association of Asphalt Paving Technologists Proceedings*, *46*, 1–40. https://trid.trb.org/view/87372

Wang, H., & Al-Qadi, I. L. (2010). Near-Surface Pavement Failure Under Multiaxial Stress State in Thick Asphalt Pavement. *Transportation Research Record: Journal of the Transportation Research Board*, *2154*(1), 91–99. https://doi.org/10.3141/2154-08

West, R., Rodezno, C., Leiva, F., & Yin, F. (2018). *Development of a Framework for Balanced Mix Design* (NCHRP 20-07/Task 406). National Center for Asphalt Technology at Auburn University. https://onlinepubs.trb.org/onlinepubs/nchrp/docs/NCHRP20-07(406)_Revised_final_report.pdf

Williams, M. L. (1957). On the Stress Distribution at the Base of a Stationary Crack. *Journal of Applied Mechanics*, *24*(1), 109–114. https://doi.org/10.1115/1.4011454

Yin, F., & West, R. (2021). *Balanced Mix Design Resource Guide*. National Asphalt Pavement Association. https://go.asphaltpavement.org/balanced-mix-design-resource-guide-lp

Zhang, Z., Roque, R., & Birgisson, B. (2001). Evaluation of Laboratory-Measured Crack Growth Rate for Asphalt Mixtures. *Transportation Research Record: Journal of the Transportation Research Board*, *1767*(1), 67–75. https://doi.org/10.3141/1767-09

Zhou, F., Hu, S., & Scullion, T. (2006). *Integrated Asphalt (Overlay) Mixture Design, Balancing Rutting and Cracking Requirements* (FHWA/TX-06/0-5123-1). Texas Transportation Institute, The Texas A&M University System. http://tti.tamu.edu/documents/0-5123-1.pdf

Zhou, F., Scullion, T., Walubita, L. F., & Wilson, B. (2014). Implementation of a Performance-Based Mix Design System in Texas. *In Application of Asphalt Mix Performance-Based Specifications (Transportation Research Circular No. E-C189)*, 32–50. https://onlinepubs.trb.org/onlinepubs/circulars/ec189.pdf

Appendix A: Current State of Knowledge for Cracking and Balanced Mix Design in Asphalt Pavements

Table of Contents

List of Figures

List of Tables

Scope of Appendix A

This section summarizes the contents of Appendix A to make it easier for users to navigate.

Section 1 details the motivation behind the project and introduces the reader to the problem of cracking in asphalt pavements. The section also touches on the brief history of the efforts to characterize cracking in the laboratory and its relation to actual field performance.

Section 2 delves into the various mechanisms through which cracking might occur in asphalt pavements. It gives a historical overview of theories proposed by researchers for cracking in materials in general and those applied to asphalt pavements.

Section 3 details the various factors that might influence the initiation and/or progression of cracking in asphalt pavements. It uses the mechanisms detailed in Section 2 to explain the impacts of environmental and mixture factors on cracking and its exacerbation under some conditions.

Section 4 describes the major types of cracking that occur in asphalt pavements. Developed machinery, presented in earlier sections, is described. Details on various parameters affecting specific cracks in the field are presented.

Section 5 builds on Section 4 and presents the characterization of various forms of cracking found in the field using several testing protocols. Detailed procedures for the most widely used tests for asphalt cracking are listed with their corresponding standard and motivation.

Section 6 introduces the concept of Balanced Mix Design (BMD). The motivation behind the new design philosophy is discussed, as well as its current implementation in various regions in the United States for asphalt highways.

Section 1: Introduction to Cracking in Pavements

Failure of transportation infrastructure has always been a concern to the community due to the economic, environmental, safety, and human factors associated with it. Pavement design philosophies, such as HVEEM and Marshall, were the starting points for designing flexible pavements against distresses, including cracking and permanent deformation. The earliest attempts to relate pavement fatigue life—the number of load repetitions to failure—to measured pavement strains were made by Monismith et al. (1961) and Pell (1962). Stiffness, an indication of a pavement mix's resistance to external forces, was suggested as a measure of pavement life. The Federal government and highway agencies funded the Strategic Highway Research Program (SHRP) to better understand pavement behavior. The work was accomplished through collaboration with universities and research centers nationwide. After the implementation of SHRP recommendations, pavement rutting resistance improved, but pavement cracking increased due to the use of dry and brittle mixtures (Harvey et al., 1995; Monismith & Deacon, 1969). In addition, the use of empirical approaches to predict pavement service life was questionable (Aglan & Figueroa, 1993).

In lieu of the stiffness approach, the energy approach gained traction to predict flexible pavement cracks. Fracture energy for asphalt pavements was introduced by Majidzadeh et al. (1971) and Van Dijk & Visser (1977). Several researchers adopted this approach and have applied the principles of fracture in lab testing (Kim et al., 2009; Marasteanu et al., 2012). Although Paris Law applications were initially used (Germann & Lytton, 1979), more sophisticated tools were utilized to predict pavement responses (Zhang et al., 2001). The tools were further developed to predict actual field life from laboratory experiments using shift factors (Molenaar, 2007; Ioannides, 1997). Various specimen geometries (Wagoner, 2006) and loading configurations (Myers & Roque, 2002) were considered. Further, the viscoelastic nature of asphalt pavement was investigated (Kim & Little, 1990; Roque et al., 2015). The Weibull survival function was also used to model asphalt pavement cracks as a stochastic process (Tsai et al., 2003, 2004). Roque & Ruth (1990) suggested that the effects of temperature, rest period, and age hardening should be incorporated in any prediction approach. They argued that loading cycles do not generate equal responses. Kim et al. (1997) illustrated the effectiveness of the Viscoelastic Continuum Damage (VECD) Model. This approach was further studied in the lab (Hou et al., 2010) and in the field (Norouzi et al., 2016).

Roque et al. (2010) tried to improve crack prediction accuracy by combining fracture mechanics and VECD. They suggested that crack initiation was better represented by VECD theory, and once the macrocrack formed, fracture mechanics would give better results. Finite element (FE) modeling (Kim & Buttlar, 2009) was used for crack propagation. Digital image correlation was utilized to calculate the strains and stresses being developed in lab specimens during testing (Abanto-Bueno & Lambros, 2002; Doll et al., 2017a). With new challenges in asphalt pavements, such as the use of polymer-modified binders, cracking modeling is expected to be further developed.

Section 2: Mechanisms of Cracking

The life of flexible pavement is affected by repetitive loading. Initially, the cycles to failure for a pavement were related to these properties using phenomenological models. The fatigue life (N_f), described by the number of load applications to failure, was empirically related to the maximum tensile stress (σ) and strain (ε) at the bottom of the pavement (Pell, 1962; Pell & Taylor, 1969).

$$\mathrm{N}_f = C_1\left(\frac{1}{\sigma}\right)^{m_1} \quad \text{For stress-controlled tests} \qquad (\text{A-1})$$

$$\mathrm{N}_f = C_2\left(\frac{1}{\varepsilon}\right)^{m_2} \quad \text{For strain-controlled tests} \qquad (\text{A-2})$$

The regression constants C_1, C_2, M_1, and M_2 were determined by testing asphalt beams in the laboratory and with field validation during the American Association of State Highway Officials (AASHO) Road Test sections. The applied loading on asphalt samples in the laboratory was rather simplistic and Miner's rule was applied (Miner, 1945).

$$\sum \frac{n_i}{\mathrm{N}_i} = \mathrm{K} \qquad (\text{A-3})$$

where K is fraction of fatigue life at different stress levels, N_i is the average number of cycles to failure at the i^{th} stress level, and n_i is the number of cycles accumulated at the i^{th} stress level.

The rule assumes a linear relationship between loading and damage without considering loading history. These equations were used by many engineers to estimate the design life of pavements (Huang, 1993). The failure was usually described as a 50-percent reduction in stiffness. This approach overlooked specimen geometry and size, and testing temperature, among other factors (Francken, 1979; Ramsamooj, 1993). Hence, a scientific and fundamental approach was needed.

Fracture Mechanics

Linear Elastic Fracture Mechanics

The traditional strength of materials approach to analyze failure considers applied stresses and compares them to material strength. Fracture mechanics, developed in the early 20th century (Griffith, 1921; Irwin, 1957), considers the geometrical aspects of cracks that might exist in a material in addition to material properties. They demonstrated that crack shape would directly affect energy release and stress distribution in a material during cracking. The main feature found was a significant amplification of the remotely applied stresses in the vicinity of the crack, demonstrating that a material may fail at an applied stress lower than its nominal strength. A material might fracture in three distinct modes: Mode I (Opening), Mode II (In-Plane Shear), and Mode III (Out-of-Plane Shear or Tearing), as shown in Figure A-1. The theory of linear elastic fracture mechanics was developed in two parallel paths: Stress Intensity Factor and Energy Release Rate.

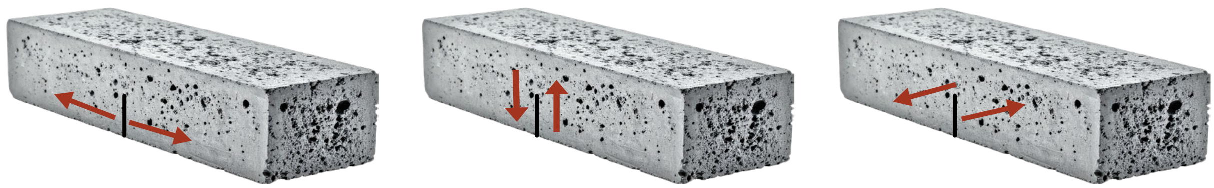

Mode I (Opening) **Mode II (In-Plane Shear)** **Mode III (Out-of-Plane Shear)**

Source: AAPTP

Figure A-1. Modes of Fracture

The crack tip autonomy of the stress field around a crack tip was seen to be universal, as long as the crack tip was far from boundary effects (Williams, 1957). However, the stress field depends on the applied load and crack length, which affect its amplitude and are quantified by stress intensity factors (one for each mode). If the stresses near a crack exceed the fracture toughness of the material, denoted as K_{IC}, crack growth occurs. Paris & Erdogan (1963) used these principles and presented the crack growth rate alongside the stress intensity factor; the relationship for Mode I is expressed as follows:

$$\frac{da}{dN} = \mathrm{A}K^{n} \qquad \text{(A-4)}$$

where crack growth rate is denoted by da/dN; K is the stress intensity factor; and A and n are coefficients obtained experimentally.

The principles, originally developed for metals (Figure A-2), were applied to asphalt pavement by Moavenzadeh and Majidzadeh (Majidzadeh et al., 1971; Moavenzadeh, 1967; Ramsamooj, 1970). They described fatigue as a damage process with three stages: damage initiation, growth, and final failure.

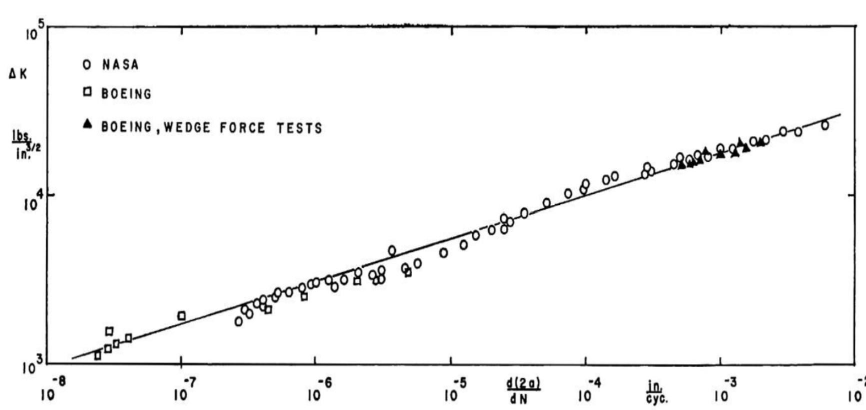

Figure A-2. Crack Growth Rate for 7075-T6 Aluminum Alloy (Paris & Erdogan, 1963)

Source: Reproduced from "A Critical Analysis of Crack Propagation Laws," by P. Paris and F. Erdogan in *Journal of Basic Engineering, 85*(4), 528–533. Permission conveyed through Copyright Clearance Center, Inc.

During the application of Paris Law, it was evident that A and n were semi-empirical parameters at best. It was shown experimentally that at low temperatures the values of A became constant, but they would not hold at intermediate and high temperatures, making A and n phenomenological constants. Also, it was noticed that Paris Law (Equation A-4) was mostly applicable during the second stage of crack growth (Jacobs et al., 1996). Stages I and III were non-linear regions, as shown in Figure A-3. Another drawback in the application to asphalt mixtures is that its viscoelastic nature is not considered.

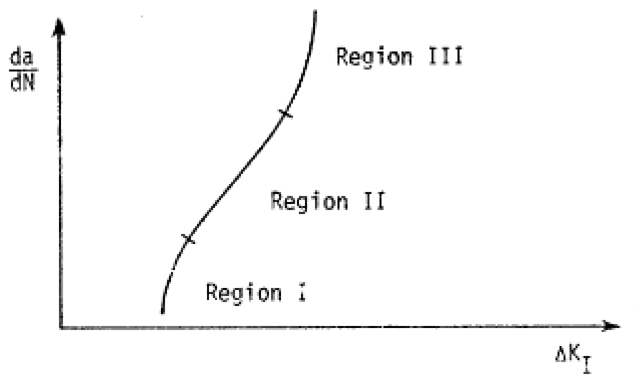

Figure A-3. Stages of Crack Growth (Paris & Erdogan, 1963)

Source: Reproduced from "A Critical Analysis of Crack Propagation Laws," by P. Paris and F. Erdogan in *Journal of Basic Engineering, 85*(4), 528–533. Permission conveyed through Copyright Clearance Center, Inc.

To account for the asphalt mixture's viscoelastic nature while still being able to use the Linear Elastic Fracture Mechanics framework, Schapery (1975) developed the "correspondence principle." Using the Dugdale-Barenblatt crack tip model (Figure A-4), he showed that the fracture parameters obtained with Paris Law, i.e., A and n, could be related to material properties such as creep compliance, tensile strength, and fracture energy. The correspondence principle, however, had many assumptions that Schapery used to derive these relations and thus made the theory not a fundamental material law that could be used to dictate the properties. The principle may only apply to relatively small strains (Rajagopal & Srinivasa, 2005). In addition, it may be valid for asphalt mixtures with high asphalt content, and breaks down for mixtures with lower asphalt content (Germann & Lytton, 1979).

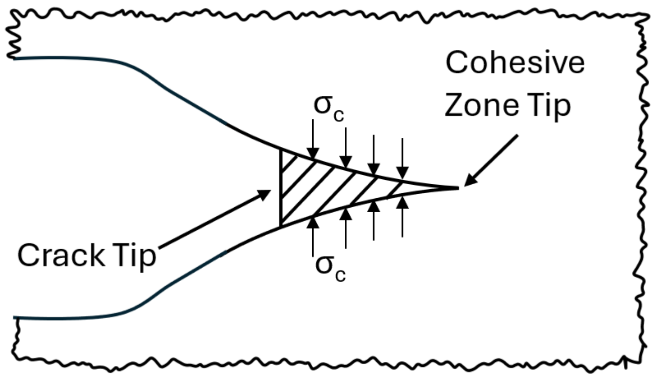

Source: AAPTP

Figure A-4. Geometry for Dugdale-Barenblatt Crack Tip Model

Energy release was also considered as a parameter that controls crack growth. This approach considers the energy of the entire system, so local stress fields need not be known. The basic principle is that the potential energy of the system near the crack is greater than the surface energy released after crack initiation and propagation. The crack growth is dictated by the rate of excess energy release near a crack tip. Griffith developed the strain energy release rate, G, in the 1920s and defined it as the energy dissipated during a fracture process per unit of newly created fracture surface area.

$$G = -\frac{1}{B}\frac{dU}{da} \quad \text{(A-5)}$$

where B is specimen thickness and dU/da is strain energy per unit crack length.

This was initially applied to asphalt pavement by Van Dijk & Visser (1977). The number of cycles to fatigue (N_f) was correlated to the energy dissipated (W_f) as follows:

$$W_f = \mathrm{B}{N_f}^z \quad \text{(A-6)}$$

where B and z were empirical constants.

Aglan & Figueroa (1993) used the thermodynamic considerations and included additional degrees of freedom such as rotation, distortion, and translation into their Crack Layer model:

$$\frac{da}{dN} = \frac{\mathrm{CW}}{\gamma a - J} \quad \text{(A-7)}$$

where W is the energy dissipated in a cycle, J is the crack driving energy, and C and γ are constants.

Numerous simplifications were used to derive this relation, and the primarily qualitative nature of the obtained results showed limited applicability for data prediction in the field (Ioannides, 1997).

Researchers attempted to define failure using the energy approach (Ghuzlan & Carpenter, 2000; Zhang et al., 2001). They defined the failure parameters in terms of dissipated energy change ratio and dissipated creep energy. These methods have shown some success in evaluating asphalt field performance.

Non-Linear Fracture Mechanics

Using the linear elastic material assumption often led to infinite stresses at the tip of the crack. In real life, these stresses lead to plasticity, microcracks, and crack branching. Therefore, this would blunt a crack tip and create a zone of non-linearity in the material near the tip. This region of non-linearity also includes the fracture process zone (FPZ). The FPZ is the region created ahead of the crack tip where the processes lead to material separation (Anderson, 2017), as shown in Figure A-5. Energy dissipation via plastic mechanisms introduces the non-linearity (Khan, 2016). For asphalt pavement, the non-linearities may also be caused by healing and aggregate interlocking, which lead to crack tortuosity. If the FPZ is small compared to the crack length, then the behavior could be approximated as linear elastic. Inclusion of stiffer materials in asphalt mixtures has been shown to decrease the FPZ size (Hill, 2016), and therefore reduce the asphalt non-linearity.

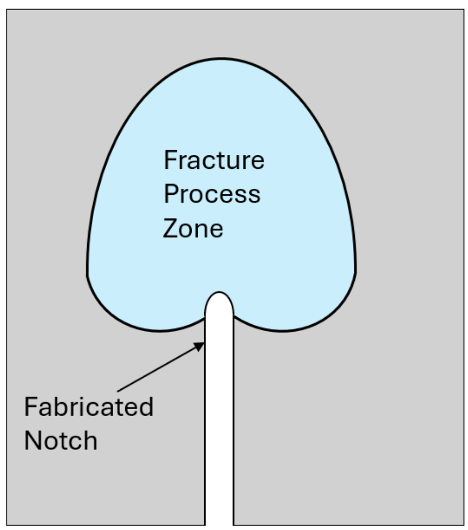

Source: AAPTP

Figure A-5. Schematic of FPZ

Mobasher et al. (1997) used non-linear fracture mechanics principles to create crack growth resistance curves (R curves) for asphalt pavement, which represent the relationship between energy release rate and crack extension. The resistance to crack growth would be a factor of the compliance of the asphalt mixture and therefore indicates the fracture toughness. This parameter may be used to differentiate asphalt mixes based on potential crack resistance.

One of the most commonly used techniques for non-linear fracture mechanics is the J-Integral approach (Rice, 1968). Parameter J was used to define the amount of energy released per unit area of crack surface increase. This was shown to be equivalent to the energy release rate from Griffith's approach in the case of Linear Elastic Fracture Mechanics. The J-Integral approach was initially used for ductile materials like metals, but was later adapted for quasi-brittle materials like Portland cement concrete (PCC) and asphalt pavement by Hillerborg et al. (1976) and Abdulshafi & Majidzadeh (1985), respectively. The J-Integral is defined as follows:

$$J = \int_{\Gamma} \left(W \, \mathrm{d}x_2 - t \cdot \frac{\partial U}{\partial x_1} \mathrm{d}s \right) \qquad \text{(A-8)}$$

where, W is strain energy density, U is the displacement vector, t is the surface traction vector, and x_1 and x_2 are coordinate directions.

J is often calculated using specimens of varying notch lengths and measuring strain energy release rates (Bhurke et al., 1997). Luo et al. (2013) combined the J-Integral approach with Paris Law. However, due to the complex and labor-intensive nature of calculating the J-Integral, this parameter is not widely used to represent fracture energy.

Quasi-brittle materials do not go through a brittle failure after peak load, but instead experience curve softening (Seo et al., 2004), as shown in Figure A-6. The area under this curve is termed fracture work (W_f), denoting the amount of work used to create the crack surface. Fracture energy (G_f) is defined by dividing the work by the surface area of the crack created. Fracture energy for asphalt mixtures has been used by researchers with reasonable success to assess cracking characteristics of mixtures (Jacobs et al., 1996; Roque et al., 2004; Zhang et al., 2001).

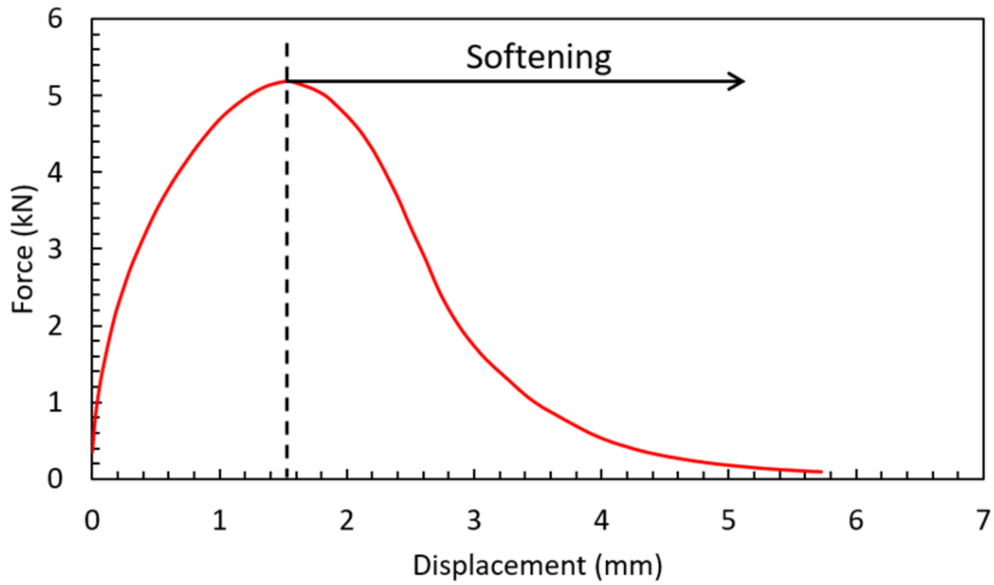

Source: AAPTP

Figure A-6. Load-Displacement Curve for Quasi-brittle Materials

Alongside the numerical approach to calculating the cracking characteristics of an asphalt mixture, there have been advances in modeling the material itself and predicting the characteristics for uncracked materials using the Cohesive Zone (CZ) Model. This approach consists of creating constitutive laws that describe the displacements and corresponding tractions along interfaces during all three stages of fracture (Hillerborg et al., 1976; Jenq & Perng, 1991).

Hillerborg et al. (1976) first applied the CZ model approach to quasi-brittle materials via PCC. Later, this approach was applied to asphalt pavement by Jenq & Perng (1991). The initial cases were simple, and later Bažant & Li (Bažant & Li, 1997; Li & Bažant, 1997) provided a much more robust application process for CZ models to viscoelastic materials. Their model included creep, compliance, and a rate-dependent softening law. A CZ model for asphalt mixture was developed, which included characteristics such as bulk properties and artificial compliance measured from laboratory asphalt mixture samples (Kim & Buttlar, 2009; Song et al., 2006). The CZ model has been shown to have good correlation between predicted and measured values (Chen et al., 2022; Kim & Aragão, 2013; Li & Guo, 2019).

Continuum Damage

Continuum damage was initially used for stochastic degradation of cohesion in a body under uniaxial loading (Murzewski, 1957; Rabotnov, 1959). This theory differs fundamentally from the fracture mechanics approach and describes the body as continuous. After the application of loading, the damage in the form of microcrack initiation and nucleation is modeled until localized damage zones are created. At this stage, the continuum damage model begins to break down because the body no longer remains continuous, and the fracture mechanics principles provide a more rigorous basis for analyzing the material response.

Schapery (1981, 1997) used a continuum damage theory applied to viscoelastic materials in both the linear and non-linear ranges, creating the VECD model. The main parameter used to derive stress, energy, and damage functions for a material was the pseudo strain function ε^R, defined by Schapery as follows:

$$\varepsilon^R = \frac{1}{E_R}\int_0^t E(\xi - \tau)\frac{d\varepsilon}{d\tau}d\tau \tag{A-9}$$

where $E(\xi)$ is the linear viscoelastic relaxation modulus, τ is the integration term, ξ is the reduced time, and E_R is the reference modulus, often taken as 1.

This convolution integral is used to account for the linear viscoelastic and time-temperature effects and creates a linear parameter, ε^R, that can be utilized using existing laws such as Hooke's Law and the energy density function. A key output of the VECD model is the relation between the amount of damage in the specimen, S, and the material integrity (pseudo secant stiffness), C, which is used to create damage characteristic curves such as those shown in Figure A-7.

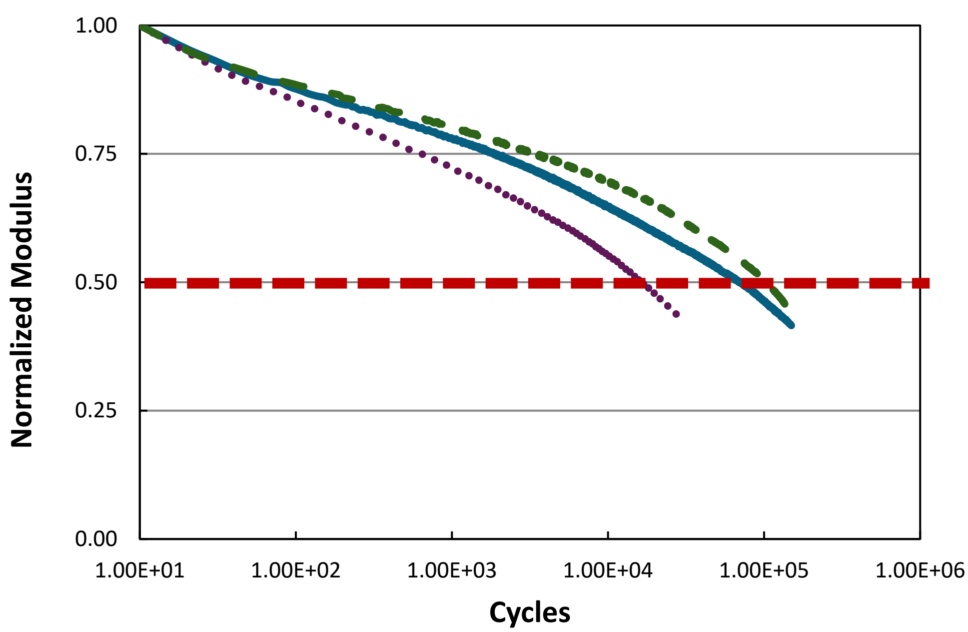

Source: AAPTP

Figure A-7. Typical VECD Damage Characteristic Curve

This work was first applied to asphalt mixes to achieve a damage relation using the pseudo-strains for sand asphalts (Kim & Little, 1990). The work was further advanced using cyclic conditions in addition to uniaxial loading (Daniel & Kim, 2002). The plastic behavior was later added, making the model applicable to both viscoelastic and viscoplastic materials under constant rate loading (Chehab et al., 2002). They also proved the applicability of time-temperature superposition during damage growth. Hence, the damage law used in the VECD model was shown to be independent of loading and time-temperature superposition. This would significantly reduce low-strain laboratory testing.

Underwood et al. (2010) simplified the VECD model by using a single function to model the fatigue characteristics, resulting in the Simplified ViscoElastic Continuum Damage (S-VECD) Model. Asphalt pavement life was then determined using the S-VECD damage characteristic curves. A failure criterion was developed by Hou et al. (2010), who proposed a pseudo stiffness value of either 0.5 for 5 °C or 0.25 for 19 °C and above.

In an effort to develop a more fundamental failure criterion, Sabouri & Kim (2014) proposed using an average dissipated pseudo-strain energy release rate, G^R, to predict the number of cycles to failure, i.e., the asphalt pavement life. The relation is a power law and is independent of test temperature, strain level, and mode of loading. To simplify testing protocols and make a linear relation for failure rather than a power law, D^R was introduced as a failure parameter (Wang & Kim, 2019). D^R was defined as the slope of the curve plotted between the number of cycles to failure and the cumulative (1-C) for the specimen. Theoretically, only one test is needed for this criterion because the relation is designed to pass through the origin. This approach has shown reasonable success in characterizing asphalt mixture cracking properties in the field (Norouzi & Kim, 2017; Wang & Kim, 2019).

In summary, this section examines the progressive deterioration of asphalt pavement under repeated loading. Early efforts to predict fatigue life relied on phenomenological models that employed empirical relationships among fatigue life, maximum tensile stress, and strain. However, such approaches overlook critical factors—including specimen geometry, size, and testing temperature—that strongly influence fatigue resistance. These limitations underscored the need for a more rigorous, science-based framework.

To address this gap, the linear elastic fracture mechanics (LEFM) approach was introduced, incorporating the mechanics of crack propagation and the role of the stress intensity factor. Subsequently, nonlinear fracture mechanics (NLFM) frameworks were explored to overcome the limitations of linear assumptions, introducing key concepts such as the FPZ and energy-based methods, including the J-integral and the crack layer model, for evaluating fracture toughness. In addition, VECD theory was discussed as a means of capturing damage evolution, from microcrack initiation and nucleation to the formation of localized damage zones. Once the material loses continuity, fracture mechanics principles provide a more rigorous basis for analysis.

Section 3: Factors Affecting Cracks in Asphalt Pavement

In addition to understanding the mechanisms of asphalt pavement cracking, it is also important to understand the factors that might influence asphalt field cracking potential, which may differ from those under controlled laboratory conditions. Several factors have been listed by various researchers (Abdel-Raouf, 1967; Monismith & Deacon, 1969).

Mixture Parameters

In designing an asphalt mixture, material properties are considered, including those of asphalt binder and aggregates, as well as mixture volumetrics, including air voids (AV). These have been shown to be important for good field performance and are easier to control compared to environmental factors.

The stiffness needed to resist and distribute loads comes from the aggregates used in the asphalt mixture. The quality and properties of aggregates play a major part in asphalt mixture performance (Monismith & Deacon, 1969). In addition, the absorptive nature of aggregates has been shown to affect the cracking potential of the asphalt mixture (Zhou & Scullion, 2005). Therefore, the quality of the aggregates should be kept in mind when designing an asphalt mixture.

One of the primary components that dictate asphalt mixture cracking potential is asphalt binder. The binder is responsible for dissipating induced loading and associated energy due to its viscoelastic nature. The relaxation properties could be indicated by the viscosity of a binder (Roque & Ruth, 1990). Asphalt binder is also the weaker component in the asphalt mixture, and therefore is where cracks appear to originate (Doll et al., 2017a).

In addition to relaxation properties, binder low-temperature properties are important (Collop & Cebon, 1995). However, higher flexibility does not always lead to better cracking-resistance (Ali et al., 2019). Asphalt binder chemistry might also affect pavement performance due to steric hardening (Wang, 2018). Hence, polymers and fibers have been used to modify neat binders to reduce asphalt cracking potential (Lee et al., 2005; Norouzi et al., 2016).

After selecting both aggregates and asphalt binder, a mixture design is developed. Increasing asphalt binder content would generally lead to more dissipation of energy and, therefore, less cracking potential (Jacobs et al., 1996; Mobasher et al., 1997). Harvey et al. (1995) showed that AV also play a significant role in characterizing asphalt cracking potential. Increasing AV would increase asphalt cracking potential due to the introduction of relatively weaker points in the mixture matrix and a decrease in the cohesive energy of the asphalt binder (Pirmohammad et al., 2016).

Today, the use of reclaimed asphalt pavement (RAP) and recycled asphalt shingles (RAS) is common in asphalt mixture design. These materials make the asphalt mixture stiffer and reduce its energy dissipation properties (Doll et al., 2017b). The increased stiffness is valuable for strength (Krishna Swamy et al., 2011) and resistance to moisture (Mogawer et al., 2011); however, it adversely impacts cracking potential. These stiffer materials lead to a relatively smaller FPZ and therefore reduce the energy dissipation mechanism of an asphalt mixture (Behnia et al., 2011; Doll et al., 2017a; Li & Gibson, 2016).

To overcome this drawback and increase energy dissipation, softeners and warm mix additives (WMA) have been added proportionally to asphalt mixtures with recycled materials. Both techniques have been shown to work well in the field, but long-term performance has yet to be demonstrated (McDaniel et al., 2012).

Environmental and Traffic Impact

In addition to vehicular loading, weather changes affect pavement life and are difficult to control. Temperature variation of asphalt pavements greatly affects the latter's structural capacity. Due to asphalt binder thermal properties, asphalt exhibits a thermal gradient within the pavement structure. The difference in thermal coefficients of aggregates and asphalt binder results in thermal stresses (Kim, 2005). At relatively low temperatures, adhesive failure may occur (Chen et al., 2022).

In addition to stresses, temperature also impacts asphalt pavement's fracture toughness (Mobasher et al. , 1997). This leads to the creation of a stiffness gradient that is also affected by aging (Kim et al., 2009; Roque et al., 2010). The stiffness gradient amplifies the loading stress intensity and increases cracking potential (Germann & Lytton, 1979). This could be aggravated by thermal cycles (Wang et al., 2005).

In addition to axle loading, tire configuration has a significant impact on asphalt pavement crack development (Ann Myers et al., 1999; Ann Myers & Roque, 2002; Baek & Al-Qadi, 2006; Gamez & Al-Qadi, 2019; Hernandez & Al-Qadi, 2015; Jacobs, 1995; Wang, Al-Qadi, et al., 2013). The presence of defects during construction could be detrimental to the overall health of the pavement due to stress concentration (Roque et al., 2010; Wang & Al-Qadi, 2010). The next section details the various cracks resulting from the aforementioned factors.

Section 4: Asphalt Pavement Cracking Types

When the stresses in asphalt pavement reach a relatively high level, the material seeks a lower energy state. Cracks may develop within the material as it evolves toward a lower energy state. Crack initiation dissipates the stored energy via surface energy release, heat dissipation, and plasticity. The crack may be classified as load-related, which is directly affected by traffic loading, or as non-load-related, which encompasses weather and pavement foundation effects. The following sections discuss asphalt pavement crack types and mechanisms.

Thermal Cracking

Asphalt pavement cracking may be caused by low temperatures or high rates of cooling. Thermally induced tensile stresses coupled with a reduction in stress relaxation capacity in the asphalt layer are the main cause of thermal cracking (Marasteanu et al., 2012). Pavements in northern regions of the United States are more prone to low-temperature cracking due to the extremely low temperatures throughout the winter.

In a restrained surface layer, contraction induced by cooling leads to the generation of thermal tensile stresses. Because there is greater constraint in a pavement's longitudinal direction compared to the vertical direction, thermal stresses often develop along the pavement's longitudinal direction (Kim, 2005). However, for relatively large airports, thermal cracks may develop in both the transverse and longitudinal directions of runways, aprons, and taxiways. Minor thermal stresses may also develop in the vertical direction due to differential thermal contraction of the asphalt binder and aggregates (Kim & El Hussein, 1995).

Source: Imad L. Al-Qadi

Figure A-8. Thermal Cracking

The friction between the asphalt layer and the underlying material can affect the restraint of the asphalt layer. Lower friction leads to greater crack spacing. The developed thermal stress might cause slippage to relieve some stress and cause thermal cracking to appear in the longitudinal direction. Thermal stresses are typically greatest on the pavement surface because the pavement surface temperature is lowest throughout the cooling phase (Collop & Cebon, 1995).

The coalescence of these thermal cracks leads to the formation of block cracking. Block cracking is highly influenced by the stiffness gradient near the pavement surface, which usually results in higher stress concentrations on the surface itself forming a network of thermal cracks. The relatively higher asphalt mix elastic modulus at low temperatures leads to the curvature pattern near a cracked boundary (Wang, 2018).

Reflective Cracking

One of the most common rehabilitation techniques used in the United States is placement of an asphalt overlay over a distressed pavement surface. The overlay is usually bonded with the underlying layer. Any movement of the joints or cracks in the underlying layer develops highly localized stresses in the overlay. These stresses are magnified by traffic and/or thermal loading, as shown in Figure A-9.

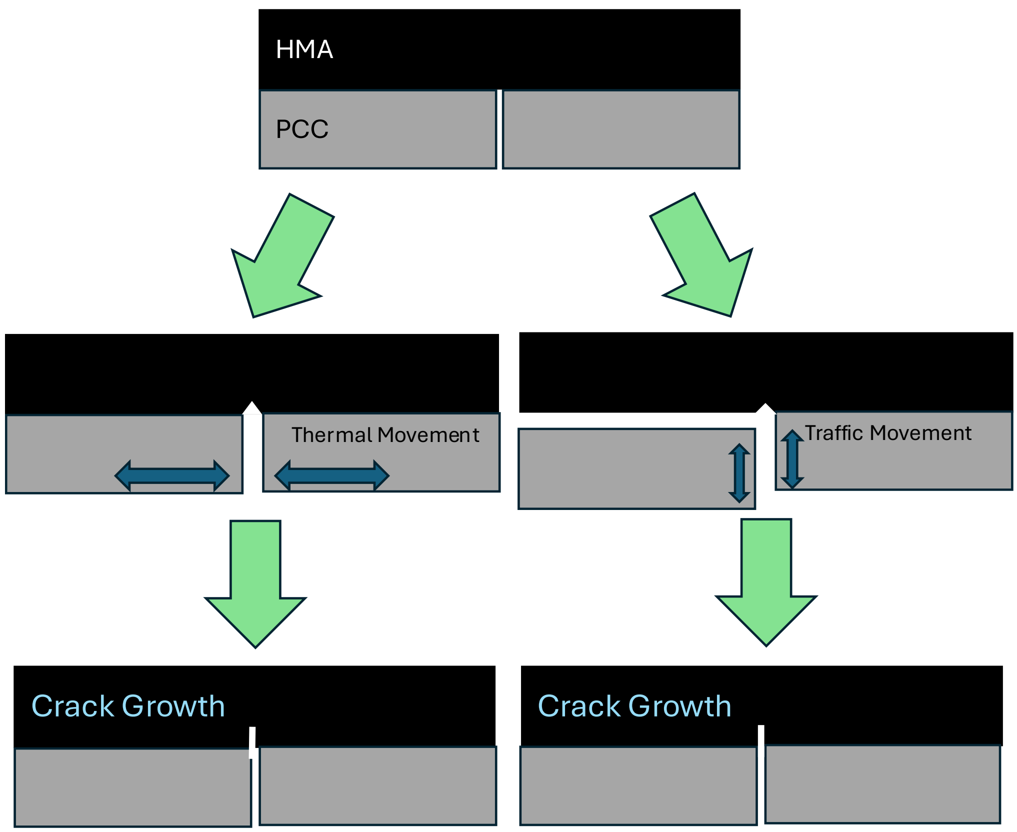

HMA = hot mix asphalt; PCC = Portland Cement Concrete.

Source: AAPTP

Figure A-9. Mechanisms of Reflection Cracking

The induced stresses are calculated using the relaxation properties of the asphalt mix and the movement occurring at the joint/crack. When the tensile stresses exceed the tensile strength of the overlay, macrocrack initiation and propagation begin. Crack initiation is best investigated using fatigue methods, while crack propagation may be estimated using fracture mechanics principles (Son, 2014). These cracks can lead to stress localizations on the surface and poor load transfers, which make them a precursor to fatigue cracking (Germann & Lytton, 1979).

Source: Imad L. Al-Qadi

Figure A-10. Reflective Cracking

Fatigue Cracking

Fatigue cracking is a load-associated distress that results from repeated heavy traffic loading and is one of the primary distresses for pavements at intermediate temperatures. Tensile and shear stresses (mixed-mode) are the primary contributors to fatigue cracks in asphalt pavements (Myers et al., 2001; Little et al., 1999). Fatigue cracks may be either adhesive (form between aggregates and asphalt mastic) or cohesive (form within the asphalt mastic).

Moving vehicle tires cause complex stress states in the pavement. The tires might exert bending-induced surface tensile stresses in the longitudinal direction for relatively thin pavements. For thicker pavements, shear induces near-surface tensile stresses, which may be more critical. Pavement thickness affects the induced stresses and, therefore, the resulting cracks (Myers & Roque, 2002; Molenaar, 1984; Roque et al., 2010). In addition to traffic, age hardening influences fatigue stresses. Roque et al. (2004) showed that tensile and shear stresses increased with asphalt pavement aging due to the reduction in its energy dissipative abilities.

Source: Imad L. Al-Qadi

Figure A-11. Fatigue Cracking

Fatigue cracking can be further divided into subcategories depending on initial crack originations.

Bottom-up Cracking

Fatigue cracking is generally considered a bottom-up distress (Huang, 1993). Miner's Law is used to predict total fatigue life. An empirical relationship is used to correlate field cracking with tensile strains at the bottom of the asphalt layer, which is considered to be the damage zone. The primary damage mechanism was thought to be bending stresses induced under wheel loads that propagate through the asphalt layer. Therefore, earlier mechanistic designs considered bottom-up cracking as the most prevalent fatigue distress. To improve resistance to fatigue damage, the concept of thicker, perpetual pavements was applied.

Top-Down and Near Surface Cracking

As the use of relatively thick pavement sections has increased, an increase in top-down cracks has been reported. These cracks resulted from surface tensile stresses in the longitudinal direction as well as shear-induced stresses at the tire edges (Canestrari & Ingrassia, 2020; Roque et al., 2010). The presence of defects in the asphalt layer could also affect crack propagation. The likelihood of top-down cracking has been shown to increase with increasing temperature and asphalt pavement thickness (Zhao et al., 2018). These cracks initially appear as single cracks in the wheel path or along construction joints in pavements, but with repeated loading new cracks tend to appear in the vicinity of the original crack. With time, they start to form an alligator cracking pattern on the pavement, interlinking with each other (Ling et al., 2019). The asphalt pavement surface is more susceptible to cracking due to aging.

However, studies showed that these cracks are mainly due to vertical shear strain in the upper part of the asphalt layer, referring to them as near-surface cracks (Wang & Al-Qadi, 2010). The vertical shear strain developed due to high contact stresses of tire ribs. These cracks coalesce below the surface, and due to the complex stress states, they propagate in both upward and downward directions (Wang et al., 2013). Hence, tire acceleration, deceleration, and cornering tend to increase the potential for near-surface cracking significantly. In addition, poor construction and debonding between asphalt layers can increase the stress intensity factors at these depth levels, leading to near-surface cracks being easier to initiate and propagate. These cracks usually initiate at approximately 2–3 inches below the surface for highway pavements and 3–4 inches below for airports.

Section 5: Characterization of Cracks in Asphalt Materials

The fracture process in asphalt mixtures is complex due to the heterogeneous nature of the mixtures (asphalt binder, aggregates, and AV are primary phases) and vehicular and environmental loading. It has been shown that a fracture process zone of appreciable size (often more than 15 mm) exists ahead of the potential crack path in asphalt mixtures (Rivera-Pérez et al., 2021). Hence, tests that measure only peak stress fail to fully evaluate cracking progression in asphalt mixtures.

Depending on the predominant mode of cracking in asphalt materials, laboratory tests are often classified into three categories: low-temperature cracking, intermediate-temperature cracking, and cyclic degradation or fatigue cracking tests. This section presents a summary of various asphalt mixture cracking tests that have been developed and applied to assess cracking in asphalt pavements. A literature review was performed to identify cracking tests for typical asphalt mixture designs that could be part of a BMD framework. Current laboratory cracking tests include the following:

- Disk-shaped Compact Tension Test (ASTM D7313, 2020)
- Semi-Circular Bend Test (Low Temperature) (AASHTO T 394, 2021)
- Indirect Tensile Creep and Strength Test (AASHTO T 322, 2007)
- Illinois Flexibility Index Test (AASHTO T 393, 2021)
- Louisiana Semi-Circular Bend Test (ASTM D8044, 2016)
- Asphalt Mixture Performance Tester Cyclic Fatigue Test (AASHTO T 400, 2022)
- Texas Overlay Test (Texas DOT, 2022)
- Flexural Bending Beam Test (AASHTO T 321, 2022)
- Cyclic Disk-shaped Compact Tension Test
- Complex (Dynamic) Modulus Test (AASHTO T 342, 2022)
- Cracking Tolerance Index Test (ASTM D8225, 2019)

Thermal Cracking

Disk-Shaped Compact Tension (DCT) Test

The DCT test for asphalt mixtures was proposed by Wagoner et al. (2005) and has been refined through subsequent efforts, including Marasteanu et al. (2012), to measure the cracking potential of asphalt mixtures at low temperatures. This test was modified from the compact tension test originally developed for measuring fracture toughness (K_{IC}) in metals. The test procedure has been refined and revised to make it better suited for asphalt mixture design and production control through efforts supported by the Minnesota Department of Transportation (DOT) (Dave et al., 2019). ASTM D7313 (2020) covers a standard test method to conduct the DCT test, and the Minnesota DOT has a modified version with tighter specimen dimension tolerances and test temperature control.

In this test, a disk-shaped specimen with a notch (Figure A-12) is pulled apart until the post-peak load level is reduced to 0.1 kN. The DCT test is conducted in a crack-mouth opening displacement (CMOD)-controlled mode with an opening rate of 1 mm/min at a temperature 10 °C warmer than the required low-temperature performance grade (PGL) for the study mixture. The area under the load-CMOD curve obtained represents the fracture energy (G_f), and the ratio of fracture energy to peak strength before failure is called the fracture strain tolerance (FST) parameter (Zhu et al., 2017). Higher values of both these parameters indicate a higher cracking resistance of asphalt mixtures. The test can be performed on gyratory-compacted, laboratory-prepared specimens and specimens obtained from field cores.

Source: AAPTP

Figure A-12. Typical DCT Test Setup

Standard test method: ASTM D7313 (2020), *Standard Test Method for Determining Fracture Energy of Asphalt Mixtures Using the Disk-Shaped Compact Tension Geometry*.

Test parameters:

- Specimen geometry: 150±10 mm diameter and 50±3.5 mm thick, two 25±1 mm holes, and a 62.5±5 mm notch
- CMOD opening rate: 1 mm/min
- Test temperature: PGL + 10 °C
- Measured parameters: fracture energy (G_f) and FST

Semi-Circular Bend (SCB) Test

The SCB test for low-temperature cracking was developed by Li & Marasteanu (2004). It was subsequently revised (Marasteanu et al., 2012) to measure the cracking potential of asphalt mixtures at low temperatures and presented in AASHTO T 394-21 (2021). Similar to the DCT test, the SCB is often conducted in a CMOD-controlled mode with an opening rate of 0.0005 mm/s at 10 °C warmer than the PGL of the binder. However, the fracture work measure is determined using the load line displacement (LLD). Figure A-13 shows the SCB test setup for asphalt mixtures. Like the DCT test, the SCB test may be performed on laboratory-prepared specimens and specimens obtained from the field. Fracture toughness, K_{IC}, can be computed using Equation A-10. Recall that K_{IC} is defined as the stress intensity factor corresponding to the initiation of the crack and can be considered a material property. The stiffness (S) is calculated as the slope of the linear part of the ascending load-LLD curve.

Source: AAPTP

Figure A-13. Typical SCB Test Setup with CMOD Gauge

$$K_{IC} = Y_{I(0.8)}\sigma_0\sqrt{\pi a} \qquad \text{(A-110)}$$

where,

Y_I = dimensionless geometric factor,

σ_0 = applied stress (MPa), calculated as $\frac{P}{2rt}$,

r = specimen radius (m),

t = specimen thickness (m),

a = notch length (m), and

$$Y_{I(0.8)} = 4.782 - 1.219\frac{a}{r} + 0.063\ exp\left[7.045\left(\frac{a}{r}\right)\right]$$

Dave & Behnia (2018) utilized low-temperature SCB tests conducted in a CMOD-controlled mode with a CMOD rate of 0.7 mm/min to obtain fracture properties of asphalt mixtures.

They demonstrated that by using a cohesive zone fracture model, local fracture properties of the asphalt mix could be calculated, which were independent of test geometry and CMOD rate. They used the cohesive zone model and DCT test to predict low-temperature SCB test results.

Standard test method: AASHTO T 394-21 (2021), *Determining the Fracture Energy of Asphalt Mixtures Using the Semicircular Bend Geometry (SCB)*.

Test parameters:

- Specimen geometry: 150±9 mm in diameter and 24.7±2 mm thick, a notch with 15±0.5 mm length and no wider than 1.5 mm
- CMOD opening rate: 0.0005 mm/s
- Test temperature: PGL+10 °C
- Measured parameters: fracture energy (G_f), fracture toughness (K_{IC}), and stiffness (S)

Indirect Tensile (IDT) Test

Building on the indirect tensile test for asphalt mixes presented by Kennedy in the 1970s (Kennedy, 1977), Roque and colleagues at Pennsylvania State University developed the Superpave IDT test (AASHTO T 322) for low-temperature cracking during the SHRP (Buttlar & Roque, 1994; Roque & Buttlar, 1992). The test measures both creep compliance and tensile strength of asphalt mixes at low temperatures. These parameters are used as inputs in the AASHTOWare® Pavement ME Design software to predict low-temperature cracking of asphalt pavements.

In this test, a cylindrical specimen with a diameter of 150 mm and a thickness of 38–50 mm is subjected to a compressive load across the diametral plane. The creep test involves holding a load level constant for 1,000 s, which produces a horizontal displacement between 0.00125 mm and 0.019 mm. During the loading process, the horizontal and vertical displacements are recorded and used to determine creep compliance and stiffness as a function of time. In the strength test, the specimen is loaded at a constant LLD rate of 12.5 mm/min until failure to determine tensile strength, and strength is calculated based on specimen dimensions and peak load. Figure A-14 shows the IDT test setup and typical creep compliance curves. The test may be performed on laboratory-prepared specimens and cores obtained from the field.

Standard test method: AASHTO T 322 (2007), *Determining the Creep Compliance and Strength of Hot Mix Asphalt (HMA) Using the Indirect Tensile Test Device*.

Test parameters:

- Specimen geometry: 150±9 mm in diameter and 38- to 50-mm thick
- Loading rate for tensile strength test: 12.5 mm/min
- Measured parameters: creep compliance and tensile strength

Source: AAPTP

Figure A-14. Typical IDT Test Setup

Intermediate Temperature Cracking

Illinois Flexibility Index Test (I-FIT)

Research efforts at the Illinois Center for Transportation resulted in the development of the I-FIT to determine the fracture-potential parameters of an asphalt mixture at an intermediate temperature (AASHTO T 393, 2021). The I-FIT setup and a schematic of typical test outcomes are shown in Figure A-15 (Al-Qadi et al., 2015; Ozer et al., 2016). I-FIT specimens are prepared by cutting the cylindrical disc specimen in half to produce two dimensionally equivalent test specimens. Semicircular specimens should have smooth, parallel faces, a thickness of 50±1 mm, a diameter of 150±1 mm, and a notch length of 15±1 mm at center. The test is conducted using LLD control at a rate of 50 mm/min and the test is stopped when the load drops below 0.1 kN.

Source: AAPTP

Figure A-15. Typical I-FIT Test Setup

The Flexibility Index (FI) of an asphalt mixture is calculated from the fracture energy (G_f) and post-peak slope (m) of the LLD curve. FI is defined as the ratio of the fracture energy to the slope of inflection point at the post-peak stage of the load-displacement curve. A higher value of FI is generally preferred, indicating a better ability to resist cracking (Al-Qadi et al., 2015). Conversely, a relatively low FI provides a means of identifying brittle mixtures that may be prone to premature cracking. FI can be calculated using Equation A-11. Nemati et al. (2019) developed the Rate-Dependent Cracking Index (RDCI) to better discriminate asphalt mixtures with various mixture variables. The calculation of RDCI is shown in Equation A-12. This test can be easily performed on specimens obtained from gyratory-compacted cylinders or pavement cores with a diameter of 150 mm.

$$FI = A \times \frac{G_{\mathrm{f}}}{|\mathrm{m}|} \tag{A-12}$$

where,

G_f = fracture energy,
$|\mathrm{m}|$ = slope at the post-peak inflection point, and
A = unit correction coefficient taken as 0.01.

$$RDCI = \frac{\int_{t_{peak}}^{t_{0.1\,peak}} W_C \, dt}{P_{t_{peak}} \times ligament\ area} \times C \tag{A-13}$$

where,

$\int_{t_{peak}}^{t_{0.1\,peak}} W_C \; dt$ = post-peak area under the cumulative work versus time curve,
P_{tpeak} = instantaneous power at peak force,
C = unit correction factor set to 0.01, and
ligament area = specimen thickness × the ligament length.

Standard test method: AASHTO T 393-21 (2021), *Determining the Fracture Potential of Asphalt Mixtures Using the Illinois Flexibility Index Test (I-FIT)*.

Test parameters:

- Specimen geometry: 150±1 mm in diameter, 50±1 mm in thickness, notch 15±1 mm long and no wider than 2.25 mm
- Loading rate: 50 mm/min using LLD control
- Test temperature: 25±0.5 °C
- Measured parameters: fracture energy (G_f), post-peak slope (m), FI, and RDCI

Louisiana Semi-Circular Bend Test

Researchers at the Louisiana Transportation Research Center (LTRC) have proposed the Semi-Circular Bend (SCB) test at intermediate temperature for asphalt pavement fatigue cracking performance evaluation (Elseifi et al., 2012; Z. Wu et al., 2005). There are five differences between the LTRC-SCB test and the SCB for low-temperature cracking test as per ASTM D8044 (2016), which are as follows:

- Test temperature: (PGH +PGL)/2+4 °C
- SCB specimen thickness: 57 mm
- Three notch depths are required: 25, 32, and 37.5 mm
- Loading rate: cross-head controlled and deformation rate of 0.5 mm/min
- Calculated fracture property is critical energy release rate (J_c)

The LTRC-SCB test setup and typical test outcomes are shown in Figure A-16. The critical strain energy release rate is obtained by determining the change in strain energy to failure, U*,* with respect to notch depth, a. The strain energy to failure, U*,* is calculated as the strain energy up to the peak load, which can be calculated as shown in Equation A-13. The higher the J_c value, the better the fracture resistance of the asphalt mixture.

$$J_c = -\frac{1}{b}\left(\frac{dU}{da}\right) \qquad \text{(A-14)}$$

where,

J_c = critical strain energy release rate (kJ/m^2),
b = sample thickness (m),
a = notch depth (m),
U = strain energy to failure (kJ), and
dU/da = change of strain energy with notch depth (kJ/m).

Source: AAPTP
Figure A-16. LTRC-SCB Test Specimens

Standard test method: ASTM D8044 (2016), *Standard Test Method for Evaluation of Asphalt Mixture Cracking Resistance using the Semi-Circular Bend Test (SCB) at Intermediate Temperatures*.

Test parameters:

- Specimen geometry: 150±9 mm in diameter, 57±1 mm thick, notch no wider than 1.5 mm
- Loading rate: 0.5 mm/min
- Test temperature: $\frac{PG\ High\ Temperature + PG\ Low\ Temperature}{2} + 4$ (in °C)
- Measured parameters: critical strain energy release rate (J_c)

Fatigue Cracking

Asphalt Mixture Performance Tester (AMPT) Cyclic Fatigue (CF) Test

The original viscoelastic continuum damage fatigue model and related laboratory tests were simplified by Underwood et al. (2010) and Hou et al. (2010) and renamed the Cyclic Fatigue (CF) test, as described in AASHTO T 400 (2022). Complex modulus (E*) results are required to complete the fatigue damage analysis, even though E* values are not part of the CF test itself and thus must be obtained separately. Both E* and CF tests can be performed on an AMPT (shown in Figure A-17) or any other closed-loop control universal test machine. The CF test includes a dynamic modulus fingerprint test and two cyclic fatigue damage tests at different strain levels.

The viscoelastic continuum damage parameters, D^R (average reduction in integrity up to failure) and S_{app} (the accumulated damage when C [pseudo stiffness] is equal to 1-D^R), are determined from the test data using the FlexMAT™ software developed by the Federal Highway Administration (FHWA). D^R is calculated based on reduction of stiffness of the sample during the test and is therefore more closely related to the damage tolerance of the asphalt mixture. The S_{app} parameter is calculated based on dissipated energy in the sample with increasing numbers of cycles and therefore is more representative of the tradeoff between applied stress and strain, i.e., the material's stiffness and relaxation capability. D^R and S_{app} may be calculated using Equations 14 and 15, respectively. Typically, a higher value for both parameters indicates higher fatigue resistance.

Source: AAPTP

Figure A-17. AMPT Cyclic Fatigue Test Specimen and Setup

$$D^R = \frac{\int_0^{N_f}(1-C)dN}{N_f} = \frac{\sum(1-C)}{N_f} \quad \text{(A-15)}$$

where,

N = number of load cycles,
N_f = maximum number of load cycles up to failure, and
C = normalized pseudo-stiffness, which decreases from the value of 1 as the damage accumulates.

$$S_{app} = 1000^{\frac{\alpha}{2}-1} \frac{a_t^{\frac{1}{\alpha}+1}\left(\frac{D^r}{C_{11}}\right)^{\frac{1}{C_{12}}}}{|E^*|^{\alpha/4}} \quad \text{(A-16)}$$

where,

C_{11}, C_{12} = the model coefficients in C-S curve determined from S-VECD theory,
α = damage model power term, and
E^* = dynamic modulus.

Standard test method: AASHTO T 400 (2022), *Determining the Damage Characteristic Curve and Failure Criterion Using the Asphalt Mixture Performance Tester (AMPT) Cyclic Fatigue Test*.

Test parameters:

- Specimen geometry: 100 mm in diameter and 130±2.5 mm in height
- Loading frequency: 10 Hz at a target strain range of 50 to 75 microstrain
- Test temperature: between 5 and 25 °C

- Measured parameters: damage characteristic curve, average reduction in integrity up to failure (D^R), and accumulated damage (S_{app})

Texas Overlay Test

Germann & Lytton (1979) initially developed the Texas Overlay Test (OT) in the late 1970s. TxDOT (Texas DOT, 2022) and New Jersey DOT (NJDOT B-10, 2007) have both adopted the revised OT method that Zhou & Scullion (2005) thoroughly updated and standardized later on. The key components of the OT device consist of two steel plates, one fixed and the other able to move horizontally (Figure A-18), simulating the opening and closing of joints or cracks in the old pavements beneath an overlay. OT specimens are 150-mm long, 75-mm wide, and 37.5-mm thick. The specimen may be laboratory-prepared or obtained from the field. The OT is a cyclic displacement-controlled test that uses a triangular loading wave pattern with a period of 10 s/cycle. Although both test temperature and opening displacement can vary, the OT is typically run at room temperature (25 °C) with a maximum opening displacement of 0.006 mm.

Source: AAPTP

Figure A-18. Texas Overlay Tester Setup

The specimen is considered failed when the cycle peak load drops by 93 percent with respect to the first peak loading cycle or, alternatively, if a pre-set value of cycles (e.g., 1,000) is reached. The number of load cycles until failure is recorded at the termination of the test. Additionally, the measured load versus displacement curve can be used to infer the fracture parameters (A and n) (Zhou et al., 2007).

Standard test methods:

- *Tex-248-F (Revised) (2022), Test Procedure for Overlay Test*
- *NJDOT B-10 (2007), Overlay Test for Determining Cracking Resistance of HMA*

Test parameters:

- Specimen geometry: 150-mm-long, 75-mm-wide, and 37.5-mm-thick
- Loading frequency: 0.1 Hz
- Test temperature: 25 °C
- Maximum opening displacement: 0.006 mm
- Measured parameter: number of cycles to failure

Flexural Bending Beam Test

Monismith and colleagues at the University of California, Berkeley, proposed the Flexural Beam Fatigue Test under the SHRP Project A-003A (Strategic Highway Research Program, 1994). The current AASHTO T 321 (2022) is a refined version of the proposed test. The beam specimen is 380 mm long, 50 mm wide, and 63 mm thick, and the applied loading rate is variable but is normally set at 10 Hz. Generally, testing is performed at intermediate temperatures, usually 20 °C. The test can be conducted in either stress- or strain-controlled mode. The strain-controlled mode is widely used because it appears to provide results comparable to field observations. The test involves four clamps holding the beam in place while a repeated haversine (or sinusoidal squared) loading is supplied to the two inner clamps, and a reaction load is applied to the outer clamps (Figure A-19). Consequently, there is a continuous bending moment over the center of the beam between the two inside clamps.

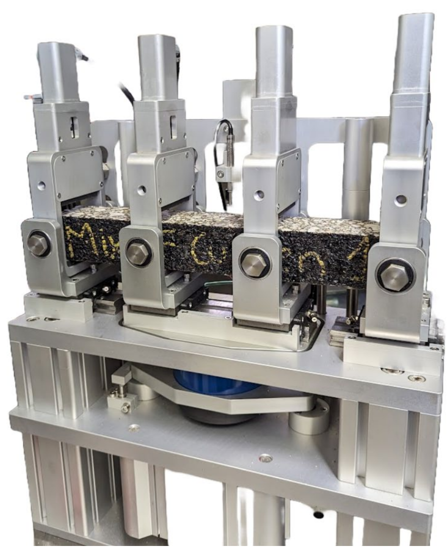

Source: AAPTP

Figure A-19. Typical Four-Point Flexural Beam Fatigue Test Setup

Standard test method: AASHTO T 321 (2022), *Standard Method of Test for Determining the Fatigue Life of Compacted Hot-Mix Asphalt (HMA) Subjected to Repeated Flexural Bending*.

Test parameters:

- Specimen geometry: 380-mm-long, 50-mm-wide, and 63-mm-thick
- Loading frequency: 10 Hz
- Test temperature: 20 °C
- Measured parameters: number of cycles to failure, dissipated energy

Cyclic Disk-shaped Compact Tension Test

The DCT test can also be performed under cyclic loading, a configuration called the Cyclic DCT Test (CDCT) (Chiangmai, 2014). Loading rates for CDCT are generally selected based on the peak load obtained during a standard DCT test. CDCT uses specimens with a modified geometry with a crack tip opening displacement (CTOD) gauge fixed with a 10-mm offset instead of the CMOD gauge used in a standard DCT test. Currently, there is no standardized test protocol for CDCT. Initial-stage fracture energy (Gf_{ini}) and initial and total dissipated energy (IDE and TDE) are fracture parameters that can be obtained from a CDCT test. Gf_{ini} is defined as the ratio of released energy dissipated at the 50th cycle (RE_{ini}) to the cracked area of the specimen.

Strength and Modulus Approach

Complex (Dynamic) Modulus Test

Complex modulus (E*) is one of the most critical parameters used to evaluate both the rutting and fatigue cracking distress predictions needed for flexible pavement design using the AASHTOWare Pavement ME Design software. AASHTO T 342 (2022) covers the standard test method to determine the dynamic modulus. The complex modulus is the ratio of the peak dynamic stress (σ_o) to the peak recoverable axial strain (ε_o) for a linear viscoelastic material under a continuous harmonic loading. A sinusoidal (haversine) axial compressive stress is applied to a specimen of asphalt at a given temperature and loading frequency. The viscous behavior of asphalt is indicated by the phase angle (δ), which is the angle by which ε_o lags behind σ_o. In a purely elastic material, strain will follow stress immediately, i.e., a phase angle of 0 degrees. The closer the phase angle is to 90 degrees, the more viscous the material is.

A cylindrical specimen with a diameter of 102 mm and a height of 150 mm is subjected to a series of cyclic loading at frequencies of 0.1, 0.5, 1.0, 5, 10, and 25 Hz at different temperatures. Figure A-20 shows the test specimen for the dynamic modulus test inside the AMPT machine. The applied stress and the resulting recoverable axial strain response of the specimen are measured and used to calculate the dynamic modulus and phase angle. Generally, dynamic modulus values measured over a range of temperatures and loading frequencies are shifted into a master curve for characterizing asphalt mixtures for pavement thickness design and performance analysis.

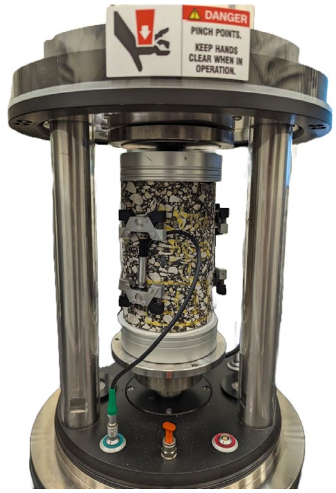

Source: AAPTP

Figure A-20. Typical Dynamic Modulus Test Specimen

Standard test method: AASHTO T 342 (2022), *Determining Dynamic Modulus of Hot Mix Asphalt (HMA)*.

Test parameters:

- Specimen geometry: 102±2 mm in diameter and 150±2.5 mm in height
- Loading frequency: 0.1, 0.5, 1.0, 5, 10, and 25 Hz
- Test temperature: –10, 4.4, 21.1, 37.8, and 54 °C
- Measured properties: complex modulus (E*) and phase angle (δ)

Cracking Tolerance (CT) Index Test

Zhou et al. (2017) proposed the Indirect Tensile Asphalt Cracking Test (IDEAL-CT) to characterize the fracture potential of an asphalt mixture at an intermediate temperature (ASTM D8225, 2019). A cylindrical specimen 150 mm in diameter and 62 mm thick is subjected to compressive loads across the diametral plane (Figure A-21). The test is conducted using LLD control at a rate of 50 mm/min and is stopped when the load drops below 0.1 kN. During testing, a data acquisition system records time, load, and displacement at a minimum sampling rate of 40 data points per second. The recorded data are then used to calculate the Cracking Tolerance Index (CT Index). The CT Index, which combines total energy dissipation during the test with the post-peak shape of the load-displacement curve, is calculated using Equation A-16. Generally, a higher CT_{Index} value indicates a lower cracking potential. The test may be performed on laboratory-prepared specimens and specimens obtained from field cores.

$$CT_{\text{Index}} = \frac{G_f}{|m_{75}|} \times \left(\frac{l_{75}}{D}\right) \quad \text{(A-17)}$$

where,

G_f = failure energy (total shaded area under the load-displacement curve),
l_{75} = displacement at the 75 percent point,
$|m_{75}|$ =slope at the 75 percent point, and
D = specimen diameter (mm).

Source: AAPTP
Figure A-21. Typical CT Index Test Setup

Standard test method: ASTM D8225 (2019), *Standard Test Method for Determination of Cracking Tolerance Index of Asphalt Mixture Using the Indirect Tensile Cracking Test at Intermediate Temperature*.

Test parameters:

- Specimen geometry: 150±2 mm in diameter, 62±1 mm in height (for nominal maximum aggregate size [NMAS] ≤19 mm)
- Loading rate: 50±2 mm/min using LLD control
- Test temperature: (PGH + PGL)/2+4 (in °C)
- Measured parameter: Cracking Tolerance Index (CT_{Index})

Indirect Tensile Strength Test

The procedure for conducting the IDT test to characterize the strength of asphalt mixtures is described previously under "Thermal Cracking" in Section 5.

Application of Fracture Tests in Airfield Asphalt Mixtures

Bennert et al. (2022) identified three different asphalt binder parameters that are sensitive to asphalt mixture fatigue cracking: the Glover–Rowe parameter at the intermediate temperature, the $(\text{loss tangent})^2$ at the intermediate temperature, and the $(\text{loss tangent})^2$ at

G*=10 MPa and found that these parameters correlated with the SCB FI and CT Index of two different airport mixtures. Similarly, Saqer et al. (2021) evaluated the effects of asphalt binder and aggregate gradation on cracking resistance of asphalt mixtures used in airport pavements using ITS and SCB tests. Although the asphalt mixtures had similar rankings based on the normalized fracture energy (NFE) and FI characteristics, the study's main finding was that the NFE exhibited less variability than the FI. The study concluded that NFE was effective in distinguishing the effect of the binder type on the cracking potential.

Yin & Barbagallo (2013) incorporated the OT to measure the reflective cracking potential of asphalt overlays. They tested five specimens at loading rates of one cycle per 30, 60, and 120 s at 32 °F and reported the average of the results. It was observed that the number of cycles to failure varied widely, ranging from a single digit to over 200 cycles. Also, Mandal et al. (2018) used a customized overlay tester (COT) and CDCT test to evaluate the fracture and fatigue performance of asphalt material collected from the full-scale pavement constructed at the National Airport Pavement Test Facility at low temperatures. They developed field shift factors as the primary output of their study to match full-scale test data to laboratory test findings.

Su et al. (2009) investigated warm mix asphalt (WMA) mixture performance and compared it with conventional HMA used for airfields through various laboratory tests. Results from the four-point flexural fatigue bending test and static three-point bending test showed that WMA mixtures produced at temperatures 30 °C lower than those used for conventional HMA exhibited comparable performance at intermediate and low temperatures compared to the control HMA mixture. Mirzaiyanrajeh et al. (2022) investigated the cracking performance of asphalt mix, WMA, and asphalt mix with RAP for airfields using complex modulus, SCB, and direct-tension cyclic fatigue tests. To accurately capture the fatigue performance limit in the airport pavement design model, the study underlined the need to develop performance-based specifications based on the nonlinear viscoelastic properties of asphalt mixtures and other useful aspects such as aging.

Bell (2009) investigated field and laboratory evaluations of aged asphalt pavements from several military airfields to develop a method for improving the prediction of fatigue life. The study proposed fatigue performance prediction models from field and laboratory test results. Shang et al. (2013) investigated the necessary Bailey parameters to obtain satisfactory performance of Superpave asphalt mixtures from Tokyo International Airport (HND) pavements. Fatigue bending test results indicated that the blends designed with the Bailey method provided better fatigue life than those designed by the conventional Superpave method.

Several studies used numerical modeling. For example, Kim & Buttlar (2009) incorporated fracture energy from the DCT test and creep compliance from the IDT test into an FE fracture model to evaluate cracking potential for airfield pavements. They observed that fracture energy of the asphalt mix depended on the loading rates and test temperatures.

Section 6: Balanced Mix Design

Introduction and History

BMD is an asphalt mixture design method that incorporates performance test results into the mixture design process. FHWA's Special Task Force on Asphalt Mixtures defined it as "asphalt mix design using performance tests on appropriately conditioned specimens that address multiple modes of distress taking into consideration mix aging, traffic, climate and location within the pavement structure." BMD incorporates two or more sets of performance tests to evaluate minimum rut depth and cracking potential to assess the asphalt mixture's ability to resist common forms of distress (West et al., 2018).

The most common approach is to optimize pavement performance by balancing the two major distress types: cracking and rutting. The balance between the two distress types is demonstrated in Figure A-22 using a pendulum analogy that was first introduced by Buchanan (Buchanan, 2016). The midpoint of the pendulum represents the optimum performance of the asphalt mixture between cracking and rut depth potential. This balance can be adjusted by modifying different volumetric characteristics or materials used in the mixture design process.

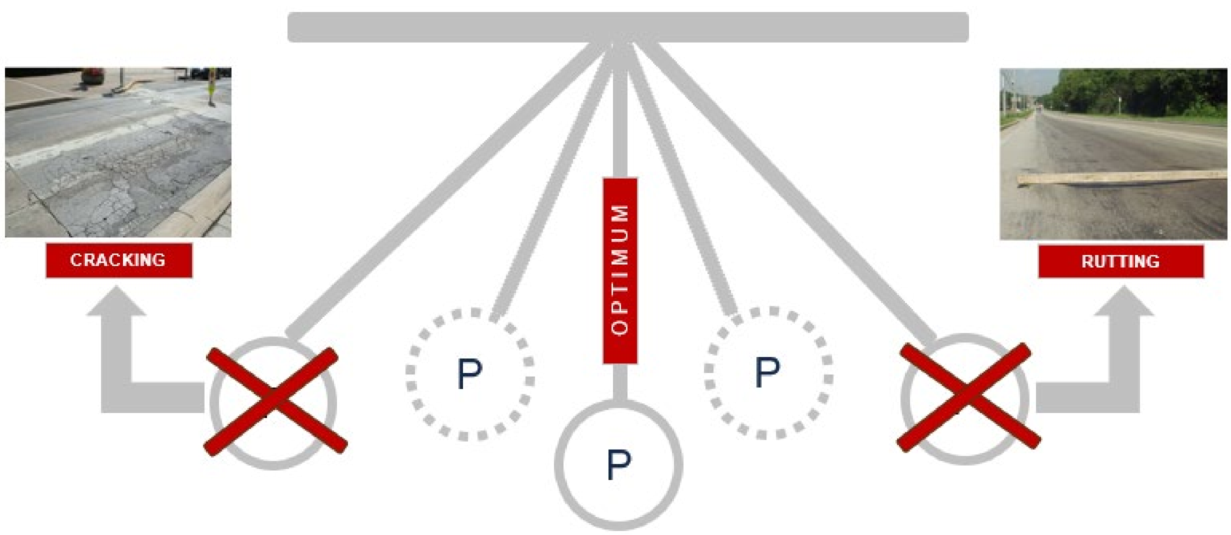

Source: AAPTP

Figure A-22. Performance Pendulum

In addition to traditional volumetric mixture design, various approaches have been developed to implement BMD. BMD can be implemented by finding the optimum binder content while targeting maximum performance from the rutting and cracking tests. Zhou and colleagues addressed this approach by setting a maximum asphalt binder content at which the rut-depth criterion was exceeded and putting the minimum asphalt content by the failure point of the cracking bar (Newcomb & Zhou, 2018). They suggested that the general goal of BMD is to reach an optimum combination of binder, aggregate, and other ingredients (e.g., RAP, mixture and binder modifiers, and rejuvenators) to meet permanent deformation and cracking criteria for a given level of traffic, climate, and pavement structure. Jichkar (2021) used the performance interaction diagram formulated with cracking and rut depth parameters to evaluate the characteristics of asphalt mixtures. The diagram allows using cracking (OT) and rut depth results from the Hamburg Wheel-Tracking Test (HWTT) to classify mixtures into four quadrants.

Researchers also proposed similar performance interaction diagrams incorporating other cracking tests and associated parameters such as I-FIT, DCT, and SCB. Al-Qadi and his colleagues developed the performance interaction diagrams using I-FIT and HWTT parameters (Al-Qadi et al., 2015) as shown in Figure A-23. The diagram was later expanded to a three-dimensional (3D) framework with the inclusion of a stiffness parameter, as seen in Figure A-24 (Ali et al., 2019). Buttlar and colleagues developed a similar space diagram using DCT and HWTT parameters (Buttlar et al., 2017).

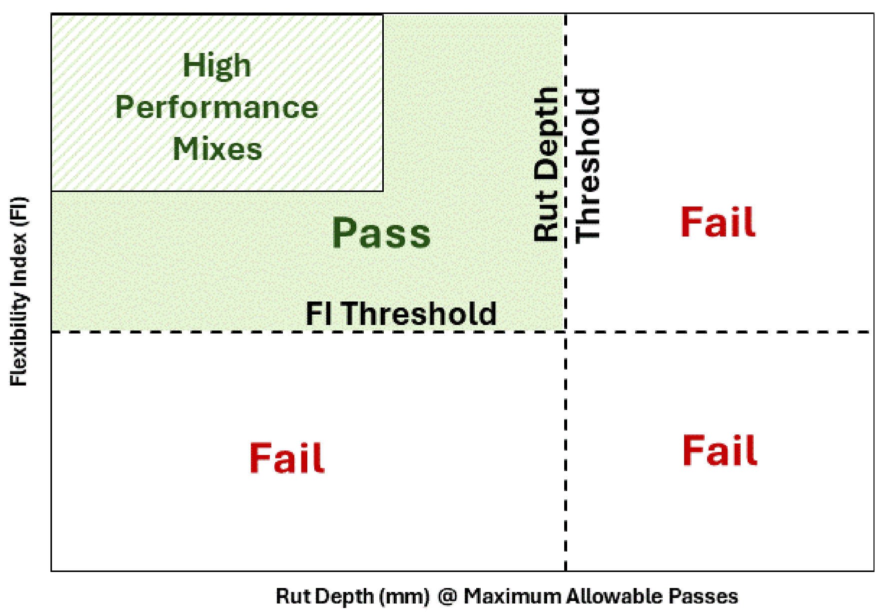

Source: Imad L. Al-Qadi

Figure A-23. Performance Interaction Diagrams (Al-Qadi et al., 2015)

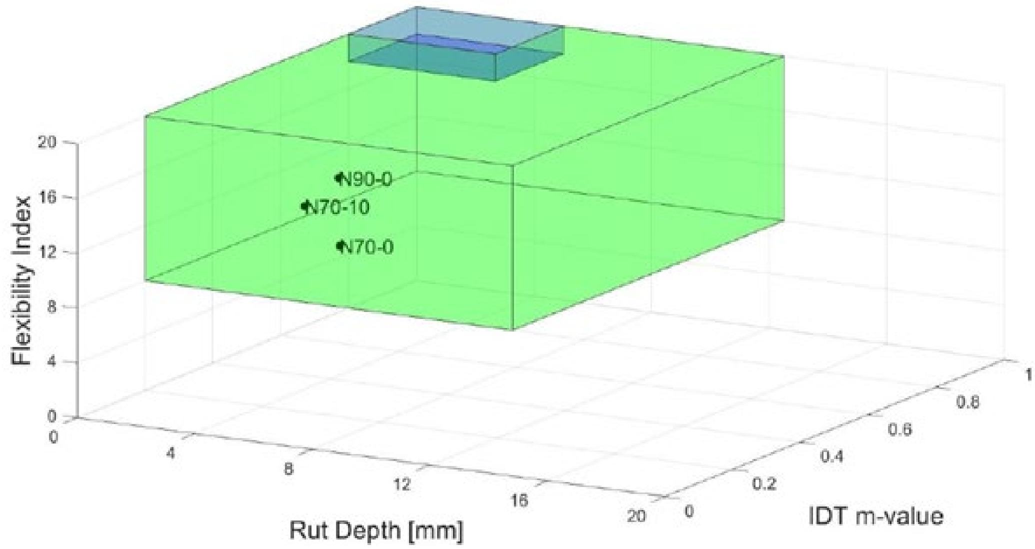

Source: Imad L. Al-Qadi

Figure A-24. 3D Interaction Diagram Showing Performance of the Mixes (Ali et al., 2019)

BMD Approaches

FHWA established the Performance Engineered Mixture Design (PEMD) program. PEMD focuses on engineering analysis and testing of asphalt mixtures on constituent material and mixtures to meet or exceed the pavement design requirements and performance life cycle. It also seeks to ensure that the mixture meets the performance criteria for a variety of pavement distresses, as BMD is designed for a specified level of traffic, climate, and pavement. PEMD can be categorized as index-based PEMD or predictive PEMD because it uses index tests to evaluate mixture design or mechanistic-empirical models to predict pavement performance.

The BMD approach can be considered part of FHWA's PEMD effort for asphalt mixtures. FHWA defines four approaches to implement BMD, as shown in Table A-1, that cover volumetric requirements, performance requirements, flexibility, and innovation potential. Approach A verifies mix performance after volumetric mixture design. Approach B complements volumetric design by adding performance tests as an optimization constraint. Both approaches retain the volumetric mixture design principles. However, performance becomes the primary basis for adjusting or improving the mixture design for Approaches C and D, in which volumetric parameters are partially or fully relaxed.

Table A-1. BMD Approaches (Hajj et al., 2021a, 2021b, 2021c, 2021d; Hajj & Aschenbrener, 2021)

Approach	Volumetric Requirements	Performance Requirements	Flexibility	Innovation Potential
A: Volumetric Design with Performance Verification	Full compliance	Full compliance	Most conservative	Lowest
B: Volumetric Design with Performance Optimization	Full compliance at preliminary optimum binder content	Performance optimization through moderate changes in the binder content	Slightly more flexible	Limited
C: Performance-Modified Volumetric Design	Some requirements may be relaxed or eliminated	Performance optimization by adjusting initial binder content or mixture component properties or proportions	Less conservative than A and B	Medium
D: Performance Design	Limited or no requirements	Performance optimization by adjusting mixture components and proportions	Least conservative	Highest

Figure A-25 illustrates FHWA's four BMD approaches in detail, offering guidance for States implementing BMD. To facilitate BMD implementation, FHWA's BMD Task Force established eight tasks as part of the mixture design approval and quality assurance (QA) process for agencies, some of which may be applied simultaneously:

1. Understanding the why and benefits of performance specifications.
2. Overall planning.
3. Selecting performance tests.
4. Performance testing equipment: acquiring, managing resources, training, and evaluation.
5. Establishing baseline data.
6. Specifications and program development.
7. Training, certifications, and accreditations.
8. Initial implementation.

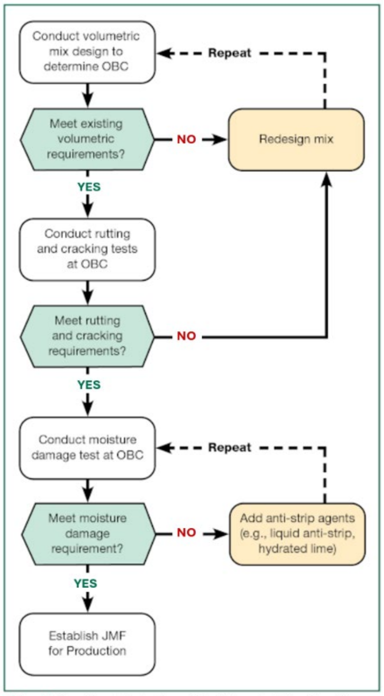

Figure1. Graphical Illustration of the Volumetric Design with Performance Verification Approach (**Approach A**)

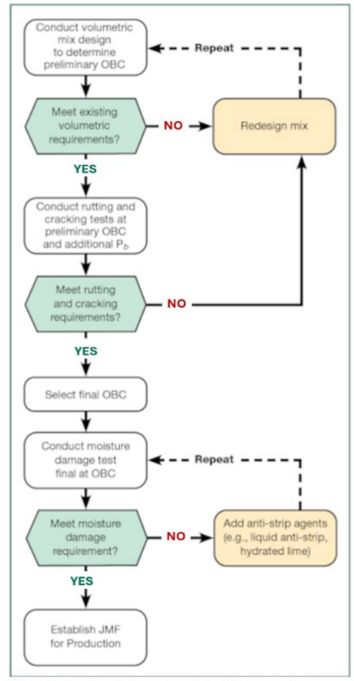

Figure 2. Graphical Illustration of the Volumetric Design with Performance Optimization Approach (**Approach B**)

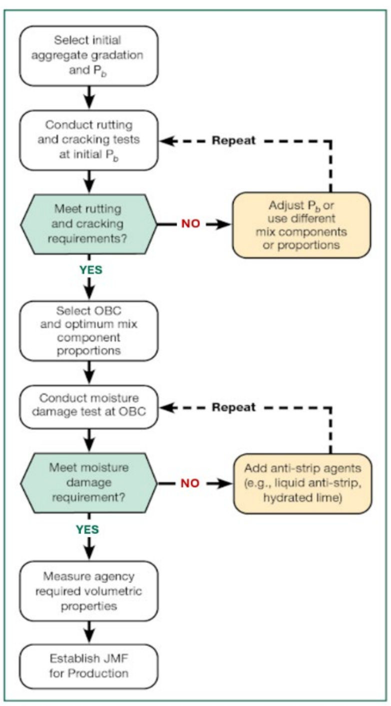

Figure 3. Graphical Illustration of the Performance-Modified Volumetric Design Approach (**Approach C**)

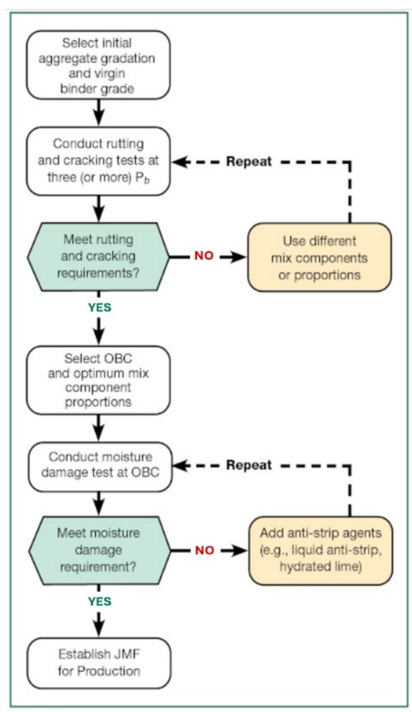

Figure 4. Graphical Illustration of the Performance Design Approach (**Approach D**)

JMF = job mix formula, OBC = optimum binder content.

Figure A-25. The Four BMD Approaches (Yin & West, 2021)

Current Implementation of BMD

According to a recent survey conducted by the National Center for Asphalt Technology (NCAT) for a National Asphalt Pavement Association (NAPA) study, some States have already started implementing BMD in their mixture design process (Yin & West, 2021). The map in Figure A-26 shows which States are employing the different BMD approaches introduced earlier and their implementation status.

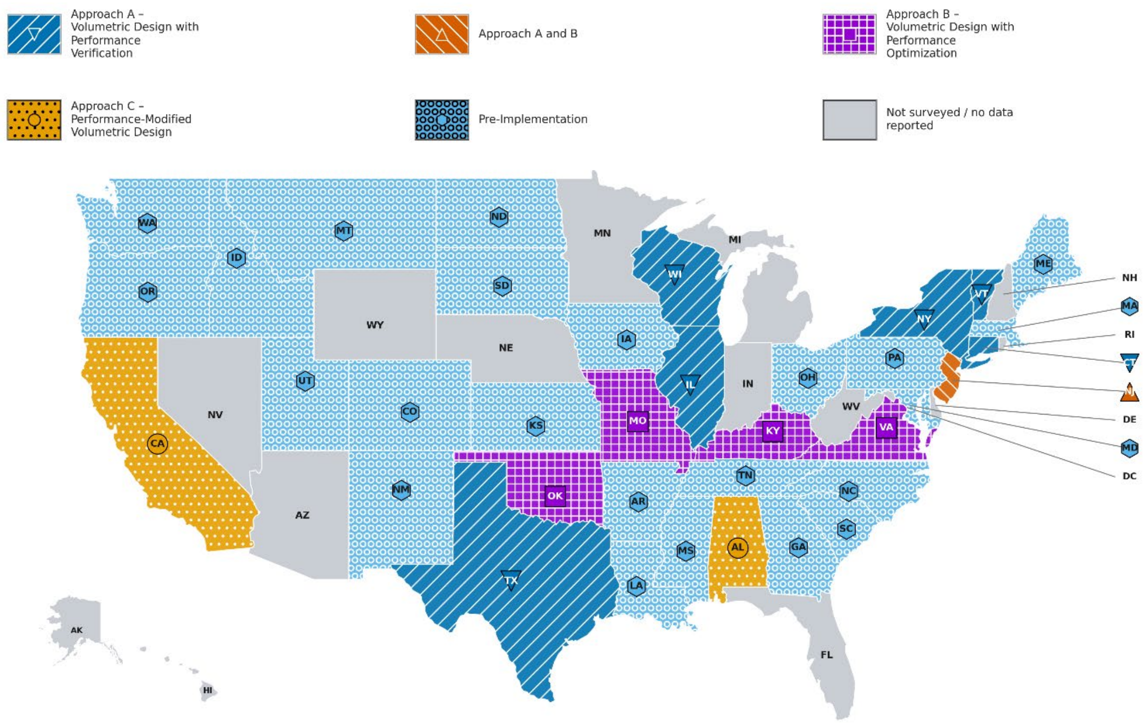

Source: AAPTP

Figure A-26. Map of States that Implement BMD (NAPA, 2026)

One of the primary steps in the BMD methodology is selecting the performance tests. Identifying the key or common distresses for a region or State is essential because test selection depends on the asphalt mixture type and the type of distresses of interest in the region (Zhou et al., 2021).

The following two maps (Figures A-27 and A-28) present the test selection for cracking and rutting potentials, respectively, for each State that is either implementing or has implemented the BMD methodology. A summary of selected State implementation examples follows.

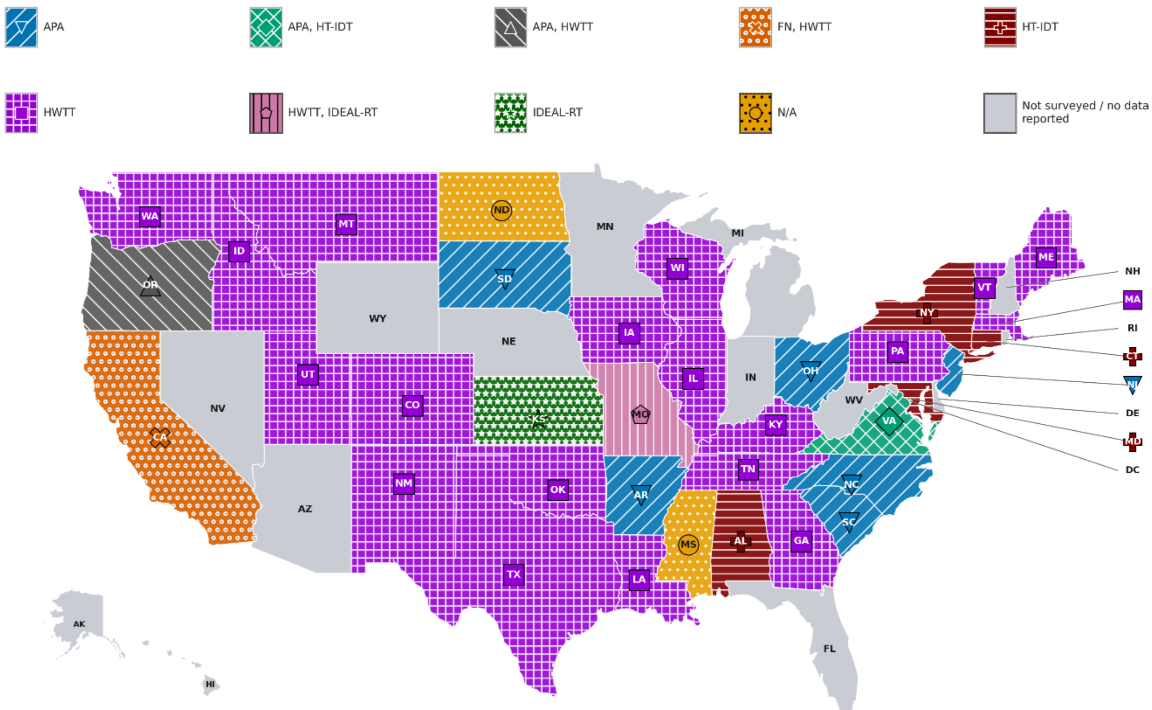

Source: AAPTP

Figure A-27. Rutting Test Selected for BMD by State (NAPA, 2026)

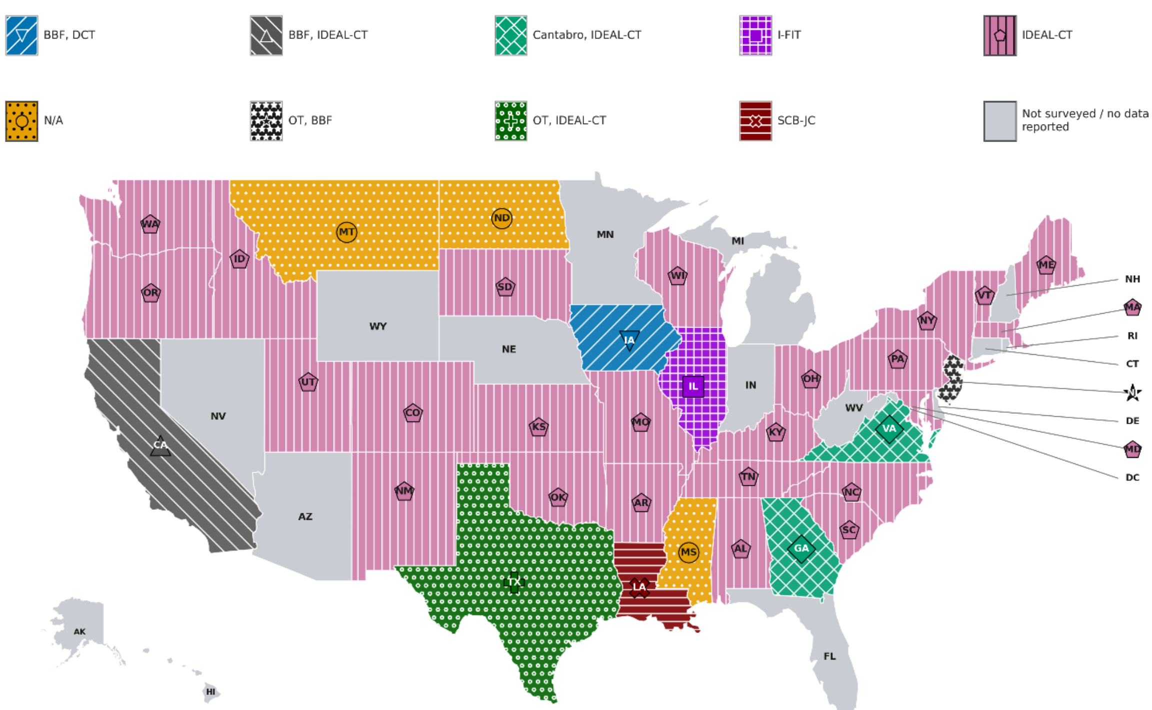

Source: AAPTP

Figure A-28. Cracking Test Selected for BMD by State (NAPA, 2026)

California

The California DOT (Caltrans) began implementing its Performance-Related Specification (PRS) based on mechanistic-empirical (ME) design in the late 1990s. In 2000, the University of California Pavement Research Center, Dynatest Consulting Inc., and Caltrans developed the CalME flexible pavement design software based on incremental-recursive damage models and material parameters from repeated load tests for fatigue and rutting and frequency sweeps for stiffness. Some of the critical elements of the PRS included efforts to increase compaction, use of stiffer binders in thick sections and polymer-modified binders in the surface layer, and testing of the mixtures using flexural beam fatigue (FBF) and repeated simple shear tests (RSST) (Wu et al., 2018).

Caltrans implemented the Superpave methodology for asphalt mix design into its Standard Specifications until 2014. This specification required using HWTT (AASHTO T 324, 2023) to identify rut depth potential and tensile strength (TS) for moisture susceptibility. Table A-2 shows the categories of mixtures used by Caltrans. Each category requires a specific PRS specification with different testing requirements and BMD approach. Mixtures are grouped into categories of PRS, Non-PRS, and Long-Life Asphalt Pavement (LLAP). Caltrans used this approach in five projects from 2003 to 2020.

Table A-2. Asphalt Mixture Types Used by Caltrans (Hajj et al., 2021a)

Mixture Type		Application
PRS and Non-PRS	Type A Asphalt	Surface, intermediate, or bottom course
	RHMA-G	Surface course
LLAP	AC-LL Polymer Modified Mixture	Surface course
	AC-LL Stiff Mixture	Intermediate course
	AC-LL Rich Binder Mixture	Bottom course

RHMA-G = Rubberized Hot Mix Asphalt-Gap Graded; AC-LL = asphalt concrete.

Caltrans has implemented BMD Approach A (Volumetric Design with Performance Verification) for their Non-PRS Type A Asphalt and Rubberized Hot Mix Asphalt-Gap Graded (RHMA-G) mixes. BMD Approach C (Performance-Modified Volumetric Design) is preferred for the LLAP mixes. Some Superpave volumetric requirements, such as the AV at N_{des} and voids in mineral aggregate (VMA), were relaxed or removed for the LLAP mixes. They are only reported for job mix formula (JMF) submittal. Table A-3 shows the essential modifications that Caltrans implemented to its volumetric design criteria; in some cases, the thresholds were shortened or decreased.

Table A-3. Modifications to AASHTO Standard Volumetric Design Criteria (Hajj et al., 2021a)

Requirements	Mixture Types	
	Type A Asphalt	RHMA-G
Number of Design Gyrations (N_{des})	↓	↓
Density at N_{des}	↔ / ↓	↔
Density at Initial Number of Gyrations ($N_{initial}$)	↑	–
Density at Maximum Number of Gyrations (N_{max})	↔	–
Design Asphalt Binder Content	–	–
Voids in Mineral Aggregate (VMA)	↑	↑
Voids Filled with Asphalt (VFA)	–	–
Dust-to-Asphalt Binder Ratio	↑ UL	R
HWT Passes at 12.5 mm Rut Depth	Min	Min
TS – Dry	Min	Min
TS – Wet	Min	Min

– Not applicable or not specified; Min = minimum; Max = maximum; ↔ = no change to requirement; ↓ = decreased; ↑ = increased; ↑ UL = increased upper limit; R = report only.

Table A-4 presents the performance test methods used by Caltrans (Wu et al., 2018). The critical factors for Caltrans in selecting a performance test for routine use are material sensitivity, field validation, and repeatability. The test must be sensitive to asphalt mixture component properties or proportions, AV, and aging.

Table A-4. Summary of Performance Tests Considered by Caltrans for BMD (Hajj et al., 2021a)

Elements	Rutting	Cracking	Moisture Damage
Test Name and Method	Non-PRS: HWTT (AASHTO T 324) PRS: RLT (AASHTO T 378 Modify)	Non-PRS: None. PRS: FBF (AASHTO T 321 Modify) I-FIT (AASHTO T 393)	Non-PRS: TS (AASHTO T 283) HWTT (AASHTO T 324) PRS: HWTT (AASHTO T 324)
JMF Requirement	Refer to Table A-3	Refer to Table A-3	Refer to Table A-3
QA/QC Implementation	Yes	Yes	Yes
Aging Protocol	Design verification is based on plant-produced asphalt mixtures. No additional laboratory aging is specified.	Design verification is based on plant-produced asphalt mixtures. No additional laboratory aging is specified.	Design verification is based on plant-produced asphalt mixtures. No additional laboratory aging is specified.
Notes	RLT implemented for I-5 (Sacramento) LLAP project. Prior LLAP projects used RSST.	Caltrans is exploring the use of I-FIT (AASHTO T 393) or CT Index test (ASTM D8225) to evaluate cracking potential of asphalt for typical mixture design and QA/QC testing.	

QA/QC = quality assurance/quality control.

Illinois

The Illinois DOT (IDOT) incorporated HWTT in its asphalt mix specifications in 2012 for rutting potential evaluation. In January 2016, the agency developed a special provision requiring the FI parameter for identifying cracking potential. In September 2020, the special provision was revised to make I-FIT a contract requirement for all asphalt mixtures.

In Illinois, RAP and RAS are widely used in asphalt mixes; RAS is mainly used in the Chicago area. With the increased use of RAP in asphalt pavements, the benefit of reduced rut depth potential is realized. However, the asphalt mixtures started getting drier, brittle, and more susceptible to premature cracking, especially in those with higher content of RAP and RAS; hence the importance of adding a cracking potential test requirement in the specifications. IDOT has three types of asphalt mixtures in its specification: high equivalent single axle load (ESAL) mixtures, low ESAL mixtures, and stone matrix asphalt (SMA) mixtures. Table A-5 summarizes the asphalt mixtures and their application.

Table A-5. Asphalt Mixture Types Used by IDOT (Hajj et al., 2021b)

Mixture Type		Application
High ESAL	IL-19.0	Binder course
	IL-9.5	Binder and surface course
	IL-4.75	Binder course
Low ESAL	IL-19.0L	Binder course
	IL-9.5L	Binder and surface course
SMA-12.5, SMA-9.5	≤10 MESALs	Binder and surface course
	>10 MESALs	Binder and surface course

IDOT uses BMD Approach A (Volumetric Design with Performance Verification) to design all asphalt mixtures and approve JMFs. Table A-6 summarizes the changes to the Superpave volumetric design criteria, allowing more asphalt binder in the asphalt mixture without jeopardizing the asphalt mixture's ability to withstand rutting. It targets an increase in the durability and reduction in the cracking potential of the asphalt mixes.

Table A-6. Modifications to AASHTO Standard Volumetric Design Criteria (Hajj et al., 2021b)

Requirements	Mixture Type					
	IL-19.0	IL-9.5	IL-4.75	IL-19.0L	IL-9.5L	SMA
Number of Design Gyrations (N_{des})	↓	↓	↓	↓	↓	↓
Density at N_{des}	↔	↔	↔	↔	↔	↔
Density at Maximum Number of Gyrations (N_{max})	↔	↔	↔	↔	↔	↔
Design Asphalt Binder Content	–	–	–	Range	Range	–
Voids in Mineral Aggregate (VMA)	↑	↔	↑	↑	↔	↑
Voids Filled with Asphalt (VFA)	↑UL / ↔	↑UL / ↔	↑	–	↔	↑

Requirements	Mixture Type					
	IL-19.0	IL-9.5	IL-4.75	IL-19.0L	IL-9.5L	SMA
Dust-to-Asphalt Binder Ratio[1]	↓	↓	↓	↓	↓	–
Draindown (%)	–	–	Min	–	–	–
HWT Passes at 12.5 mm Rut Depth	Min	Min	Min	–	–	Min
FI – Short-term Aging	Min	Min	Min	Min	Min	Min
FI – Long-term Aging	Min	Min	–	Min	Min	Min
TS – Conditioned	Min	Min	Min	Min	Min	Min
TS – Unconditioned	Max	Max	Max	Max	Max	Max
TSR	Min	Min	Min	Min	Min	Min

– Not applicable or not specified; Min = minimum; Max = maximum; ↔ = no change to requirement; ↓ = decreased; ↑ = increased; ↑UL = increased upper limit; TSR = tensile strength ratio.

[1] IDOT uses dust-to-asphalt binder ratio as opposed to dust-to-effective asphalt binder ratio.

IDOT uses HWTT for rutting, I-FIT for cracking, and tensile strength ratio (TSR) for moisture susceptibility. During the asphalt mixture design process, the contractor submits prepared samples to IDOT for a performance verification test. Table A-7 summarizes the required testing to verify performance.

Table A-7. Summary of Performance Tests Considered by IDOT for BMD (Hajj et al., 2021b)

Elements	Rutting	Cracking	Moisture Damage
Test Name and Method	HWTT (AASHTO T 324)	I-FIT (AASHTO T 393)	TS (AASHTO T 283)
JMF Requirement	Refer to Table A-6	Refer to Table A-6	Refer to Table A-6
QA/QC Implementation	Yes	Yes	Yes
Aging Protocol	AASHTO R 30 (Illinois-modified version)	AASHTO R 30 (Illinois-modified version)	AASHTO R 30 Illinois modified version
Notes	Compacted gyratory bricks are interchangeable between HWTT and I-FIT. Test specimens specific to each test are cut from gyratory bricks.	Compacted gyratory bricks are interchangeable between HWTT and I-FIT. Test specimens specific to each test are cut from gyratory bricks.	No freeze-thaw (F-T) cycle (IDOT found no F-T to be harsher than including one F-T cycle in most cases)

Virginia

The Virginia DOT (VDOT) has been using RAP since the 1980s. After a couple of successful initial experimental projects, it became common practice throughout the State. RAP contents in VDOT's asphalt mixtures range from 10 to 50 percent. Binder grade is changed for performance benefits for asphalt mixtures with more than 20 percent RAP. In the mid to late 1990s, VDOT adopted the Superpave method as specified in AASHTO M 323 and AASHTO R 35 to identify the optimal aggregate blend and its corresponding optimal binder content. As a result, the agency's mixtures became coarser and had less binder. With those changes, asphalt mixture performance did not meet the requirements. VDOT had to modify the volumetric parameters for its specification to move the mixtures to the finer side, increase binder content, and limit the RAP content to 20 percent.

With a goal to implement a higher RAP content (30 percent and 35 percent) in surface asphalt mixtures, in 2007, VDOT started a project to compare its 20-percent RAP mixture with a 30-percent RAP mixture (Diefenderfer et al., 2021). The agency evaluated the mixture using the flexural beam fatigue test for fatigue cracking (AASHTO T 321, 2022), Asphalt Pavement Analyzer (APA) test for rutting (Virginia Test Method – 110, 2000), and TSR test for moisture damage (AASHTO T 283, 2022).

In late 2017, VDOT began benchmarking asphalt mixtures to support higher-RAP pilot projects. These projects provided the benchmark results to evaluate different cracking tests used for mixtures with different NMAS and high RAP content. As an outcome of this benchmark study, the agency recommended using the Cantabro Test for cracking, the APA Test for rutting, and IDT for moisture susceptibility, including recommendations for initial performance test criteria (Hajj et al., 2021d). This set the basis to develop a few BMD provisions, including the different types of asphalt mixtures used. Figure A-29 shows the timeline for BMD implementation, which involves developing performance criteria for cracking and rutting.

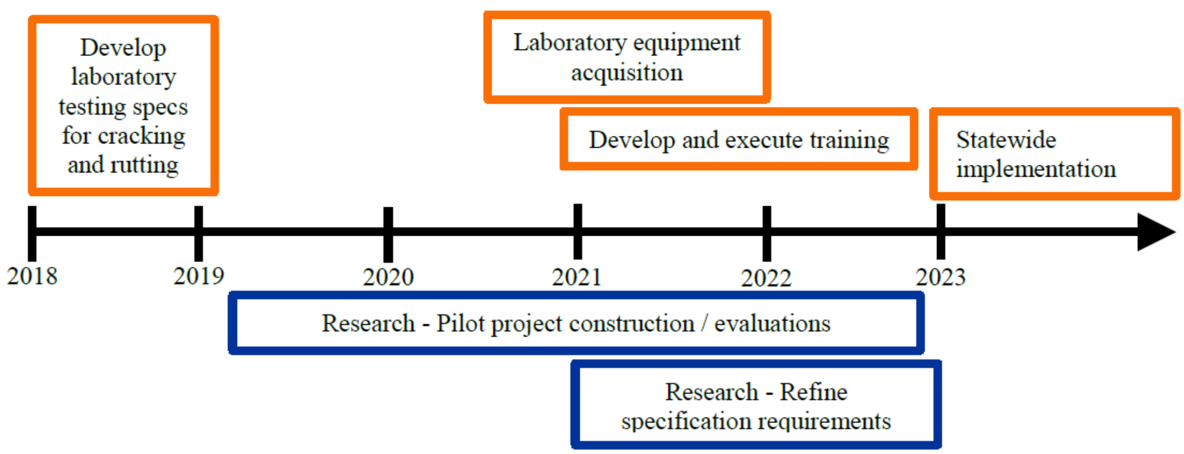

Source: University of Nevada Reno

Figure A-29. VDOT Timeline for Statewide Implementation of BMD (Hajj et al., 2021d)

VDOT uses Approach A (Volumetric Design with Performance Verification) and Approach D (Performance Design). The specific volumetric requirements and gyratory compaction effort for surface mixtures are shown in Table A-8.

Table A-8. Mixture Design Volumetric Requirements and Gyratory Compaction Effort for Performance + Volumetric-Type Surface Mixes (Hajj et al., 2021d)

Mixture Type	Required Density (% of Theoretical Max. Specific Gravity)	VMA (Minimum %)					VFA (%)	Dust-to-Binder Ratio	N_{des}
		NMAS (mm)							
	N_{design}	25	19	12.5	9.5	4.75			
SM-9.5A	96.0	–	–	–	16.0	–	75–80	0.7–1.3	50
SM-9.5D	96.0	–	–	–	16.0	–	75–80	0.7–1.3	50
SM-12.5A	96.0	–	–	15.0	–	–	73–79	0.7–1.3	50
SM-12.5D	96.0	–	–	15.0	–	–	73–79	0.7–1.3	50

– Not applicable.

Table A-9 summarizes the performance test methods, JMF requirements, and aging protocols for different specimens.

Table A-9. Summary of Performance Tests Considered by VDOT for BMD (Hajj et al., 2021d)

Elements	Rutting	Cracking	Moisture Damage
Test Name and Method	APA (AASHTO T 340)	Cantabro (AASHTO TP 108) IDT (ASTM D8225)	TSR (AASHTO T 283)
JMF Requirement	≤8.0 mm after 8,000 passes at 64 °C	≤7.5% ≥70 at 25 °C	≥0.80 at 25 °C
QA/QC Implementation	Yes	Yes	Yes
Aging Protocol	Lab-produced mixtures: Short-term conditioning of loose mixture for 2 hr at the design compaction temperature before compacting. Plant-produced mixtures: compaction temperature and compact immediately.	Lab-produced mixtures: Short-term conditioning of loose mixture for 2 hr (Cantabro) or 4 hr (IDT cracking) at the design compaction temperature. Long-term conditioning of loose mixture for 8 hr at 135 °C. Plant-produced mixtures: Compaction temperature and compact immediately.	Lab-produced mixtures: Short-term conditioning of loose mixture for 4 hr at 135 °C. Plant-produced mixtures: compaction temperature and compact immediately.
Notes	VDOT is investigating the use of high-temperature IDT strength, IDEAL Shear Rutting Test (IDEAL-RT), or Marshall stability for acceptance.	VDOT is investigating the use of other cracking performance tests or indices for acceptance.	VDOT conducted a test on plant-produced asphalt mixtures during the production part of the approval process.

Louisiana

The Louisiana Department of Transportation and Development (LaDOTD) has two sections within its standard specifications manual that address the different types of asphalt mixtures the agency uses. Pavements constructed using these specifications started to present premature failures due to increased traffic volume on highways. Another factor that led LaDOTD to make changes in the specifications used was the increasing interest in using RAP, WMA technologies, and rubber-modified asphalt binder (Cooper et al., 2014). Table A-10 summarizes the different asphalt mixtures and applications used by LaDOTD. The agency's main mixture specification differences are variations in AV, VMA, and critical strain energy release rate (J_c) requirements that were adopted as cracking resistance parameters and criteria. Table A-11 presents the modification to the AASHTO volumetric criteria they applied.

Table A-10. Asphalt Mixture Types Used by LaDOTD (Hajj & Aschenbrener, 2021)

Specifications	Mixture Type	Application
Thin Asphalt Applications (Section 501)	Dense mix Coarse mix OGFC	New and rehabilitation construction Used as a finishing course
Asphalt Mixtures (Section 502)	Wearing course Binder course Base course SMA	New and rehabilitation construction

OGFC = open-graded friction course.

The LTRC initiated several research studies in 2011 to develop a PRS for the asphalt mixtures used in Louisiana. The LaDOTD's BMD approach for asphalt mixture design and JMF approval is Approach A (Volumetric Design with Performance Verification).

Table A-11. Modifications to AASHTO Standard Volumetric Design Criteria (Hajj & Aschenbrener, 2021)

Requirements	Asphalt Mixture Type								
	Thin Asphalt Mixtures		Asphalt Mixtures					AAC Mixtures (<1,000 ADT)	
	Dense Mix	Coarse Mix and OGFC	Inci-dental Paving	Wearing and Binder Courses	Base Course Level 1	ATB Level 1	SMA	Incidental Paving	Wearing Course
Number of Design Gyrations (N_{des})	↓	↓	↓	↓	↓	↓	↓	↓	↓
Density at N_{des}	↓	↓	↑	↑	↑	↑	↑	↓	↓
Density at Maximum Number of Gyrations (N_{max})	↔	↔	↔	↔	↔	↔	↔	↔	↔
Design Asphalt Binder Content	Min	Min	–	–	–	Min	Min	–	–

Requirements	Asphalt Mixture Type								
	Thin Asphalt Mixtures		Asphalt Mixtures					AAC Mixtures (<1,000 ADT)	
	Dense Mix	Coarse Mix and OGFC	Incidental Paving	Wearing and Binder Courses	Base Course Level 1	ATB Level 1	SMA	Incidental Paving	Wearing Course
Voids in Mineral Aggregate (VMA)	–	–	↓	↓	↓	↓	↑	↔	↔
Voids Filled with Asphalt (VFA)	–	–	–	–	–	–	–	–	↑ LL
Dust-to-Asphalt Binder Ratio	↑ UL	–	↑ UL	↑ UL	↑ UL	↑ UL	↑ UL	–	–
Natural Sands	Max	–	–	Max	Max	Max	Max	–	Max
Draindown (%)	–	Max	–	–	–	–	–	–	–
LWT Rut Depth at Specified Passes	Max	Max	Max	Max	Max	Max	Max	Max	Max
SCB, J_c	–	–	–	Min	–	–	Min	–	Min

– Not applicable or not specified; Min = minimum; Max = maximum; ↔ = no change to requirement; ↓ = decreased; ↑ = increased; ↑ UL = increased upper limit; ↑ LL = increased lower limit; AAC = aged asphalt concrete; ADT = average daily traffic; ATB = asphalt-treated base.

LaDOTD uses performance testing such as the Loaded Wheel Tester (LWT) for rutting and the SCB's critical strain energy release rate (J_c) for cracking. Table A-12 shows the performance testing requirements for each mixture type.

Table A-12. Performance Testing Requirements for LaDOTD (Hajj & Aschenbrener, 2021)

Asphalt Mixture Types		LWT, Maximum Rut-Depth @ 50 °C*	SCB, J_c @ 25 °C (kJ/m²)
Thin Asphalt Applications	Dense mix	≤12 mm @ 12,000 passes	–
	Coarse mix	≤12 mm @ 20,000 passes	–
	OGFC	≤12 mm @ 5,000 passes	–
Asphalt Mixtures	Incidental paving	≤10 mm @ 10,000 passes	–
	Wearing course – Level 1	≤10 mm @ 20,000 passes	≥0.5
	Wearing course – Level 2	≤6 mm @ 10,000 passes	≥0.6
	Binder course – Level 1	≤10 mm @ 20,000 passes	≥0.5
	Binder course – Level 2	≤6 mm @ 20,000 passes	≥0.6
	Base course – Level 1	≤12 mm @ 20,000 passes	–
	ATB – Level 1	≤10 mm @ 10,000 passes	–
	SMA	≤6 mm @ 20,000 passes	≥0.6
Asphalt Mixtures (<1,000 ADT)	Incidental paving	≤10 mm @ 10,000 passes	–
	Wearing course	≤10 mm @ 15,000 passes	≥0.5

– Not applicable or not specified; ADT = average daily traffic.

Table A-13 presents the summarized BMD requirements for performance testing for LaDOTD.

Table A-13. Summary of Performance Tests Considered by LaDOTD for BMD (Hajj & Aschenbrener, 2021)

Elements	Rutting	Cracking	Moisture Damage
Test Name and Method	LWT (AASHTO T 324)	SCB (ASTM D8044)	LWT (AASHTO T 324)
JMF Requirement	Refer to Table A-11	Refer to Table A-11	Refer to Table A-11
QA/QC Implementation	Yes	Yes	Yes
Aging Protocol	**Lab-produced mixtures**: Short-term conditioning procedure for mechanical properties per AASHTO R 30 (4 hr at 135 °C). **Plant-produced mixtures**: Short-term conditioning procedure for mechanical properties per AASHTO R 30 (4 hr at 135 °C).	**Lab-produced mixtures**: Long-term conditioning procedure per AASHTO R 30 (5 days at 85 °C). **Plant-produced mixtures**: Long-term conditioning procedure per AASHTO R 30 (5 days at 85 °C).	**Lab-produced mixtures**: Short-term conditioning procedure for mechanical properties per AASHTO R 30 (4 hr at 135 °C). **Plant-produced mixtures**: Short-term conditioning procedure for mechanical properties per AASHTO R 30 (4 hr at 135 °C).
Notes		The SCB is being evaluated for potential use during production for acceptance by establishing an aging scaling factor to estimate test results for long-term oven-aged specimens from those obtained on short-term oven-aged specimens.	

Texas

The Texas DOT (TxDOT) has approximately 197,000 lane-miles of highway infrastructure. TxDOT specifies its standard asphalt mixtures mainly under Item 341 (dense-graded mixtures) and Item 344 (Superpave mixtures). These specifications cover approximately 35 and 45 percent of the asphalt mixture placed by TxDOT, respectively (Hajj et al., 2021c). Other specification items cover thin overlay mixes, SMA, and other specialty mixtures. TxDOT developed a new standard, TxDOT SS 3074 Superpave Mixtures – Balanced Mix Design, to produce asphalt mixtures with satisfactory volumetric and mechanical performance. SS 3074 incorporates the HWTT and OT to evaluate asphalt mixture stability and durability (Zhou et al., 2014).

Recently, TxDOT has initiated a significant effort in partnership with industry and academia to revise and further develop the SS 3074 for surface mixtures with RAP (Hajj et al., 2021c). TxDOT uses BMD Approach A (Volumetric Design with Performance Verification). The agency's goal is to use BMD on 80 percent of the mixtures and implement more advanced and innovative BMD Approaches C or D. TxDOT adjusted the volumetric requirements for

BMD mixes; all mixtures are compacted at 50 gyrations (N_{des}) and a target molded density of 96 percent. Table A-14 presents the mixture design volumetric requirements.

Table A-14. TxDOT Mixture Design Volumetric Requirements (Hajj et al., 2021c)

Asphalt Mixture Type		Asphalt Binder Content (%)	Target Lab-Molded Density (%)	VMA (Minimum %)$						Dust-to-Asphalt Binder Ratio#	Drain-down (%)
				NMAS (mm)							
				37.5	25	19	12.5	9.5	4.75		
DG Mixtures	A, B, C, D, or F	–	96.5*	12.0	13.0	14.0	15.0	16.0	–	–	–
SP Mixtures	SP-A, SP-B, SP-C, or SP-D	–	96.0	13.0	14.0	15.0	16.0	–	–	0.6–1.6	
PFC	Fine (PFC-F)	6.0–7.0	≤78.0	–	–	–	–	–	–	–	≤0.1
	Coarse (PFC-C)	6.0–7.0	≤82.0	–	–	–	–	–	–	–	≤0.1
	Fine (PFCR-F)	8.0–10.0	≤82.0	–	–	–	–	–	–	–	≤0.1
	Coarse (PFCR-C)	7.0–9.0	≤82.0	–	–	–	–	–	–	–	≤0.1
SMA	SMA	6.0–7.0	96.0	–	–	–	17.5	17.5	–	–	≤0.1
	SMAR	7.0–10.0	96.0	–	–	–	19.0	19.0	–	–	≤0.1
TOM	Coarse (TOM-C)	≥6.0	97.5*	–	–	–	–	16.0	–	–	≤0.2
	Fine (TOM-F)	≥6.5	97.5*	–	–	–	–	16.5	–	–	≤0.2
TBFC	Fine (PFC-F)	6.0–7.0	≤78.0	–	–	–	–	–	–	–	≤0.1
	Coarse (PFC-C)	6.0–7.0	≤82.0	–	–	–	–	–	–	–	≤0.1
	Coarse (PFCR-C)	7.0–9.0	≤82.0	–	–	–	–	–	–	–	≤0.1
	TBWC-Type A	5.0–5.8	≤92.0	–	–	–	–	–	–	–	≤0.1
	TBWC-Type B	4.8–5.6	≤92.0	–	–	–	–	–	–	–	≤0.1
	TBWC-Type C	4.8–5.6	≤92.0	–	–	–	–	–	–	–	≤0.1
CAM	Fine	≥7.0	98.0	–	–	–	–	–	17.0	≤1.4	–
SP – BMD	SP-C Surface	–	96.0	–	–	15.0	–	–	–	0.6–1.6	–
	SP-D Fine	–	96.0	–	–	–	16.0	–	–	0.6–1.6	–

– Not applicable or not specified; DG = dense-graded; SP = Superpave; PFC = permeable friction course; SMAR = stone-matrix asphalt rubber; TOM = thin overlay mixtures; TBFC = thin bonded friction courses; TBWC = thin bonded wearing course; CAM = crack attenuating mixture.

$ Uses effective specific gravity of the aggregate (Gse) and not bulk specific gravity of the aggregate (Gsb).

* Texas gyratory compactor.

Table A-15 presents TxDOT's changes to AASHTO volumetric design criteria, including the acceptance parameters from the performance tests (HWTT and OT).

Table A-15. Modifications to AASHTO Standard Volumetric Design Criteria for TxDOT (Hajj et al., 2021c)

Requirements	Mixture Type					
	PFC	SMA	TOM	TBFC	CAM	SP – BMD
Number of Design Gyrations (N_{des})	↓	↓	↓	↓	↓	↓
Density at N_{des}	↓	↔	↑	↓	↑	↔
Density at Maximum Number of Gyrations (N_{max})	–	–	–	–	–	–
Design Asphalt Binder Content	Range	Range	Min	Range	Min	–

Requirements	Mixture Type					
	PFC	SMA	TOM	TBFC	CAM	SP – BMD
VMA*	–	↑	↑	–	↑	↑
VFA	–	–	–	–	–	–
Dust-to-Asphalt Binder Ratio	–	–	–	–	↑ UL	↑ UL
Draindown (%)	Min	Min	Min	Min	–	–
HWTT Passes @ 12.5 mm Rut Depth	Min/R	–	Min	Min/R	Min	Min
HWTT Rut Depth @ 20,000 Passes	–	Max	–	–	–	–
OT Number of Cycles	Min/R	Min	Min	Min/R	Min	–
OT CFE	–	–	–	–	–	Min
OT CPR	–	–	–	–	–	Max

– Not applicable or not specified; Min = minimum; Max = maximum; ↔ = no change to requirement; ↓ = decreased; ↑ = increased; ↑ UL = increased upper limit; CFE = critical fracture energy; CPR = crack progression rate; PFC = permeable friction course; TOM = thin overlay mixtures; TBFC = thin bonded friction courses; CAM = crack attenuating mixture; SP = Superpave mixtures.
* Uses G_{se} and not G_{sb}.

TxDOT is working to improve the performance testing criteria used by the agency since 2004 for rutting with HWTT and since 2014 for cracking with OT. Currently, the agency is evaluating the feasibility of using the Rapid Rutting Test (RRT), known as the IDEAL Shear Rutting Test (IDEAL-RT). The goal is to use it during production as a surrogate test for acceptance. Table A-16 summarizes the performance tests currently used by TxDOT for BMD of specialty and SP–BMD mixtures (Hajj et al., 2021c).

Table A-16. Summary of Performance Tests Considered by TxDOT for BMD (Hajj et al., 2021c)

Elements	Rutting	Cracking	Moisture Damage
Test Name and Method	HWTT (Tex-242-F)	OT (Tex-248-F) IDEAL-CT (Tex-250-F)	IDT (Tex-226-F) Dry Boil Test (Tex-530-C) HWTT (Tex-242-F)
JMF Requirement	Refer to Table A-14	Refer to Table A-14	Refer to Table A-14
QA/QC Implementation	Yes	Yes	Yes
Aging Protocol	**Lab-produced mixtures**: Short-term conditioning of loose mixture for 2 hr at compaction temperature (Tex-241-F). **Plant-produced mixtures**: Minimize cooling, reheat specimens to the compaction temperature, and compact within 2 hr.	**Lab-produced mixtures**: Short-term conditioning of loose mixture for 2 hr at compaction temperature (Tex-241-F). **Plant-produced mixtures**: Minimize cooling, reheat specimens to the compaction temperature, and compact within 2 hr.	

Elements	Rutting	Cracking	Moisture Damage
Notes	TxDOT is investigating the use of IDEAL-RT for acceptance. A correlation between the HWTT and IDEAL-RT is being investigated.	A correlation between the OT and the IDEAL-CT for acceptance is established on a mixture-by-mixture basis. TxDOT is looking into extended aging as a side study in the test projects to potentially require an extended aging protocol in the future.	

Delhi International Airport

A performance-based mixture design was implemented in the Phase 3 of expansion of Delhi International Airport in India (Tipnis et al., 2023). The project faced significant challenges due to restricted construction windows, strict security measures, and varying weather conditions. A binder was selected to balance workability with asphalt mixture stiffness at high temperatures.

The study evaluated three JMFs: JMF 1 had an NMAS of 26.5 mm, JMF 2 had an NMAS of 19 mm, and JMF 3 had an NMAS similar to JMF 2. Marshall mix design was performed for all three JMFs, and their performance was evaluated through various performance tests. These tests included HWTT to assess rutting potential, IDEAL-CT to assess cracking potential, and TSR to predict moisture damage susceptibility.

Field trials were conducted to validate the selected mixture, ensuring it could withstand extended delivery times and maintain compaction at lower temperatures. Friction testing in wet conditions was also performed. Based on all these parameters, JMF 2 was selected as the ideal mixture for surface course. The pavement surface has performed well. This case study demonstrates how a performance-based approach can produce a balanced and improved asphalt mixture design.

Section 7: Summary

BMD is an asphalt mixture design approach that incorporates performance tests into the mixture design process. This method seeks to optimize pavement performance by balancing the two major distress types: cracking and rutting. BMD has been successfully implemented by various State DOTs. Its application to airfield pavement design can be crucial in predicting potential asphalt mixture performance. This would allow contractors to design balanced asphalt mixtures prior to production, ensuring material quality with greater confidence.

Cracking in asphalt pavement is influenced by two primary factors: mixture parameters and environmental impacts. Mixture parameters include the properties of asphalt binders, such as their relaxation properties and behavior at low temperatures, and aggregate quality, such as shape, texture, and gradation. The incorporation of RAP and RAS has led to stiffer asphalt mixtures. While beneficial in some respects, stiffer mixtures have lower energy-dissipation properties, resulting in early-stage cracking under stress. Environmental and heavy traffic loading factors further worsen the pavement condition and contribute to the failure of asphalt pavements through various forms of cracking. A thorough understanding of the types of cracking—thermal, reflective, and fatigue—is important in addressing these challenges. Thermal cracking occurs at low temperatures or due to rapid cooling, whereas reflective cracking is induced by stress from movement at existing cracks or joints beneath the asphalt layer. Fatigue cracking, a major concern at intermediate temperatures, results from repetitive heavy vehicle loading.

A thorough understanding of pavement cracking mechanisms remains a challenge. Recent developments, such as asphalt binder modification and increased traffic loads, have further underscored the importance of accurately determining the cracking potential of asphalt mixtures. Various cracking models have been developed to predict the behavior of asphalt mixtures under different conditions. The cracking models have evolved from empirical methods to more fundamental ones, such as J-integral and crack layer models. Despite these advancements, no cracking model accurately captures crack initiation and propagation.

To characterize cracking in asphalt pavements, various laboratory tests are used to evaluate asphalt mixture resistance to thermal, intermediate-temperature, and cyclic loading. Tests include DCT, SCB, and ITS for thermal cracking; I-FIT and the Louisiana SCB test for intermediate-temperature cracking; and cyclic fatigue, FBF, and OT for fatigue cracking. Furthermore, E*, CT Index, and IDT tests are used to evaluate the strength and modulus of the asphalt mixture. Many studies have been conducted to evaluate the fracture toughness of airfield asphalt mixtures through various tests. These findings underscore the need to develop performance-based specifications that account for the non-linear viscoelastic properties of asphalt mixtures, their dependence on loading rate and temperature, and other aspects such as aging effects critical to airfield pavements.

Table A-17. Laboratory Cracking Tests Summary

Test Name	Test Standard	Loading Condition	Mode of Loading	Notched/ Unnotched[1]	Specimen Geometry[2]	Test Temperature[3]	Test Parameter
DCT	(ASTM D7313, 2020)	Monotonic	CMOD controlled	N	D: 150 mm T: 50 mm ND: 62.5 mm	PGL + 10° C	Fracture energy (G_f), Fracture strain tolerance (FST)
SCB	(AASHTO T 394, 2021)	Monotonic	CMOD controlled	N	D: 150 mm T: 24.7 mm ND: 15 mm	PGL + 10 °C	Fracture energy (G_f), Fracture toughness (K_{IC}), Stiffness (S)
IDT	(AASHTO T 322, 2007)	Monotonic	LLD controlled for strength	UN	D: 150 mm T: 38 to 50 mm	−30 to 10 °C	Tensile strength, Creep compliance
I-FIT	(AASHTO T 393, 2021)	Monotonic	LLD controlled	N	D: 150 mm T: 50 mm ND: 15 mm	25 °C	Fracture energy (G_f), Post-peak slope (m), Flexibility Index (FI) Rate-dependent cracking index (RDCI)
LTRC SCB	(ASTM D8044, 2016)	Monotonic	CMOD controlled	N	D: 150 mm T: 57 mm ND: 15 mm	(PGH + PGL)/2 + 4 °C	Critical strain energy release rate (J_c)
CT-Index	(ASTM D8225, 2019)	Monotonic	LLD controlled	UN	D: 150 mm T: 62 mm	(PGH + PGL)/2 + 4 °C	Cracking tolerance index (CT Index)
DTCF	(AASHTO T 400, 2022)	Cyclic	Displacement controlled	UN	D: 150 mm T: 62 mm	5 to 25 °C	Damage characteristic curve, D^R and S_{app}
Texas Overlay Test	(Texas DOT, 2022)	Cyclic	Displacement controlled	UN	L: 150 mm W: 75 mm T: 37.5 mm	25 °C	Number of cycles to failure, Paris law crack growth parameters
Flexural Bending Beam Test	(AASHTO T 321, 2022)	Cyclic	Strain controlled (Usually)	UN	L: 380 mm W: 50 mm T: 63 mm	20 °C	Number of cycles to failure, Dissipated energy

[1]N – notched, UN – unnotched

[2]D – diameter, W – width, T – thickness, ND – notch depth

[2]PGL – low-temperature PG, PGH – high-temperature PG

References

AASHTO M 323. (2022). *Standard Specification for Superpave Volumetric Mix Design*. American Association of State Highway and Transportation Officials.

AASHTO R 35. (2022). *Standard Practice for Superpave Volumetric Design for Asphalt Mixtures*. American Association of State Highway and Transportation Officials.

AASHTO T 283. (2022). *Standard Method of Test for Resistance of Compacted Asphalt Mixtures to Moisture-Induced Damage*. American Association of State Highway and Transportation Officials.

AASHTO T 321. (2022). *Standard Method of Test for Determining the Fatigue Life of Compacted Asphalt Mixtures Subjected to Repeated Flexural Bending*. American Association of State Highway and Transportation Officials.

AASHTO T 322. (2007). *Standard Method of Test for Determining the Creep Compliance and Strength of Hot Mix Asphalt (HMA) Using the Indirect Tensile Test Device*. American Association of State Highway and Transportation Officials.

AASHTO T 324. (2023). *Standard Method of Test for Hamburg Wheel-Track Testing of Compacted Asphalt Mixtures*. American Association of State Highway and Transportation Officials.

AASHTO T 342. (2022). *Standard Method of Test for Determining Dynamic Modulus of Hot Mix Asphalt (HMA)*. American Association of State Highway and Transportation Officials.

AASHTO T 393. (2021). *Standard Method of Test for Determining the Fracture Potential of Asphalt Mixtures Using Illinois Flexibility Index Test (I-FIT)*. American Association of State Highway and Transportation Officials.

AASHTO T 394. (2021). *Standard Method of Test for Determining the Fracture Energy of Asphalt Mixtures Using the Semicircular Bend Geometry (SCB)*. American Association of State Highway and Transportation Officials.

AASHTO T 400. (2022). *Standard Method of Test for Determining the Damage Characteristic Curve and Failure Criterion Using the Asphalt Mixture Performance Tester (AMPT) Cyclic Fatigue Test*. American Association of State Highway and Transportation Officials.

Abanto-Bueno, J., & Lambros, J. (2002). Investigation of Crack Growth in Functionally Graded Materials Using Digital Image Correlation. *Engineering Fracture Mechanics*, *69*(14), 1695–1711. https://doi.org/10.1016/S0013-7944(02)00058-9

Abdel-Raouf, A.-G. (1967). *Brittle Behavior and Crack Propagation in Asphaltic Mixtures* [Doctoral dissertation, University of Illinois at Urbana-Champaign]. http://hdl.handle.net/2142/60334

Abdulshafi, A. A., & Majidzadeh, K. (1985). J-Integral and Cyclic Plasticity Approach to Fatigue and Fracture of Asphaltic Mixtures. *Transportation Research Record*, (1034), 112–123. https://trid.trb.org/view/276662

Aglan, H. A., & Figueroa, J. L. (1993). Damage-Evolution Approach to Fatigue Cracking in Pavements. *Journal of Engineering Mechanics*, *119*(6), 1243–1259. https://doi.org/10.1061/(ASCE)0733-9399(1993)119:6(1243)

Ali, U. M., Hernandez, J., Al-Qadi, I., & Ozer, H. (2019). Three-Dimensional Balanced Mix Design for Asphalt Concrete. *Airfield and Highway Pavements 2019*, 178–188. https://doi.org/10.1061/9780784482452.018

Al-Qadi, I. L., Ozer, H., Lambros, J., Khatib, A. E., Singhvi, P., Khan, T., Rivera-Perez, J., & Doll, B. (2015). *Testing Protocols to Ensure Performance of High Asphalt Binder Replacement Mixes Using RAP and RAS* (FHWA-ICT-15-017). Illinois Center for Transportation.

Anderson, T. L. (2017). *Fracture Mechanics: Fundamentals and Applications, Fourth Edition* (4th ed.). CRC Press. https://doi.org/10.1201/9781315370293

Ann Myers, L., & Roque, R. (2002). Top-Down Crack Propagation in Bituminous Pavements and Implications For Pavement Management. *Journal of the Association of Asphalt Paving Technologists*, *71*. https://trid.trb.org/view/698756

Ann Myers, L., Roque, R., & Birgisson, B. (2001). Propagation Mechanisms for Surface-Initiated Longitudinal Wheelpath Cracks. *Transportation Research Record*, *1778*(1), 113–122. https://doi.org/10.3141/1778-14

Ann Myers, L., Roque, R., Ruth, B. E., & Drakos, C. (1999). Measurement of Contact Stresses for Different Truck Tire Types to Evaluate Their Influence on Near-Surface Cracking and Rutting. *Transportation Research Record*, *1655*(1), 175–184. https://doi.org/10.3141/1655-23

ASTM D7313. (2020). *Standard Test Method for Determining Fracture Energy of Asphalt Mixtures Using the Disk-Shaped Compact Tension Geometry*. ASTM International.

ASTM D8044. (2016). *Standard Test Method for Evaluation of Asphalt Mixture Cracking Resistance using the Semi-Circular Bend Test (SCB) at Intermediate Temperatures*. ASTM International.

ASTM D8225. (2019). *Standard Test Method for Determination of Cracking Tolerance Index of Asphalt Mixture Using the Indirect Tensile Cracking Test at Intermediate Temperature*. ASTM International.

Baek, J., & Al-Qadi, I. L. (2006). Finite Element Method Modeling of Reflective Cracking Initiation and Propagation: Investigation of the Effect of Steel Reinforcement Interlayer on Retarding Reflective Cracking in Hot-Mix Asphalt Overlay. *Transportation Research Record: Journal of the Transportation Research Board*, *1949*(1), 32–42. https://doi.org/10.1177/0361198106194900104

Bažant, Z. P., & Li, Y.-N. (1997). Cohesive Crack with Rate-Dependent Opening and Viscoelasticity: I. Mathematical Model and Scaling. *International Journal of Fracture*, *86*(3), 247–265. https://doi.org/10.1023/A:1007486221395

Behnia, B., Dave, E. V., Ahmed, S., Buttlar, W. G., & Reis, H. (2011). Effects of Recycled Asphalt Pavement Amounts on Low-Temperature Cracking Performance of Asphalt Mixtures Using Acoustic Emissions. *Transportation Research Record*, *2208*(1), 64–71. https://doi.org/10.3141/2208-09

Bell, H. P. (2009). *Fatigue Evaluation Criteria for Aged Hot-Mix Asphalt Surfaces*. Mississippi State University.

Bennert, T., Garg, N., Ericson, C., & Cytowicz, N. (2023). Evaluation of Test Methods to Identify Asphalt Binders Prone to Surface-initiated Cracking. *Transportation Research Record*, *2677*(3), 897–910. https://doi.org/10.1177/03611981221119191

Bhurke, A. S., Shin, E. E., & Drzal, L. T. (1997). Fracture Morphology and Fracture Toughness Measurement of Polymer-Modified Asphalt Concrete. *Transportation Research Record*, *1590*(1), 23–33. https://doi.org/10.3141/1590-04

Buchanan, S. (2016, September 20). *Balanced Mix Design (BMD) for Asphalt Mixtures*. SHRP2 Peer to Peer Exchange 2016. AASHTO Strategic Highway Research Program 2. https://shrp2.transportation.org/documents/presentations/10_Buchanan_SHRP2BalancedMixDesignforAsphaltMixtures.pdf

Buttlar, W. G., Hill, B. C., Wang, H., & Mogawer, W. (2017). Performance Space Diagram for the Evaluation of High- and Low-temperature Asphalt Mixture Performance. *Road Materials and Pavement Design*, *18*(sup1), 336–358. https://doi.org/10.1080/14680629.2016.1267446

Buttlar, W. G., & Roque, R. (1994). Development and Evaluation of the Strategic Highway Research Program Measurement and Analysis System for Indirect Tensile Testing at Low Temperatures. *Transportation Research Record*, (1454), 163–171. https://trid.trb.org/view/424722

Canestrari, F., & Ingrassia, L. P. (2020). A Review of Top-Down Cracking in Asphalt Pavements: Causes, Models, Experimental Tools and Future Challenges. *Journal of Traffic and Transportation Engineering (English Edition)*, *7*(5), 541–572. https://doi.org/10.1016/j.jtte.2020.08.002

Chehab, G. R., Kim, Y. R., Schapery, R. A., Witczak, M. W., & Bonaquist, R. (2002). Time-Temperature Superposition Principle for Asphalt Concrete with Growing Damage in Tension State. *Journal of the Association of Asphalt Paving Technologists*, *71*, 559–593. https://trid.trb.org/view/698753

Chen, A., Airey, G. D., Thom, N., Li, Y., & Wan, L. (2022). Simulation of Micro-Crack Initiation and Propagation Under Repeated Load in Asphalt Concrete Using Zero-Thickness Cohesive Elements. *Construction and Building Materials*, *342*, 127934. https://doi.org/10.1016/j.conbuildmat.2022.127934

Chiangmai, C. N. (2014). *Experimental Evaluation of Monotonic and Cyclic Fracture Behaviour Using Disk-shaped Compact Tension Test and Released Energy Approach* [Doctoral dissertation, University of Illinois at Urbana-Champaign]. https://hdl.handle.net/2142/73043

Collop, A. C., & Cebon, D. (1995). A Theoretical Analysis of Fatigue Cracking in Flexible Pavements. *Proceedings of the Institution of Mechanical Engineers, Part C: Journal of Mechanical Engineering Science*, *209*(5), 345–361. https://doi.org/10.1243/PIME_PROC_1995_209_163_02

Cooper, S. B., Mohammad, L. N., Kabir, S., & King, W. (Bill). (2014). Balanced Asphalt Mixture Design through Specification Modification: Louisiana's Experience. *Transportation Research Record: Journal of the Transportation Research Board*, *2447*(1), 92–100. https://doi.org/10.3141/2447-10

Daniel, J. S., & Kim, Y. R. (2002). Development of a Simplified Fatigue Test and Analysis Procedure Using a Viscoelastic Continuum Damage Model. *Journal of the Association of Asphalt Paving Technologists*, *71*, 619–650.

Dave, E. V., & Behnia, B. (2018). Cohesive Zone Fracture Modelling of Asphalt Pavements with Applications to Design of High-Performance Asphalt Overlays. *International Journal of Pavement Engineering*, *19*(3), 319–337. https://doi.org/10.1080/10298436.2017.1353393

Dave, E. V., Oshone, M., Schokker, A., & Bennett, C. E. (2019). *Disc Shaped Compact Tension (DCT) Specifications Development for Asphalt Pavement* (MN/RC 2019-24). Department of Civil and Environmental Engineering University of New Hampshire. http://dot.state.mn.us/research/reports/2019/201924.pdf

Diefenderfer, S. D., Boz, I., & Habbouche, J. (2021). *Balanced Mix Design for Surface Asphalt Mixtures: Phase I: Initial Roadmap Development and Specification Verification* (FHWA/VTRC 21-R15). Virginia Transportation Research Council.

Doll, B., Ozer, H., Rivera-Perez, J., Al-Qadi, I. L., & Lambros, J. (2017a). Damage Zone Development in Heterogeneous Asphalt Concrete. *Engineering Fracture Mechanics*, *182*, 356–371. https://doi.org/10.1016/j.engfracmech.2017.06.002

Doll, B., Ozer, H., Rivera-Perez, J. J., Al-Qadi, I. L., & Lambros, J. (2017b). Investigation of Viscoelastic Fracture Fields in Asphalt Mixtures using Digital Image Correlation. *International Journal of Fracture*, *205*(1), 37–56. https://doi.org/10.1007/s10704-017-0180-8

Elseifi, M. A., Mohammad, L. N., Ying, H., & Cooper, S. (2012). Modeling and Evaluation of the Cracking Resistance of Asphalt Mixtures Using the Semi-Circular Bending Test at Intermediate Temperatures. *Road Materials and Pavement Design*, *13*(sup1), 124–139. https://doi.org/10.1080/14680629.2012.657035

Epps, J. A., & Monismith, C. L. (1969). *Asphalt Mixture Behavior in Repeated Flexure* (D-6-1). Univ. of California, Berkeley. https://trid.trb.org/View/97796

Francken, L. (1979). Fatigue Performance of a Bituminous Road Mix Under Realistic Test Conditions. *Transportation Research Record*, (712), pp 30-37. https://trid.trb.org/view/146461

Gamez, A., & Al-Qadi, I. L. (2019). Turning Maneuver Effect on Near-Surface Airfield Pavement Responses. *Transportation Research Record: Journal of the Transportation Research Board*, *2673*(8), 275–283. https://doi.org/10.1177/0361198119841861

Germann, F. P., & Lytton, R. L. (1979). *Methodology for Predicting the Reflection Cracking Life of Asphalt Concrete Overlays* (FHWA/TX-79/09+207-5). Texas Transportation Institute. https://trid.trb.org/view/142495

Ghuzlan, K. A., & Carpenter, S. H. (2000). Energy-Derived, Damage-Based Failure Criterion for Fatigue Testing. *Transportation Research Record*, *1723*(1), 141–149. https://doi.org/10.3141/1723-18

Griffith, A. A. (1921). The Phenomena of Rupture and Flow in Solids. *Philosophical Transactions of the Royal Society of London. Series A, Containing Papers of a Mathematical or Physical Character*, *221*, 163–198. https://www.jstor.org/stable/91192

Hajj, E. Y., & Aschenbrener, T. B. (2021). *Case Studies on the Implementation of Balanced Mix Design and Performance Tests for Asphalt Mixtures: Louisiana Department of Transportation & Development (LaDOTD)* (WRSC-TR-21-04). University of Nevada, Reno.

Hajj, E. Y., Aschenbrener, T. B., & Nener-Plante, D. (2021a). *Case Studies on the Implementation of Balanced Mix Design and Performance Tests for Asphalt Mixtures: California Department of Transportation (Caltrans)* (WRSC-TR-21-02). University of Nevada, Reno.

Hajj, E. Y., Aschenbrener, T. B., & Nener-Plante, D. (2021b). *Case Studies on the Implementation of Balanced Mix Design and Performance Tests for Asphalt Mixtures: Illinois Department of Transportation (IDOT)* (WRSC-TR-21-03). University of Nevada, Reno.

Hajj, E. Y., Aschenbrener, T. B., & Nener-Plante, D. (2021c). *Case Studies on the Implementation of Balanced Mix Design and Performance Tests for Asphalt Mixtures: Texas Department of Transportation (TxDOT)* (WRSC-TR-21-07). University of Nevada, Reno.

Hajj, E. Y., Aschenbrener, T. B., & Nener-Plante, D. (2021d). *Case Studies on the Implementation of Balanced Mix Design and Performance Tests for Asphalt Mixtures: Virginia Department of Transportation (VDOT)* (WRSC-TR-21-08). University of Nevada, Reno.

Harvey, J. T., Deacon, J. A., Tsai, B.-W., & Monismith, C. L. (1995). *Fatigue Performance of Asphalt Concrete Mixes and Its Relationship to Asphalt Concrete Pavement Performance in California* (RTA-65W485-2). University of California, Berkeley. https://ucprc.ucdavis.edu/pdf/Fatigue%20Performance%20of%20AC.pdf

Hernandez, J. A., & Al-Qadi, I. L. (2015). Airfield Pavement Response Caused by Heavy Aircraft Takeoff: Advanced Modeling for Consideration of Wheel Interaction. *Transportation Research Record: Journal of the Transportation Research Board*, *2471*(1), 40–47. https://doi.org/10.3141/2471-06

Hill, B. (2016). *Asphalt Mixture Evaluation Using Performance Space Diagrams, Digital Image Correlation, and Discrete Element Modeling* [Dissertation, University of Illinois Urbana Champaign]. http://hdl.handle.net/2142/95586

Hillerborg, A., Modéer, M., & Petersson, P.-E. (1976). Analysis of Crack Formation and Crack Growth in Concrete by Means of Fracture Mechanics and Finite Elements. *Cement and Concrete Research*, *6*(6), 773–781. https://doi.org/10.1016/0008-8846(76)90007-7

Hou, T., Underwood, B. S., & Kim, Y. R. (2010). Fatigue Performance Prediction of North Carolina Mixtures Using the Simplified Viscoelastic Continuum Damage Model. *Journal of the Association of Asphalt Paving Technologists*, *79*, 35–80. https://trid.trb.org/view/1086607

Huang, Y. H. (1993). *Pavement Analysis and Design*. Prentice Hall.

Ioannides, A. M. (1997). Fracture Mechanics in Pavement Engineering: The Specimen-Size Effect. *Transportation Research Record*, *1568*(1), 10–16. https://doi.org/10.3141/1568-02

Irwin, G. R. (1957). Analysis of Stresses and Strains Near the End of a Crack Traversing a Plate. *Journal of Applied Mechanics*, *24*(3), 361–364. https://doi.org/10.1115/1.4011547

Jacobs, M., Hopman, P. C., & Molenaar, A. A. A. (1996). Application of Fracture Mechanics Principles to Analyze Cracking in Asphalt Concrete. *Journal of the Association of Asphalt Paving Technologists*, *65*, 1–39. https://trid.trb.org/view/487700

Jacobs, M. M. J. (1995). *Crack Growth in Asphaltic Mixes* [Dissertation]. Delft University of Technology.

Jenq, Y.-S., & Perng, J.-D. (1991). Analysis of Crack Propagation in Asphalt Concrete Using Cohesive Crack Model. *Transportation Research Record*, (1317), 90–99. https://trid.trb.org/view/365394

Jichkar, P. D. (2021). *Implementation of HMA Design Tool to Develop Balanced Mix Design Based on Gradation Parameters* [Master's thesis, University of Texas at El Paso]. https://scholarworks.utep.edu/open_etd/3278/

Kennedy, T. W. (1977). Characterization of Asphalt Pavement Materials Using the Indirect Tensile Test. *In Association of Asphalt Paving Technologists Proc*, *Vol 46*, 132–150. https://trid.trb.org/View/87356

Khan, A. T. U. (2016). *Displacement Rate and Temperature Effect on Asphalt Concrete Cracking Potential* [Thesis, University of Illinois Urbana Champaign]. http://hdl.handle.net/2142/90483

Kim, H., & Buttlar, W. G. (2009). Multi-Scale Fracture Modeling of Asphalt Composite Structures. *Composites Science and Technology*, *69*(15), 2716–2723. https://doi.org/10.1016/j.compscitech.2009.08.014

Kim, K. W., & El Hussein, H. M. (1995). Effect of Differential Thermal Contraction on Fracture Toughness of Asphalt Materials at Low Temperatures. *Journal of the Association of Asphalt Paving Technologists*, *64*, 474–499. https://trid.trb.org/view/468086

Kim, M., Buttlar, W. G., Baek, J., & Al-Qadi, I. L. (2009). Field and Laboratory Evaluation of Fracture Resistance of Illinois Hot-Mix Asphalt Overlay Mixtures. *Transportation Research Record*, *2127*(1), 146–154. https://doi.org/10.3141/2127-17

Kim, S.-S. (2005). Direct Measurement of Asphalt Binder Thermal Cracking. *Journal of Materials in Civil Engineering*, *17*(6), 632–639. https://doi.org/10.1061/(ASCE)0899-1561(2005)17:6(632)

Kim, Y. R., Lee, H.-J., & Little, D. N. (1997). Fatigue Characterization of Asphalt Concrete Using Viscoelasticity and Continuum Damage Theory. *Journal of the Association of Asphalt Paving Technologists*, *66*, 520–569. https://trid.trb.org/view/488044

Kim, Y. R., & Little, D. N. (1990). One-Dimensional Constitutive Modeling of Asphalt Concrete. *Journal of Engineering Mechanics*, *116*(4), 751–772. https://doi.org/10.1061/(ASCE)0733-9399(1990)116:4(751)

Kim, Y.-R., & Aragão, F. T. S. (2013). Microstructure Modeling of Rate-Dependent Fracture Behavior in Bituminous Paving Mixtures. *Finite Elements in Analysis and Design*, *63*, 23–32. https://doi.org/10.1016/j.finel.2012.08.004

Krishna Swamy, A., Mitchell, L. F., Hall, S. J., & Sias Daniel, J. (2011). Impact of RAP on the Volumetric, Stiffness, Strength, and Low-Temperature Properties of HMA. *Journal of Materials in Civil Engineering*, *23*(11), 1490–1497. https://doi.org/10.1061/(ASCE)MT.1943-5533.0000245

Lee, S. J., Rust, J. P., Hamouda, H., Kim, Y. R., & Borden, R. H. (2005). Fatigue Cracking Resistance of Fiber-Reinforced Asphalt Concrete. *Textile Research Journal*, *75*(2), 123–128. https://doi.org/10.1177/004051750507500206

Li, C., & Guo, J. (2019). Cracking Simulation of Asphalt Concrete Beam Specimen using Cohesive Zone Model. *Construction and Building Materials*, *214*, 49–60. https://doi.org/10.1016/j.conbuildmat.2019.04.122

Li, Q., Chen, X., Li, G., & Zhang, S. (2018). Fatigue Resistance Investigation of Warm-Mix Recycled Asphalt Binder, Mastic, and Fine Aggregate Matrix. *Fatigue & Fracture of Engineering Materials & Structures*, *41*(2), 400–411. https://doi.org/10.1111/ffe.12692

Li, X., & Marasteanu, M. (2004). Evaluation of the Low Temperature Fracture Resistance of Asphalt Mixtures Using the Semi Circular Bend Test. *Journal of the Association of Asphalt Paving Technologists*, *73*, 401–426. https://trid.trb.org/view/749998

Li, Y.-N., & Bažant, Z. P. (1997). Cohesive Crack Model with Rate-Dependent Opening and Viscoelasticity: II. Numerical Algorithm, Behavior and Size Effect. *International Journal of Fracture*, *86*(3), 267–288. https://doi.org/10.1023/A:1007497104557

Ling, M., Luo, X., Chen, Y., Hu, S., & Lytton, R. L. (2019). A Calibrated Mechanics-Based Model for Top-Down Cracking of Asphalt Pavements. *Construction and Building Materials*, *208*, 102–112. https://doi.org/10.1016/j.conbuildmat.2019.02.090

Little, D. N., Lytton, R. L., Williams, D., & Kim, Y. R. (1999). An Analysis of the Mechanism of Microdamage Healing Based on the Application of Micromechanics First Principles of Fracture and Healing. *Journal of the Association of Asphalt Paving Technologists*, *68*, 501–542. https://trid.trb.org/view/639721

Luo, X., Luo, R., & Lytton, R. L. (2013). Modified Paris's Law to Predict Entire Crack Growth in Asphalt Mixtures. *Transportation Research Record*, *2373*(1), 54–62. https://doi.org/10.3141/2373-06

Majidzadeh, K., Kauffmann, E. M., & Ramsamooj, D. V. (1971). Application of Fracture Mechanics in the Analysis of Pavement Fatigue. *In Association of Asphalt Paving Technologists Proceedings*, *40*, 227–246. https://trid.trb.org/view/103438

Mandal, T., Yin, H., & Ji, R. (2018). Correlating Laboratory and Full-Scale Reflective Cracking Tests for Airfield Pavements. *Construction and Building Materials*, *169*, 47–58. https://doi.org/10.1016/j.conbuildmat.2018.02.182

Marasteanu, M., Buttlar, W., Bahia, H., Williams, C., Moon, K. H., Teshale, E. Z., Falchetto, A. C., Turos, M., Dave, E., Paulino, G., Ahmed, S., Leon, S., Braham, A., Behnia, B., Tabatabaee, H., Velasquez, R., Arshadi, A., Puchalski, S., Mangiafico, S., ... Kvasnak, A. (2012). *Investigation of Low Temperature Cracking in Asphalt Pavements National Pooled Fund Study – Phase II* (Report MN/RC 2012-23). Minnesota Department of Transportation. http://conservancy.umn.edu/handle/11299/135177

McDaniel, R. S., Shah, A., & Huber, G. (2012). *Investigation of Low- and High-Temperature Properties of Plant-Produced RAP Mixtures* (FHWA-HRT-11-058). https://rosap.ntl.bts.gov/view/dot/41731

Miner, M. A. (1945). Cumulative Damage in Fatigue. *Journal of Applied Mechanics*, *12*(3), A159–A164. https://doi.org/10.1115/1.4009458

Mirzaiyanrajeh, D., Dave, E. V., Sias, J. E., & Garg, N. (2022). Exploration of Cracking-Related Performance-Based Specification Indexes for Airfield Asphalt Mixtures. *Journal of Transportation Engineering, Part B: Pavements*, *148*(4), 04022057. https://doi.org/10.1061/JPEODX.0000401

Moavenzadeh, F. (1967). *Asphalt Fracture*. *36*, 51–72. https://trid.trb.org/view/100870

Mobasher, B., Mamlouk, M. S., & Lin, H.-M. (1997). Evaluation of Crack Propagation Properties of Asphalt Mixtures. *Journal of Transportation Engineering*, *123*(5), 405–413. https://doi.org/10.1061/(ASCE)0733-947X(1997)123:5(405)

Mogawer, W. S., Austerman, A. J., Bonaquist, R., & Roussel, M. (2011). Performance Characteristics of Thin-Lift Overlay Mixtures: High Reclaimed Asphalt Pavement Content, Recycled Asphalt Shingles, and Warm-Mix Asphalt Technology. *Transportation Research Record*, *2208*(1), 17–25. https://doi.org/10.3141/2208-03

Molenaar, A. A. A. (1984). Fatigue and Deflection Cracking Due to Traffic Loads. *Journal of the Association of Asphalt Paving Technologists*, *53*, 440–474. https://trid.trb.org/view/725970

Molenaar, A. A. A. (2007). Prediction of Fatigue Cracking in Asphalt Pavements: Do We Follow the Right Approach? *Transportation Research Record*, *2001*(1), 155–162. https://doi.org/10.3141/2001-17

Monismith, C. L., & Deacon, J. A. (1969). Fatigue of Asphalt Paving Mixtures. *Transportation Engineering Journal of ASCE*, *95*(2), 317–346. https://doi.org/10.1061/TPEJAN.0000023

Monismith, C. L., Secor, K. E., & Blackmer, E. W. (1961). Asphalt Mixture Behavior in Repeated Flexure. *In Association of Asphalt Paving Technologists Proceedings*, *30*, 188–222. https://trid.trb.org/view/728292

Murzewski, J. (1957). Une Theorie Statistique du Corps Fragile Quasihomogene. *Proc. IUTAM 9th Congrès*, 313–320.

NAPA. (2026). *Implementation Efforts*. National Asphalt Pavement Association. https://www.asphaltpavement.org/resources/key-initiatives/balanced-mix-design/implementation-efforts/

Nemati, R., Haslett, K., Dave, E. V., & Sias, J. E. (2019). Development of a Rate-Dependent Cumulative Work and Instantaneous Power-based Asphalt Cracking Performance Index. *Road Materials and Pavement Design*, *20*(sup1), S315–S331. https://doi.org/10.1080/14680629.2019.1586753

Newcomb, D., & Zhou, F. (2018). *Balanced Design of Asphalt Mixtures* (MN/RC 2018-22). Texas A&M Transportation Institute. https://mdl.mndot.gov/_flysystem/fedora/2023-01/201822.pdf

NJDOT B-10. (2007). *Overlay Test for Determining Crack Resistance of HMA*. New Jersey Department of Transportation.

Norouzi, A., Kim, D., & Richard Kim, Y. (2016). Numerical Evaluation of Pavement Design Parameters for the Fatigue Cracking and Rutting Performance of Asphalt Pavements. *Materials and Structures*, *49*(9), 3619–3634. https://doi.org/10.1617/s11527-015-0744-x

Norouzi, A., & Richard Kim, Y. (2017). Mechanistic Evaluation of Fatigue Cracking in Asphalt Pavements. *International Journal of Pavement Engineering*, *18*(6), 530–546. https://doi.org/10.1080/10298436.2015.1095909

Ozer, H., Al-Qadi, I. L., Lambros, J., El-Khatib, A., Singhvi, P., & Doll, B. (2016). Development of the Fracture-Based Flexibility Index for Asphalt Concrete Cracking Potential Using Modified Semi-Circle Bending Test Parameters. *Construction and Building Materials*, *115*, 390–401. https://doi.org/10.1016/j.conbuildmat.2016.03.144

Paris, P., & Erdogan, F. (1963). A Critical Analysis of Crack Propagation Laws. *Journal of Basic Engineering*, *85*(4), 528–533. https://doi.org/10.1115/1.3656900

Pell, P. S. (1962). Fatigue Characteristics of Bitumen and Bituminous Mixes. *International Conference on the Structural Design of Asphalt Pavements*, *203*(1), 43–58. https://trid.trb.org/View/717074

Pell, P. S., & Taylor, I. F. (1969, February). *Asphaltic Road Materials in Fatigue*. Association of Asphalt Paving Technologists Proc. https://trid.trb.org/View/105024

Pirmohammad, S., Khoramishad, H., & Ayatollahi, M. R. (2016). Effects of Asphalt Concrete Characteristics on Cohesive Zone Model Parameters of Hot Mix Asphalt Mixtures. *Canadian Journal of Civil Engineering*, *43*(3), 226–232. https://doi.org/10.1139/cjce-2014-0504

Rabotnov, Y. N. (1959). On the Long-Rerm Fracture Mechanism. In *Problems of Strength of Materials and Structures* (pp. 5–7). Izd. Akad. Nauk SSSR.

Rajagopal, K. R., & Srinivasa, A. R. (2005). A Note on a Correspondence Principle in Nonlinear Viscoelastic Materials. *International Journal of Fracture*, *131*(4), L47–L52. https://doi.org/10.1007/s10704-005-2599-6

Ramsamooj, D. V. (1970). *Analysis and Design of the Flexibility of Pavements*. [Doctoral dissertation, The Ohio State University]. https://www.proquest.com/dissertations-theses/analysis-design-flexibility-pavements/docview/302444857/se-2

Ramsamooj, D. V. (1993). Fracture of Highway and Airport Pavements. *Engineering Fracture Mechanics*, *44*(4), 609–626. https://doi.org/10.1016/0013-7944(93)90102-X

Rice, J. R. (1968). A Path Independent Integral and the Approximate Analysis of Strain Concentration by Notches and Cracks. *Journal of Applied Mechanics*, *35*(2), 379–386. https://doi.org/10.1115/1.3601206

Rivera-Pérez, J., Ozer, H., Lambros, J., & Al-Qadi, I. L. (2021). Illinois Flexibility Index Test: Effect of Specimen Geometry and Test Configuration on the Asphalt Concrete Damage Zone. *Journal of Transportation Engineering, Part B: Pavements*, *147*(1), 04020085. https://doi.org/10.1061/JPEODX.0000243

Roque, R., Birgisson, B., Drakos, C., & Dietrich, B. (2004). Development and Field Evaluation of Energy-Based Criteria for Top-Down Cracking Performance of Hot Mix Asphalt. *Journal of the Association of Asphalt Paving Technologists*, *73*, 229–260. https://trid.trb.org/view/749993

Roque, R., & Buttlar, W. G. (1992). Development of a Measurement and Analysis System to Accurately Determine Asphalt Concrete Properties Using the Indirect Tensile Mode. *Journal of the Association of Asphalt Paving Technologists*, *61*, 304–332. https://trid.trb.org/view/486940

Roque, R., & Ruth, B. E. (1990). Mechanisms and Modeling of Surface Cracking in Asphalt Pavements. *Journal of the Association of Asphalt Paving Technologists*, *59*, 396–421. https://trid.trb.org/view/487374

Roque, R., Zou, J., & Hernando, D. (2015). Cracking Mechanisms in Asphalt Mixtures. In *Advances in Asphalt Materials* (pp. 135–167). Elsevier. https://doi.org/10.1016/B978-0-08-100269-8.00005-2

Roque, R., Zou, J., Kim, Y. R., Baek, C., Thirunavukkarasu, S., Underwood, B. S., & Guddati, M. N. (2010). *Top-Down Cracking of Hot-Mix Asphalt Layers: Models for Initiation and Propagation* (p. 22935). Transportation Research Board. https://doi.org/10.17226/22935

Sabouri, M., & Kim, Y. R. (2014). Development of a Failure Criterion for Asphalt Mixtures under Different Modes of Fatigue Loading. *Transportation Research Record*, *2447*(1), 117–125. https://doi.org/10.3141/2447-13

Saqer, H., Nazzal, M. D., & Abbas, A. (2021). Evaluation of the Performance of Asphalt Mixes for Airport Pavements. *Journal of Materials in Civil Engineering*, *33*(4), 04021029. https://doi.org/10.1061/(ASCE)MT.1943-5533.0003629

Schapery, R. A. (1975). A Theory of Crack Initiation and Growth in Viscoelastic Media. *International Journal of Fracture*, *11*(1), 141–159. https://doi.org/10.1007/BF00034721

Schapery, R. A. (1981). On Viscoelastic Deformation and Failure Behavior of Composite Materials with Distributed Flaws. In *Advances in Aerospace Structures and Materials 1981* (pp. 5–20). ASME.

Schapery, R. A. (1997). Nonlinear Viscoelastic and Viscoplastic Constitutive Equations Based on Thermodynamics. *Mechanics of Time-Dependent Materials*, *1*(2), 209–240. https://doi.org/10.1023/A:1009767812821

Seo, Y., Kim, Y. R., Schapery, R. A., Witczak, M. W., & Bonaquist, R. (2004). A Study of Crack-Tip Deformation and Crack Growth in Asphalt Concrete Using Fracture Mechanics. *Journal of the Association of Asphalt Paving Technologists*, *73*, 697–730. https://trid.trb.org/view/750007

Shang, G. T., Takahashi, O., & Maekawa, R. (2013). Recommended Combination of the Bailey Parameters in Superpave Gradation Design for Japanese Airfield Pavements. *International Journal of Pavement Research and Technology*, *6*(6), 704–713. https://trid.trb.org/view/1279745

Son, S. (2014). *Development of a Phenomenological Constitutive Model for Fracture Resistance Degradation of Asphalt Concrete with Damage Growth Due to Repeated Loading* [Doctoral dissertation, University of Illinois Urbana Champaign]. http://hdl.handle.net/2142/49825

Song, S. H., Paulino, G. H., & Buttlar, W. G. (2006). A Bilinear Cohesive Zone Model Tailored for Fracture of Asphalt Concrete Considering Viscoelastic Bulk Material. *Engineering Fracture Mechanics*, *73*(18), 2829–2848. https://doi.org/10.1016/j.engfracmech.2006.04.030

Strategic Highway Research Program. (1994). *Fatigue Response of Asphalt-Aggregate Mixes* (SHRP-A-404; p. 309). National Research Council. https://trid.trb.org/View/405685

Su, K., Maekawa, R., & Hachiya, Y. (2009). Laboratory Evaluation of WMA Mixture for Use in Airport Pavement Rehabilitation. *Construction and Building Materials*, *23*(7), 2709–2714. https://doi.org/10.1016/j.conbuildmat.2008.12.011

Texas DOT. (2022). *Test Procedure for the Overlay Test. Tex-248-F (Revised)*. Texas Department of Transportation.

Tipnis, M., Kataware, A. V., Chowdary, K., Gupta, A., & Das, S. K. (2023). Case Study—Delhi International Airport Phase 3 Expansion Performance Based Mix Design for Bituminous Surface Course. *Airfield and Highway Pavements 2023*, 213–228. https://doi.org/10.1061/9780784484913.020

Tsai, B.-W., Harvey, J. T., & Monismith, C. L. (2003). Application of Weibull Theory in Prediction of Asphalt Concrete Fatigue Performance. *Transportation Research Record*, *1832*(1), 121–130. https://doi.org/10.3141/1832-15

Tsai, B.-W., Harvey, J. T., & Monismith, C. L. (2004). Two-Stage Weibull Approach for Asphalt Concrete Fatigue Performance Prediction. *Journal of the Association of Asphalt Paving Technologists*, *73*, 623–655. https://trid.trb.org/view/750005

Underwood, B. S., Kim, Y. R., & Guddati, M. N. (2010). Improved Calculation Method of Damage Parameter in Viscoelastic Continuum Damage Model. *International Journal of Pavement Engineering*, *11*(6), 459–476. https://doi.org/10.1080/10298430903398088

Van Dijk, W., & Visser, W. (1977). Energy Approach to Fatigue for Pavement Design. *In Association of Asphalt Paving Technologists Proceedings*, *46*, 1–40. https://trid.trb.org/view/87372

Virginia Test Method – 110. (2000). *Method of Test For Determining Rutting Susceptibility Using The Asphalt Pavement Analyzer*. Virginia Department of Transportation.

Wagoner, M. P. (2006). *Fracture Tests for Bituminous-Aggregate Mixtures: Laboratory and Field Investigations* [Doctoral dissertation, University of Illinois at Urbana-Champaign]. http://hdl.handle.net/2142/83316

Wagoner, M. P., Buttlar, W. G., Paulino, G. H., & Blankenship, P. (2005). Investigation of the Fracture Resistance of Hot-Mix Asphalt Concrete Using a Disk-Shaped Compact

Tension Test. *Transportation Research Record*, *1929*(1), 183–192. https://doi.org/10.1177/0361198105192900122

Wang, H. (2018). *Investigation on the Mechanisms of Block Cracking in Asphalt Pavements* [Doctoral dissertation, University of Illinois at Urbana-Champaign]. https://hdl.handle.net/2142/102469

Wang, H., & Al-Qadi, I. L. (2010). Near-Surface Pavement Failure Under Multiaxial Stress State in Thick Asphalt Pavement. *Transportation Research Record: Journal of the Transportation Research Board*, *2154*(1), 91–99. https://doi.org/10.3141/2154-08

Wang, H., Al-Qadi, I. L., Portas, S., & Coni, M. (2013). Three-Dimensional Finite Element Modeling of Instrumented Airport Runway Pavement Responses. *Transportation Research Record: Journal of the Transportation Research Board*, *2367*(1), 76–83. https://doi.org/10.3141/2367-08

Wang, H., Ozer, H., Al-Qadi, I. L., & Duarte, C. A. (2013). Analysis of Near-Surface Cracking under Critical Loading Conditions Using Uncracked and Cracked Pavement Models. *Journal of Transportation Engineering*, *139*(10), 992–1000. https://doi.org/10.1061/(ASCE)TE.1943-5436.0000562

Wang, Y., & Kim, Y. (2019). Development of a Pseudo Strain Energy-based Fatigue Failure Criterion for Asphalt Mixtures. *International Journal of Pavement Engineering*, *20*(10), 1182–1192. https://doi.org/10.1080/10298436.2017.1394100

Wang, Y., Mahboub, K. C., & Hancher, D. E. (2005). Survival Analysis of Fatigue Cracking for Flexible Pavements Based on Long-Term Pavement Performance Data. *Journal of Transportation Engineering*, *131*(8), 608–616. https://doi.org/10.1061/(ASCE)0733-947X(2005)131:8(608)

West, R., Rodezno, C., Leiva, F., & Yin, F. (2018). *Development of a Framework for Balanced Mix Design* (NCHRP 20-07/Task 406). National Center for Asphalt Technology at Auburn University. https://onlinepubs.trb.org/onlinepubs/nchrp/docs/NCHRP20-07(406)_Revised_final_report.pdf

Williams, M. L. (1957). On the Stress Distribution at the Base of a Stationary Crack. *Journal of Applied Mechanics*, *24*(1), 109–114. https://doi.org/10.1115/1.4011454

Wu, R., Harvey, J., Buscheck, J., & Mateos, A. (2018). *Mechanistic-Empirical (ME) Design: Mix Design Guidance for Use with Asphalt Concrete Performance-Related Specifications* (UCPRC-RR-2017-12). University of California Pavement Research Center. https://escholarship.org/uc/item/0jg6f2qp

Wu, Z., Mohammad, L. N., Wang, L. B., & Mull, M. A. (2005). Fracture Resistance Characterization of Superpave Mixtures Using the Semi-Circular Bending Test. *Journal of ASTM International*, *2*(3), 1–15. https://doi.org/https://doi.org/10.1520/JAI12264

Yin, F., & West, R. (2021). *Balanced Mix Design Resource Guide*. National Asphalt Pavement Association. https://go.asphaltpavement.org/balanced-mix-design-resource-guide-lp

Yin, H., & Barbagallo, D. (2013). Development of Full-Scale Reflective Cracking Test at the FAA National Airport Pavement Test Facility. *Transportation Research Record*, *2368*(1), 81–91. https://doi.org/10.3141/2368-08

Zhang, Z., Roque, R., & Birgisson, B. (2001). Evaluation of Laboratory-Measured Crack Growth Rate for Asphalt Mixtures. *Transportation Research Record: Journal of the Transportation Research Board*, *1767*(1), 67–75. https://doi.org/10.3141/1767-09

Zhao, Y., Alae, M., & Fu, G. (2018). Investigation of Mechanisms of Top-Down Fatigue Cracking of Asphalt Pavement. *Road Materials and Pavement Design*, *19*(6), 1436–1447. https://doi.org/10.1080/14680629.2017.1303394

Zhou, F., Hu, S., Scullion, T., Chen, D.-H., Qi, X., & Claros, G. (2007). Development and Verification of the Overlay Tester Based Fatigue Cracking Prediction Approach. *Journal of the Association of Asphalt Paving Technologists*, *76*, 627–662. https://trid.trb.org/View/839509

Zhou, F., Im, S., Sun, L., & Scullion, T. (2017). Development of an IDEAL Cracking Test for Asphalt Mix Design and QC/QA. *Road Materials and Pavement Design*, *18*(sup4), 405–427. https://doi.org/10.1080/14680629.2017.1389082

Zhou, F., & Scullion, T. (2005). *Overlay Tester: A Rapid Performance Related Crack Resistance Test* (FHWA/TX-05/0-4467-2). Federal Highway Administration. https://trid.trb.org/view/760186

Zhou, F., Scullion, T., Walubita, L. F., & Wilson, B. (2014). Implementation of a Performance-Based Mix Design System in Texas. *In Application of Asphalt Mix Performance-Based Specifications (Transportation Research Circular No. E-C189)*, 32–50. https://onlinepubs.trb.org/onlinepubs/circulars/ec189.pdf

Zhou, F., Steger, R., & Mogawer, W. (2021). Development of a Coherent Framework for Balanced Mix Design and Production Quality Control and Quality Acceptance. *Construction and Building Materials*, *287*, 123020. https://doi.org/10.1016/j.conbuildmat.2021.123020

Zhu, Y., Dave, E. V., Rahbar-Rastegar, R., Daniel, J. S., & Zofka, A. (2017). Comprehensive Evaluation of Low-Temperature Fracture Indices for Asphalt Mixtures. *Road Materials and Pavement Design*, *18*(sup4), 467–490. https://doi.org/10.1080/14680629.2017.1389085

Appendix B: Field Core Mixture Designs

National Airport Pavement and Materials Research Center (NAPMRC)

Table B-1. Gradation Design for NAPMRC Test Lane 1
(PG 76-22, P_b = 5%)

Sieve Size	Cumulative Percent Passing (%)
25 mm (1")	100
19 mm (3/4")	97.1
12.5 mm (1/2")	84.0
9.5 mm (3/8")	74.4
4.75 mm (#4)	52.0
2.36 mm (#8)	36.0
1.18 mm (#16)	25.2
0.6 mm (#30)	17.8
0.3 mm (#50)	11.4
0.15 mm (#100)	7.2
0.075 mm (#200)	4.0

Table B-2. Gradation Design for NAPMRC Test Lane 2
(PG 76-22, P_b = 5%, 0.5% Chemical WMA Additive)

Sieve Size	Cumulative Percent Passing (%)
25 mm (1")	100
19 mm (3/4")	97.1
12.5 mm (1/2")	84.0
9.5 mm (3/8”)	74.4
4.75 mm (#4)	52.0
2.36 mm (#8)	36.0
1.18 mm (#16)	25.2
0.6 mm (#30)	17.8
0.3 mm (#50)	11.4
0.15 mm (#100)	7.2
0.075 mm (#200)	4.0

WMA = warm mix asphalt.

Table B-3. Gradation Design for NAPMRC Test Lane 3 (PG 76-22, P_b = 5%, 1.5% Organic WMA Additive)

Sieve Size	Cumulative Percent Passing (%)
25 mm (1")	100
19 mm (3/4")	97.1
12.5 mm (1/2")	84.0
9.5 mm (3/8")	74.4
4.75 mm (#4)	52.0
2.36 mm (#8)	36.0
1.18 mm (#16)	25.2
0.6 mm (#30)	17.8
0.3 mm (#50)	11.4
0.15 mm (#100)	7.2
0.075 mm (#200)	4.0

WMA = warm mix asphalt.

Table B-4. Gradation Design for NAPMRC Test Lane 4 (PG 76-22, P_b = 5%, 0.25% Hybrid WMA Additive)

Sieve Size	Cumulative Percent Passing (%)
25 mm (1")	100
19 mm (3/4")	97.1
12.5 mm (1/2")	84.0
9.5 mm (3/8")	74.4
4.75 mm (#4)	52.0
2.36 mm (#8)	36.0
1.18 mm (#16)	25.2
0.6 mm (#30)	17.8
0.3 mm (#50)	11.4
0.15 mm (#100)	7.2
0.075 mm (#200)	4.0

WMA = warm mix asphalt.

Table B-5. Gradation Design for NAPMRC Test Lane 5
(PG 76-22, P_b = 5%, 1.5% Organic WMA Additive, 4% Latex)

Sieve Size	Cumulative Percent Passing (%)
25 mm (1")	100
19 mm (3/4")	97.1
12.5 mm (1/2")	84.0
9.5 mm (3/8")	74.4
4.75 mm (#4)	52.0
2.36 mm (#8)	36.0
1.18 mm (#16)	25.2
0.6 mm (#30)	17.8
0.3 mm (#50)	11.4
0.15 mm (#100)	7.2
0.075 mm (#200)	4.0

WMA = warm mix asphalt.

Table B-6. Gradation Design for NAPMRC Test Lane 6
(PG 76-22, P_b = 5%, 1.5% Organic WMA Additive, 4% Latex, 20% RAP)

Sieve Size	Cumulative Percent Passing (%)
25 mm (1")	100
19 mm (3/4")	97.1
12.5 mm (1/2")	83.7
9.5 mm (3/8")	74.0
4.75 mm (#4)	51.1
2.36 mm (#8)	36.0
1.18 mm (#16)	26.0
0.6 mm (#30)	18.7
0.3 mm (#50)	12.1
0.15 mm (#100)	7.4
0.075 mm (#200)	4.7

WMA = warm mix asphalt; RAP = reclaimed asphalt pavement.

University of Illinois–Willard Airport (CMI)

Table B-7. Gradation Design for CMI S3
(PG 70-22, P_b = 6.4%)

Sieve Size	Cumulative Percent Passing (%)
25 mm (1")	100
19 mm (3/4")	100
12.5 mm (1/2")	97.0
9.5 mm (3/8")	84.0
4.75 mm (#4)	65.0
2.36 mm (#8)	47.0
1.18 mm (#16)	29.0
0.6 mm (#30)	18.0
0.3 mm (#50)	11.0
0.15 mm (#100)	7.0
0.075 mm (#200)	6.0

Table B-8. Gradation Design for CMI S3 RAP
(PG 70-22, P_b = 5.9%, 20% RAP)

Sieve Size	Cumulative Percent Passing (%)
25 mm (1")	100
19 mm (3/4")	99.0
12.5 mm (1/2")	87.0
9.5 mm (3/8")	81.0
4.75 mm (#4)	57.0
2.36 mm (#8)	37.0
1.18 mm (#16)	23.0
0.6 mm (#30)	15.0
0.3 mm (#50)	10.0
0.15 mm (#100)	7.0
0.075 mm (#200)	5.6

RAP = reclaimed asphalt pavement.

Note: Designs for CMI S1 and CMI S2 were not available.

Kansas City International Airport (MCI)

Table B-9. Gradation Design for MCI
(PG 70-28, P_b = 6.3%)

Sieve Size	Cumulative Percent Passing (%)
25 mm (1")	100
19 mm (3/4")	100
12.5 mm (1/2")	92.0
9.5 mm (3/8")	85.0
4.75 mm (#4)	65.0
2.36 mm (#8)	44.0
1.18 mm (#16)	28.0
0.6 mm (#30)	18.0
0.3 mm (#50)	11.0
0.15 mm (#100)	6.0
0.075 mm (#200)	4.3

Appendix C: Dynamic Modulus and Texas Overlay Test Results

Dynamic Modulus (AASHTO T 342)

Testing Temperatures: −10 °C (14 °F), 4 °C (39 °F), 21.1 °C (70 °F), 37.8 °C (100 °F), 54.0 °C (129.2 °F)

Test Frequencies: 0.1, 0.5, 1, 5, 10, 25 Hz

Fitting Model and Parameters:

$$Log\ |E^*| = \delta + \frac{\alpha}{1 + e^{\beta + \gamma\ \mathrm{Log}(F_r)}}$$

$$Log(F_r) = Log\ (F) + \ a_1(T_r - T) + a_2(T_r - T)^2$$

E^* = dynamic Modulus

F = loading frequency at test temperature T

T_r = reference temperature 20 °C (68 °F)

F_r = reduced frequency

α, β, γ, δ, a_1, a_2 = fitting coefficients

Acronyms and abbreviations used in Figures C-1 through C-11 and Tables C-1 through C-8:

AV	Air voids
EWR	Newark Liberty International Airport
FAA	Federal Aviation Administration
ORAP	Chicago O’Hare International Airport’s reclaimed asphalt pavement mixture
ORD	Chicago O’Hare International Airport
PMLC	Plant-mixed, laboratory-compacted
RTS	Reno Stead Airport
SFO	San Francisco International Airport
SMF	Sacramento International Airport
TEB	Teterboro Airport
TPA	Tampa International Airport

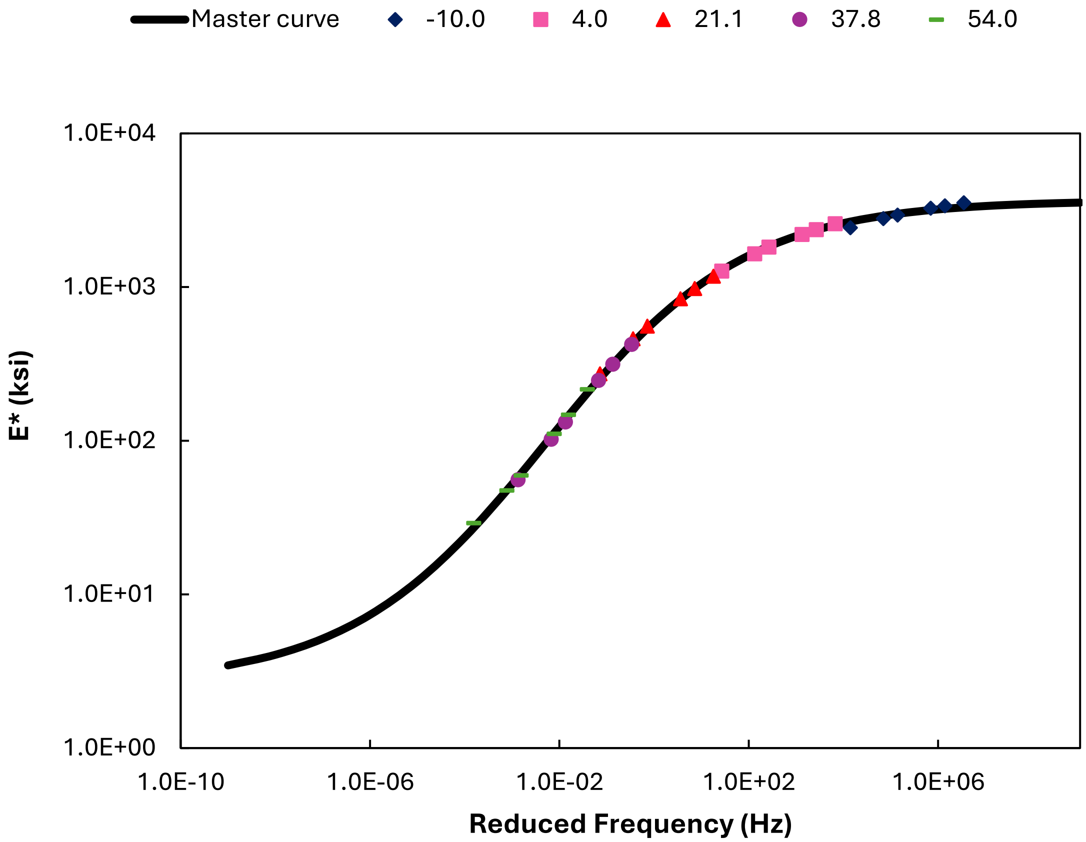

Source: AAPTP

Figure C-1. Dynamic Modulus Master Curve for EWR PMLC

Table C-1. Fitting Coefficients for EWR

α	β	δ	γ	a_1	a_2
3.14E+00	-1.09E+00	4.19E-01	-4.81E-01	1.30E-01	1.39E-03

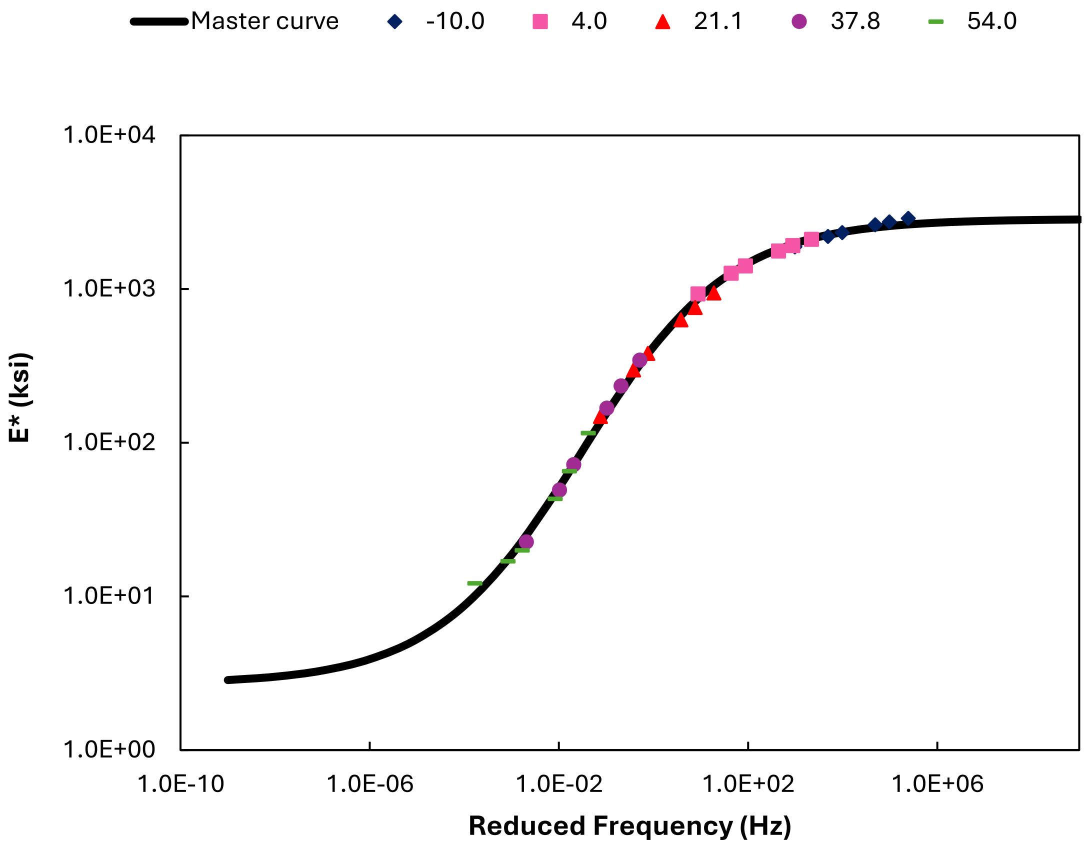

Source: AAPTP

Figure C-2. Dynamic Modulus Master Curve for TEB PMLC

Table C-2. Fitting Coefficients for TEB

α	β	γ	δ	a_1	a_2
3.03E+00	-9.70E-01	4.31E-01	-6.42E-01	1.09E-01	8.04E-04

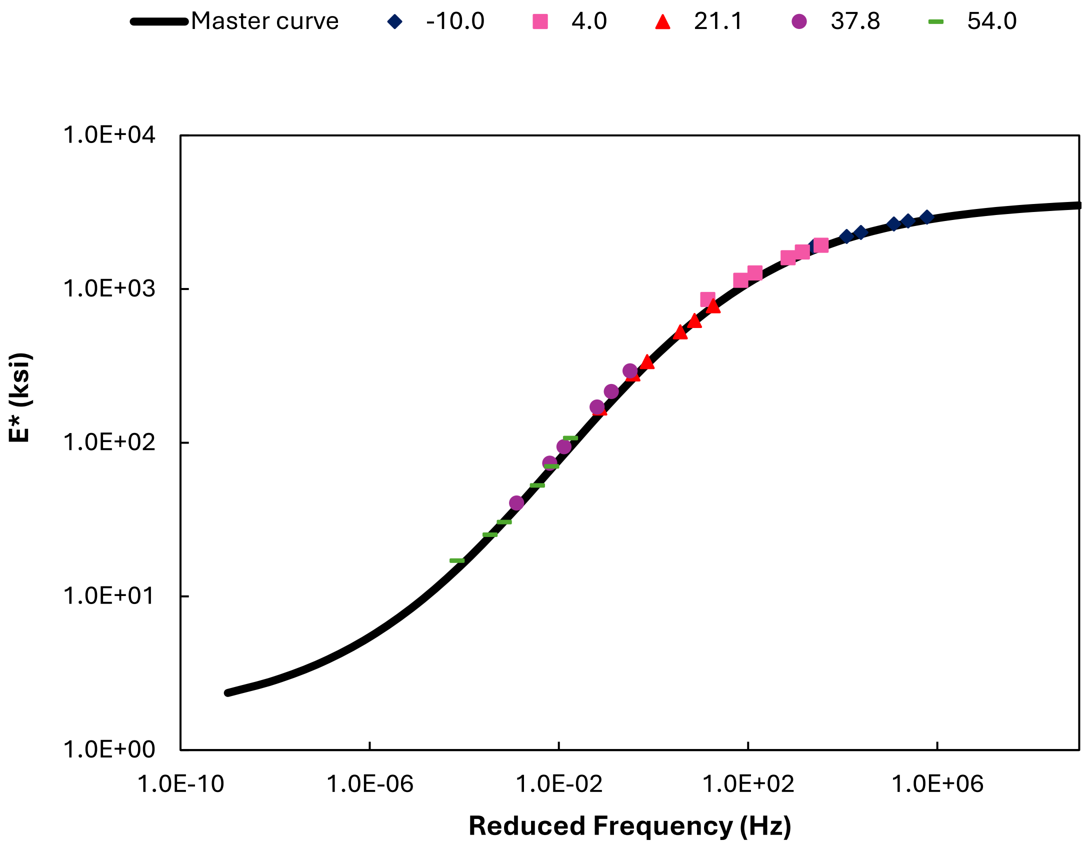

Source: AAPTP

Figure C-3. Dynamic Modulus Master Curve for TPA PMLC

Table C-3. Fitting Coefficients for TPA

α	β	γ	δ	a_1	a_2
3.38E+00	-8.30E-01	1.97E-01	-4.15E-01	1.21E-01	8.38E-04

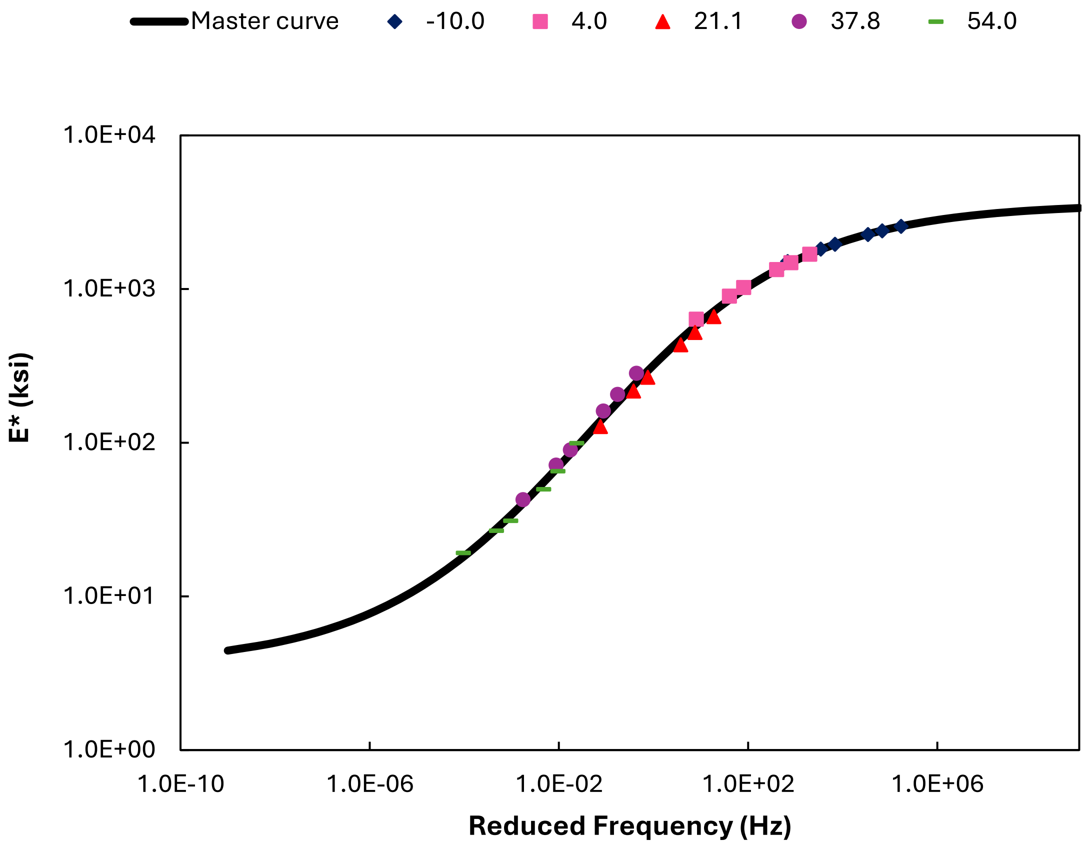

Source: AAPTP

Figure C-4. Dynamic Modulus Master Curve for RTS PMLC

Table C-4. Fitting Coefficients for RTS

α	β	γ	δ	a_1	a_2
3.00E+00	-6.20E-01	5.51E-01	-4.48E-01	1.10E-01	6.13E-04

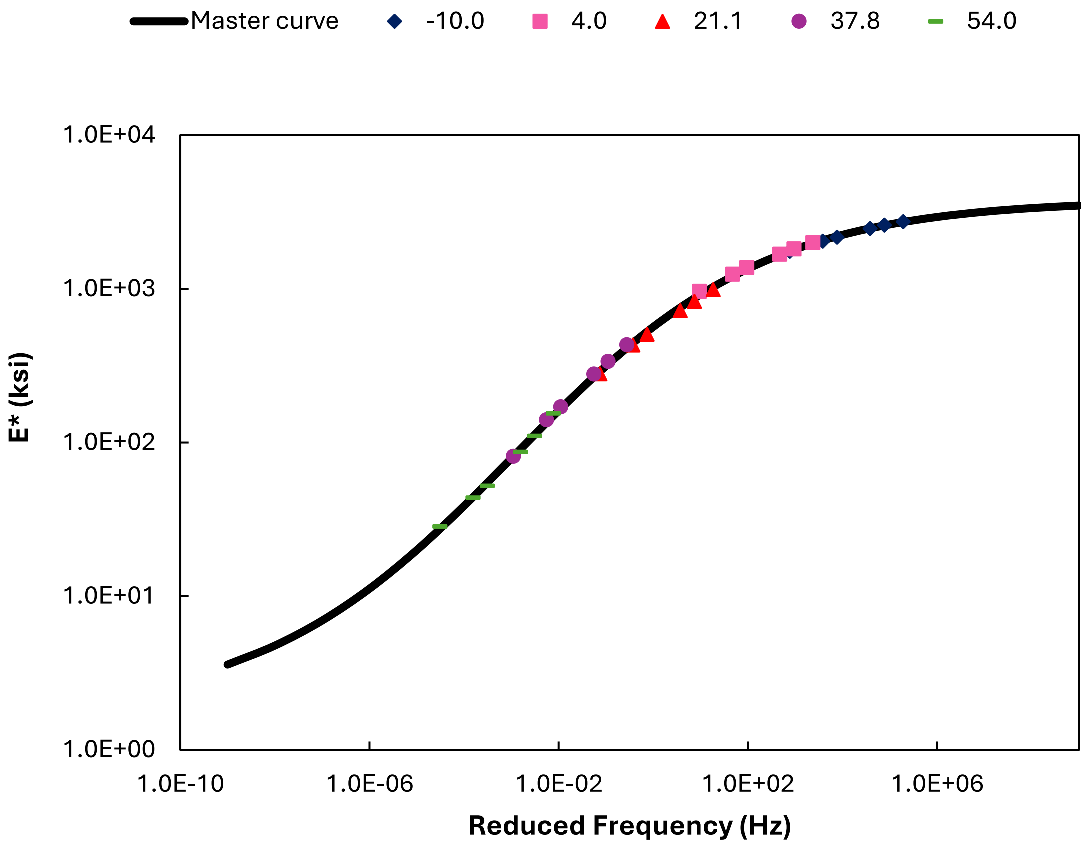

Source: AAPTP

Figure C-5. Dynamic Modulus Master Curve for SMF PMLC

Table C-5. Fitting Coefficients for SMF

α	β	γ	δ	a_1	a_2
3.34E+00	-1.11E+00	2.43E-01	-3.76E-01	1.17E-01	4.14E-04

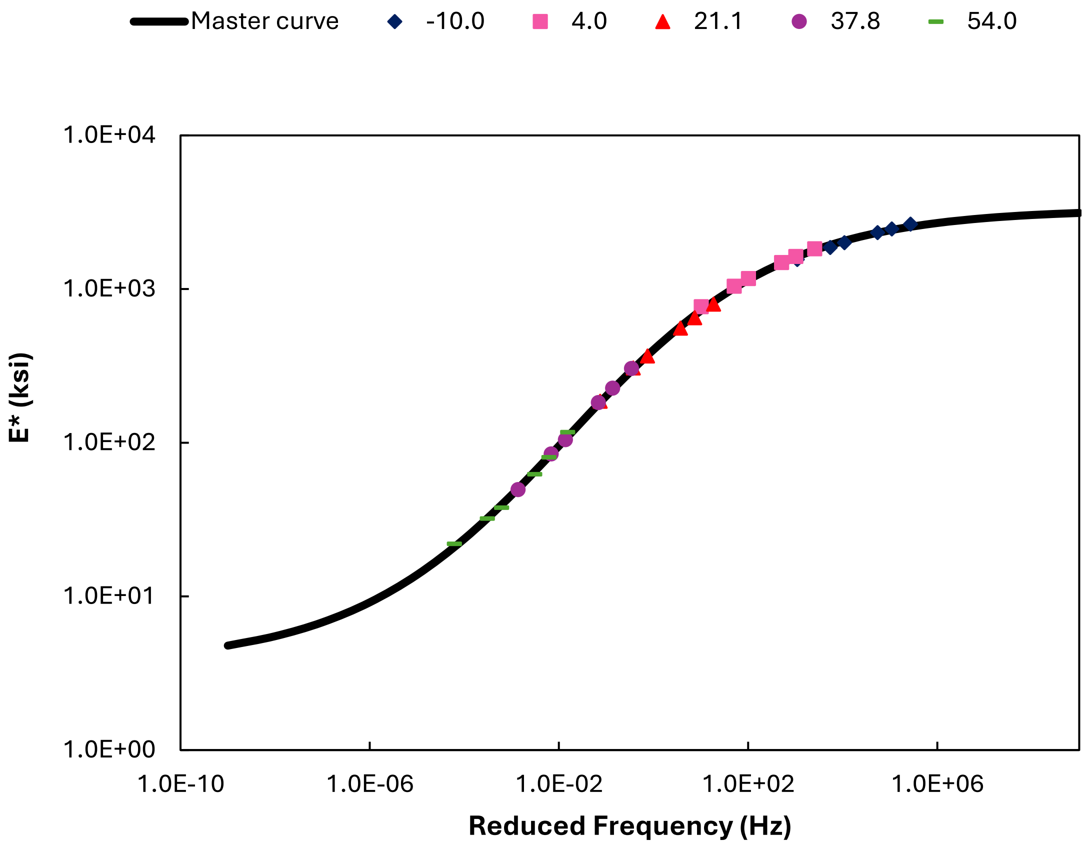

Source: AAPTP

Figure C-6. Dynamic Modulus Master Curve for SFO PMLC

Table C-6. Fitting Coefficients for SFO

α	β	γ	δ	a_1	a_2
2.96E+00	-8.03E-01	5.63E-01	-4.44E-01	1.16E-01	6.30E-04

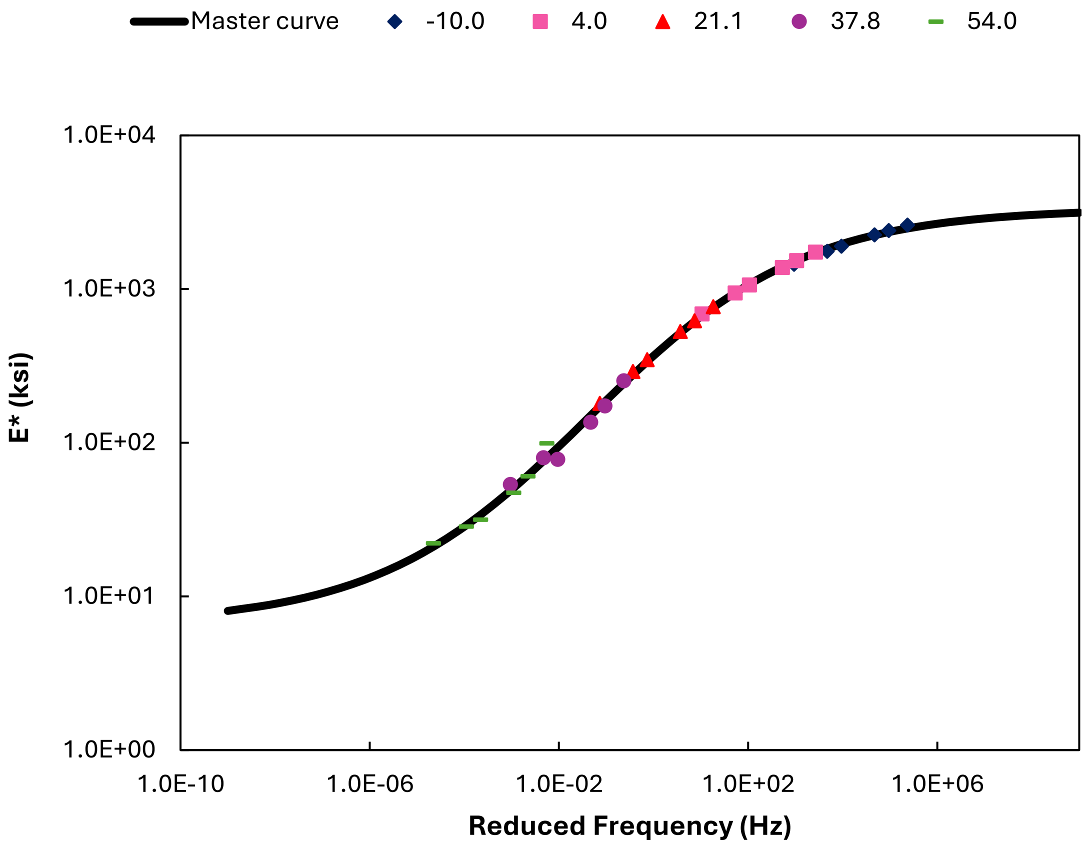

Source: AAPTP

Figure C-7. Dynamic Modulus Master Curve for ORD PMLC

Table C-7. Fitting Coefficients for ORD

α	β	γ	δ	a_1	a_2
2.70E+00	-6.00E-01	8.19E-01	-4.46E-01	1.21E-01	3.93E-04

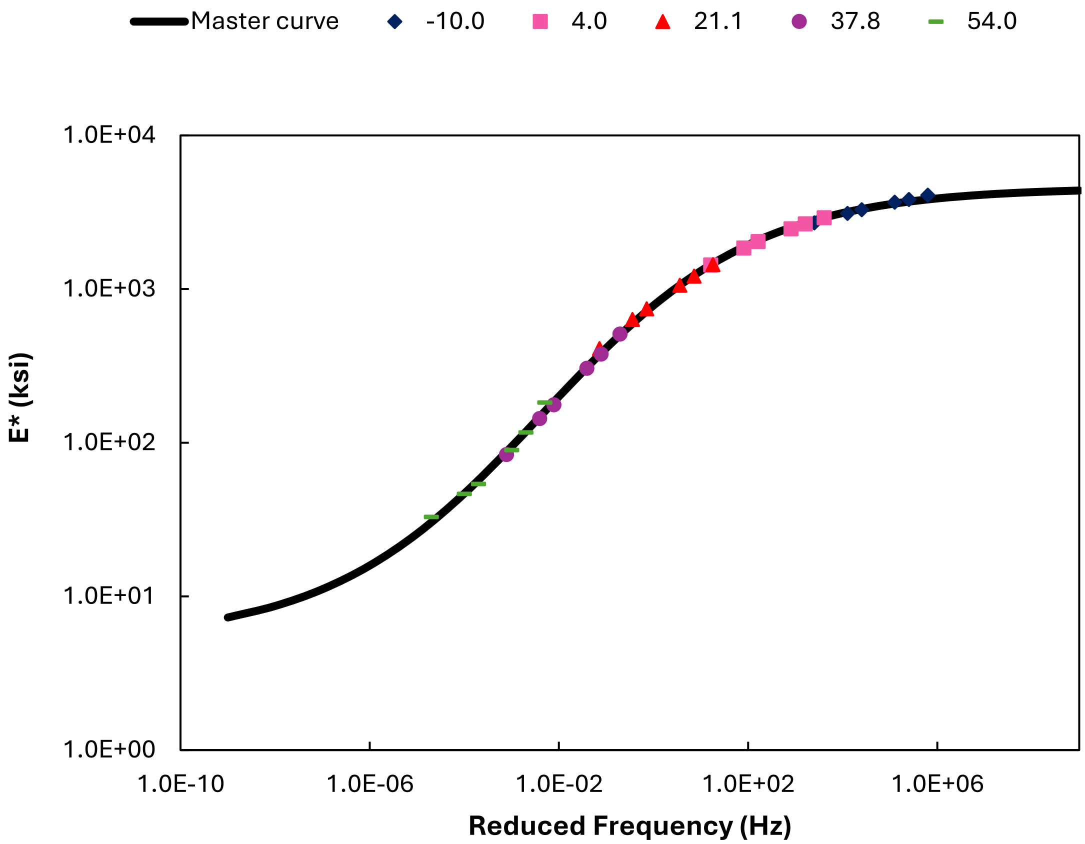

Source: AAPTP

Figure C-8. Dynamic Modulus Master Curve for ORAP PMLC

Table C-8. Fitting Coefficients for ORAP

α	β	γ	δ	a_1	a_2
2.94E+00	-1.04E+00	7.19E-01	-4.45E-01	1.29E-01	5.96E-04

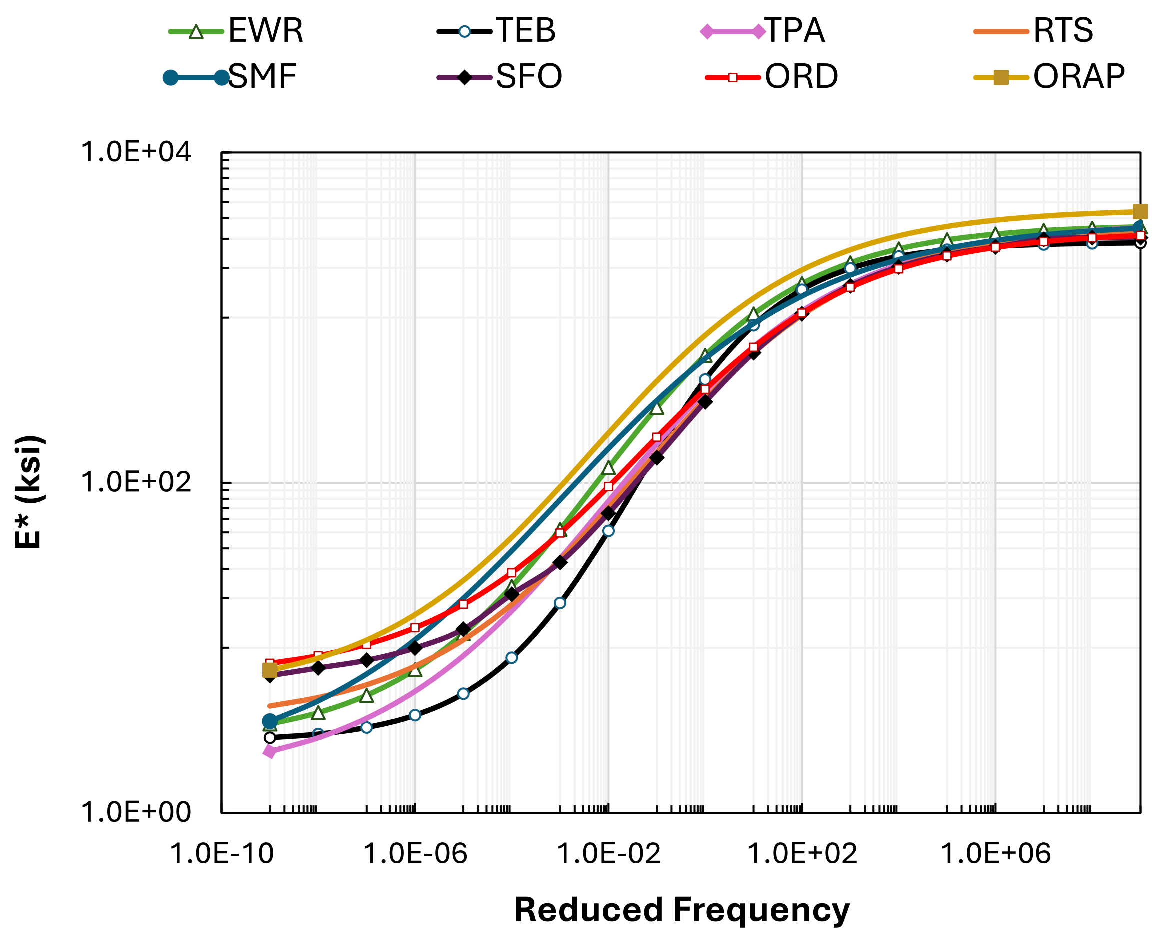

Source: AAPTP

Figure C-9. Comparison of Dynamic Modulus Master Curve for PMLC

Texas Overlay Test (Tex-248-F)

The Texas Overlay Test (OT) was conducted in accordance with *Tex-248-F*, developed by the Texas Department of Transportation. The tests were conducted using a universal testing machine load frame equipped with a customized testing fixture (Figure C-10). The test was conducted at 25 °C for the collected plant mixture, laboratory-produced mixture, and collected field cores. Rectangular asphalt concrete specimens were sawed from laboratory-compacted gyratory pills or field cores and trimmed to dimensions of 76±0.5 mm (3±0.02 inches) wide by 38±0.5 mm (1.5±0.02 inches) thick, following precise cutting templates and guidelines. Each specimen was glued using a high-strength, two-part epoxy between two steel plates: one fixed and one mounted to a vertically sliding block. A 4.2-mm (0.165-inch) spacer bar was used to maintain consistent gap alignment during mounting. A 6.8-kg (15-lb) weight was applied to each specimen during epoxy curing to ensure full plate contact.

(a)

(b)

Source: AAPTP

Figure C-10. OT (a) Specimen and (b) Vertical Setup

After curing for at least 24 hr, the mounted assemblies were conditioned at 25±0.5 °C (77±1 °F) for a minimum of 1 hr before testing. Cyclic direct tension was applied via a triangular waveform at a constant maximum displacement of 0.635 mm (0.025 inches) per cycle, with each cycle lasting 10 s. Testing commenced following a 10-min relaxation period to stabilize specimen temperature and seating stress. The test was terminated once a 70- or 93-percent reduction in maximum load from the first cycle was observed or after 1,000 cycles, whichever occurred first. Testing was conducted on short-term aged (STA) specimens only.

Three key parameters derived from the OT describe the fatigue behavior of asphalt mixtures:

- **Number of Cycles to Failure (Nf):** Number of cycles needed to reach a 70-percent reduction in maximum load, provided it occurs within 1,200 cycles. The number of cycles threshold for the maximum load reduction was set based on the machine and rigidity of the OT fixture. The standard OT fixture, which uses 93-percent reduction in force, was found to be more rigid than the universal testing machine custom fixture, so the threshold for maximum load reduction was set at 70 percent for this test setup.

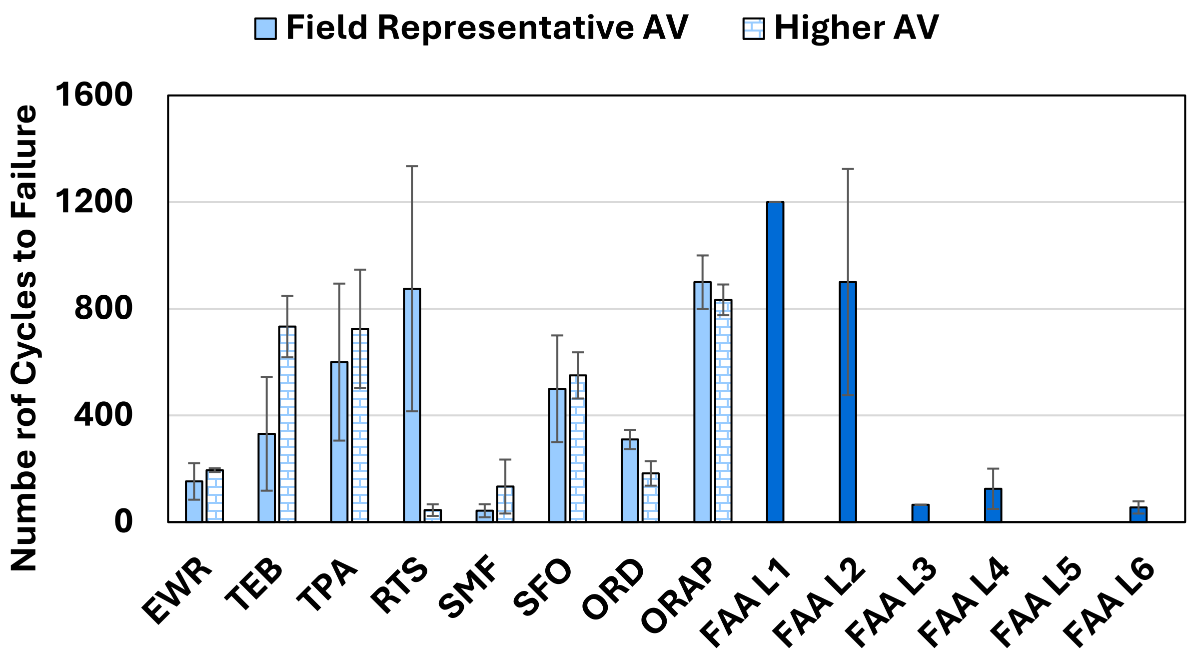

Source: AAPTP

Figure C-11. Number of Cycles to Failure for PMLC and Field Core Specimens

- **Crack Progression Rate (β):** This describes how quickly a crack propagates under repeated loading and is determined by fitting the load and cycle data to a power model.

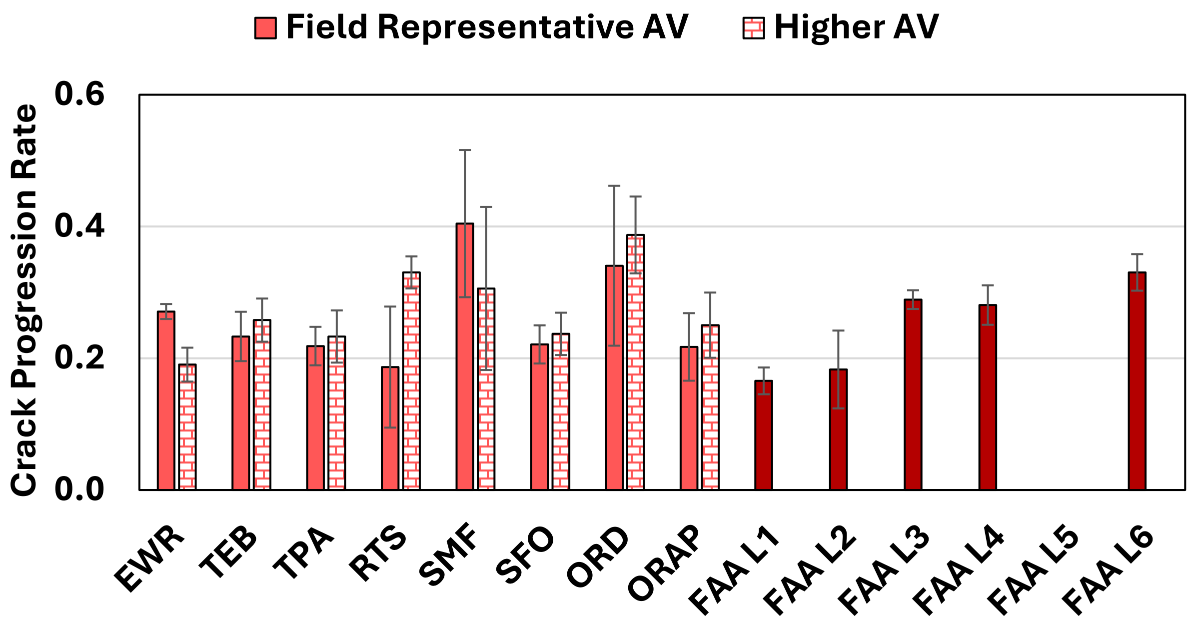

Source: AAPTP

Figure C-12. Crack Progression Rate for PMLC and Field Core Specimens

- **Critical Fracture Energy (Gc):** This parameter is calculated as the area under the load-displacement curve up to the peak load during the first cycle divided by the specimen cross-sectional area. The parameter represents the total energy required to initiate damage or cracking.

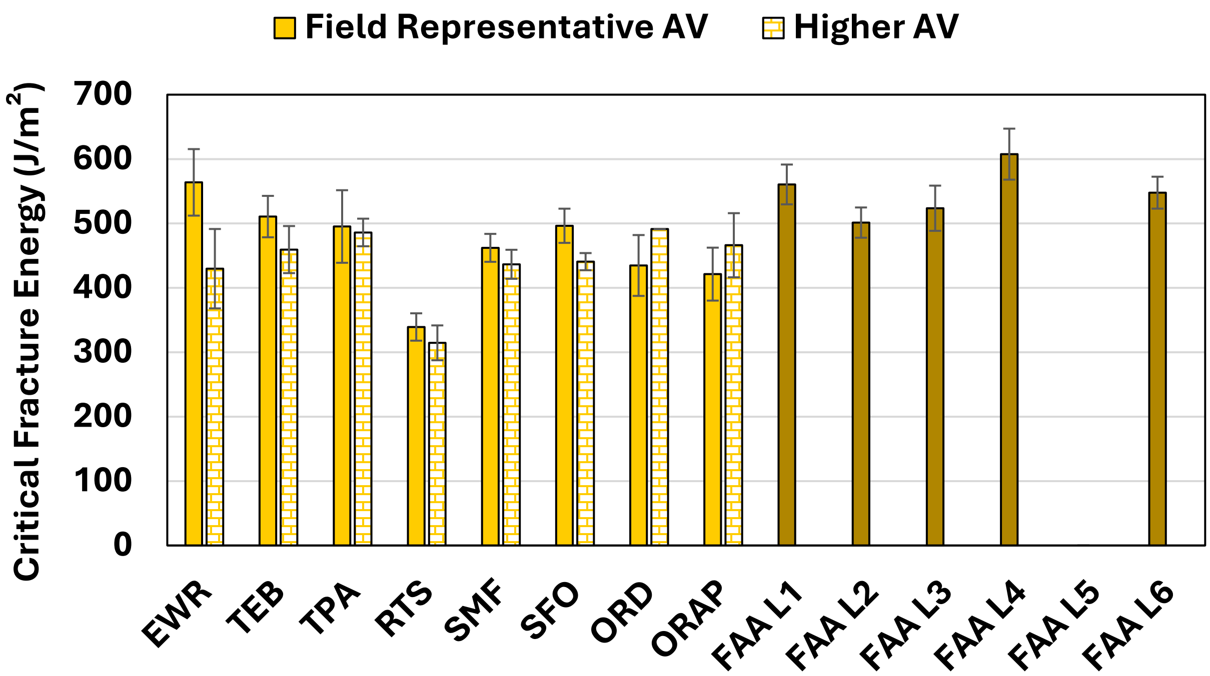

Source: AAPTP

Figure C-13. Critical Fracture Energy for PMLC and Field Core Specimens

The test showed limited potential to distinguish mixtures with varying design variables and field cores with known performance. Binder-rich and polymer-modified mixtures exhibited higher critical fracture energy, lower crack progression rate, and higher number of cycles to failure, while stiff mixtures or mixtures with lower voids in mineral aggregate (VMA) or binder volume generally performed poorly in the test. Preliminary thresholds of 0.3 for crack progression rate and 200 for number of cycles to failure are recommended for further investigation.

Appendix D: Laboratory-Mixed, Laboratory-Compacted Mixture Designs

Newark Liberty International Airport (EWR)

Table D-1. Gradation Design for EWR (PG 82-22, P_b = 4.49%)

Sieve Size	JMF Cumulative Percent Passing (%)	LMLC Cumulative Percent Passing (%)
25 mm (1")	100	100
19 mm (3/4")	95.1	95.6
12.5 mm (1/2")	75.5	76.4
9.5 mm (3/8")	57.7	59.4
4.75 mm (#4)	37.1	37.9
2.36 mm (#8)	32.0	33.3
1.18 mm (#16)	21.1	22.0
0.6 mm (#30)	15.4	16.2
0.3 mm (#50)	10.7	11.8
0.15 mm (#100)	7.2	8.2
0.075 mm (#200)	4.4	5.5

JMF = job mix formula; LMLC = laboratory-mixed, laboratory-compacted.

Teterboro Airport (TEB)

Table D-2. Gradation Design for TEB (PG 64-22, P_b = 5.03%)

Sieve Size	JMF Cumulative Percent Passing (%)	LMLC Cumulative Percent Passing (%)
25 mm (1")	100	100
19 mm (3/4")	100	100
12.5 mm (1/2")	89.0	89.2
9.5 mm (3/8")	74.7	75.7
4.75 mm (#4)	46.8	46.6
2.36 mm (#8)	32.9	32.6
1.18 mm (#16)	21.9	22.4
0.6 mm (#30)	16.2	17.4
0.3 mm (#50)	10.4	11.3
0.15 mm (#100)	6.4	7.5
0.075 mm (#200)	3.1	4.3

JMF = job mix formula; LMLC = laboratory-mixed, laboratory-compacted.

Tampa International Airport (TPA)

Table D-3. Gradation Design for TPA (PG 82-22, P_b = 6.80%)

Sieve Size	JMF Cumulative Percent Passing (%)	LMLC Cumulative Percent Passing (%)
25 mm (1")	100	100
19 mm (3/4"	100	100
12.5 mm (1/2")	100	100
9.5 mm (3/8")	97.3	97.4
4.75 mm (#4)	71.3	71.6
2.36 mm (#8)	49.5	49.0
1.18 mm (#16)	36.9	37.0
0.6 mm (#30)	28.6	28.6
0.3 mm (#50)	20.7	21.1
0.15 mm (#100)	7.0	7.8
0.075 mm (#200)	4.0	3.9

JMF = job mix formula; LMLC = laboratory-mixed, laboratory-compacted.

Reno Stead Airport (RTS)

Table D-4. Gradation Design for RTS (PG 64-28, P_b = 5.70%)

Sieve Size	JMF Cumulative Percent Passing (%)	LMLC Cumulative Percent Passing (%)
25 mm (1")	100	100
19 mm (3/4")	100	100
12.5 mm (1/2")	95.5	95.8
9.5 mm (3/8")	88.4	88.6
4.75 mm (#4)	60.7	60.7
2.36 mm (#8)	48.6	49.0
1.18 mm (#16)	33.4	33.5
0.6 mm (#30)	23.4	23.7
0.3 mm (#50)	14.7	15.1
0.15 mm (#100)	8.9	9.1
0.075 mm (#200)	6.0	6.4

JMF = job mix formula; LMLC = laboratory-mixed, laboratory-compacted.

San Francisco International Airport (SFO)

Table D-5. Gradation Design for SFO (PG 76-22, P_b = 5.50%)

Sieve Size	JMF Cumulative Percent Passing (%)	LMLC Cumulative Percent Passing (%)
25 mm (1")	100	100
19 mm (3/4")	96.9	96.5
12.5 mm (1/2")	86.6	86.6
9.5 mm (3/8")	78.8	79.1
4.75 mm (#4)	63.4	63.2
2.36 mm (#8)	47.1	46.6
1.18 mm (#16)	33.2	32.5
0.6 mm (#30)	21.6	21.0
0.3 mm (#50)	12.1	11.5
0.15 mm (#100)	5.7	5.3
0.075 mm (#200)	3.5	3.0

JMF = job mix formula; LMLC = laboratory-mixed, laboratory-compacted.

Chicago O'Hare International Airport (ORD)

Table D-6. Gradation Design for ORD (PG 76-28, P_b = 6.20%)

Sieve Size	JMF Cumulative Percent Passing (%)	LMLC Cumulative Percent Passing (%)
25 mm (1")	100	100
19 mm (3/4")	100	100
12.5 mm (1/2")	98.0	98.1
9.5 mm (3/8")	88.2	88.3
4.75 mm (#4)	59.9	60.5
2.36 mm (#8)	37.5	38.2
1.18 mm (#16)	22.1	22.9
0.6 mm (#30)	13.8	14.4
0.3 mm (#50)	9.0	9.5
0.15 mm (#100)	6.1	6.9
0.075 mm (#200)	4.9	5.3

JMF = job mix formula; LMLC = laboratory-mixed, laboratory-compacted.

Chicago O'Hare International Airport's Reclaimed Asphalt Pavement Mixture (ORAP)

Table D-7. Gradation Design for ORAP (PG 76-22, P_b = 5.02%)

Sieve Size	JMF Cumulative Percent Passing (%)	LMLC Cumulative Percent Passing (%)
25 mm (1")	100	100
19 mm (3/4")	97.7	96.8
12.5 mm (1/2")	88.8	88.7
9.5 mm (3/8")	82.7	82.8
4.75 mm (#4)	47.2	47.6
2.36 mm (#8)	27.9	27.3
1.18 mm (#16)	17.4	16.7
0.6 mm (#30)	12.6	11.4
0.3 mm (#50)	8.7	7.9
0.15 mm (#100)	6.3	5.7
0.075 mm (#200)	4.9	5.0

JMF = job mix formula; LMLC = laboratory-mixed, laboratory-compacted.

Appendix E: Development of the Simplified Low-Temperature Semi-Circular Bend Test

Table of Contents

List of Figures

List of Tables

Loading Rate Selection

A crack mouth opening displacement (CMOD) rate (i.e., crack propagation rate) of 0.7 mm/min in Semi-Circular Bend (SCB) geometry was reported as analogous to a 1 mm/min CMOD rate in the Disk-shaped Compact Tension (DCT) geometry (Dave & Behnia, 2018; Son et al., 2019). Therefore, experimental trials were performed for three mixtures with varying nominal maximum aggregate size (NMAS), ranging from 4.75 mm to 19 mm, to establish the load line displacement (LLD) rate necessary for maintaining the target CMOD rate of ≤0.7 mm/min at a test temperature of −12 °C. The 4.75-mm NMAS mixture (RR) was a highway mixture, explicitly chosen to account for smaller NMAS asphalt mixtures. The procedure for conducting the trials is illustrated in Figure E-1.

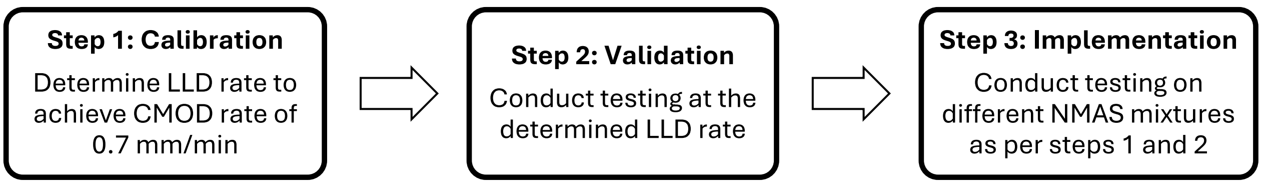

Source: AAPTP

Figure E-1. LLD Loading Rate Determination Trial Procedure

Table E-1 summarizes the test results of Newark Liberty International Airport (EWR), Teterboro Airport (TEB), and RR mixture specimens. The procedure suggests a loading rate of 0.19 mm/min for EWR, 0.21 mm/min for TEB, and 0.23 mm/min for RR to match a CMOD rate of ≤0.7 mm/min. The results indicated that the LLD rate required to achieve the target CMOD rate was influenced by the NMAS of the mixture. Specifically, the LLD rate was inversely proportional to the NMAS, varying from 0.17 mm/min to 0.23 mm/min. Therefore, a 0.15 mm/min LLD rate was selected for the study to ensure a CMOD rate of ≤0.7 mm/min across all airfield mixtures. The selected loading rate effectively reduced the likelihood of plastic deformation, creep effects, and softening behavior of the material that could occur at slower loading rates, while also mitigating the risk of sudden failure associated with faster loading rates.

Table E-1. LLD Loading Rate Determination for Asphalt Mixtures

Mixture Type	Step	Fracture Energy LLD (J/m^2)	Peak Load (kN)	LLD Rate (mm/min)	Crack Propagation Rate (mm/min)
EWR (19-mm NMAS)	Step 1	953	6.97	0.17	0.53
		862	6.31	0.17	0.50
		886	7.47	0.18	0.61
		1032	7.28	0.18	0.61
		680	6.50	0.19	0.70
		715	7.55	0.19	0.70
	Step 2	902	6.85	0.19	0.65
		792	7.54	0.19	0.71
TEB (12.5-mm NMAS)	Step 1	638	6.30	0.20	0.66
		603	5.68	0.21	0.67
		630	6.12	0.21	0.64
		716	5.62	0.21	0.68
		751	6.39	0.21	0.68
		482	4.81	0.21	0.67
	Step 2	612	6.65	0.21	0.63
		452	5.62	0.21	0.60
RR (4.75-mm NMAS)	Step 1	599	5.89	0.19	0.55
		548	5.79	0.19	0.57
		492	5.64	0.19	0.55
		673	6.00	0.21	0.63
		553	5.68	0.23	0.66
		577	6.17	0.23	0.71
		655	6.31	0.25	0.80
	Step 2	1152	6.72	0.23	0.75
		677	5.63	0.23	0.71
		792	6.26	0.23	0.75

Loading Rate Effect

Experimental

The loading device ram displacement was not an accurate representation of specimen deformation due to the higher stiffness of asphalt mixtures at low testing temperatures. Therefore, in subsequent testing, a linear variable differential transformer (LVDT) was used to measure the specimen deformation. However, the initial experimental trials, as described in Figure E-1, were not repeated with on-specimen LVDTs, as their primary purpose was limited to the LLD rate selection process.

The effect of loading rate on the fracture behavior of asphalt mixtures was further evaluated by comparing the load-LLD plots of EWR and TEB mixtures tested at two distinct LLD rates. As shown in Figure E-2, both mixtures exhibited a clear sensitivity to loading rate. Specifically, specimens tested at higher LLD rates (0.19 mm/min for EWR and 0.21 mm/min for TEB) demonstrated steeper load-LLD curves in the pre-peak region than those tested at the slower rate of 0.05 mm/min, indicating reduced deformation capacity and a more brittle failure behavior under faster loading conditions. This difference was attributed to the reduced time for binder relaxation at higher loading rates, which promotes a less viscous response, in contrast to slower loading rates, which promote a time-dependent viscoelastic deformation. The findings emphasize the importance of selecting an appropriate loading rate that achieves a balance between the material's low-temperature viscoelastic behavior and a completely brittle failure of the specimen. The latter would result in uncontrolled crack growth with inadequate machine control and data acquisition.

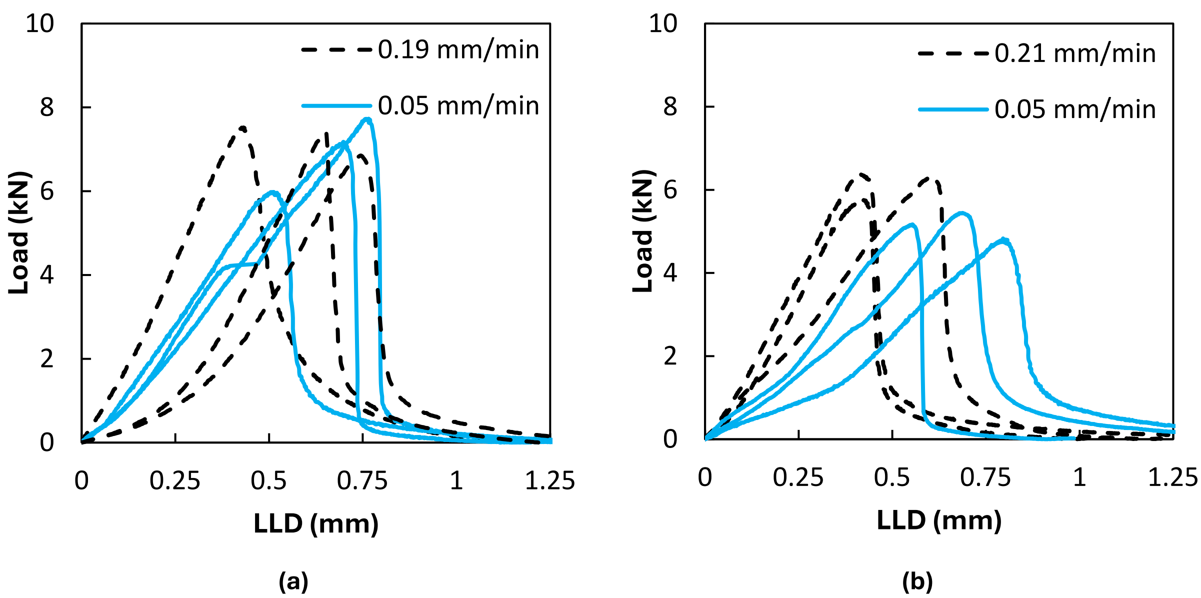

Source: AAPTP

Figure E-2. Load-LLD Plots of (a) EWR and (b) TEB Mixtures Tested at Two Different Loading Rates

Numerical Simulation

To complement the experimental results, a numerical simulation was performed using commercial software (ABAQUS) to assess the influence of loading rate on the fracture process in the SLT-SCB configuration. A finite element (FE) model of the Simplified Low-Temperature Semi-Circular Bend (SLT-SCB) test was developed, as shown in Figure E-3, including the mesh details with loading conditions. The mesh was built using quadrilateral, two-dimensional, plane strain elements with linear shape interpolation functions.

The cracking behavior was modeled using zero-thickness cohesive elements inserted along the ligament length. The response of these cohesive elements is represented by a bi-linear cohesive zone model (CZM) (Dave & Behnia, 2018), which characterizes fracture through a traction-separation relationship. In this relationship, traction refers to the stresses that connect the fracture surfaces, while separation refers to the displacement jump between the surfaces. The CZM requires two parameters: the tensile strength, which refers to the maximum stress a cohesive element can resist before crack initiation, and the local fracture energy parameter, defined as the area under the traction-separation curve for each cohesive element (Dave & Behnia, 2018). FE simulations were conducted using bulk material properties that were linear viscoelastic, with Prony series and Williams–Landel–Ferry (WLF) parameters obtained from the AASHTO T 342 test procedure. The model uses a Poisson's ratio of 0.3. ABAQUS calculates the Prony series coefficients using the user-defined instantaneous modulus E_0. For the simulated mixture in this model, E_0 = 21678.35 MPa, which is also comparable with reported findings (Li & Marasteanu, 2005) for asphalt mixtures tested by SCB geometry at low temperatures.

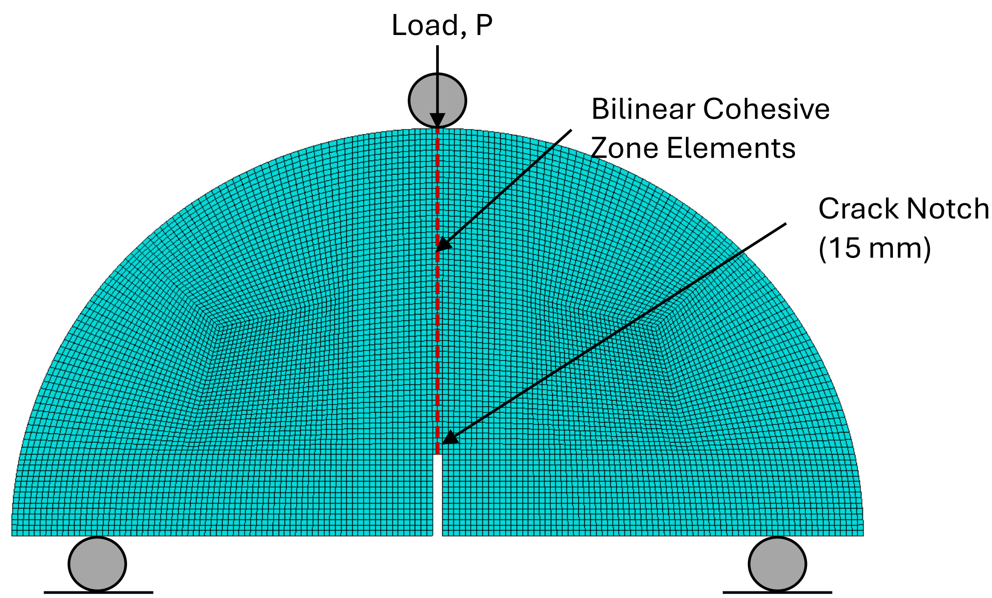

Note: The average element side length of the CZ elements is 1 mm.

Source: AAPTP

Figure E-3. FE Models for Semi-Circular Bend (SCB) Fracture Test

The FE analysis conducted in the study assumed the asphalt mixture is homogeneous, without considering the presence of aggregates and their effects on crack propagation. This assumption was made as the primary purpose of the FE simulations was to gain mechanistic insight into the evolution of fracture and energy dissipation with different loading rates. To calibrate the model and determine the optimal local fracture parameters, load-LLD curves for the experimental and simulation results at 0.15 mm/min LLD rate were matched for the Tampa International Airport (TPA) mix, as shown in Figure E-4(a). The optimum local fracture energy and tensile strength values were 1,400 J/m^2 and 11 MPa, respectively. Next, simulations with slower loading rates of 0.05 mm/min (three times slower) and 0.015 mm/min (10 times slower) were performed with the same optimal local fracture parameters to assess the loading rate effect.

Figure E-4(a) compares FE simulation and experimental results using the load-LLD curves at three monotonic loading rates. As expected, decreasing the loading rate resulted in lower peak load and a corresponding higher deformation at peak load. Furthermore, Figure E-4(b) compares the energies calculated by ABAQUS (DS Simulia Corp., 2015), where the total energy is equal to the external applied work. Viscoelastic dissipation energy is the dissipated energy due to specimen deformation, and the damage-released energy is the energy released from cohesive element failure. These energies were extracted from all monotonic loading-rate simulations to obtain insights into energy evolution, as shown in Figure E-4(b).

The results demonstrate that the loading rate has a direct effect on the partitioning of total energy into viscoelastic dissipation and damage-released energies within the specimen. Lower loading rates resulted in substantially higher viscoelastic dissipation energy, indicating that a larger fraction of the total energy was consumed by time-dependent viscoelastic deformation rather than crack formation, which can increase the applied work required to break the specimen, in addition to increased testing time. Simultaneously, the damage-released energy decreased marginally with a slower loading rate, confirming that rate-dependent viscoelastic relaxation delays crack growth and reduces the available driving energy for the material fracture. Moreover, excessively fast loading rates may trigger unstable crack propagation and premature failure. Therefore, a loading rate of 0.15 mm/min was finalized for the SLT-SCB protocol based on these results, as it reduces the potential for undesirable creep deformation, increases the proportion of energy contributing to material fracture, and provides a controlled and stable fracture response. Table E-2 summarizes the energy components and proportions of viscoelastic dissipation and damage-released energies for the simulated loading rates.

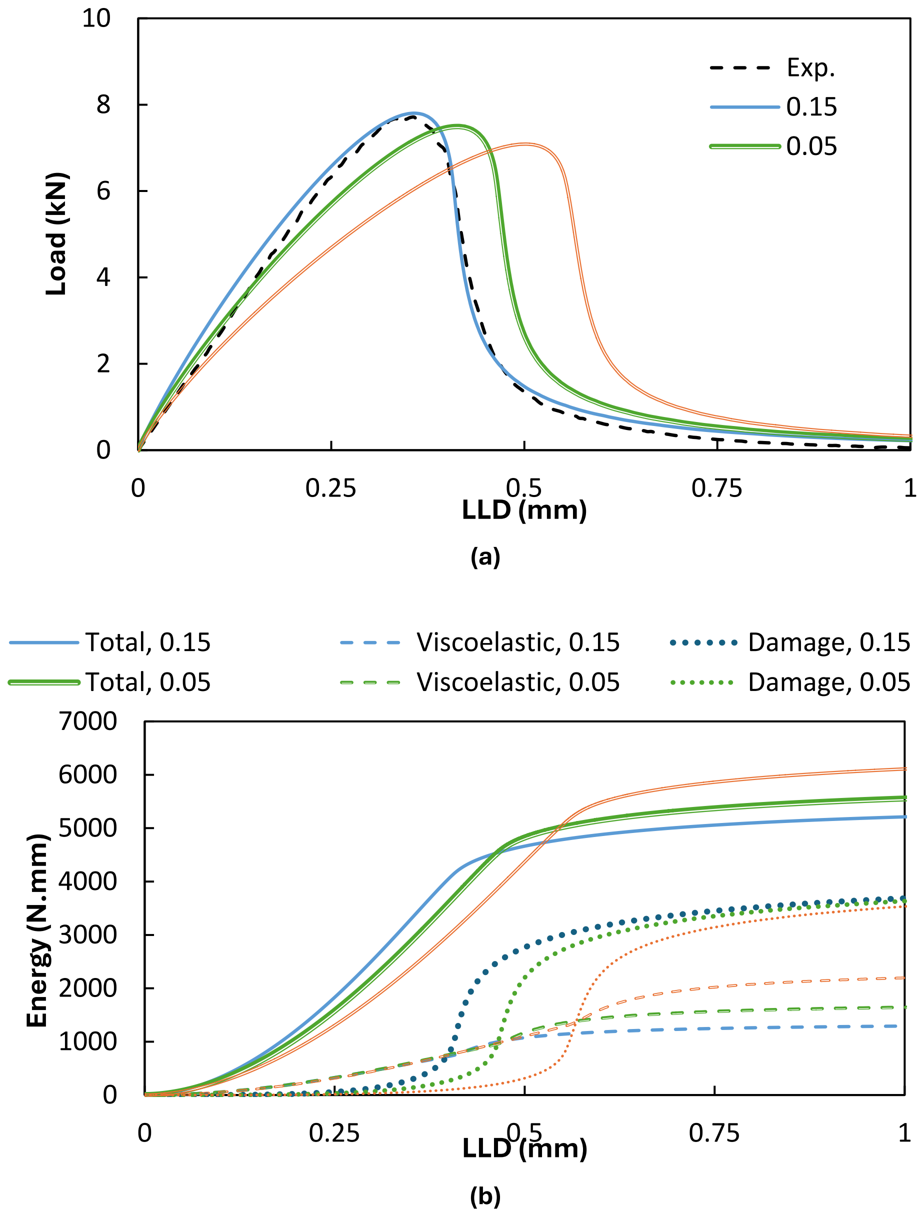

Note: Test temperature was −12 °C.

Source: AAPTP

Figure E-4. Numerical Simulation Showing Effect of Loading Rate on (a) the Load-Displacement Curve and (b) Energy Evolution Components, including Creep Dissipation and Damage Dissipation

Table E-2. Energy Components and Proportions of Creep Dissipation and Damage Dissipation

Loading Rate (mm/min)	Total Energy (N.mm)	Viscoelastic Dissipation Energy (N.mm)	Viscoelastic Dissipation/ Total Energy	Damage-Released Energy (N.mm)	Damage-Released Energy/ Total Energy
0.15	5312	1315	0.248	3841	0.723
0.05	5672	1683	0.297	3808	0.671
0.015	6256	2271	0.363	3746	0.599

Load-LLD Plot Parameters

Figure E-5 shows a typical load-LLD and load-CMOD plot for an LLD-controlled test. In the load-LLD plot, an initial curvature is observed upon loading, resulting from the seating of the specimen on the supports and the development of the contact area, followed by the material's linear behavior (Figure E-5(a)). Finally, a sudden drop in load is observed due to the release of bulk-response energy (i.e., the pre-fracture overall stress build-up in the specimen) stored in the specimen at a low temperature. On the other hand, the load-CMOD plot in Figure E-5(b) shows the gradual crack opening during the test. Both plots confirm that once the crack initiates at low temperature, the material's load carrying capacity decreases significantly with further increase in loading during crack propagation.

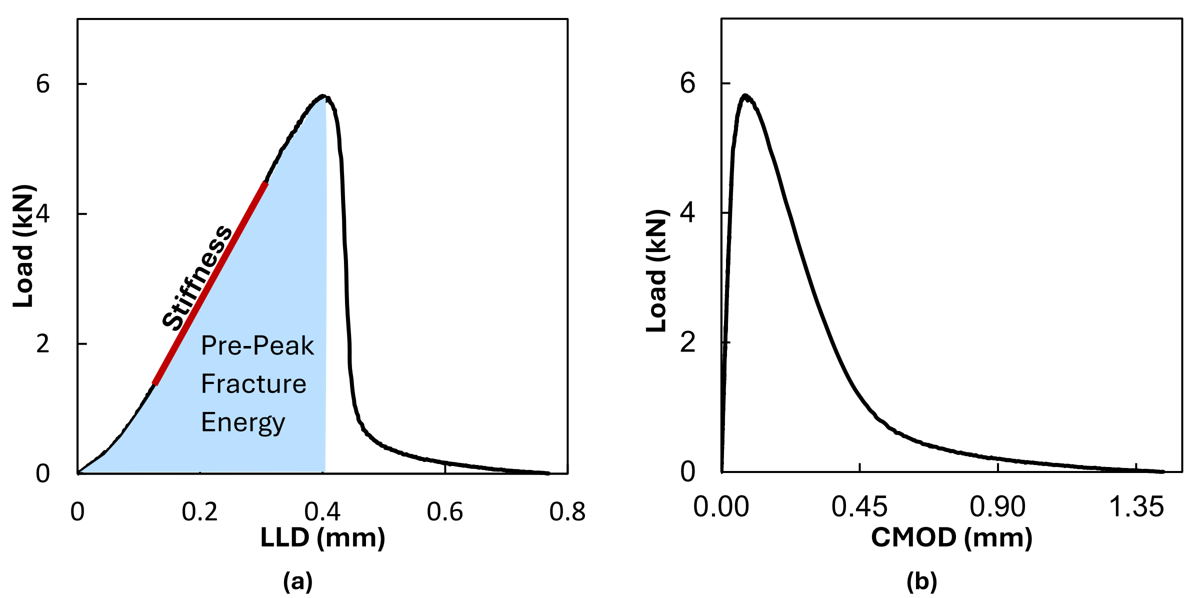

Source: AAPTP

Figure E-5. Typical (a) Load-LLD and (b) Load-CMOD Plots for SLT-SCB

At low temperatures, asphalt behaves predominantly in an elastic manner with limited viscous dissipation, especially at higher loading rates, and crack initiation becomes the dominant factor in the fracture response. By monitoring CMOD as a measure of crack growth, the CMOD-time plot, shown in Figure E-6, exhibits a sharp increase near the peak load, marking a transition from crack initiation to propagation. For practicality and ease of implementation, the study approximated the initiation energy by calculating the pre-peak area under the load-LLD curve, as illustrated schematically by the shaded area in Figure E-5(a), yielding a simple yet effective metric for comparing the crack-initiation resistance of asphalt mixtures.

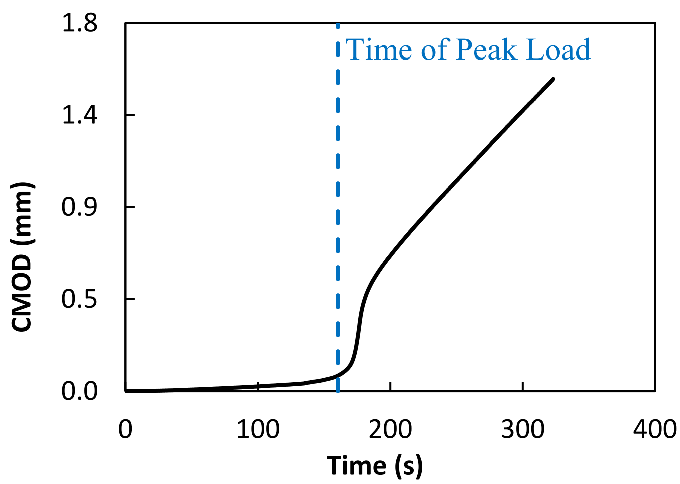

Source: AAPTP

Figure E-6. Typical CMOD-Time Plot for SLT-SCB

In addition to pre-peak fracture energy (PFE), the study considered the loading characteristics of the asphalt mixture during testing by measuring loading stiffness, as shown in Figure E-5(a) by the thicker line segment. The stiffness was calculated from the linear portion of the load-LLD curve at the mid 50-percent pre-peak region using a sliding window regression enhanced with a penalty term (α). This approach helped minimize the influence of noise near the region's bounds and focuses on computing the most stable and consistent region. To evaluate linearity, a window was incrementally translated through the loading data with a least-squares fit to obtain an unpenalized coefficient of determination, $R^2_{unpenalized}$. A penalized coefficient of determination, $R^2_{penalized}$, was then defined as follows:

$$R^2_{penalized} = R^2_{unpenalized} - \alpha d^2 \quad \text{(E-1)}$$

where,

d = (average load in the window/ peak load) – 0.5, representing the normalized offset from the mid-point of the pre-peak region.

The window yielding the highest $R^2_{penalized}$ was selected as the optimal linear segment for estimating the loading stiffness (S). This approach was applied using window lengths ranging from 10 to 30 percent of the pre-peak curve. Based on repeatability and flexibility across replicates, a window length of 15 percent and a penalty factor, $\alpha = 0.05$, were selected as optimal parameters for stiffness determination. This approach ensured that stiffness was calculated from the most representative linear portion of the curve while minimizing the influence of localized curvature in the load-LLD curve, experimental measurement noise, and accumulated damage in the specimen, as observed in numerical analysis. The resulting stiffness values demonstrated good consistency across specimens, reinforcing the robustness of this method.

To provide a single index parameter, the study proposes the Low-temperature Cracking Index (LCI) to assess the cracking potential of asphalt mixtures at low temperatures. LCI was defined as the ratio of PFE to the determined stiffness (S) from the SLT-SCB test, as shown in Equation E-2. A higher LCI indicates higher energy required for crack initiation, or lower stiffness, implying an increased strain tolerance before fracture for materials with similar fracture energies. A higher LCI would thus signify a lower potential of low-temperature cracking.

Low-temperature Cracking Index, LCI = PFE/S (E-2)

where,

PFE = pre-peak fracture energy (J/m^2); S = stiffness (kN/mm), calculated using 15-percent window length and $\alpha = 0.05$, as described above.

Test Temperature Selection

Figure E-7 illustrates the temperature sensitivity of the SLT-SCB test by comparing the LCI values of two asphalt mixtures—RTS and ORD—tested at two different temperatures selected based on geographical location. Error bars in the plot denote 1 standard deviation of the mean LCI from replicate tests. As expected, a consistent decrease in LCI is observed with decreasing test temperature, reflecting reduced fracture energy and increased stiffness at lower temperatures. For the RTS mixture, the LCI decreased from approximately 58 at −12 °C to 28 at −18 °C, indicating a strong temperature dependence of fracture properties. The decline reflects the PG 64-28 binder’s greater temperature dependence within the tested range and a more ductile response at −12 °C, transitioning to an increased glassy response at −18 °C. A similar decreasing trend in LCI with temperature was observed for the ORD mixture, but at a smaller magnitude. The LCI dropped from around 33 at −18 °C to 21 at −27 °C. The decline in this case was not as steep because the response of the PG 76-28 binder was dominated by elastic responses at both testing temperatures. These results confirm that the test is sensitive to temperature changes and can capture the temperature-dependent fracture behavior of asphalt mixtures. The consistent reduction in

LCI with decreasing temperature underscores the importance of testing at appropriate temperatures to assess a mixture's resistance to low-temperature cracking accurately.

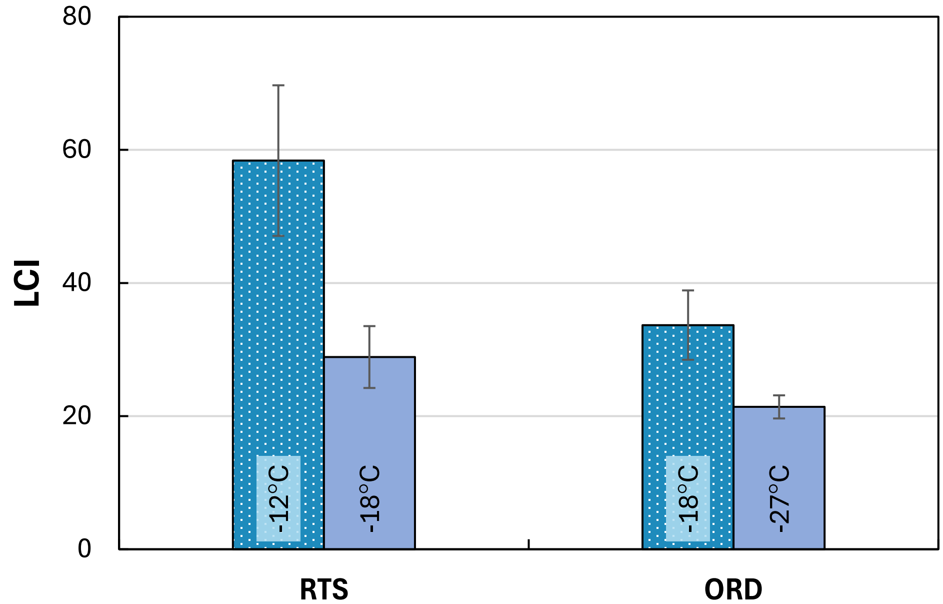

Source: AAPTP

Figure E-7. LCI Values for Asphalt Mixtures from RTS and ORD at Different Temperatures

The next critical step was to finalize the appropriate test temperature for specimen conditioning. The test temperature was selected based on site-specific low-temperature data obtained from the LTPPBind™ database (FHWA, n.d.), which reflects the actual in-service geographical conditions of the asphalt mixture. This site-specific approach was preferred over the conventional method of using a low-temperature binder PG as the basis for selecting the test temperature. The rationale for this deviation lies in the inherent limitations of PG-based selection, which prevents contractors from using a softer binder in a mixture. Hence, adopting site-specific low temperatures ensures testing conditions that mirror the real-world environment where the asphalt mixture will be deployed, thereby enhancing the relevance, reliability, and accuracy of the test outcomes in evaluating mixture performance.

To facilitate this approach, airports were selected to represent a wide range of climatic regions across the United States. For each airport, the lowest annual pavement surface temperatures were obtained from the LTPPBind datasets at the 50th and 98th percentiles. Based on the data, the 50th percentile low temperature is a practical and effective choice, as it aligns well with the binder grade traditionally used for airfield pavements. An upper limit of −12 °C is proposed to avoid creep effects that could potentially occur for mixtures from warmer regions. This threshold aligns with the Federal Aviation Administration (FAA) requirement for a minimum binder grade of PG XX-22 (FAA, 2018), ensuring compliance with stringent performance specifications for warmer-weather airport conditions that may still occasionally experience colder weather and/or high cooling rates during storm events. The final test temperature for each location was determined using the following relation:

Test temperature (°C) = colder of (True $LTPG_{50}$ + 10 °C, −12 °C) (E-3)

where,

test temperature = rounded down to the nearest whole number; and true $LTPG_{50}$ = location-specific low-temperature performance grade from LTPPBind datasets at 50th percentile reliability.

Results and Analysis

Impact of Binder Grade and Content

Binder grade impact was evaluated using cross-combination mixtures (XCM). Figure E-8 compares the load–LLD responses of the four XCM at −12 °C and −18 °C. At −12 °C, all PG XX-28 formulations outperformed their PG XX-22 counterparts, exhibiting higher PFE and lower stiffness. This performance was controlled primarily by the binder's low-temperature performance grade (PGL), with neither binder source nor high-temperature performance grade (PGH) producing discernible differences. For −18 °C, however, the load–LLD curves of the four binder grades converged into a tight band, and their fracture properties became nearly identical—an indication that the asphalt mixtures had shifted into a predominantly glassy, brittle regime once the test temperature fell below their PGL.

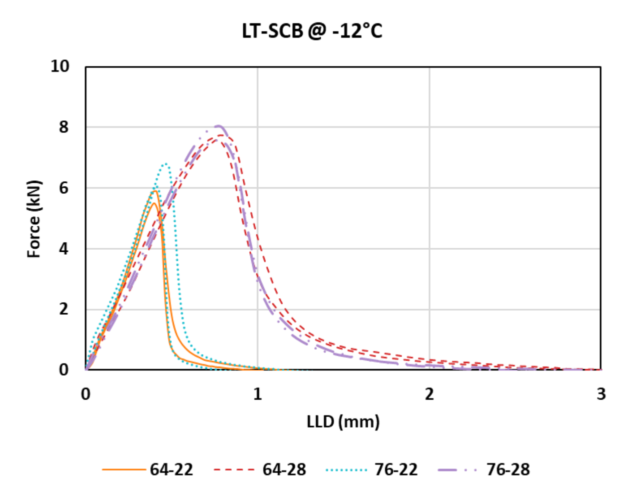

(a)

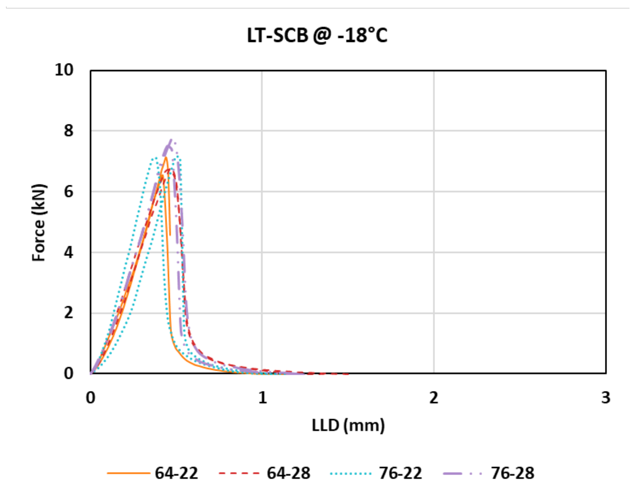

(b)

Source: AAPTP

Figure E-8. Effect of Binder PG on XCM at (a) −12 °C and (b) −18 °C

To verify the non-glassy-to-glassy transition, load-LLD plots at three different temperatures (PGL+10 °C and one PG difference [6 °C] on either side) for each binder XCM are shown in Figure E-9. All mixtures clearly showed viscoelastic responses at a grade higher than

PGL+10 °C. At PGL+10 °C and below, the load–LLD curves and fracture parameters changed only marginally, consistent with an elastic-dominated response. The minimal change in PFE further underscored the onset of brittle behavior.

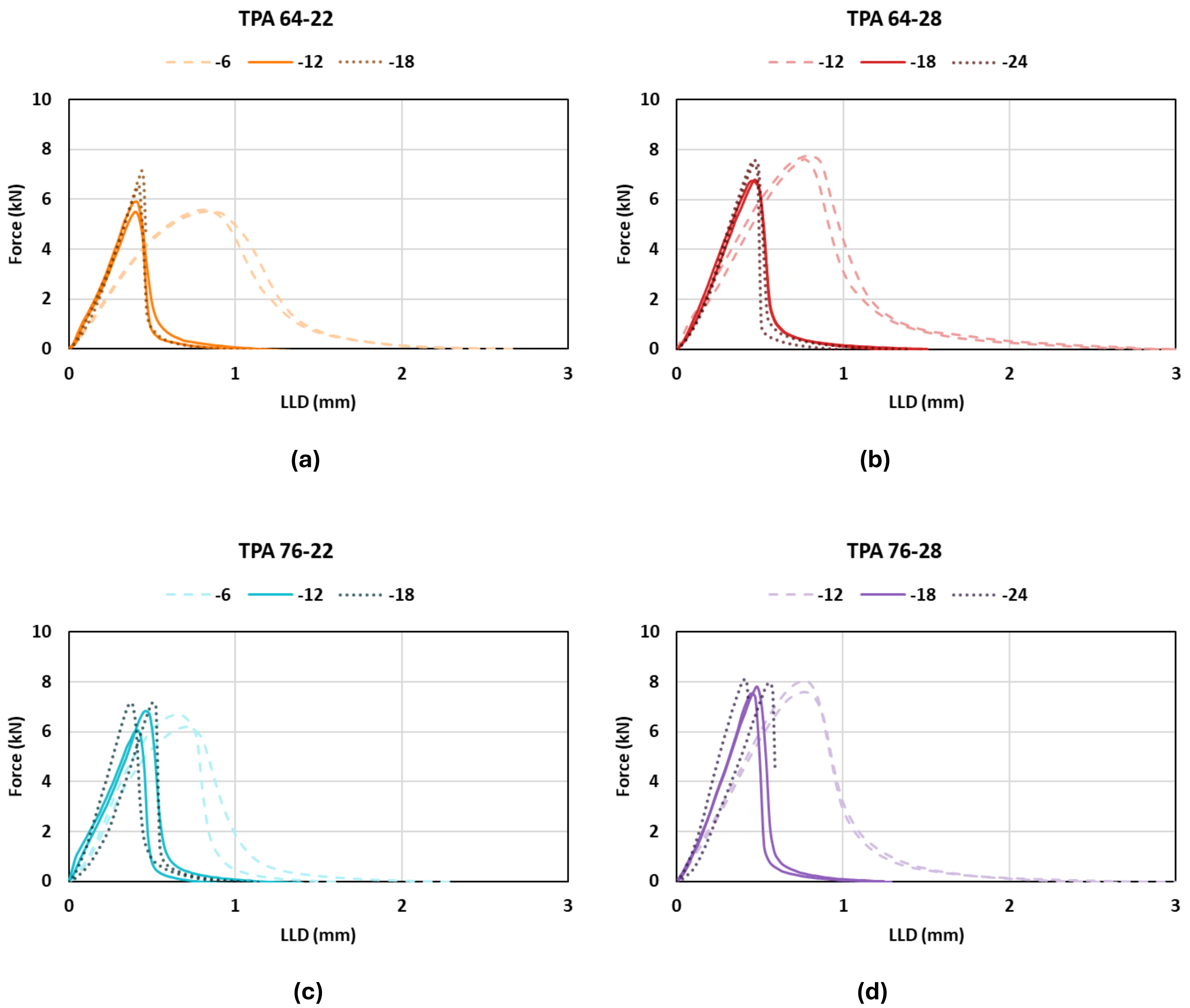

Source: AAPTP

Figure E-9. Effect of Test Temperature on XCM with (a) PG 64-22, (b) PG 64-28, (c) PG 76-22, and (d) PG 76-28 Binders Tested at PGL+10 °C and ± 6 °C (one PG difference on both sides)

The shear stress relaxation modulus, G(t = 60 s), and its time-dependent slope, m_r(t = 60 s), for each binder were measured at the same three testing temperatures (Figure E-10). The higher loading stiffnesses of the mixtures correlated with increasing G(t) and decreasing (less negative) m_r(t) values. A power-law fit with R^2 = 0.83 for stiffness and G(t), and a linear fit with R^2 = 0.90 for stiffness and m_r, were observed. This further validated the use of loading stiffness as a key binder-characterization metric for low-temperature cracking and supports the inclusion of stiffness in LCI.

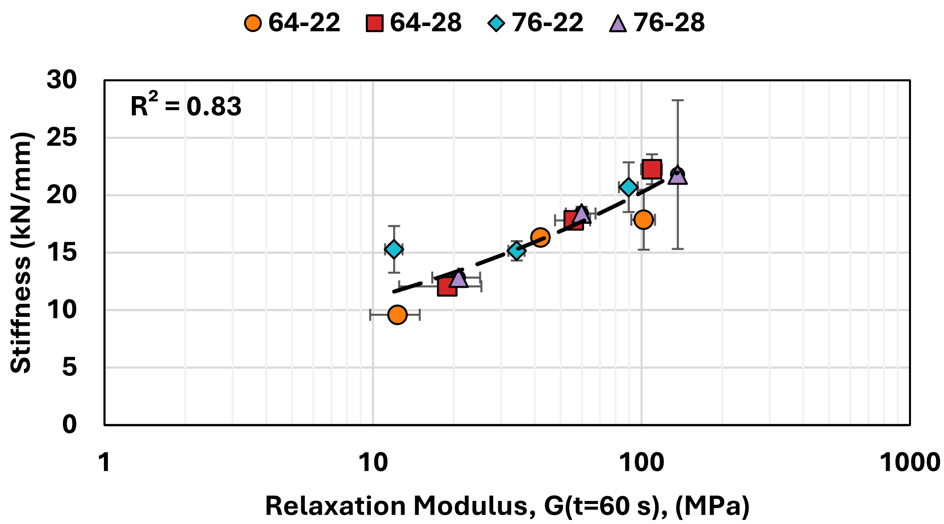

(a)

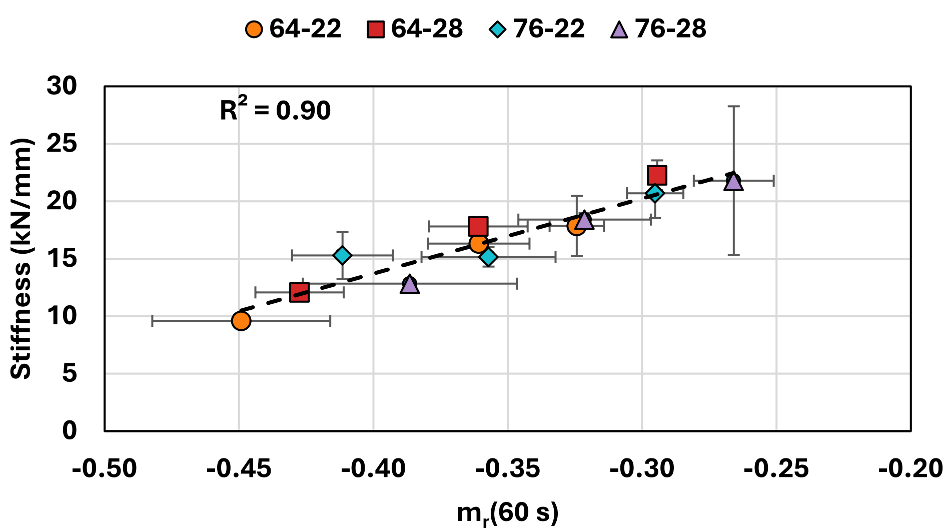

(b)

Note: Error bars represent 1 standard deviation.

Source: AAPTP

Figure E-10. Relation of Mixture Loading Stiffness with (a) G(t=60 s) and (b) m_r(t=60 s) for Binders at Three Test Temperatures

The results of the statistical analysis of outputs from the Student's t-test (i.e., connecting letters groups) are presented by the letters shown at the bottom of the bars. These results are used to assess the sensitivity of test parameters by the number of distinct groups they can statistically separate. In the study, Group A indicates the group that has the best value of the property concerning cracking resistance. The bars that do not have the same letter are considered to be significantly different from each other at a significance level of 0.05.

For instance, as shown in Figure E-11, the stiffness parameter for TPA 64-22 is statistically the same for −12 °C and −18 °C conditions but different than that for −6 °C. A connecting-letter designation (e.g., AB) indicates that a result is statistically part of both groups (e.g., A and B) but can still be distinguished as a different group.

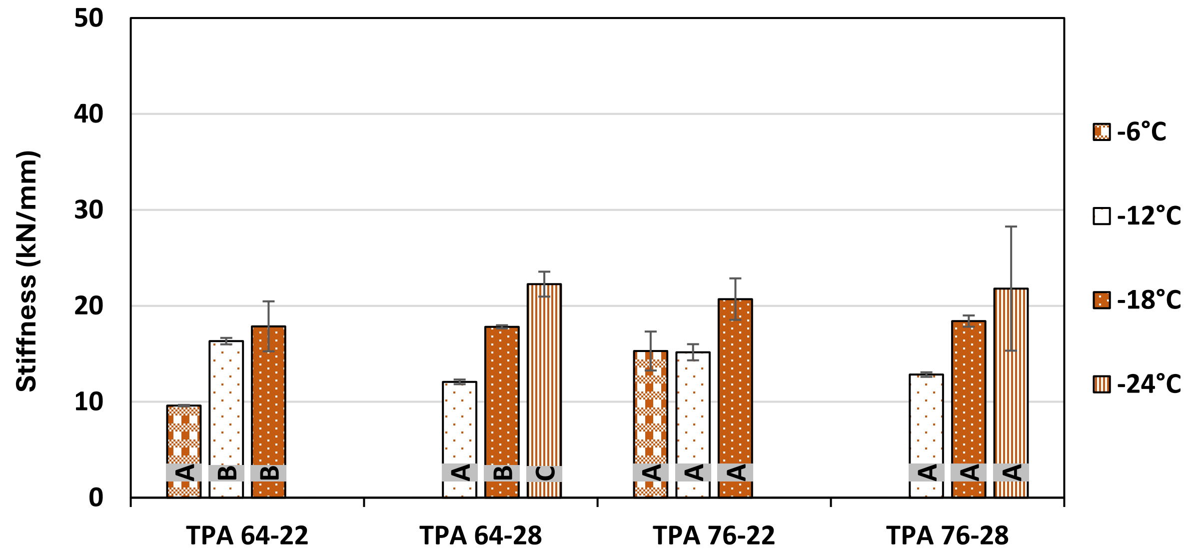

(a)

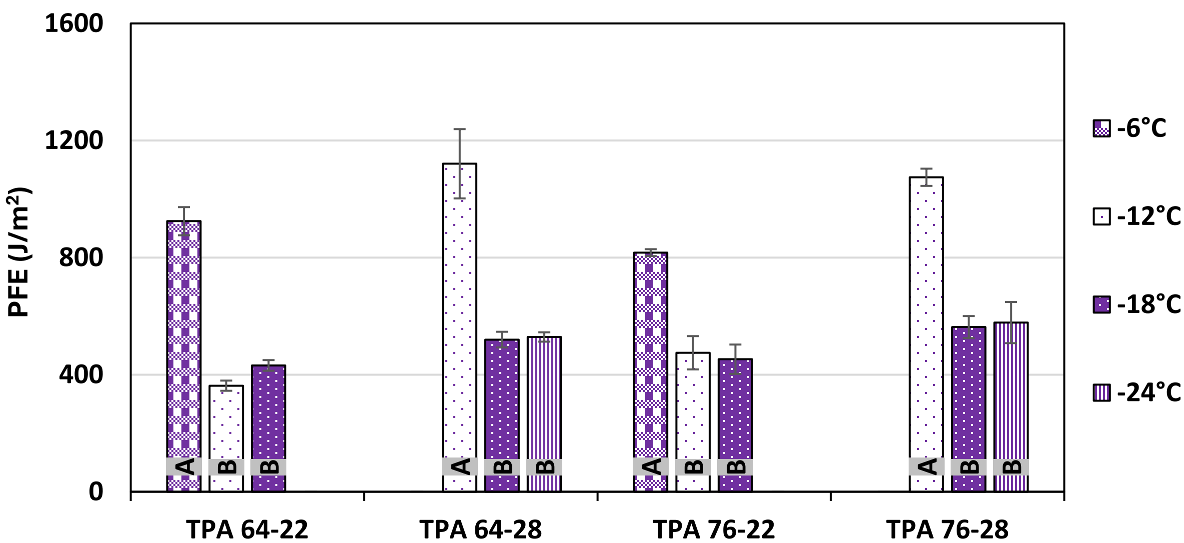

(b)

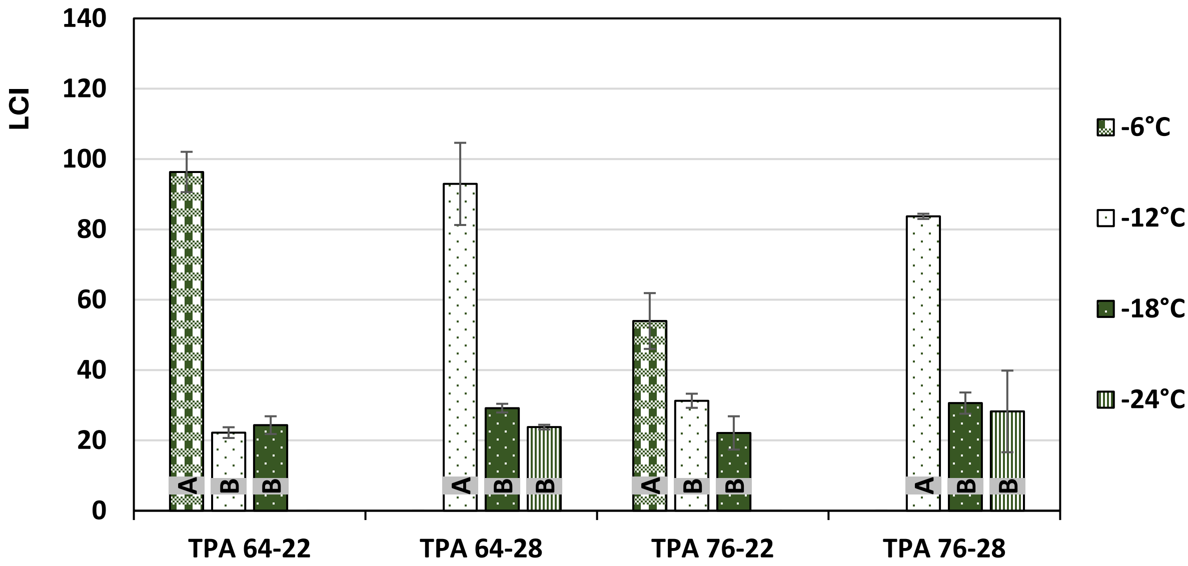

(c)

Note: Error bars represent 1 standard deviation; letters at the bottom of the bars represent the statistical groupings of variations within each mixture type.

Source: AAPTP

Figure E-11. Effect of Test Temperature and Binder Grade on (a) Stiffness, (b) PFE, and (c) LCI for XCM

The results illustrate the influence of testing temperature on stiffness, PFE, and LCI. Stiffness increased as the temperature decreased, while the PFE plateaued beyond PGL+10 °C. At the same testing temperature, binders with lower PGL exhibited lower stiffness and higher PFE. As expected, LCI increased at higher temperatures and with lower PGL binders, reflecting enhanced energy dissipation and reduced stiffness under viscoelastic conditions. The results highlight the critical role of binder grade in mitigating low-temperature cracking.

The effect of binder content variability was tested at ±0.5 percent from the optimum binder content (OBC) for TPA. Labels "O−," "O," and "O+" denote OBC−0.5 percent, OBC, and OBC+0.5 percent, respectively. Specimens for all three binder contents were tested at −12 °C and −18 °C. Small binder content adjustments did not significantly affect stiffness, fracture energy, or LCI at −18 °C, as presented in Figure E-12. Binder volume had little impact on crack initiation under brittle conditions, which was consistent with prior findings (Li et al., 2008). However, at a warmer temperature, −12 °C (likely warmer than the glassy state), the O+ specimens for PG XX-28 exhibited a modest decrease in stiffness and a modest increase in fracture energy. As a result, the LCI values of O− and O+ specimens were statistically different. This suggests that an additional binder could enhance energy absorption before cracking when the material exhibits partial viscoelastic behavior.

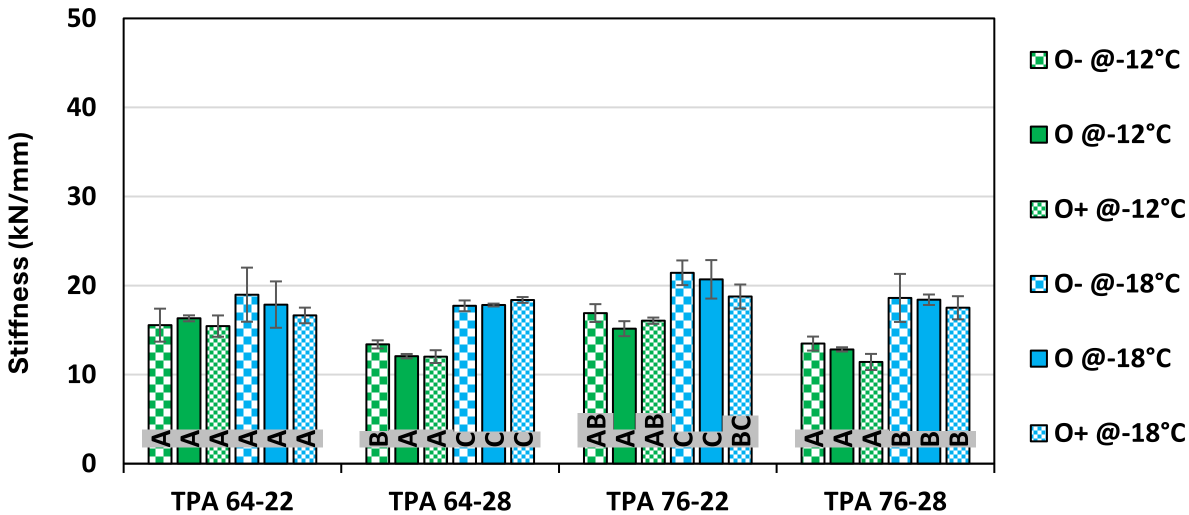
Stiffness (kN/mm)
0
10
20
30
40
50
TPA 64-22
TPA 64-28
TPA 76-22
TPA 76-28
A A A A A A
B A A C C C
AB A AB C C BC
A A A B B B
O- @-12°C
O @-12°C
O+ @-12°C
O- @-18°C
O @-18°C
O+ @-18°C

(a)

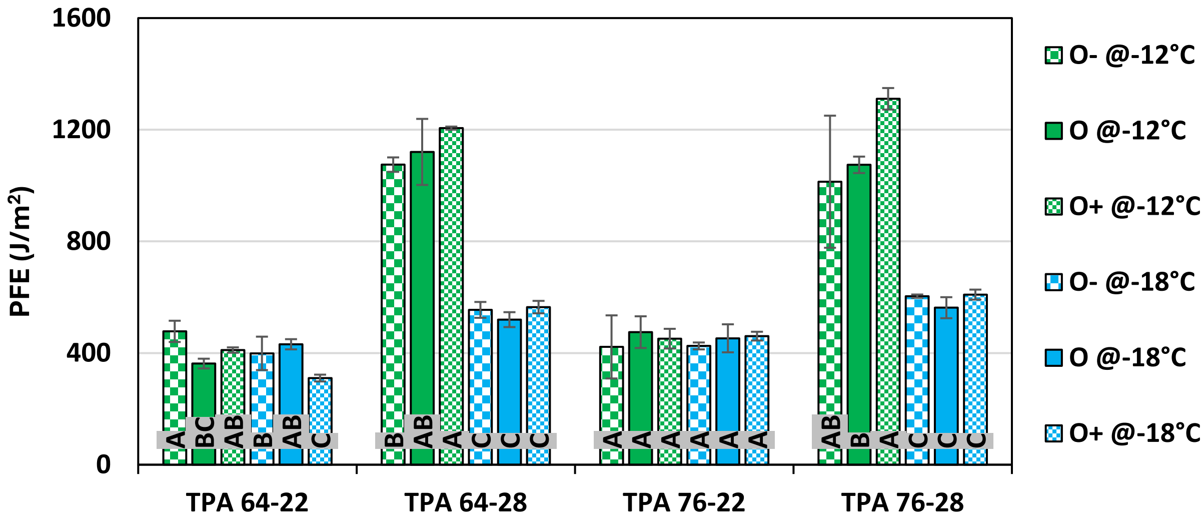
PFE (J/m²)
0
400
800
1200
1600
TPA 64-22
TPA 64-28
TPA 76-22
TPA 76-28
A BC AB B AB C
B AB A C C C
A A A A A A
AB B A C C C
O- @-12°C
O @-12°C
O+ @-12°C
O- @-18°C
O @-18°C
O+ @-18°C

(b)

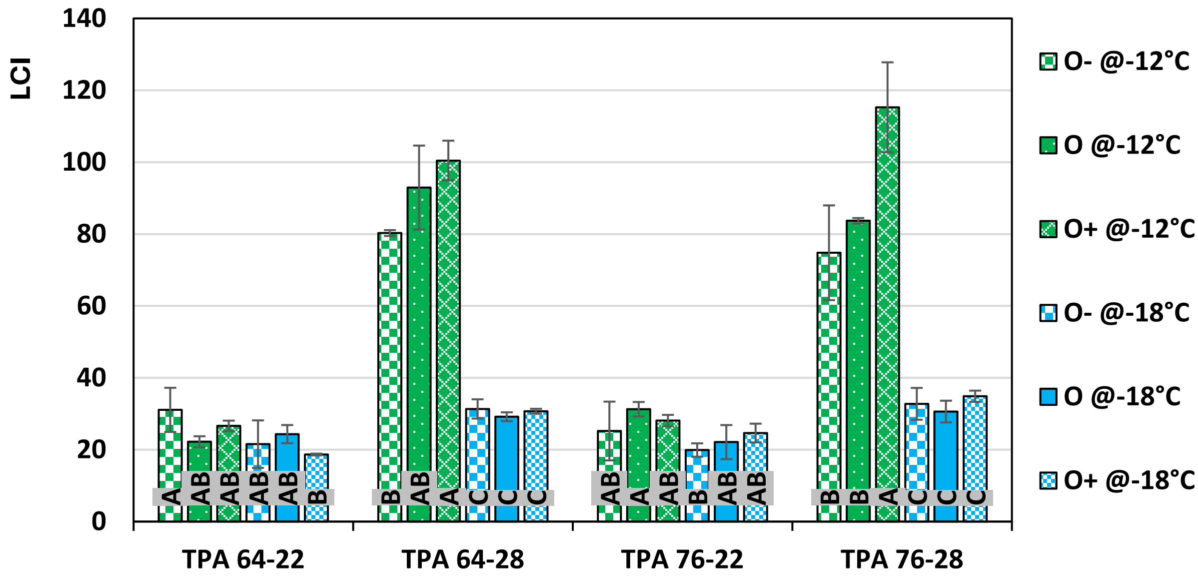

(c)

Note: Error bars represent 1 standard deviation; letters at the bottom of the bars represent the statistical groupings of variations within each mixture type.

Source: AAPTP

Figure E-12. Effect of Binder Content Variability at −12 °C and −18 °C on (a) Stiffness, (b) PFE, and (c) LCI for XCM

Impact of Aging and Air Void Content

Seven laboratory-mixed, laboratory-compacted (LMLC) asphalt mixtures were evaluated at two air void (AV) levels—average (3 percent for the TPA mix, 5 percent for the others) and high (5 percent for TPA, 7 percent for the rest)—under both short-term aging (STA) and long-term aging (LTA). Figure E-13 shows stiffness, PFE, and LCI for these specimens. The variability in measured properties for EWR was likely due to the coarse aggregate skeleton in this mix, while the variability of the Chicago O’Hare International Airport’s reclaimed asphalt pavement mixture (ORAP) likely reflects the 25-percent RAP content.

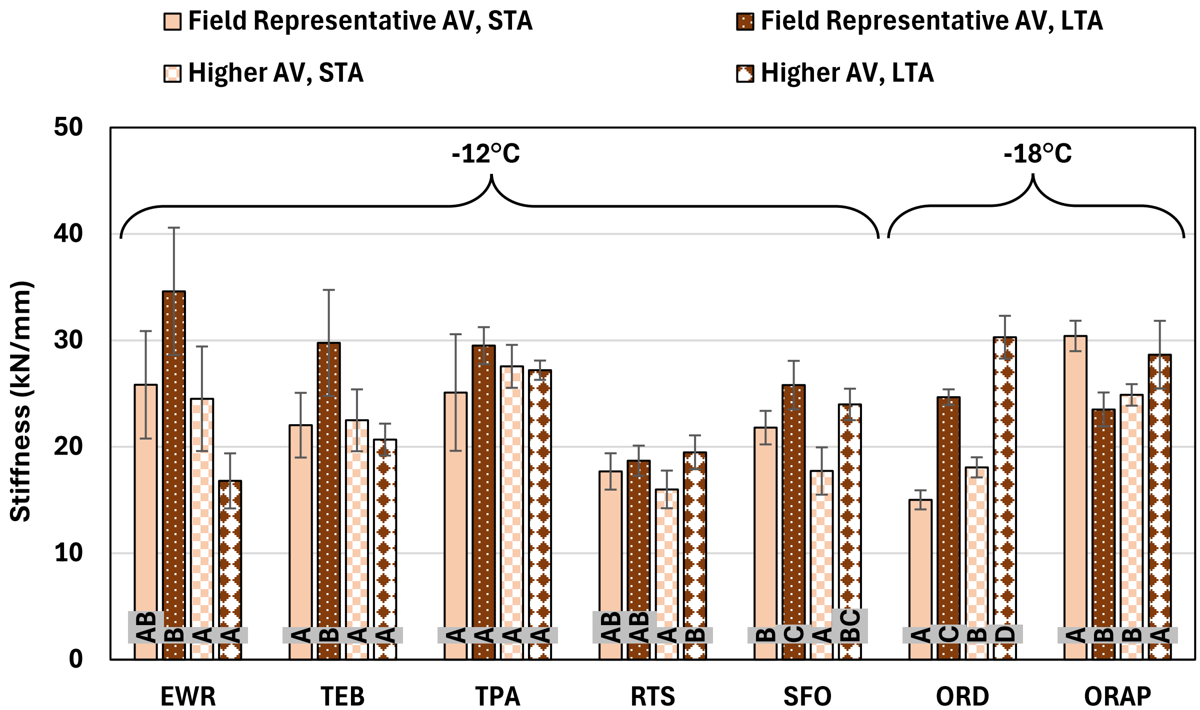
Field Representative AV, STA
Field Representative AV, LTA
Higher AV, STA
Higher AV, LTA
Stiffness (kN/mm)
50
40
30
20
10
0
-12°C
-18°C
EWR
TEB
TPA
RTS
SFO
ORD
ORAP

(a)

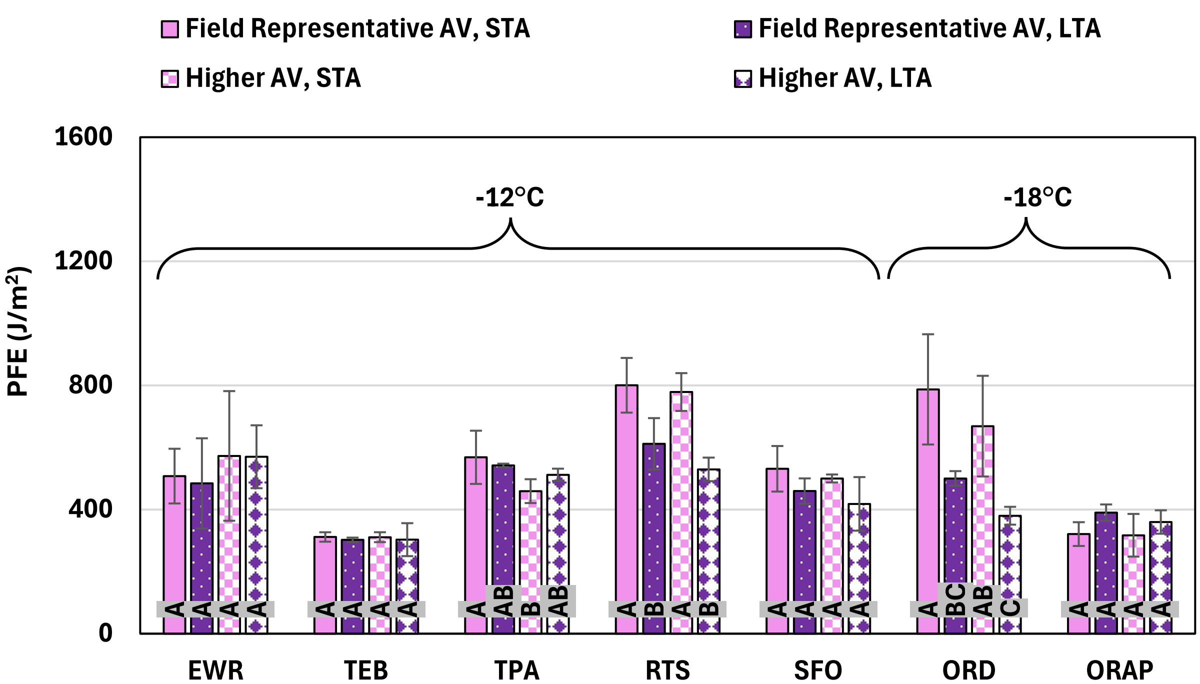
Field Representative AV, STA
Field Representative AV, LTA
Higher AV, STA
Higher AV, LTA
PFE (J/m²)
1600
1200
800
400
0
-12°C
-18°C
EWR
TEB
TPA
RTS
SFO
ORD
ORAP

(b)

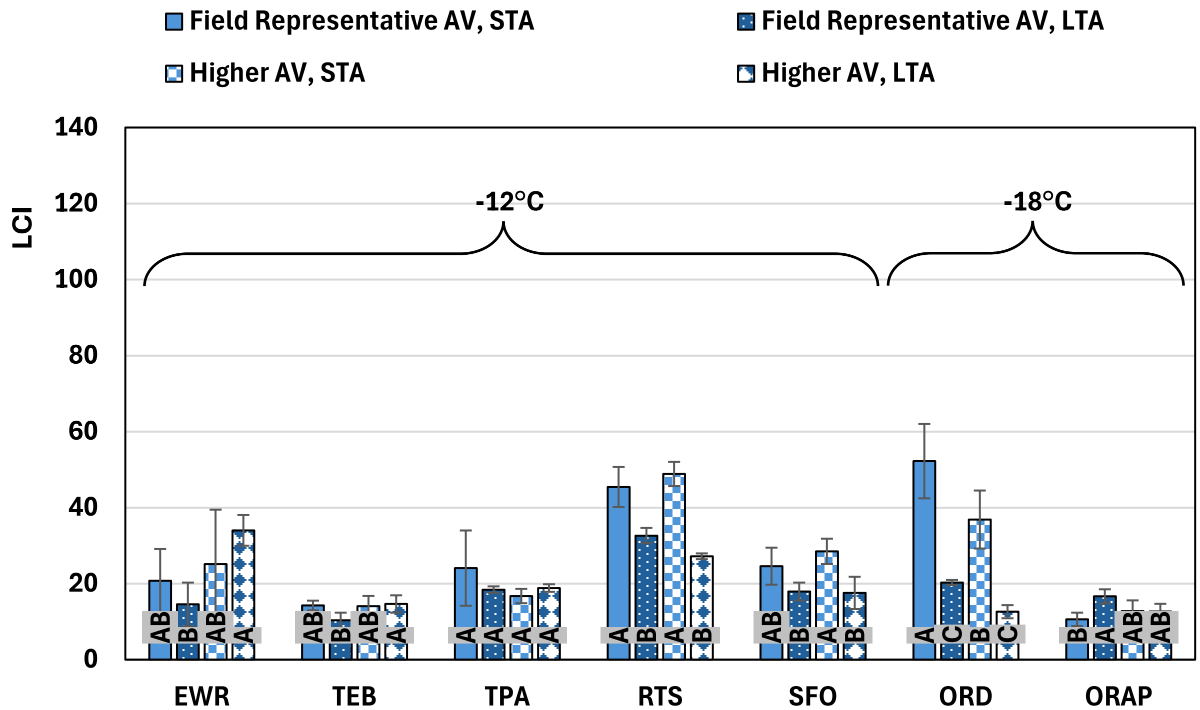

(c)

RTS = Reno Stead Airport; SFO = San Francisco International Airport, ORD = Chicago O'Hare International Airport.
Note: Error bars represent 1 standard deviation; letters at the bottom of the bars represent the statistical groupings of variations within each mixture type.

Source: AAPTP

Figure E-13. Effect of Aging and AV on (a) Stiffness, (b) PFE, and (c) LCI for LMLC Asphalt Mixtures

ORD and RTS exhibited the highest LCI values, reflecting their combination of high PFE and relatively low loading stiffness. Both asphalt mixtures incorporated a PGL XX-28 binder, exemplifying the binder grade's role in controlling low-temperature cracking. Even at −18 °C, the ORD mixture maintained exceptional low-temperature cracking properties, further underscoring the importance of appropriate binder grade selection.

Increasing AV content had no consistent significant effect on PFE or on loading stiffness for either aged or unaged specimens. As a result, asphalt mixtures with higher AV showed similar or slightly reduced LCI values. This limited effect of increased AV on low-temperature cracking has been reported by Li et al. (Li et al., 2008). The SLT-SCB test was specifically designed to probe crack initation under near-brittle conditions, where a marginal increase in AV content would have little influence on measured fracture properties. This may not apply to cracking at room temeprature, where AV typically act as crack-blunting pockets, slowing crack propogation (Rivera-Perez et al., 2018).

Aging of asphalt specimens produced modest changes in PFE for most mixes, however, RTS and ORD experienced a pronounced drop after LTA. This could be attributed to a shift toward a more glassy—and thus more brittle—response post aging, which reduces the energy dissipated before crack initiation. In parallel, loading stiffness increased after aging in most cases, except with EWR and ORAP, which showed high variability as explained earlier. Accordingly, LCI values either decreased or remained statistically unchanged after aging, consistent with expected trends in cracking potential.

PMLC Test Results

In addition to LMLC, plant-mixed, laboratory-compacted (PMLC) specimens for each asphalt formulation were also tested. Figure E-14 compares LCI values for LMLC and PMLC specimens for the seven asphalt mixtures. Variability was generally low, with coefficients of variation (COVs) for both LMLC and PMLC replicates less than 20 percent. A Student's t-test (α = 0.05) showed no significant difference between LMLC and PMLC LCI values for all mixes except ORD. Further investigation indicated that the ORD plant sample was likely overheated and not representative of the job-mix, leading to excessive aging and a lower PMLC LCI. Excluding ORD, LCI values clustered closely between lab and plant specimens, supporting its use in asphalt mixture design as well as process control during production.

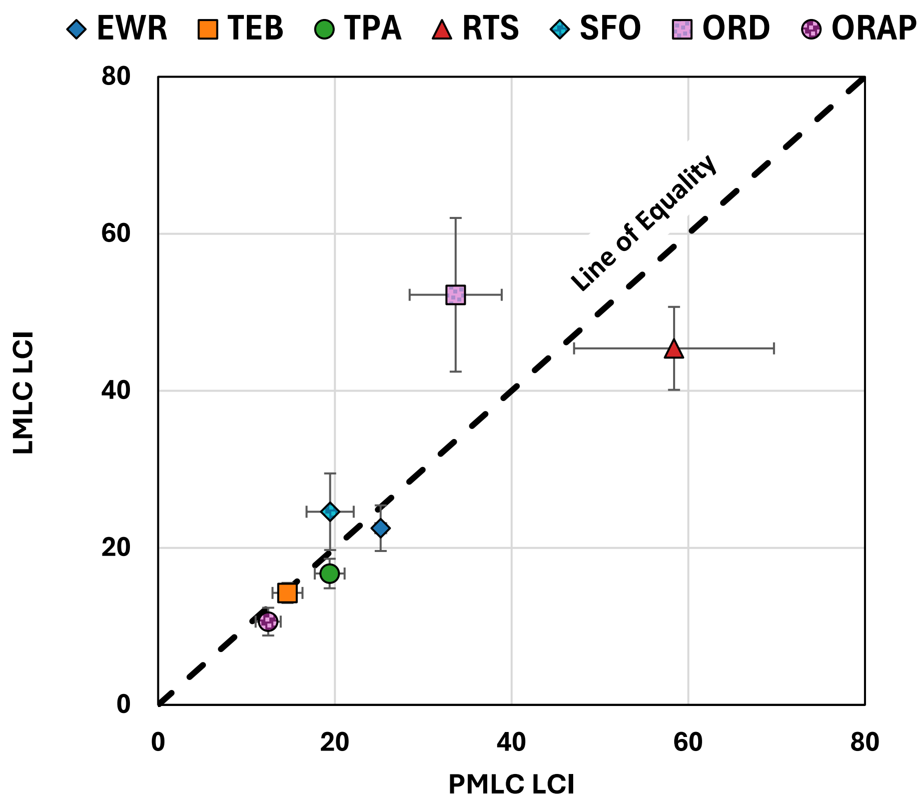

Note: Error bars represent 1 standard deviation.

Source: AAPTP

Figure E-14. Comparison of LCI Determined from LMLC and PMLC Mixtures at 5% AV

Lastly, the LCI from the SLT-SCB was compared with results from the established DCT test. Fracture energy from DCT has been reported to be correlated with field performance (Dave & Hoplin, 2015; Marasteanu et al., 2012). Figure E-15 presents a comparison between the DCT fracture energy and the SLT-SCB-derived LCI for PMLC specimens. Under the ASTM D7313 protocol, RTS mixtures are tested in DCT at −18 °C; however, the SLT-SCB method prescribes −12 °C for RTS based on climate considerations. To align the two methods, RTS specimens were, therefore, tested in the SLT-SCB at both −12 °C and −18 °C, and Figure E-15 showed the value at only −18 °C for a fair comparison. The plot shows a clear positive trend, with higher DCT fracture energy often having higher SLT-SCB LCI. The COV for DCT results ranged from 5 percent (SFO) to 13 percent (ORAP), whereas the LCI COV lay between 2 percent (EWR) and 16 percent (RTS). Therefore, LCI showed robust and repeatable results that could be used in a quality assurance process with confidence.

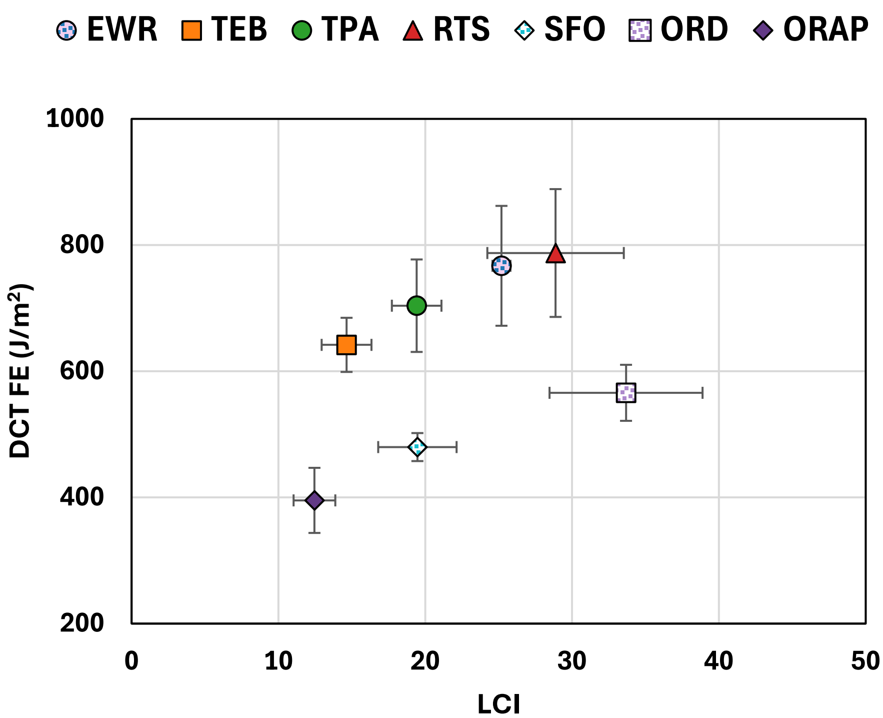

Note: Error bars represent 1 standard deviation.

Source: AAPTP

Figure E-15. Comparison of DCT and LCI for PMLC Mixtures at 5% AV

Figure E-16 presents the results of the SLT-SCB test conducted on field cores obtained from three locations—the University of Illinois–Willard Airport (CMI), Kansas City International Airport (MCI), and six FAA test lanes at the National Airport Pavement and Materials Research Center. As expected, the LCI values of the field cores were generally lower than those of the PMLC mixtures, primarily due to the aging in field-exposed pavements. Among the FAA test lanes (all constructed in 2019), L3 and L4 exhibited cracking after accelerated loading. During the first winter cycle, the cracks became more prominent and propagated to the surface, indicating a higher cracking potential of L3 and L4 (Alvarez et al., 2024). The SLT-SCB results aligned with the observations, as both L3 and L4 had notably lower LCI values, confirming their aging susceptibility to low-temperature cracking. Greater variability in the LCI of L6 may be attributed, in part, to the presence of latex in the mixture.

At CMI, two different pavement sections, constructed in 2004 and 2014, were sampled and tested. Both sections exhibited low LCI values, consistent with the expected increase in cracking potential of asphalt mixtures with aging in older surfaces. During the most recent condition assessment before reconstruction, both CMI pavement sections exhibited medium-severity cracking, including longitudinal, transverse, alligator, and block cracking (Illinois DOT, n.d.). Meanwhile, the MCI cores, collected from a newly resurfaced pavement in 2022, showed better LCI values than the CMI cores, even at a lower test temperature (−18 °C), reflecting their satisfactory performance. Collectively, the findings confirm that the SLT-SCB test can reliably differentiate asphalt mixtures and effectively identify cracked pavements by reduced LCI values.

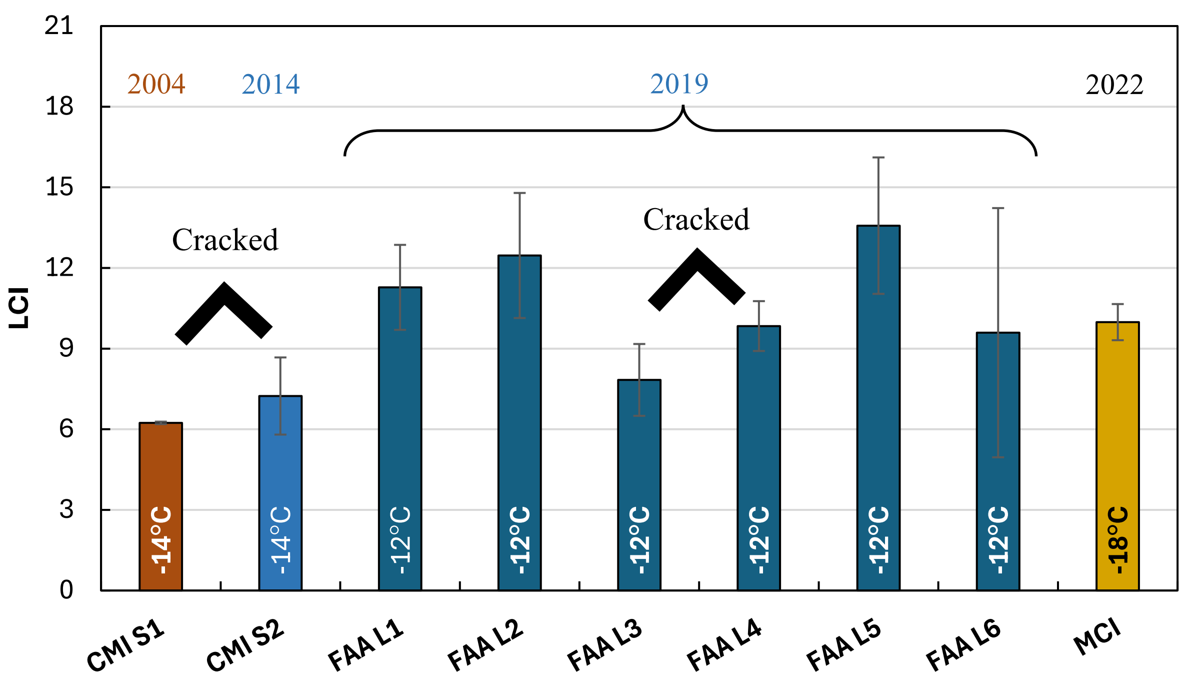

Note: Test temperatures are listed at the bottom of each bar.

Source: AAPTP

Figure E-16. LCI Values of Field Cores

References

AASHTO T 342. (2022). *Standard Method of Test for Determining Dynamic Modulus of Hot Mix Asphalt (HMA)*. American Association of State Highway and Transportation Officials.

Alvarez, D. B., Kazmee, H., & Garg, N. (2024). Laboratory and Field Performance Evaluation of Cracking of Airfield Warm Mix Asphalt with Reclaimed Asphalt Pavement at the National Airport Pavement and Materials Research Center. *Transportation Research Record: Journal of the Transportation Research Board*, *2678*(11), 530–546. https://doi.org/10.1177/03611981241242071

ASTM D7313. (2020). *Standard Test Method for Determining Fracture Energy of Asphalt Mixtures Using the Disk-Shaped Compact Tension Geometry*. ASTM International.

Dave, E. V., & Behnia, B. (2018). Cohesive Zone Fracture Modelling of Asphalt Pavements with Applications to Design of High-Performance Asphalt Overlays. *International Journal of Pavement Engineering*, *19*(3), 319–337. https://doi.org/10.1080/10298436.2017.1353393

Dave, E. V., & Hoplin, C. (2015). Flexible Pavement Thermal Cracking Performance Sensitivity to Fracture Energy Variation of Asphalt Mixtures. *Road Materials and Pavement Design*, *16*(sup1), 423–441. https://doi.org/10.1080/14680629.2015.1029697

DS Simulia Corp. (2015). *Abaqus Analysis User's Manual, Version 6.14*. Dassault Systèmes Simulia Corp.

FAA. (2018). *Standard Specifications for Construction of Airports, Advisory Circular 150/5370-10H*. Federal Aviation Administration.

FHWA. (n.d.). *LTPP InfoPave*. Federal HIghway Administration. Retrieved https://infopave.fhwa.dot.gov/

Illinois DOT. (n.d.). *Illinois 2022–2025 IDEA — Airport Details*. Illinois Department of Transportation. Retrieved June 23, 2025, from https://idea.appliedpavement.com/hosting/illinois/airport-details/airport-details.html

Li, X., Braham, Andrew F., Marasteanu, M. O., Buttlar, W. G., & Williams, R. C. (2008). Effect of Factors Affecting Fracture Energy of Asphalt Concrete at Low Temperature. *Road Materials and Pavement Design*, *9*(sup1), 397–416. https://doi.org/10.1080/14680629.2008.9690176

Li, X., & Marasteanu, M. O. (2005). Cohesive Modeling of Fracture in Asphalt Mixtures at Low Temperatures. *International Journal of Fracture*, *136*(1–4), 285–308. https://doi.org/10.1007/s10704-005-6035-8

Marasteanu, M., Buttlar, W., Bahia, H., Williams, C., Moon, K. H., Teshale, E. Z., Falchetto, A. C., Turos, M., Dave, E., Paulino, G., Ahmed, S., Leon, S., Braham, A., Behnia, B., Tabatabaee, H., Velasquez, R., Arshadi, A., Puchalski, S., Mangiafico, S., … Kvasnak, A. (2012). *Investigation of Low Temperature Cracking in Asphalt Pavements National Pooled Fund Study – Phase II* (Report MN/RC 2012-23). Minnesota Department of Transportation. http://conservancy.umn.edu/handle/11299/135177

Rivera-Perez, J., Ozer, H., & Al-Qadi, I. L. (2018). Impact of Specimen Configuration and Characteristics on Illinois Flexibility Index. *Transportation Research Record*, *2672*(28), 383–393. https://doi.org/10.1177/0361198118792114

Son, S., Said, I. M., & Al-Qadi, I. L. (2019). Fracture Properties of Asphalt Concrete Under Various Displacement Conditions and Ttemperatures. *Construction and Building Materials*, *222*, 332–341. https://doi.org/10.1016/j.conbuildmat.2019.06.161

Appendix F: Technical Note Template for Disc with O-Notch for Uniaxial Testing (DONUT)

ote technical note technica

Standard Test Method for Determining the Cracking Potential of Asphalt Mixtures Using the Disc with O-Notch for Uniaxial Testing (DONUT)

Author name (if the report was authored only by the FAA)

Date

DOT/FAA/TC-TNxx/xx

This document is available to the U.S. public through the National Technical Information Services (NTIS), Springfield, Virginia 22161.

This document is also available from the Federal Aviation Administration William J. Hughes Technical Center at actlibrary.tc.faa.gov.

U.S. Department of Transportation

Federal Aviation Administration

NOTICE

Technical Report Documentation Page

1. Report No.	2. Government Accession No.	3. Recipient's Catalog No.
DOT/FAA/TC-TNxx/xx		

4. Title and Subtitle	5. Report Date
Disc with O-Notch for Uniaxial Testing (DONUT)	November 2025
	6. Performing Organization Code
7. Author(s)	8. Performing Organization Report No.
9. Performing Organization Name and Address	10. Work Unit No. (TRAIS)
	11. Contract or Grant No.
12. Sponsoring Agency Name and Address Sponsoring Agency name and address	13. Type of Report and Period Covered
	14. Sponsoring Agency Code

15. Supplementary Notes

The Federal Aviation Administration Aviation Research Division COR was

16. Abstract

17. Key Words	18. Distribution Statement
	This document is available to the U.S. public through the National Technical Information Service (NTIS), Springfield, Virginia 22161. This document is also available from the Federal Aviation Administration William J. Hughes Technical Center at actlibrary.tc.faa.gov.

19. Security Classif. (of this report)	20. Security Classif. (of this page)	21. No. of Pages	22. Price
Unclassified	Unclassified		

Form DOT F 1700.7 (8-72) Reproduction of completed page authorized

ACKNOWLEDGEMENTS

(Optional)

TABLE OF CONTENTS

LIST OF FIGURES

Figure Page

LIST OF TABLES

LIST OF ACRONYMS

DI	DONUT Index
DONUT	Disc with O-Notch for Uniaxial Testing
FAA	Federal Aviation Administration
LLD	Load line displacement
LMLC	Laboratory-mixed, laboratory-compacted
LVDT	Linear variable differential transducer
NMAS	Nominal maximum aggregate size
PMLC	Plant-mixed, laboratory-compacted
SGC	Superpave gyratory compactor

EXECUTIVE SUMMARY

1 SCOPE

1.1. This test method covers the determination of asphalt mixture cracking potential at an intermediate test temperature. A cylindrical specimen with a central circular hole is loaded diametrically at a constant load line displacement rate. Work of fracture (W_f), apparent fracture energy (G_f), post-peak secant slope ($|S_{75}|$), and DONUT Index (DI) are determined from recorded load versus load line displacement curve. The DI may be used as part of an asphalt mixture approval process.

1.2. The test is applied to laboratory-compacted specimens and pavement cores of various asphalt mixtures having a nominal maximum aggregate size (NMAS) of 19 mm or less. The specimen thickness is 62 ± 1 mm. Applicability to mixtures of larger than 19 mm NMAS, to gap-graded or open-graded mixtures, and to specimen thicknesses outside this range has not been established.

1.3. The standard test temperature is 25 °C. Another intermediate test temperature may be used when specified.

1.4. The values stated in SI units are to be regarded as standard. Values given in parentheses are inch-pound equivalents provided for information only and are not requirements of this standard. No other units of measurement are included in this standard.

1.5. The text of this standard references notes and footnotes that provide explanatory material. The notes and footnotes (excluding those in tables and figures) shall not be considered as requirements of the standard.

1.6. *This standard does not purport to address all safety concerns, if any, associated with its use. It is the responsibility of the user of this standard to establish appropriate safety, health, and environmental practices and determine the applicability of regulatory limitations prior to use.*

1.7. *This international standard was developed in accordance with internationally recognized principles on standardization established in the Decision on Principles for the Development of International Standards, Guides and Recommendations issued by the World Trade Organization Technical Barriers to Trade (TBT) Committee.*

2 REFERENCED DOCUMENTS

2.1 ASTM STANDARDS

- D8, Standard Terminology Relating to Materials for Roads and Pavements
- D2041/D2041M, Test Method for Theoretical Maximum Specific Gravity and Density of Asphalt Mixtures
- D2726/D2726M, Test Method for Bulk Specific Gravity and Density of Non-Absorptive Compacted Asphalt Mixtures
- D3203/D3203M, Test Method for Percent Air Voids in Compacted Asphalt Mixtures
- D3666, Specification for Minimum Requirements for Agencies Testing and Inspecting Road and Paving Materials
- D6373, Specification for Performance Graded Asphalt Binder
- D6925, Test Method for Preparation and Determination of the Relative Density of Asphalt Mix Specimens by Means of the Superpave Gyratory Compactor

- E4, Practices for Force Verification of Testing Machines
- E177, Practice for Use of the Terms Precision and Bias in ASTM Test Methods
- E691, Practice for Conducting an Interlaboratory Study to Determine the Precision of a Test Method

2.2 AASHTO STANDARDS:
- R 30, Practice for Mixture Conditioning of Hot Mix Asphalt (HMA)
- M 320, Specification for Performance-Graded Asphalt Binder
- M 332, Specification for Performance-Graded Asphalt Binder Using Multiple Stress Creep Recovery (MSCR) Test

2.3 OTHER PUBLICATIONS:
- Bajaj, A., Al-Qadi, I. L., & Lambros, J. (2026). A Novel Fracture-Inspired Cored Brazil Disc Test to Characterize Cracking Potential for Asphalt Concrete. *International Journal of Pavement Engineering*, *27(1)*. DOI: 10.1080/10298436.2026.2670562.

3 TERMINOLOGY

3.1. *Definitions:*

3.1.1. For definitions of terms used in this standard, refer to Terminology in ASTM D8.

3.2. *Definitions of Terms Specific to This Standard:*

3.2.1. *DI, n*—DONUT Index, a dimensionless index used to evaluate the potential of an asphalt mixture to cracking, calculated from G_f and $|S_{75}|$ in accordance with this test method.

3.2.2. *W_f, n*—work of fracture (Joules) calculated as the area under the load displacement curve. The area is taken between the contact load and the load at which the test is terminated.

3.2.3. *G_f, n*—fracture energy (Joules/m^2) required to induce a unit surface area of a crack and calculated as the work of fracture divided by specimen ligament and thickness. The ligament area is the total projected fracture area of the two ligaments, one on each side of the central hole.

3.2.4. *LLD, n*—load line displacement, the relative displacement (mm) between the upper and lower loading strips measured along the axis of loading.

3.2.5. *l_{100}, n*—displacement (mm) corresponding to peak load during the test. See **Figure 1**.

3.2.6. *l_{75}, n*—displacement (mm) corresponding to 75 % of the peak load at the post-peak stage. See **Figure 1**.

3.2.7. *$|S_{75}|$, n*—secant slope (kN/mm) calculated as $\left|\frac{P_{75}-P_{100}}{l_{75}-l_{100}}\right|$. See **Figure 1**.

3.2.8. *P_{100}, n*—peak load (kN) during the test. See **Figure 1**.

3.2.9. *P_{75}, n*—75 % of the peak load (kN) at the post-peak stage. See **Figure 1**.

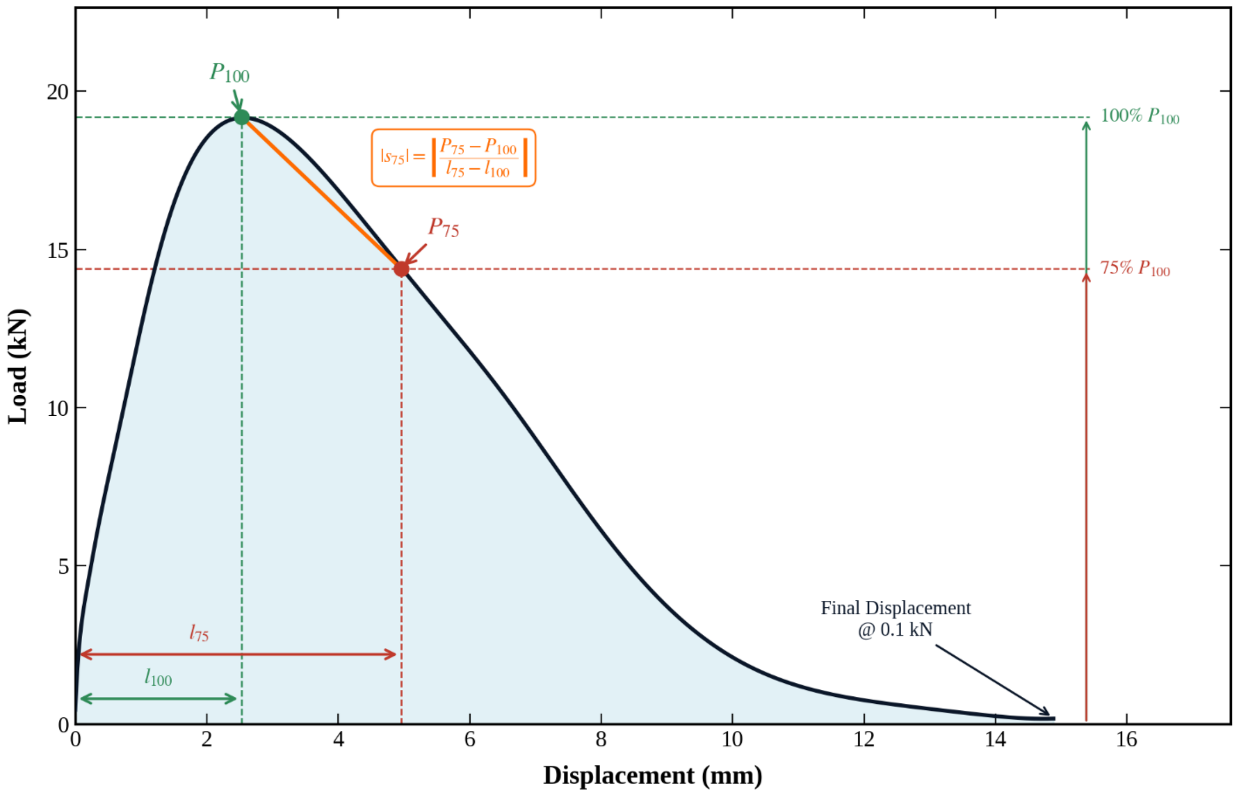

Figure 1: Recorded Load (P) versus Load Line Displacement (l) Curve

4 SUMMARY OF TEST METHOD

4.1. This test procedure considers both crack initiation and propagation in asphalt mixtures and is developed based on fracture mechanics.

4.2. A cylindrical compacted asphalt mixture specimen, using a Superpave gyratory compactor (SGC), or an asphalt pavement core with a central circular hole is fabricated. The specimen is conditioned and maintained through testing at 25 ± 1 °C or selected temperature. The specimen is positioned in the fixture, and the load is applied diametrically such that a constant load line displacement (LLD) rate of 50.0 ± 2.0 mm/min is obtained and maintained for the duration of the test. Both the load and LLD are measured during the entire duration of the test and are used to calculate work of fracture (W_f), fracture energy (G_f), post-peak secant slope ($|S_{75}|$), and DONUT Index (DI).

5 SIGNIFICANCE AND USE

5.1. The DONUT is used to determine the cracking potential of an asphalt mixture at an intermediate temperature selected for the local climate. Test specimens are readily obtained by sawing Superpave gyratory compacted cylinders 150 ± 2 mm in diameter to a thickness of 62 ± 1 mm, and a core drill is used to fabricate the central hole. Field cores, from a layer thick enough to yield a 62 ± 1 mm specimen, may be tested in the same configuration to assess the cracking potential of an in-place asphalt mixture.

5.2. The hole establishes the location of crack initiation at a known, geometrically defined stress concentration rather than at an arbitrary flaw in the aggregate skeleton or beneath the loading strips. Fixing the initiation location removes one of the principal sources of specimen-to-specimen scatter in unnotched configurations. Hence, the measured response is directly attributable to the asphalt mixture.

5.3. The hole and the wide loading strips together redistribute the stress field. As a result, a larger fraction of the externally supplied work is consumed by the fracture process, and a smaller fraction by bulk viscoelastic deformation and by damage beneath the loading contacts. The fracture energy computed by this test method is nevertheless an apparent fracture energy. It includes energy dissipated by crack growth, by time-dependent deformation remote from the crack front, and by inelastic deformation at the loading strips. It is not a material constant, and it is not transferable between geometries.

5.4. Crack growth in this geometry is not purely opening mode. The curved ligament boundary, the viscoelastic response of the binder, and the size of the aggregate relative to the ligament width together produce a mixed-mode crack path. The secant slope $|S_{75}|$ is used as a surrogate for the rate at which the specimen sheds load after peak, and therefore for the rate at which the crack traverses the ligament.

5.5. The DONUT Index combines the energy consumed in fracture with the rate of post-peak load shedding. A mixture that absorbs a large amount of energy and unloads gradually yields a high DONUT Index. An asphalt mixture that absorbs little energy and unloads abruptly yields a low DONUT Index. The DONUT Index is used to rank asphalt mixtures containing different binders, binder modifiers, aggregate blends, fibers, and recycled materials, and to identify crack-susceptible mixtures during mixture design and production quality control and acceptance.

5.6. Acceptance criteria are not part of this test method. Threshold values of the DONUT Index depend on mixture type, layer function, traffic or aircraft loading, climate, and the aging protocol used to prepare the specimens or age of the mixture in service. Any criterion stated by a specifying agency shall be accompanied by the aging protocol and the specimen preparation route to which it applies.

5.7. This test method is not intended for the direct determination of fracture toughness, of critical energy release rate, or of any parameter used as a direct input to a mechanistic pavement response model.

Note 1—The quality of the results produced by this standard is dependent on the competence of the personnel performing the procedure and the capability, calibration, and maintenance of the equipment used. Agencies that meet the criteria of Specification D3666 are generally considered capable of competent and objective testing, sampling, inspection, etc. Users of this standard are cautioned that compliance with Specification D3666 alone does not completely ensure reliable results. Reliable results depend on many factors; following the suggestions of Specification D3666 or some similar acceptable guideline provides a means of evaluating and controlling some of those factors.

6 APPARATUS

6.1. *Test Apparatus*—The test apparatus consists of an axial loading device, a load cell, loading strips, specimen deformation measurement devices, and a data acquisition system. Alternatively, the load cell, loading strips, specimen deformation measurement devices, data acquisition system, or combinations thereof can be integrated into a test fixture.

6.1.1. *Axial Loading Device*—The loading apparatus shall be capable of delivering loading in compression with a capacity of at least 25 kN. It shall be capable of maintaining a constant deformation rate of 50 ± 2.0 mm/min, which may require a closed-loop, feedback-controlled servo-hydraulic load frame. An electromechanical, screw-driven frame may be used if it can maintain the constant deformation rate.

6.1.2. *Load Cell*— The load cell shall have a resolution of 0.01 kN and a capacity of at least 25 kN. The load cell shall be accurate to within ± 1 % of the indicated load over the range from 0.10 kN to the peak load. The peak load shall fall between 10 % and 90 % of the load cell capacity.

6.1.3. *Loading Strips*—The loading strips shall be made of steel and have a concave surface with a radius of curvature equal to the nominal radius of the test specimen. For specimens with a nominal diameter of 150 ± 2 mm, the loading strips shall be 30 ± 0.3 mm wide. The length of the loading strips shall exceed the thickness of the specimen as in **Figure 2**. The outer edges of the loading strips shall be beveled slightly to remove sharp edges. The loading faces of the two strips shall be parallel to within 0.1 mm over the width of the strip, and their longitudinal axes shall be aligned to within 1.0 mm in the direction perpendicular to the loading axis. Before each test the strip faces shall be free of grooving, burrs, and adhering asphalt.

6.1.3.1. *Option A*—The loading strips can be part of a test fixture similar to that shown in **Figure 2**, in which the lower loading strip is mounted on a base having two perpendicular guide rods or posts extending upward. The upper loading strip shall be clean and slide freely on the posts. Guide sleeves in the upper segment of the test fixture shall direct the two loading strips together without appreciable binding or loose motion in the guide rods.

6.1.3.2. *Option B*—The upper and lower loading strips, as shown in **Figure 3**, are parts of an axial loading device. They are permanently attached to the top loading actuator and the base plate, respectively.

6.1.3.3. *Option C*—The upper and lower loading strips, as shown in **Figure 4**, are part of a test fixture integrated with a load cell, loading strips, specimen deformation measurement devices, and a data acquisition system.

6.1.4. *Internal Displacement Measuring Device*—The displacement shall be measured to a resolution of ±0.01 mm. The machine stroke linear variable differential transducer (LVDT) or other type of displacement transducer can be used if its resolution is sufficient to meet the requirement. The displacement data measured during the test may need to be corrected for system compliance through standardizing the test system.

6.1.5. *External Displacement Measuring Device*—If an internal displacement measuring device does not exist or has insufficient precision, one or more external displacement measuring devices such as LVDTs can be used (**Figure 3**).

6.1.6. *Data Acquisition System*—Time, load, and LLD (using either internal or external displacement measuring devices) data are collected at a minimum of 50 sampling data points per second to obtain a smooth load LLD curve.

6.2. *Conditioning Chamber*—An environmental chamber or water bath capable of maintaining the target intermediate test temperature ± 1.0 °C for conditioning specimens before testing.

6.3. *Gyratory Compactor*—A gyratory compactor and associated equipment for preparing laboratory specimens in accordance with Test Method D6925 are needed.

6.4. *Core Drill*—A core drill shall be a coring machine with a cooling system and a diamond bit capable of producing a central hole 27.5 mm ± 2 mm in diameter through the full thickness of the test specimen. The axis of the hole shall be perpendicular to the specimen faces to within 1°. A bit with a 25.5 mm (1.00 in) inside diameter is generally suited to produce the finished hole size once kerf is accounted for. The bit shall be selected by measuring the finished hole diameter on trial specimens rather than by assuming the kerf.

Note 2—A coring machine with adjustable vertical feed and rotational speed is recommended. The variable feeds and speeds may be controlled by various methods. A vertical feed rate of approximately 0.05 mm/rev (0.002 in/rev) and a rotational speed of approximately 450 r/min has been found to be satisfactory for several Superpave asphalt mixtures. Use of a standard electric core drill with a holder for the specimen is also acceptable.

6.5. *Saw*—A water-cooled laboratory masonry saw capable of producing plane, parallel faces on gyratory-compacted cylinders and on field cores. The saw shall hold the specimen so that sawn faces are parallel to within 2.0 mm across the specimen diameter.

6.6. *Sample Measurement Device*—A caliper accurate to ± 0.1 mm shall be used to measure specimen thickness and diameter.

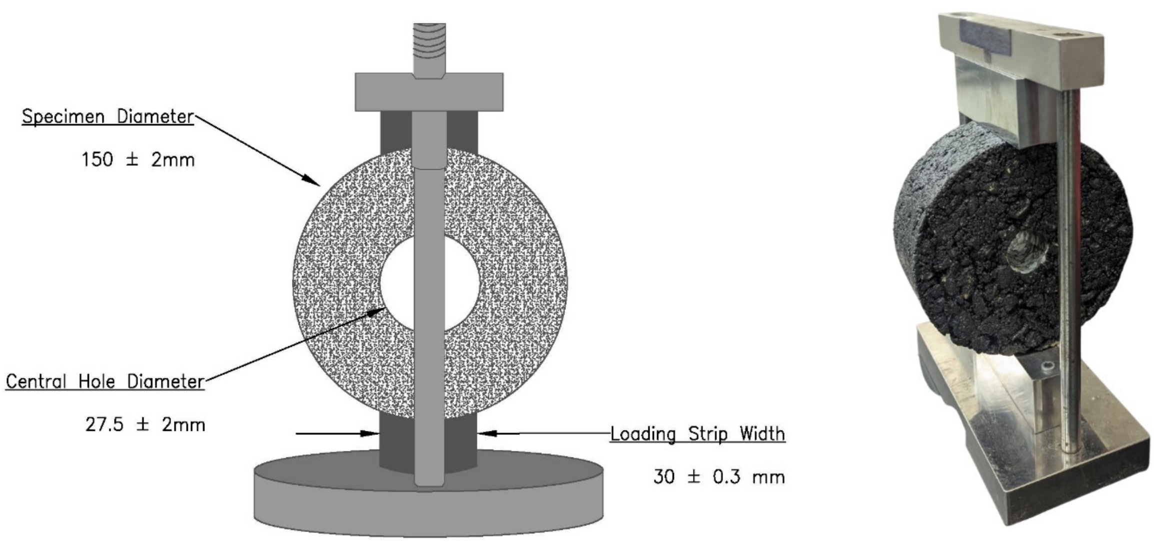

Figure 2: Modified Indirect Tension Test Fixture

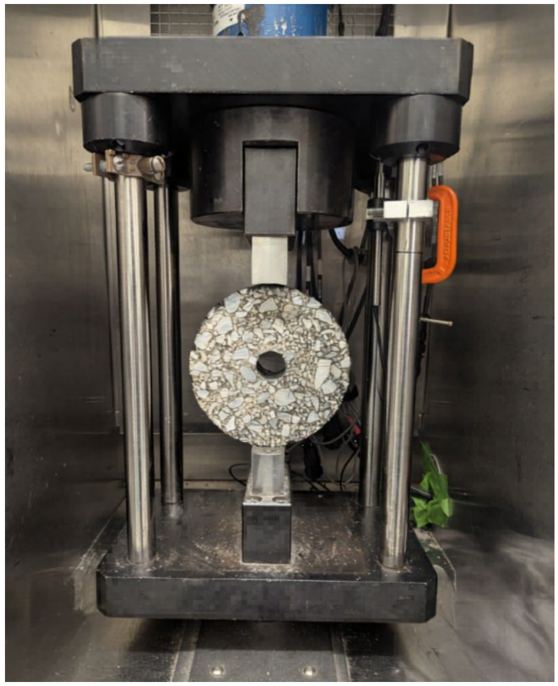

Figure 3: Loading Strips Embedded in an Axial Loading Device

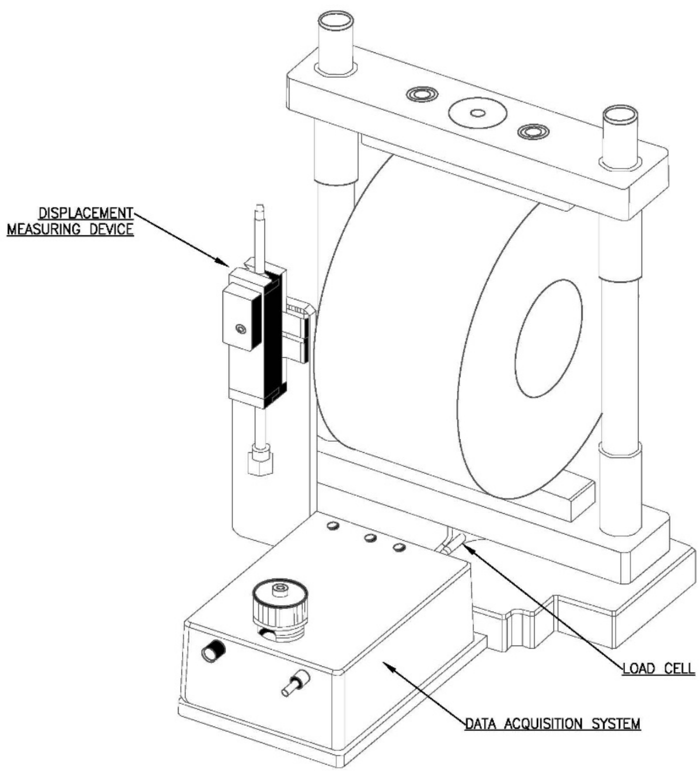

Figure 4: Loading Strips Embedded in a Test Fixture with Load Cell, Displacement Measurement Device, and Data Acquisition System

7 HAZARDS

7.1. Standard laboratory caution should be exercised when handling, compacting, and fabricating test specimens and asphalt mixtures.

8 SAMPLING, TEST SPECIMENS, AND TEST UNITS

8.1. The DONUT may be conducted on laboratory-prepared test specimens or field cores.

8.2. *Laboratory-Compacted Asphalt Mixture Samples:*

8.2.1. *Specimen Size*—For the mixtures with a nominal maximum aggregate size (NMAS) of 19 mm or smaller, the specimens shall be 150 ± 2 mm in diameter and 62 ± 1 mm in thickness. Specimens can be sawed from a larger gyratory compacted pill. Direct compaction to the final 62 mm thickness shall not be used unless the specifying agency permits it, in which case the report shall state that direct compaction was used.

Note 3—Direct molding of 62-mm-thick disc specimens at representative air void levels for airfield pavements is discouraged. It leads to a significantly higher number of gyrations and consequently potential aggregate breakage.

8.2.2. *Specimen Fabrication by Sawing:*

8.2.2.1. Compact a cylinder 150 ± 2 mm in diameter and 160 ± 1 mm in height in accordance with Test Method D6925, using a mass selected to give the target air void content in the finished test specimens. If a lab does not have the capability to compact 160 ± 1 mm tall gyratory specimens, then two 115 ± 1 mm tall gyratory specimens may be compacted and used instead to replace each 160 ± 1 mm tall gyratory specimen.

8.2.2.2. Discard not less than 10 mm from the top face and not less than 10 mm from the bottom face of the cylinder. The air void structure of these regions is not representative of the interior of the cylinder. Saw the test specimens, each 62 ± 1 mm thick, from the remaining central portion. Where a single specimen is taken from a cylinder, it shall be taken from the central portion.

8.2.2.3. The two sawn faces of each specimen shall be plane and parallel to within 2.0 mm across the specimen diameter. Verify this as the difference between the maximum and the minimum thickness measured at four locations spaced 45° apart around the perimeter.

8.2.3. Measure the thickness at four locations and the diameter at two orthogonal locations. Use the average of these measurements in all calculations.

8.2.4. *Circular Holes for Stress Concentration*—A 27.5 ± 2 mm diameter hole will be fabricated at the center of the cylindrical specimen using a core drill as described in Section 6. The location of the hole shall not deviate more than 2 mm from the center.

8.2.5. *Aging*—Loose mixture for laboratory-mixed, laboratory-compacted (LMLC) specimens shall be short-term conditioned for 2 h ± 5 min at the compaction temperature in accordance with AASHTO R 30 before compaction, unless a different protocol is specified by the agency. Plant-mixed, laboratory-compacted (PMLC) specimens shall be compacted after reheating the sampled mixture to its compaction temperature, and the reheating time and temperature shall be recorded. The aging protocol used shall be stated in the report and shall accompany any DONUT Index criterion.

8.2.6. *Air Void Content*— Prepare a minimum of three specimens at the target air void content ± 0.5 %. Discard specimens that fall outside the target range, and do not include them in the reported set.

Note 4—The specimen air voids can be calculated using ASTM Test Method D3203/D3203M. The typical air void target for highway pavement is 7 %, P-401 airfield pavements is 5 %, and for P-404 airfield pavements it is 3 %. Other target air voids can be used, but specimens with significantly different air voids (larger than ± 0.5 %) are not comparable.

8.3. *Samples Cored from Asphalt Pavements:*

8.3.1. Field cores can be used if the pavement layer is thicker than 62 mm. Field core specimens shall be 150 ± 2 mm in diameter. The axis of the core shall be perpendicular to the pavement surface, and the deviation of the core axis from perpendicular shall not exceed 1°. Trim the top and bottom surfaces of all cores to the specimen thickness required by this test method.

8.3.2. Where the layer thickness does not permit a 62 mm specimen, record and report the actual thickness. DONUT Index values from specimens thinner than 62 mm shall not be compared with values from 62 mm specimens unless a locally established thickness correction has been applied and reported.

Note 5—Care shall be taken to avoid damage to the cores during handling and transportation prior to testing. A core bit of 156 mm in diameter may be needed in order to obtain cores 150 ± 2 mm in diameter. The air voids of the core specimens should be determined. Additionally, the DONUT Index values of core specimens are relatively comparable but may not be equal to those of laboratory-compacted specimens due to different aging conditions.

Note 6—DONUT Index correction factors for pavement core specimen thickness and differences between field and lab compaction may be needed. A thickness correction factor may be applied for pavement cores tested at thickness less than 62 mm. The correction factors may require local calibration to consider locally available materials and mixture design requirements.

8.4. A minimum of three specimens shall be tested for LMLC or PMLC specimens. A minimum of three field core specimens shall be tested.

9 PROCEDURE

9.1. *Conditioning*—Precondition test specimens in an environmental chamber or water bath at a target intermediate test temperature ± 1.0 °C for 2 h ± 10 min. Surface dry water-bath specimens immediately before testing. State the conditioning medium and the conditioning time in the report.

Note 7—The typical target intermediate test temperature is 25 °C. Other target intermediate test temperatures can be used. One choice for the target intermediate test temperature is *PG IT* defined in ASTM Specification D6373, AASHTO M 320, or AASHTO M 332 and provided in Eq 1:

$$PG\ IT = \frac{PG\ HT + PG\ LT}{2} + 4 \qquad (1)$$

where:

PG IT	=	intermediate performance grade temperature (°C),
PG HT	=	climatic high-performance grade temperature (°C), and
PG LT	=	climatic low-performance grade temperature (°C).

9.2. *Test Temperature Control*—Immediately after removing the test specimen from the conditioning water bath or environmental chamber, complete positioning and testing of the DONUT specimen within 5 min to ensure that the specimen temperature is maintained.

9.3. *Check Fixture*—Inspect the fixture to ensure all contact surfaces are clean and free of debris and that the loading strip is of the correct width.

9.4. *Position Specimen*—Place the specimen in the fixture so that it is centered on the lower loading strip and the loading axis passes through the center of the central hole. Confirm that both loading strips make uniform contact across the full thickness of the specimen before load is applied.

9.5. *Contact Load*—First, impose a contact load in LLD control at a rate of 1.0 ± 0.5 mm/min until the measured load reaches 0.10 ± 0.01 kN. Record the contact load to ensure it is achieved. At the contact load, set the LLD reading to zero. Do not re-zero the load cell. All load values shall be reported as measured. Confirm that the recorded displacement increases monotonically once the contact load is reached. A record in which displacement reverses, or in which load rises with no corresponding displacement, indicates that the specimen was not fully seated, and shall be reported as invalid.

Note 8—Incomplete seating produces a load rise over the first few hundredths of a millimeter that does not reflect the mixture, and it displaces the origin of the load versus LLD curve. A slower approach to the contact load, or a brief hold at the contact load before the test rate is applied, reduces its occurrence.

9.6. *Loading*—Apply load to the specimen in LLD control at a rate of 50 ± 2.0 mm/min. Terminate the test when the load falls below 0.10 kN after the peak load has been reached, or when the LLD reaches 25 mm, whichever occurs first. During testing, record the time, load, and displacement at a minimum sampling rate of 50 data points per second.

9.7. Repeat Sections 9.1 through 9.6 for each test specimen.

9.8. Testing shall be completed in 5 min or less after removal from the environmental chamber to maintain a uniform specimen temperature.

10 CALCULATION OR INTERPRETATION OF RESULTS

10.1. The work of fracture (W_f) is calculated as the area under the load versus LLD curve (see **Figure 1**) using the trapezoidal rule provided in Eq 2. The summation is carried out over every recorded data point from the contact load through termination of test.

$$W_f = \sum_{i=1}^{n-1} \left(\frac{1}{2} \times (l_{i+1} - l_i) \times (P_{i+1} + P_i) \right) \tag{2}$$

where:

W_f	=	work of fracture (Joules),
P_i	=	applied load (kN) at the *i* load step application,
P_{i+1}	=	applied load (kN) at the *i* + 1 load step application,
l_i	=	LLD (mm) at the *i* step, and
l_{i+1}	=	LLD (mm) at the *i* + 1 step.

10.2. *Fracture Energy (G_f)* is calculated by dividing the work of fracture (the area under the load versus the average LLD curve; see **Figure 1**) by the cross-sectional area of the specimen ligament. Use the mean measured diameter and the mean measured thickness of the individual specimen, not the nominal values.

$$G_f = \frac{W_f}{(D-d)\times t} \times 10^6 \tag{3}$$

where:

G_f	=	fracture energy (Joules/m^2),
W_f	=	work of fracture (Joules),
D	=	specimen diameter (mm),
d	=	hole diameter (mm), and
t	=	specimen thickness (mm).

10.3. Secant slope ($|S_{75}|$) is the slope between the peak load and load at 75 % peak load point after the peak; see **Figure 1**.

10.4. *Curve Fitting for Noisy Data*—Where noise in the recorded load versus LLD curve prevents P_{100}, l_{100}, or l_{75} from being located directly from the recorded data, the curve may be fitted in accordance with Appendix A and the fitted curve used to determine these quantities. W_f shall be computed from the recorded data in every case. State in the report whether a fit was applied.

Note 9—Fitting is a remedy for measurement noise. It is not a remedy for a poorly conducted test. A record showing a load discontinuity, a second peak, or a seating step should be investigated rather than fitted.

10.5. DONUT Index (*DI*) is calculated from the parameters obtained using the load displacement curve, as listed below:

$$DI = \frac{G_f}{|S_{75}|} \times 0.001 \tag{4}$$

where:

DI	=	DONUT Index,
G_f	=	fracture energy (Joules/m^2), and
$\lvert S_{75}\rvert$	=	absolute value of the secant slope S_{75} (kN/mm).

Note 10—0.001 is a scale factor in Eq 4. The DONUT Index is reported as a dimensionless number.

11 REPORT

11.1. *The report shall include the following parameters for each test specimen:*

11.1.1. Asphalt mixture type.

11.1.2. Test temperature, °C.

11.1.3. Specimen preparation method and aging condition.

11.1.4. Theoretical maximum specific gravity of the asphalt concrete mixture, to the nearest 0.001.

11.1.5. Bulk specific gravity of the asphalt concrete mixture, to the nearest 0.001.

11.1.6. Specimen air voids, %.
11.1.7. Specimen thickness, mm.
11.1.8. Compaction method, and whether the specimen was sawn from a taller cylinder or compacted directly to thickness.
11.1.9. Specimen diameter, mm.
11.1.10. Peak load, P_{100}, kN, and displacement at peak load, l_{100}, mm.
11.1.11. Displacement at 75 % of the peak load, l_{75}, mm.
11.1.12. Whether the load versus LLD curve was fitted in accordance with Appendix A.
11.1.13. Secant slope, $|S_{75}|$, kN/mm.
11.1.14. Fracture energy, G_f, Joules/m^2.
11.1.15. Work of fracture, W_f, Joules.
11.1.16. DONUT Index, *DI*.
11.1.17. Report P_{100} to the nearest 0.01 kN, displacements to the nearest 0.01 mm, $|S_{75}|$ to the nearest 0.01 kN/mm, G_f to the nearest 1 J/m^2, W_f to the nearest 0.1 J, and DI to the nearest 0.1.

12 PRECISION AND BIAS

12.1. *Precision*: The precision of this test method has not been determined. An interlaboratory study conducted in accordance with Practice E691 is planned.
12.2. *Bias*: No accepted reference material suitable for determining the bias of this test method is available. Therefore, bias cannot be determined.

13 KEYWORDS

13.1. Asphalt mixture cracking potential; Disc with O-Notch for Uniaxial Testing; DONUT Index; fracture energy; secant slope; work of fracture; balanced mix design; crack propagation.

APPENDIX A— CURVE FITTING PROCEDURE FOR NOISY LOAD VERSUS LLD DATA

A.1. *SCOPE*:

A.1.1. This appendix presents the algorithm used to fit the recorded load versus load line displacement curve where noise prevents the peak load or the post-peak characteristic points from being located directly from the recorded data. The algorithm consists of the following steps:

A.1.1.1. Preprocessing the raw load–LLD curve;

A.1.1.2. Determination of the peak; and

A.1.1.3. Post-peak calculations.

A.1.2. The fitted curve is used only to determine P_{100}, l_{100}, P_{75}, and l_{75}. The work of fracture is determined from the recorded data in accordance with the Calculation section of this test method.

Note A1—The work of fracture is integrated from the recorded data rather than from the fitted curve, so no fit of the ascending branch is required.

A.2. *PREPROCESSING:*

A.2.1. Remove from the recorded file all data points whose load is less than 0.10 kN.

A.2.2. Identify the maximum recorded load. Assign the data preceding it to the ascending segment and the remaining data to the post-peak segment. Denote the provisional peak (l'_{100}, P'_{100}) and the end of the record (l_f, P_f). Let L be the displacement span of the post-peak segment, $L = l_f - l'_{100}$.

A.3. *DETERMINATION OF THE PEAK:*

A.3.1. Fit a polynomial of degree three by least squares to the recorded data lying within ± 0.5 mm of l'_{100}. P_{100} is the maximum of the fitted polynomial over that interval and l_{100} is the displacement at which it occurs:

$$P_1(l) = c_1 \times l^3 + c_2 \times l^2 + c_3 \times l + c_4$$

A.3.2. where: c_i = polynomial coefficients.

Note A2—Do not fit the full ascending branch. A high-order polynomial fitted over the whole ascending branch is dominated by the low-load region and displaces the apparent peak.

A.4. *POST-PEAK FITTING:*

A.4.1. Fit by least squares a sum of four Gaussian terms to the post-peak segment of the load–LLD curve:

$$P_2(l) = \Sigma\, d_i \exp[-((l - e_i)/f_i)^2],\ \ i = 1 \text{ to } n,\ n = 4$$

where: d, e, f = fitting coefficients, and n = number of exponential terms.

A.4.2. Constrain the coefficients as follows, scaling each bound to the record being fitted:

d_i between $-1.5P_{100}$ and $1.5P_{100}$;

e_i between $l'_{100} - L$ and $l'_{100} + L$; and

f_i not less than the lower bound selected in accordance with A4.3.

A.4.3. Constrain f from below, since an unbounded f may approach zero and produce a spurious derivative, while a bound set too high degrades the accuracy of the fit. Candidate lower bounds are $0.20L$, $0.15L$, $0.10L$, $0.06L$, $0.03L$, $0.02L$, and $0.01L$. Begin with the largest and proceed in descending order until the criterion of A4.6 is satisfied.

A.4.4. Use the following starting estimate. Take d_1 to d_4 as P'_{100}, $0.5P'_{100}$, $0.3P'_{100}$, and $0.1P'_{100}$; take e_1 to e_4 as $l'_{100} + 0$, $0.25L$, $0.50L$, and $0.85L$; and take f_1 to f_4 as $L/4$, $L/3$, $L/2$, and L, each raised to the current lower bound on f where necessary.

A.4.5. Generate a displacement vector from l'_{100} to l_f in increments of 0.005 mm and compute the corresponding loads from $P_2(l)$.

A.4.6. Accept the fit where the coefficient of determination of the post-peak segment is not less than 0.997 and the fitted curve decreases monotonically between l_{100} and the displacement at which it reaches P_{75}. Otherwise, select the next lower bound for f and repeat A4.1 through A4.5.

A.5. *DETERMINATION OF PARAMETERS:*

A.5.1. P_{100} and l_{100} are determined in accordance with A3.1.

A.5.2. P_{75} is $0.75 \times P_{100}$.

A.5.3. l_{75} is the smallest displacement greater than l_{100} at which $P_2(l)$ equals P_{75}.

A.5.4. Compute $|S_{75}|$ from these values in accordance with the Calculation section of this test method.

A.6. *REPORTING:*

A.6.1. Report that the curve was fitted, the coefficient of determination of the post-peak segment, and the lower bound of f at which the fit was accepted. Apply the procedure to every specimen in a set, or to none of them.

Appendix G: Technical Note Template for the Illinois Flexibility Index Test (I-FIT)

Standard Method of Test for Determining the Fracture Potential of Asphalt Mixtures Using the Illinois Flexibility Index Test (I-FIT)

Author name (if the report was authored only by the FAA)

Date

DOT/FAA/TC-TNxx/xx

This document is available to the U.S. public through the National Technical Information Services (NTIS), Springfield, Virginia 22161.

This document is also available from the Federal Aviation Administration William J. Hughes Technical Center at actlibrary.tc.faa.gov.

U.S. Department of Transportation

Federal Aviation Administration

NOTICE

Technical Report Documentation Page

1. Report No.	2. Government Accession No.	3. Recipient's Catalog No.
DOT/FAA/TC-TNxx/xx		

4. Title and Subtitle	5. Report Date
Standard Method of Test for Determining the Fracture Potential of Asphalt Mixtures Using the Illinois Flexibility Index Test (I-FIT)	APRIL 2025
	6. Performing Organization Code
7. Author(s)	8. Performing Organization Report No.
9. Performing Organization Name and Address	10. Work Unit No. (TRAIS)
	11. Contract or Grant No.
12. Sponsoring Agency Name and Address Sponsoring Agency name and address	13. Type of Report and Period Covered
	14. Sponsoring Agency Code

15. Supplementary Notes

The Federal Aviation Administration Aviation Research Division COR was

16. Abstract

17. Key Words	18. Distribution Statement
	This document is available to the U.S. public through the National Technical Information Service (NTIS), Springfield, Virginia 22161. This document is also available from the Federal Aviation Administration William J. Hughes Technical Center at actlibrary.tc.faa.gov.

19. Security Classif. (of this report)	20. Security Classif. (of this page)	21. No. of Pages	22. Price
Unclassified	Unclassified		

Form DOT F 1700.7 (8-72) Reproduction of completed page authorized

ACKNOWLEDGEMENTS

(Optional)

TABLE OF CONTENTS

LIST OF FIGURES

LIST OF TABLES

LIST OF ACRONYMS

COV	Coefficient of variation
FAA	Federal Aviation Administration
FI	Flexibility index
I-FIT	Illinois flexibility index test
LLD	Load line displacement
LVDT	Linear variable differential transducer
NMAS	Nominal maximum aggregate size
SCB	Semi-circular bend
SGC	Superpave gyratory compactor

EXECUTIVE SUMMARY

1. SCOPE

1.1. This test method covers the determination of Mode I (tensile opening mode during crack propagation) cracking resistance properties of asphalt mixtures at intermediate test temperatures. Specimens are tested in the semi-circular bend geometry, which is a half disc with a notch parallel to the direction of load application. The data analysis procedure associated with this test determines the fracture energy (G_f) and post-peak slope (m) of the load load line displacement (LLD) curve. These parameters are used to develop a flexibility index (FI) to predict the fracture resistance of an asphalt mixture at intermediate temperatures. The FI can be used as part of the asphalt mixture approval process.

1.2. These procedures apply to test specimens having a nominal maximum aggregate size (NMAS) of 19 mm or less. Lab compacted and pavement core specimens can be tested according to this test procedure. A thickness correction factor will need to be developed and applied for pavement cores tested at a thickness less than 45 mm.

1.3. *This standard does not purport to address all the safety concerns, if any, associated with its use. It is the responsibility of the user of this standard to establish and follow appropriate health and safety practices and determine the applicability of regulatory limitations prior to use.*

1.4. *The quality of the results produced by this standard is dependent on the competence of the personnel performing the procedure and the capability, calibration, and maintenance of the equipment used. Agencies that meet the criteria of R 18 are generally considered capable of competent and objective testing/sampling/inspection/etc. Users of this standard are cautioned that compliance with R 18 alone does not completely assure reliable results. Reliable results depend on many factors; following the suggestions of R 18 or some similar acceptable guideline provides a means of evaluating and controlling some of those factors.*

2. REFERENCED DOCUMENTS

2.1. *AASHTO Standards*:
- R 18, Establishing and Implementing a Quality Management System for Construction Materials Testing Laboratories
- R 67, Sampling Asphalt Mixtures after Compaction (Obtaining Cores)
- T 166, Bulk Specific Gravity (G_{mb}) of Compacted Asphalt Mixtures Using Saturated Surface-Dry Specimens
- T 209, Theoretical Maximum Specific Gravity (G_{mm}) and Density of Asphalt Mixtures
- T 269, Percent Air Voids in Compacted Dense and Open Asphalt Mixtures
- T 283, Resistance of Compacted Asphalt Mixtures to Moisture-Induced Damage
- T 312, Preparing and Determining the Density of Asphalt Mixture Specimens by Means of the Superpave Gyratory Compactor
- TP 105, Determining the Fracture Energy of Asphalt Mixtures using Semicircular Bend Geometry (SCB)

2.2. *ASTM Standards*:
- D8, Standard Terminology Relating to Materials for Roads and Pavements

- D3549/D3549M, Standard Test Method for Thickness or Height of Compacted Bituminous Paving Mixture Specimens

2.3. *Other Publications:*

- Al-Qadi, I. L., H. Ozer, J. Lambros, A. El Khatib, P. Singhvi, T. Khan, and B. Doll. 2015. *Testing Protocols to Ensure Performance of High Asphalt Binder Replacement Mixes Using RAP and RAS*, FHWA ICT-15-07. Illinois Center for Transportation, Rantoul, IL.
- Doll, B., H. Ozer, J. Rivera-Perez, J. Lambros, and I. L. Al-Qadi. 2016. Investigation of Viscoelastic Fracture Fields in Asphalt Mixtures Using Digital Image Correlation. *International Journal of Fracture*, Vol. 205, No. 1, pp. 37–56.
- Ozer, H., I. L. Al-Qadi, J. Lambros, A. El-Khatib, P. Singhvi, and B. Doll. 2016a. Development of the Fracture-Based Flexibility Index for Asphalt Concrete Cracking Potential Using Modified Semi-Circle Bending Test Parameters. *Construction and Building Materials*, Vol. 115, pp. 390–401.
- Ozer, H., P. Singhvi, T. Khan, J. Rivera, I. L. Al-Qadi. 2016b. Fracture Characterization of Asphalt Mixtures with RAP and RAS Using the Illinois Semi-Circular Bending Test Method and Flexibility Index. *Transportation Research Record*, Transportation Research Board, National Research Council, Washington, DC, Vol. 2575, pp. 130–137.
- Ozer, H., I. L. Al-Qadi, P. Singhvi, J. Bausano, R. Carvalho, X. Li, and N. Gibson. 2017. Assessment of Asphalt Mixture Performance Tests to Predict Fatigue Cracking in an Accelerated Pavement Testing Trial. *International Journal of Pavement Engineering*, Special Issue for Cracking in Flexible Pavements and Asphalt Mixtures: Theories to Modeling and Testing to Mitigation.
- RILEM Technical Committee 50-FMC. 1985. "Determination of the Fracture Energy of Mortar and Concrete by Means of Three-Point Bend Tests on Notched Beams." *Materials and Structures*, Springer Netherlands for International Union of Laboratories and Experts in Construction Materials, Systems and Structures (RILEM), Dordrecht, The Netherlands, No. 106, July–August 1985, pp. 285–290.

3. <u>TERMINOLOGY</u>

3.1. *Definitions*:

3.1.1. *critical displacement, u_1*—displacement at the intersection of the post-peak slope with the displacement-axis.

3.1.2. *displacement at peak load, u_0*—recorded displacement at peak load.

3.1.3. *final displacement*, u_{final}—recorded displacement at the 0.1 kN cut-off load.

3.1.4. *flexibility index,* FI—index intended to characterize the cracking resistance of an asphalt mixture, calculated by multiplying the ratio of fracture energy to post-peak slope by a constant multiplier.

3.1.5. *fracture energy, G_f*—energy required to create a unit surface area of a crack.

3.1.6. *ligament area,* Area_{lig}—cross-sectional area of the specimen through which the crack propagates, calculated by multiplying ligament width (test specimen thickness) and ligament length.

3.1.7. *linear variable differential transducer (LVDT)*—sensor device for measuring linear displacement.

3.1.8. *load line displacement (LLD)*—displacement measured in the direction of the load application.

3.1.9. *post-peak slope, m*—slope at the first inflection point of the load–LLD curve after the peak.

3.1.10. *semi-circular bend (SCB) geometry*—a half disc with a notch parallel to the direction of load application.

3.1.11. *work of fracture (W_f)*—calculated as the area under the load–LLD curve.

4. SUMMARY OF METHOD

4.1. A Superpave gyratory compactor (SGC)-compacted asphalt mixture specimen or an asphalt pavement core is trimmed and cut in half to create a semicircular test specimen. A notch is sawn in the flat side of the semicircular specimen opposite the curved edge. The specimen is conditioned and maintained through testing at 25 ± 0.5 °C. The specimen is positioned in the fixture with the notched side down, centered on two rollers. A load is applied along the vertical radius of the specimen, and the load and load line displacement (LLD) are measured during the entire duration of the test. The load is applied such that a constant LLD rate of 50 mm/min is obtained and maintained for the duration of the test. The I-FIT fixture and I-FIT specimen geometry for an SGC laboratory-compacted specimen are shown in **Figure 1**.

4.2. Fracture energy (G_f), post-peak slope (m), displacement at peak load (u_0), critical displacement (u_1), and a flexibility index (FI) are calculated from the load and LLD results.

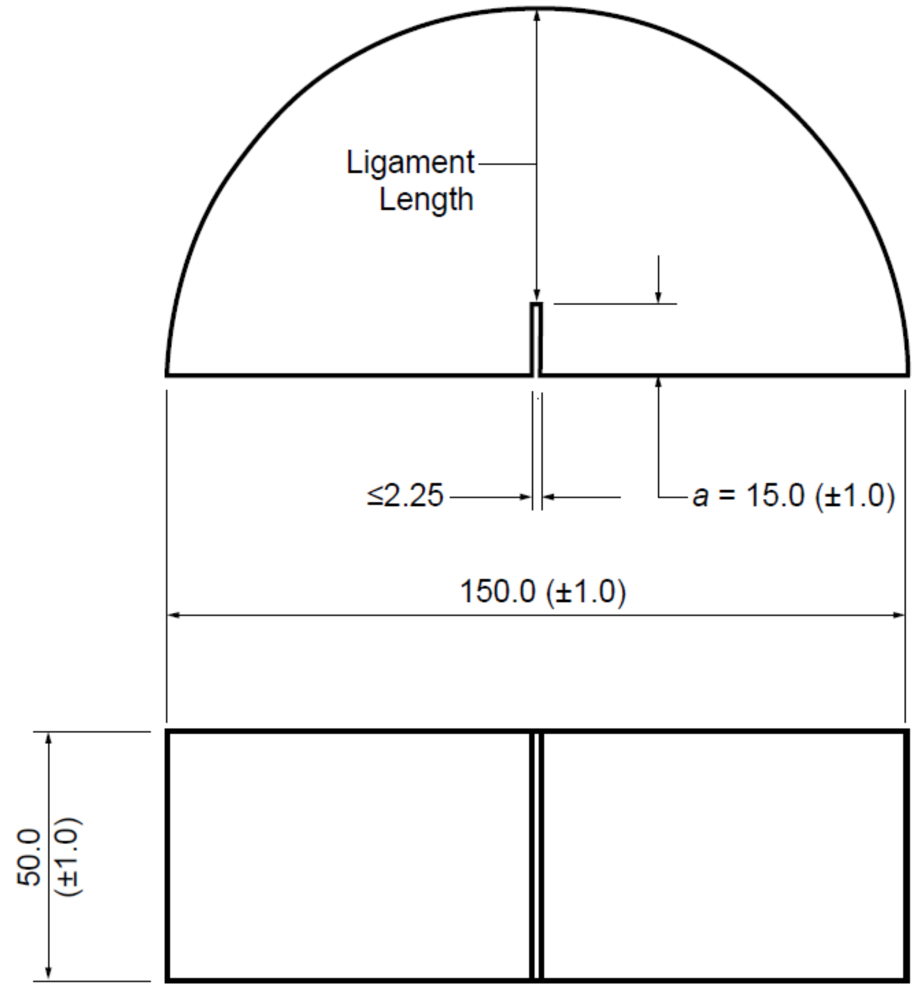

Figure 1: I-FIT SGC Laboratory Compacted Specimen Configuration (dimensions in millimeters)

5. SIGNIFICANCE AND USE

5.1. The I-FIT is used to determine fracture resistance parameters of an asphalt mixture at an intermediate temperature (Al-Qadi et al., 2015; Ozer et al., 2016a; Ozer et al., 2016b). From the fracture parameters of G_f and *m* obtained, the FI of an asphalt mixture is calculated. The FI provides a means to identify brittle mixtures that may be prone to premature cracking. The range for an acceptable FI will vary according to local environmental conditions, application of the mixture, nominal maximum aggregate size (NMAS), asphalt binder content, asphalt binder performance grade (PG), air voids, expectation of service life, etc. (Al-Qadi et al., 2015; Ozer et al., 2016a; Ozer et al., 2016b; Ozer et al., 2017).

5.2. The calculated FI indicates an asphalt mixture's overall capacity to resist cracking-related damage (Al-Qadi et al., 2015). Generally, a mixture with higher FI can resist crack propagation for a longer time duration under tensile stress. The FI should not be directly used in structural design and analysis of pavements. FI values obtained using this procedure are used in ranking the cracking resistance of alternative mixtures for a given layer in a structural design. The *Gf* parameter is dependent on specimen size, loading time, and temperature. Fracture mechanisms for viscoelastic materials are influenced by crack front viscoelasticity and bulk material (far from the crack front) viscoelasticity. Total calculated G_f from this test includes the amount of energy dissipated by crack propagation, viscoelastic mechanisms away from the crack front, and other inelastic irreversible processes (frictional and damage processes at the loading support points) (Doll et al., 2016).

5.3. G_f is one of the parameters used to calculate the FI, which is further used to predict asphalt mixture fracture potential. It also represents the main parameter input in more complex analyses based on a theoretical crack (cohesive zone) model. In order to be used as part of a cohesive zone model, fracture energy as calculated from the experiment shall be corrected to determine energy associated with crack propagation only. A correction factor may be used to eliminate other sources of inelastic energy contributing to the total fracture energy calculated directly from the experiment.

5.4. This test method and FI can be used to rank the cracking resistance of asphalt mixtures containing various asphalt binders, modifiers of asphalt binders, aggregate blends, fibers, and recycled materials.

5.5. The specimens can be readily obtained from SGC-compacted cylinders or from pavement cores with a diameter of 150 mm.

6. APPARATUS

6.1. *Testing Machine*—An I-FIT system consists of a closed-loop axial loading device, a load measuring device, a bend test fixture, specimen deformation measurement devices, and a control and data acquisition system. A constant displacement-rate device, such as a closed loop, feedback-controlled servo-hydraulic load frame, shall be used.

Note 1—An electromechanical, screw-driven machine may be used if results are comparable to a closed loop, feedback-controlled servo-hydraulic load frame.

6.1.1. *Axial Loading Device*—The loading device shall be capable of delivering loads in compression with a maximum resolution of 10 N and a capacity of at least 10 kN.

6.1.2. *Bend Test Fixture*—The fixture is composed of a loading head, a steel base plate, and two steel rollers with a nominal diameter (*D*) of 25 mm. The tip of the loading head has a contact curvature with a radius of 12.5 ± 0.05 mm. The horizontal loading head shall pivot relative to the vertical loading axis to conform to slight specimen variations. The length of the two roller supports in **Figure 2** and **Figure 3** shall be a minimum of 65 mm. Illustrations of the loading and supports are shown in **Figures 2** and **3**.

6.1.2.1. *Method A*—Typically two steel rollers with a nominal diameter of 25 mm are mounted on bearings through their axis of rotation and attached to the steel base plate with brackets. One of the steel rollers may pivot on an axis perpendicular to the axis of loading to conform to slight specimen variations. A distance of 120 ± 0.1 mm between the two steel rollers is maintained throughout the test.

6.1.2.2. *Method B*—An alternate fixture design uses two steel rollers with a nominal diameter of 25 mm that each rotate in a U-shaped roller support steel block. The initial roller position is fixed by springs and backstops that establish the initial test span dimension of 120 ± 0.1 mm. The support rollers are allowed to rotate away from the backstops during the test but should remain in contact with the sample.

6.1.3. *Internal Displacement Measuring Device*—The displacement measurement can be performed using the machine's stroke (position) transducer if the resolution of the stroke is sufficient (0.01 mm or lower). The fracture test displacement data may be corrected for system compliance, loading-pin penetration, and specimen compression by performing a calibration of the testing system.

6.1.4. *External Displacement Measuring Device*—If an internal displacement measuring device does not exist or has insufficient precision, an externally applied displacement measurement device such as a linear variable differential transducer (LVDT) accurate to 0.01 mm can be used (**Figure 2** and **Figure 3**).

6.1.5. *Control and Data Acquisition System*—Time, load, and LLD (using an external and/or internal displacement measurement device) are recorded. The control and data acquisition system is required to apply a constant LLD rate at a precision of 50 ± 1 mm/min and collect data at a minimum sampling frequency of 20 Hz in order to obtain a smooth load–LLD curve.

6.1.6. *Saw*—A laboratory saw capable of cutting asphalt specimens shall be used; it must be capable of cutting the notch described in **Figure 1**.

6.1.7. *Conditioning Chamber*—A water bath or environmental chamber shall be used; it must be capable of maintaining specimen temperature as described in Section 10.1.

6.1.8. *Measuring Device*—A caliper or ruler accurate to ± 0.1 mm shall be used for specimen thickness and area measurement.

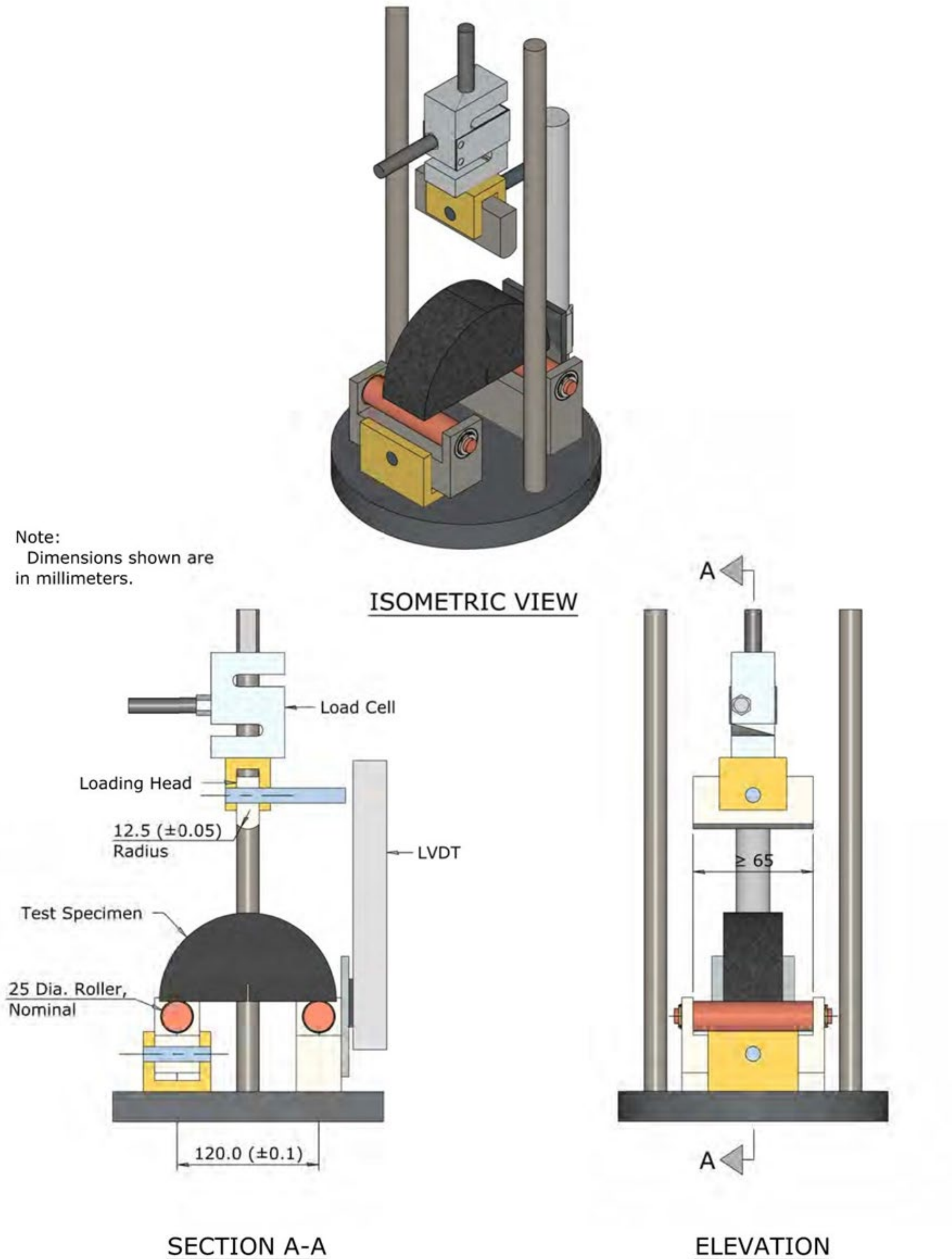

Figure 2: Method A—Isometric, Cross-Section, and Elevation of the I-FIT Fixture (dimensions in millimeters)

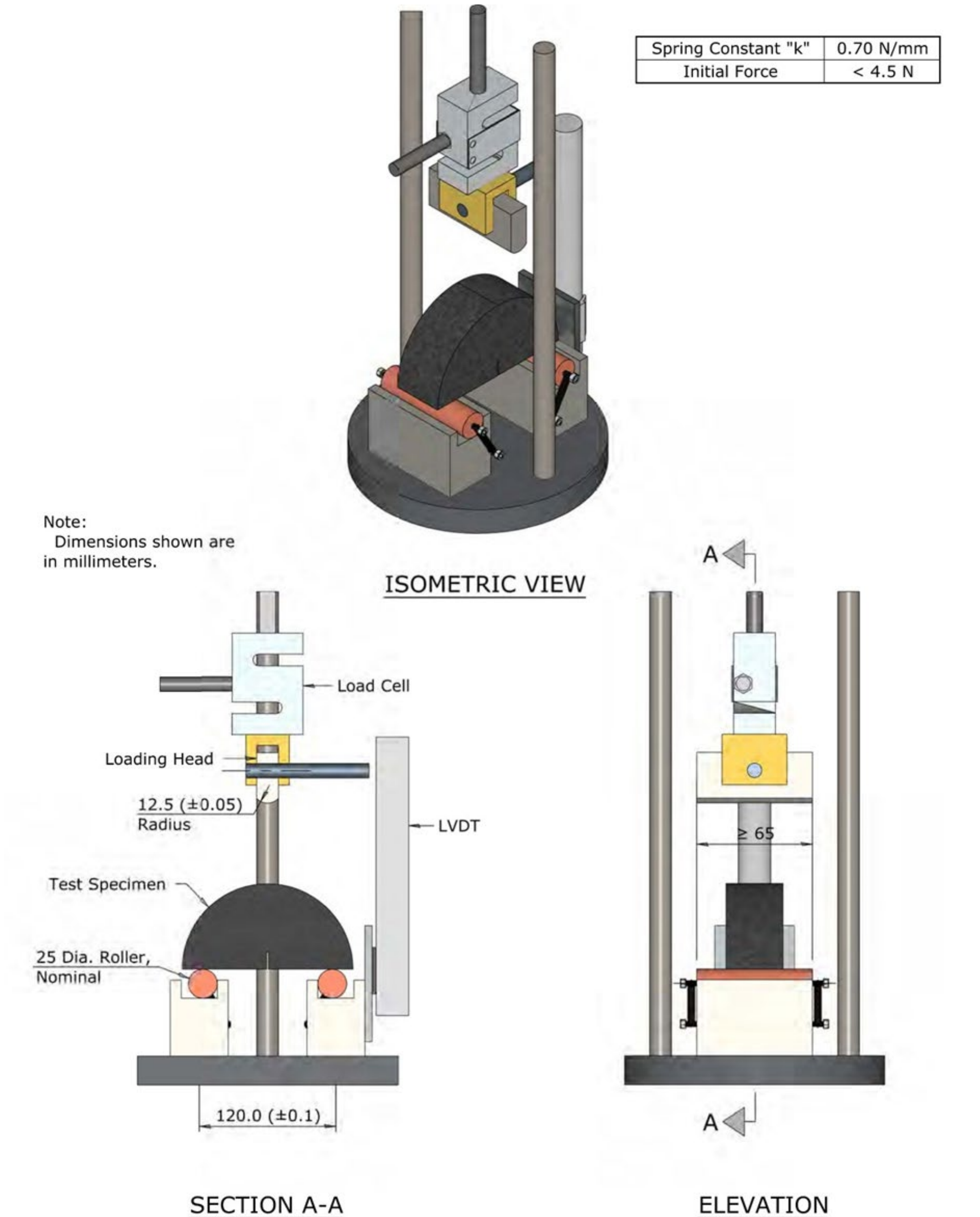

Figure 3: Method B—Isometric, Cross-Section, and Elevation of the I-FIT Fixture (dimensions in millimeters)

7. HAZARDS

7.1. Standard laboratory caution should be used in handling, compacting, and fabricating asphalt mixture test specimens in accordance with T 312 and when using a saw for cutting specimens.

8. CALIBRATION AND STANDARDIZATION

8.1. A water bath as used in AASHTO T 283 or an environmental chamber will be used to maintain the specimen at a constant and uniform temperature.

8.2. Verify the calibration of all measurement components (such as load cells and LVDTs) of the testing system.

8.3. If any of the verifications yield data that does not comply with the accuracy specified, correct the problem prior to proceeding with testing. Appropriate action may include maintenance of system components, calibration of system components (using an independent calibration agency, service by the manufacturer, or in-house resources), or replacement of the system components.

9. PREPARATION OF TEST SPECIMENS AND PRELIMINARY DETERMINATIONS

9.1. *Test Specimen Size*—For mixtures with an NMAS of 19 mm or less, prepare the test specimens from a laboratory-compacted SGC specimen or from pavement cores. If laboratory-compacted SGC specimens are used, the final I-FIT specimens shall have smooth parallel faces with a thickness of 50 ± 1 mm and a diameter of 150 ± 1 mm (see Figure 4). If pavement cores are used, refer to **Figure 1** for the notch width and notch length dimensions and tolerances. The final pavement core I-FIT specimen dimensions shall be 150 ± 8 mm in diameter with smooth parallel faces 25 to 50 ± 1 mm thick depending on available field layer thickness.

Note 3—A typical laboratory saw for mixture specimen preparation can be used to obtain cylindrical discs with smooth, parallel surfaces. A tile saw is recommended for cutting the 15 ± 1 mm notch in the individual I-FIT specimens. Diamond-impregnated cutting faces and water cooling are recommended to minimize damage to the specimen. When cutting the I-FIT specimens into semicircular halves, it is recommended not to push the two halves against each other because it may create an uneven base surface of the test specimen that can affect the I-FIT results.

9.1.1. *SGC Specimens*—Prepare one laboratory SGC specimen according to T 312 in the SGC with the compaction height a minimum of 160 ± 1 mm. From the middle of each 160 ± 1 mm-tall specimen, obtain two cylindrical 50 ± 1 mm-thick discs with smooth, parallel faces by saw cutting (see **Figure 4**). For laboratory-compacted specimens, the bulk specific gravity and the air voids shall be determined for each of the two circular discs according to T 269. The air voids for each disc shall be 5.0 ± 0.5 percent for a P-401 compliant asphalt mix and 3.0 ± 0.5 percent for a P-404 compliant asphalt mix. Cut each disc into two dimensionally equivalent halves resulting in four individual I-FIT specimens. A minimum of three individual test specimens is required for one I-FIT result.

Note 4—The height of the gyratory compacted specimens should be 160 ± 1 mm to achieve target air voids in each disc (see **Figure 4**). If a lab does not have the capability to compact 160 ± 1 mm-tall gyratory specimens, then two

115 ± 1 mm-tall gyratory specimens may be compacted and used in place of each 160 ± 1 mm-tall gyratory specimen. A 50 ± 1 mm-thick disc will be cut from the middle of each gyratory specimen, which will result in four individual I-FIT specimens (see **Figure 4**).

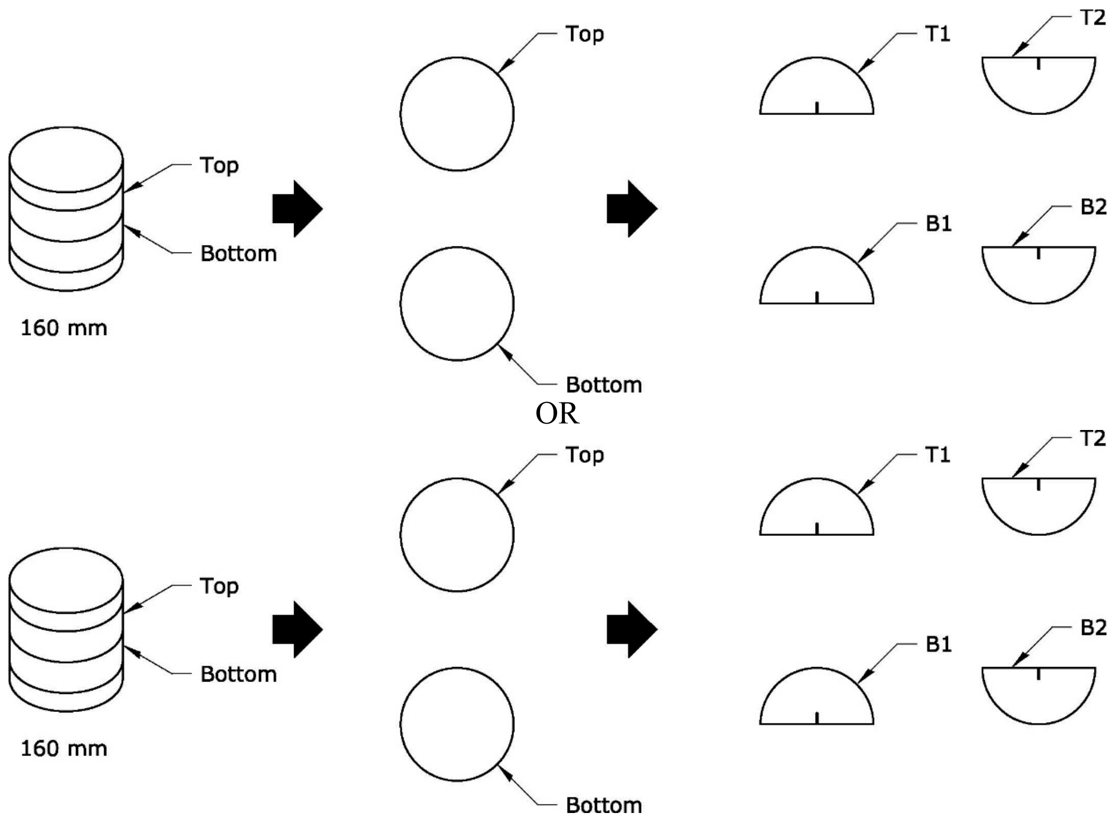

Figure 4: Specimen Preparation from 160 mm or 115 mm-Tall SGC Specimens

9.1.2. *Pavement Cores*—Obtain pavement cores in accordance with R 67. Obtain one 150 mm diameter pavement core if the lift thickness is greater than or equal to 100 mm, or two 150 mm diameter pavement cores if the lift thickness is less than 100 mm.

9.1.2.1. *Pavement Core Specimen Preparation*—Prepare four replicate I-FIT specimens using pavement cores obtained from a pavement lift, with smooth, parallel surfaces that conform to the height and diameter requirements specified herein. To preserve and maximize core thickness, the as-compacted face shall be utilized as well as a sawed face. The thickness of test specimens in most cases for pavement cores may vary from 25 to 50 ± 1 mm. If the lift thickness is less than 50 ± 1 mm, test specimens should be prepared as thick as possible but in no case be less than two times the nominal maximum aggregate size of the mixture or 25 ± 1 mm, whichever is greater. If lift thickness is greater than 50 ± 1 mm, a 50 ± 1 mm disc shall be prepared as specified in Section 9.1. Cores from pavements with lifts greater than 75 ± 1 mm may be cut to provide two cylindrical specimens of equal thickness. In the uppermost pavement layer when cored, the as-compacted face will remain intact and one cut will be made to produce a disc at least two times the nominal maximum aggregate size of the mixture or 25 ± 1 mm, whichever is greater. In all subsequent discs cut from that pavement core, two sawed faces may be used to produce smooth, parallel surfaces.

9.1.2.2. *Determining the Bulk Specific Gravity*—Determine the bulk specific gravity directly on each disc obtained from pavement cores according to T 166.

9.1.2.3. *Determining the Air Voids*—The air void contents of each disc shall be determined according to T 269. Pavement cores will not be subject to air void content tolerances.

9.1.2.4. *Cutting Semicircular Test Specimens*—Cut each cylindrical disc in half to produce two dimensionally equivalent semicircular test specimens.

9.2. *Notch Cutting*—Cut a notch along the axis of symmetry of each individual semicircular specimen to a depth of 15 ± 1 mm and ≤ 2.25 mm in width (see **Figure 1**).

Note 5—If the notch terminates in an aggregate particle 9.5 mm or larger on both faces of the specimen, the specimen shall be discarded.

9.3. *Determining Specimen Dimensions*—Measure the notch depth on both faces of the specimen and record the average value to the nearest 0.5 mm. Measure and record the ligament length (see **Figure 1**) and thickness of each specimen. The ligament length may be measured *directly* on both faces of the specimen with the average value recorded, or the ligament length may be measured *indirectly* by subtracting the notch depth from the entire width (radius) of the specimen on both faces of the specimen and averaging the two measurements. Measure the specimen thickness approximately 19.0 mm on either side of the notch and on the curved edge directly across from the notch. Average the three measurements and record as the average thickness to the nearest 0.1 mm.

10. LONG-TERM AGING

10.1. Perform a long-term aging procedure on I-FIT specimens as defined by the specifying agency.

Note 6—The I-FIT specimen long-term aging procedure in Appendix B may be used.

11. TEST PROCEDURE

11.1. *Conditioning*—Test specimens shall be conditioned in a water bath or an environmental chamber at 25 ± 0.5 °C for 2 h ± 10 min.

11.1.1. *Test Temperature Control*—Immediately after removing the test specimen from the conditioning water bath or environmental chamber, complete positioning and testing of the I-FIT specimen within 5 ± 1 min to ensure that the specimen temperature is maintained.

11.2. *Position Specimen*—Position the test specimen in the test fixture on the rollers so that it is centered in both the "x" and the "y" directions and so that the vertical axis of loading is aligned to pass from the center of the top radius of the specimen through the middle of the notch.

11.3. *Contact Load*—First, impose a contact load of 0.1 ± 0.01 kN in stroke control with a loading rate of 0.05 kN/s.

11.3.1. *Record Contact Load*—Record the contact load to ensure it is achieved.

11.3.2. *Loading*—After the contact load of 0.1 kN is reached, the test is conducted using LLD control at a rate of 50 mm/min. The test stops when the load drops below 0.1 kN.

11.3.3. Repeat Sections 11.1 through 11.3.2 for each test specimen.

12. PARAMETERS

12.1. *Determining Work of Fracture (W_f)*—The work of fracture is calculated as the area under the load–LLD curve (see **Figure 5**). If the test is stopped prior to reaching 0.1 kN, the remainder of the load–LLD curve should be produced by extrapolation techniques.

The area under the load–LLD curve is calculated using a numerical integration technique. In order to apply the numerical integration, raw load-displacement data shall be divided into two curves described by an appropriate fitting equation. A polynomial equation with a degree of six is sufficient for the curve prior to peak load (Equation 1). An exponential-based function (Equation 2) is used for the post-peak load portion of the curve. Then, analytical integration shall be applied to calculate the area under each curve (Equation 3).

For displacements (u) prior to the peak load (P_{max}):

$$P_1(u) = c_1 \times u^6 + c_2 \times u^5 + c_3 \times u^4 + c_4 \times u^3 + c_5 \times u^2 + c_6 \times u^1 + c_7 \quad (1)$$

where:

c_i = polynomial coefficients.

For displacements (u) after the peak load (P_{max}) to the cut-off displacement (u_{final}):

$$P_2(u) = \sum_i^{n=4} d_i exp\left[-\left(\frac{u-e_i}{f_i}\right)^2\right] \quad (2)$$

where:

d, e, f = polynomial coefficients, n is the number of exponential terms.

Work of fracture can be analytically or numerically calculated using the integral equation below and boundaries of displacement:

$$W_f = \int_0^{u_0} P_1(u)du + \int_{u_0}^{u_{final}} P_2(u)du \quad (3)$$

where:

u_0 = displacement at the peak load;

u_{final} = displacement at the 0.1 kN cut-off load.

Note 7—Due to the relative difference between the compliance of the testing frame and specimen, displacement recorded may vary. A correction factor may need to be considered to correct recorded displacements when applicable.

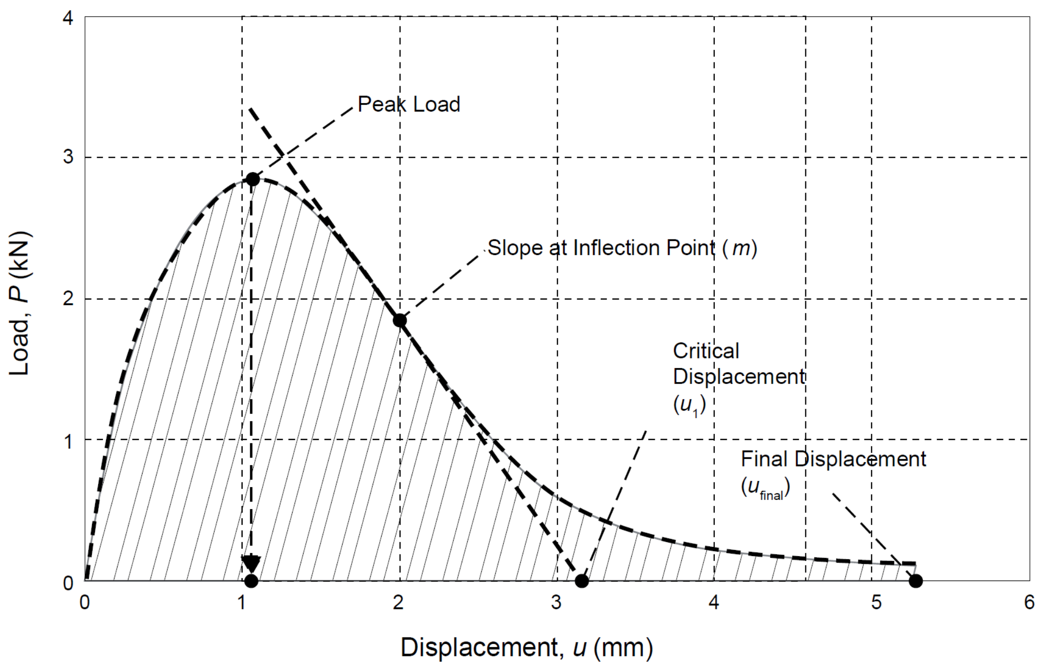

Figure 5: Recorded Load (P)–Load Line Displacement (u) Curve

12.2. *Fracture Energy (G_f)*—The fracture energy G_f, determined as per the RILEM TC 50-FMC (1985) approach, is calculated by dividing the work of fracture (the area under the load–LLD curve; see **Figure 5**) by the ligament area (the product of the ligament length and the thickness of the specimen) of the I-FIT specimen prior to testing:

$$G_f = \frac{W_f}{A_{lig}} \times 10^6 \quad (4)$$

where:

G_f	=	fracture energy (Joules/m^2);
W_f	=	work of fracture (Joules), where
W_f	=	$\int Pdu$
P	=	load (kN);
u	=	load line displacement (mm);
A_{lig}	=	ligament area (mm^2), where
A_{lig}	=	$(r - a) \times t$
r	=	specimen radius (mm);
a	=	notch length (mm); and
t	=	specimen thickness (mm).

Note 8—G_f is a size-dependent property. This specification does not aim at calculating size-independent G_f. Therefore, cracking resistance of asphalt mixtures quantified with G_f may vary when the notch length-to-radius ratio changes.

12.3. *Determining Post-Peak Slope (m)*—The inflection point is determined on the load–LLD curve (**Figure 5**) after the peak load. The slope of the tangential curve drawn at the inflection point represents post-peak slope.

12.4. *Determining Displacement at Peak Load (u_0)*—The displacement when peak load is reached.

12.5. *Determining Critical Displacement (u_1)*—The intersection of the tangential post-peak slope with the displacement axis yields the critical displacement value. A straight line is drawn connecting the inflection point and displacement axis with a slope *m*.

12.6. *Flexibility Index (FI)*—FI can be calculated from the parameters obtained using the load–LLD curve (Al-Qadi et al. 2015; Ozer et al. 2016a; Ozer et al. 2016b). The factor A is used for unit conversion and scaling. A is equal to 0.01. Complete details of the analysis procedure are provided in Appendix A.

$$FI = \frac{G_f}{|m|} \times A \quad (5)$$

where:

$|m|$ = absolute value of post-peak load slope *m* (kN/mm).

13. CORRECTION FACTORS

13.1. *Correction Factors for Flexibility Index*—Flexibility index correction factors for pavement core specimen thickness and differences between field and lab compaction may be needed. A thickness correction factor may be applied for pavement cores tested at a thickness less than 45 mm. The correction factors may require local calibration to consider locally available materials and mixture design requirements.

14. REPORT

14.1. *Report the following information*:

14.1.1. Bulk specific gravity of each specimen tested, to the nearest 0.001;

14.1.2. Air void content of each disc, to the nearest 0.1 percent;

14.1.3. The number of cut faces for each specimen tested, if pavement cores were used;

14.1.4. Average thickness *t* and average ligament length of each specimen tested, to the nearest 0.1 mm;

14.1.5. Initial notch length *a*, to the nearest 0.5 mm;

14.1.6. Average and coefficient of variation (COV) of peak load, to the nearest 0.1 kN;

14.1.7. Average and COV of recorded time at peak load, to the nearest 0.1 s;

14.1.8. Average and COV of load line displacement at the peak load (u_0), to the nearest 0.1 mm;

14.1.9. Average and COV of critical displacement (u_1), to the nearest 0.1 mm;

14.1.10. Average and COV of post-peak slope (*m*), to the nearest 0.1 kN/mm;

14.1.11. Average and COV of fracture energy G_f, to the nearest 1 J/m^2; and

14.1.12. Average and COV of flexibility index to the nearest 0.1.

15. PRECISION AND BIAS

15.1. *Precision:*

15.1.1. *Single-Operator Precision*—The single-operator coefficient of variation of flexibility index has been found to be 27.1 percent. Therefore, results of two properly conducted tests by the same operator on the same material are not expected to differ from each other by more than 75.9 percent of their average.

15.1.2. *Multi-laboratory Precision*—The multi-laboratory coefficient of variation of flexibility index has been found to be 34.1 percent. Therefore, results of two properly conducted tests by two different laboratories on specimens of the same material are not expected to differ from each other by more than 95.5 percent of their average.

Table 1: Precision Estimates[a]

Material	Average FI	Components of Variance		Variances	
		Single Operator	Between Laboratory	Single Operator	Multi-laboratory
2017	5.2	2.36	0.49	2.36	2.85
2018	23.1	36.85	7.64	36.85	44.49
2019	9.6	5.90	9.55	5.90	15.44

Material	Average FI	Standard Deviations		Coefficients of Variation (%)	
		Single Operator	Multi-laboratory	Single Operator	Multi-laboratory
2017	5.2	1.54	1.69	29.6	32.5
2018	23.1	6.07	6.67	26.3	28.9
2019	9.6	2.43	3.93	25.3	41.0

[a] Based on a multi-laboratory study of state departments of transportation, private, and academic laboratories in 2017, 2018, and 2019. Three materials (all 9.5-mm NMAS mixtures) with varying contents of RAP were used (a different mixture was used each year). Approximately 12 specimens were tested per material on at least 30 devices per year.

15.2. *Bias*—No information can be presented on the bias of the procedure because no material having an accepted reference value is available.

16. KEYWORDS

16.1. Asphalt mixture; flexibility index; fracture energy; Illinois flexibility index test (I-FIT); semi-circular bend (SCB); stiffness; work of fracture.

APPENDIX A—CALCULATIONS

A.1. *Scope*:

A.1.1. This appendix presents the framework and algorithms used to process the load–LLD curve and to compute the critical variables such as fracture energy, slope (after the crack begins propagating), and flexibility index. The algorithm consists of the following steps:

A.1.1.1. Preprocessing the raw load–LLD curve;

A.1.1.2. Pre-peak calculations; and

A.1.1.3. Post-peak calculations.

A.1.2. *Preprocessing*:

A.1.2.1. The algorithm starts with preprocessing the raw test output file containing the load and displacement data. The first step of pre-processing is to trim the tail of the curve. The data points whose load values are smaller than 0.1 kN are removed. Because the load–LLD curve exhibits different characteristics before and after the peak load, the trimmed load–LLD curve is divided into two parts: pre-peak and post-peak. To do this, the peak load at which the maximum load value is reached is identified. The values of the load–LLD curve before the peak load are assigned to the pre-peak segment; the remaining data are assigned to the post-peak segment. The calculations required for pre-peak and post-peak segments are explained in Sections A1.3 and A1.4.

A.1.3. *Pre-Peak Calculations*:

A.1.3.1. *The following steps are completed to process the pre-peak segment of the load–LLD curve*:

A.1.3.1.1. The beginning (u_i, P_i) and end (u_0, P_{max}) coordinates of the load–LLD curve are captured.

A.1.3.1.2. A polynomial equation with a degree of six is fitted to the pre-peak segment of the load–LLD curve (Equation A.1).

$$P_1(u) = c_1 \times u^6 + c_2 \times u^5 + c_3 \times u^4 + c_4 \times u^3 + c_5 \times u^2 + c_6 \times u^1 + c_7 \quad (A.1)$$

where:

c_i = polynomial coefficients.

A.1.3.1.3. A new set of data is generated with equal displacement increments using the polynomial function bounded by the beginning and end points found in Section A1.3.1.1. The increments used to divide the data are found by dividing the displacement at the peak load by 1000. A new displacement vector ($u$pre) is generated from ui to u0 with calculated increments. The new loading vector is computed by substituting the value of the displacement vector in Equation A.1. The purpose of generating a dataset with higher resolution is to increase the accuracy of the numerical integration described in Section A1.3.1.4.

A.1.3.1.4. Numerical integration is applied to calculate the area under the pre-peak segment of the load–LLD curve. The integral for the area calculation is given in Equation A.2. A trapezoidal integration technique is used for the numerical integration of Equation A.2. When analytical integration tools are available, analytical integration is recommended to improve accuracy.

$$W_f(pre - peak) = \int_0^{u_0} P_1(u)du \quad (A.2)$$

A.1.3.1.5. When the load–LLD curve starts with a residual load at zero displacement, the curve needs to be extrapolated to modify the area calculated in the previous step. In such cases, the curve is linearly extrapolated to the displacement coordinate where the load is zero. The displacement at the zero load (u_r) is found. The area under the extrapolated segment is added to calculate total pre-peak area (Equation A.1). Numerical integration is applied to find the residual area shown by the additional term in Equation A.3. The second part of the sum comes from the additional area of extrapolation.

$$W_f(pre - peak) = \int_0^{u_0} P_1(u)du + u_r \times P_r \times 0.5 \quad (A.3)$$

where:

P_r	=	residual load at zero displacement; and
u_r	=	calculated displacement at zero load.

A.1.4. *Post-Peak Calculations*:

A.1.4.1. An algorithm was developed to process the post-peak segment of the load–LLD curve to calculate area under the curve as well as the inflection point and slope at the inflection point. Explanations of each step are given in Sections A1.4.1.1 through A1.4.1.3.

A.1.4.1.1. The beginning (u_0, P_0) and end (u_f, P_f) coordinates of the post-peak load–LLD curve are captured (see **Figure A.1**). The raw data records are stored in two vectors as *u*post = $\{u_0, \ldots, u_f\}$ and $P_{post} = \{P_0, \ldots, P_f\}$.

A.1.4.1.2. In this step, candidate lower bounds for parameter *f* in Equation A.4 are initialized and kept in a vector. This parameter can govern the first derivative of the post-peak segment resulting in abnormal slope values. For example, if a lower bound is not defined for this parameter, it may go to zero, which creates a spike-like, spurious slope. On the other hand, if the bound is defined too high, accuracy of the fitted curve may be compromised. Therefore, candidate values for the lower bounds for this parameter were found to be $f_{bounds} = \{0.9, 0.7, 0.5, 0.3, 0.1, 0.05, 0.01, 0.005, 0.001\}$. The optimum value is found iteratively looping over the values initialized in the f_{bounds}. The order of the values should be descending.

$$P_2(u) = \sum_i^{n=4} d_i exp\left[-\left(\frac{u-e_i}{f_i}\right)^2\right] \quad (A.4)$$

where:

d, e, f	=	polynomial coefficients, and
n	=	number of exponential terms.

A.1.4.1.3. All model parameters in Equation A.4 are regularized by setting lower and upper bounds for each of them. Upper and lower bounds for each parameter except *f* are initialized as 10 and –10, respectively. Because of the limitations of the regression function used in MATLAB (the function called "fit"), the regularization had to be conducted in a heuristic way.

A.1.4.1.3.1. A regression function that inputs u_{post} and P_{post} is developed by fitting the Gaussian function (Equation A.4) to the post-peak segment of the data bounded by the limits defined in Section A.1.4.1.3. The number of Gaussian terms is selected as four. Then, the inflection points at which the second derivative of the fitted equation becomes zero are extracted, and the first derivatives indicating the slopes (m_i) are computed at the extracted inflection points (u_i).

A.1.4.1.3.2. It is possible that the second derivative of the fitted equation $P_2(u)$ may not have any roots (i.e., there is no inflection point; hence, no slope can be found). If $P_2(u)$ does not have any roots, the next value in the vector f_{bounds} should be selected before proceeding with the remaining steps. If a root or roots of $P_2(u)$ exist, proceed to the next step.

A.1.4.1.3.3. At each inflection point found, draw the tangential slope by extrapolating a line intersecting the displacement axis, as shown in **Figure A.1**. The first derivative value at the inflection is defined as the post-peak slope (m) as shown below.

$$m = \left[\frac{\partial P_2(u)}{\partial u}\right]_{u=u_{inf}} \tag{A.5}$$

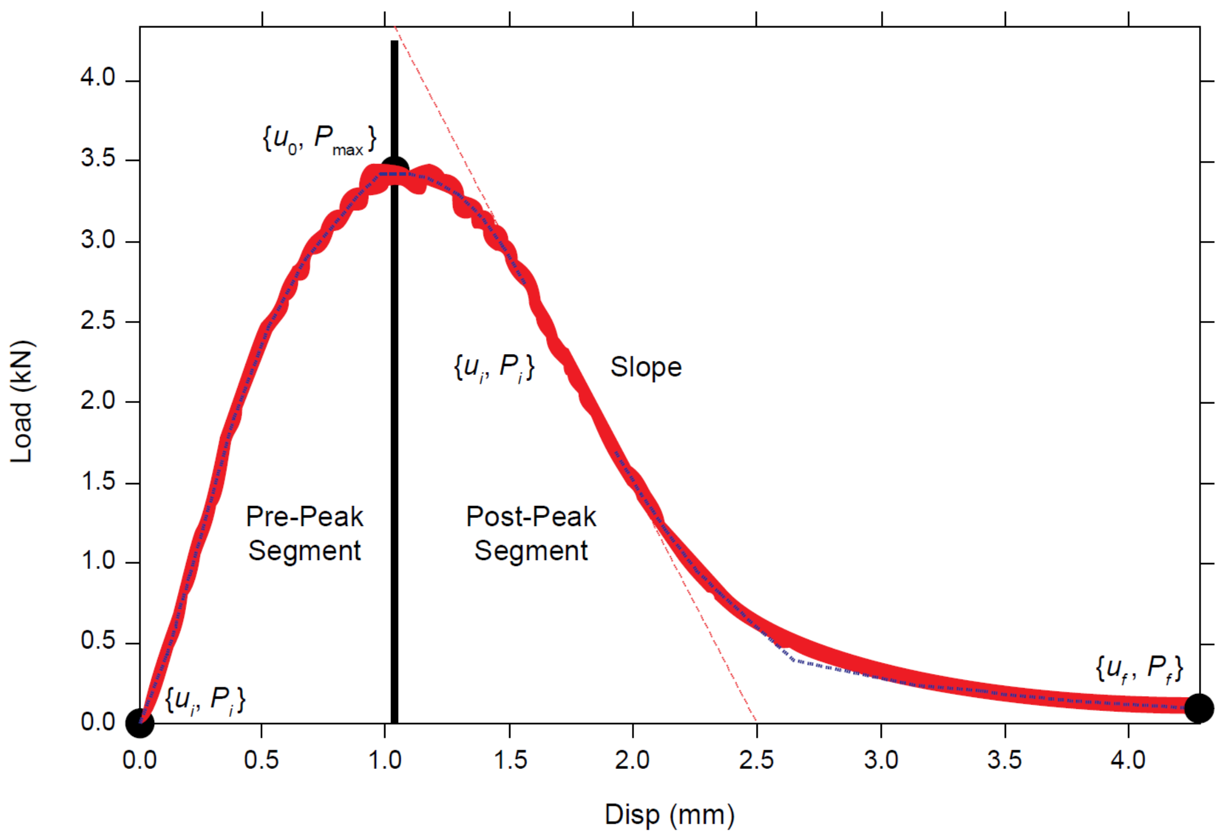

Figure A.1: Demonstration of Pre-Peak and Post-Peak Segments

A.1.4.1.3.4. It is common that the fitted equation may produce more than one slope when there is more than one root found in the previous step. There is only one slope considered consistent with the definition of the test; the remaining slopes are spurious and need to be eliminated. To find the most representative slope and eliminate the unrealistic slope(s), three visual-based criteria are implemented. The criteria, grading, and elimination processes are as follows:

- *Criterion 1*—Incremental displacement values (u_n) are generated with equal increments between u_0 and u_i. A linear slope equation, $S(u)$, is described by using the slope (see Equation A.5) and passing through the inflection point (u_i). The mean value of the difference between the slope equation and the post-peak load–LLD curve is calculated using Equation A.6.

$$C1 = \frac{\sum_{n=1}^{M}[S(u_n) - P_2(u_n)]}{M} \tag{A.6}$$

where:

M = number of displacement values such that ($u_0 < u_n < u_i$). Equal sizes of increments are used to create M-times displacement values (u_n). M may vary depending on the length between u_0 and u_i;

$S(u_n)$ = value of slope equation calculated at $u = u_n$; and

$P_2(u_n)$ = value of post-peak load–LLD curve calculated at $u = u_n$.

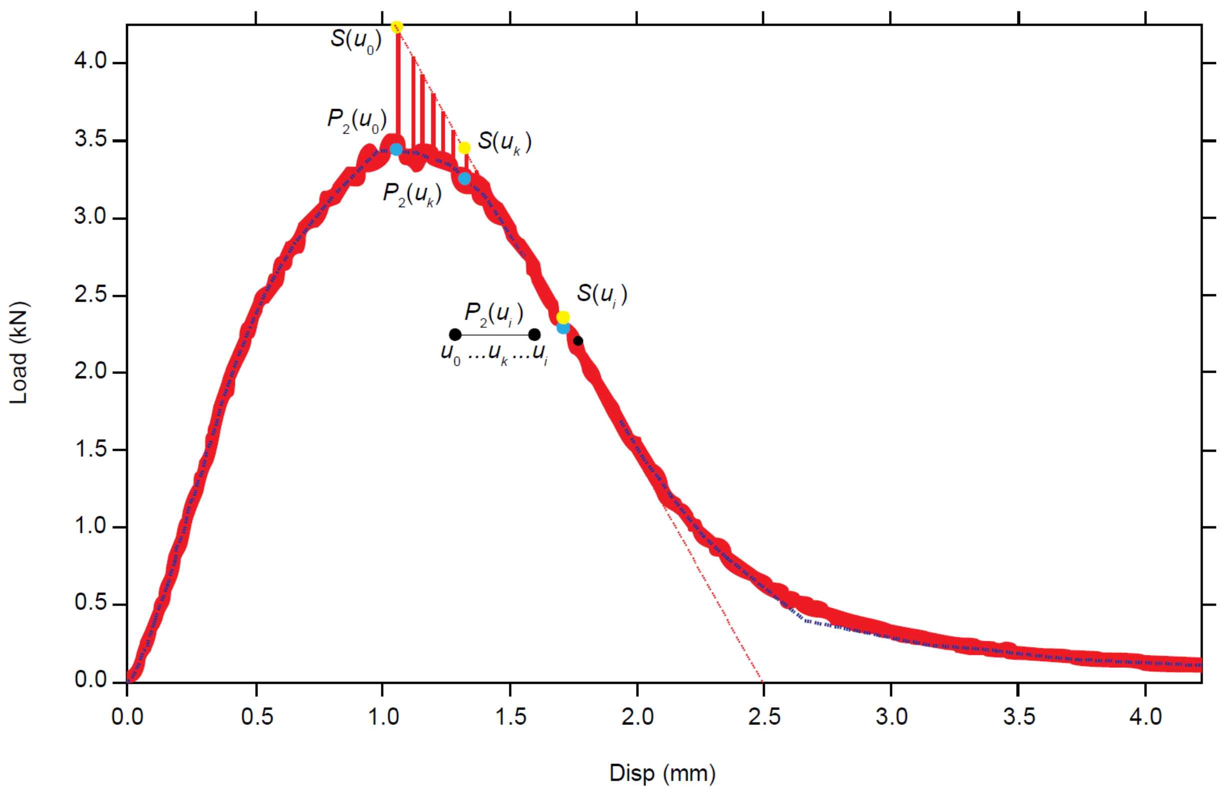

Figure A.2: Checking Mean Difference for Criterion 1

- *Criterion 2*—Incremental displacement values (u_n) are generated with equal increments between u_0 and u_t. The u_t is found by taking 30 percent of $P_i = P_2(u_i)$ (load corresponding to the inflection point) (see Figure A.3). The same linear slope equation, $S(u)$, is used as in Criterion 1. The mean value of difference between slope equation and post-peak load–LLD curve is calculated using Equation A.7.

$$C2 = \frac{\sum_{n=1}^{M}[P_2(u_n) - S(u_n)]}{M} \quad (A.7)$$

where:

M = number of displacement values such that ($u_0 < u_n < u_t$). Equal sizes of increments are used to create M-times displacement values (u_n). M may vary depending on the length between u_0 and u_t;

$S(u_n)$ = value of slope equation calculated at $u = u_n$; and

$P_2(u_n)$ = value of post-peak load–LLD curve calculated at $u = u_n$.

The ideal slope line should be perfectly tangential or remain below the fitted curve. Therefore, the slope lines with negative means are eliminated. The grading scheme for this criterion is similar to the previous one. If more than one slope remains after elimination, slopes are ranked in an ascending order according to the mean difference (C2). The slope with lowest mean difference is ranked highest.

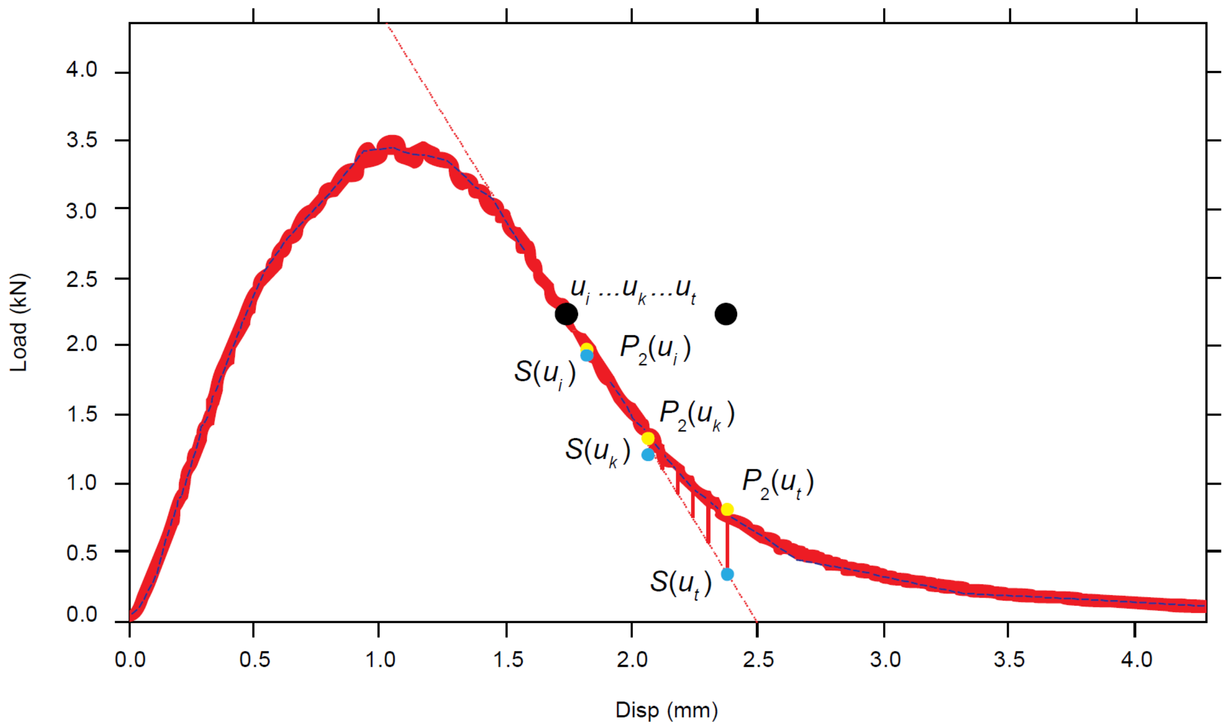

Figure A.3: Checking Mean Difference for Criterion 2

- *Criterion 3*—The value of this criterion is –x coordinate of inflection points (i.e., u_i). If there are multiple candidates for a slope line, they are ranked in ascending order according to their u_i. For example, slopes found at smaller inflection points are ranked higher than the slope found at the tail part of the curve.

A.1.4.1.3.5. If at least one realistic slope is found, and the R2 of the fit is higher than 0.997, the fit is accepted, and the loop is stopped. In that case, the framework jumps to Section A.1.4.1.4 to calculate fracture energy and report the representative slopes along with other required test outcomes. Otherwise, the loop continues—that is, the next value from f_{bound} is selected to modify the lower bound for the parameter f. Sections

A1.4.1.3.1 through A1.4.1.3.5 are repeated until a representative slope and satisfactory R2 are found.

A.1.4.1.4. Using the satisfactory fit, $P_2(u)$, and representative inflection point and post-peak slope values (m), the test parameters required in the report section of the specification are calculated.

A.1.4.1.4.1. Representative slope is reported as the one with the highest score from the grading process (Section A1.4.1.3.4).

A.1.4.1.4.2. Similar to the pre-peak area calculation, a new displacement vector between up and u_{final} by an increment of 0.005 is generated. Then corresponding load values are calculated by feeding this generated displacement vector to the fitted regression functions. The purpose of generating new sets of data with increased resolution is to increase the accuracy of the numerical integration in the next step.

A.1.4.1.4.3. A trapezoidal numerical integration technique (Figure A.2) is employed for the integral shown in Equation A.8 to calculate the area under the post-peak segment of the curve.

$$W_f(post-peak) = \int_{u_0}^{u_{final}} P_2(u)du \qquad (A.8)$$

A.1.4.1.4.4. The total area under the load–LLD curve is found by adding the pre-peak and post-peak areas. Then the work of fracture is calculated using Equation A.9.

$$W_f = W_f(post-peak) + W_f(pre-peak) \qquad (A.9)$$

A.1.4.1.4.5. Total energy and slope are input to Equations A.10 and A.11 to compute fracture energy and flexibility index.

$$G_f = \frac{W_f}{A_{lig}} \times 10^6 \qquad (A.10)$$

$$FI = \frac{G_f}{|m|} \times A_s \qquad (A.11)$$

APPENDIX B—LONG-TERM AGING PROCEDURE

B.1. *Scope*:

B.1.1. This appendix includes and summarizes the findings of the R27-175 study conducted by the Illinois Center for Transportation through the Illinois Department of Transportation to evaluate the long-term aging effects on hot mix asphalt surface mixtures using the Illinois Flexibility Index Test and to develop a corresponding long-term-aging protocol.

B.2. *Procedure*:

B.2.1. Prepare surface mixture test specimens according to Section 9.

B.2.2. Place the four test specimens, notched face down, on a tray (pan), with a barrier between the test specimens and the tray (e.g., parchment paper, a nonstick cooking mat, heavy-duty aluminum foil).

B.2.3. Place the tray with the specimens in a preheated forced-draft oven set at 95 ± 3 °C (203 ± 5 °F).

B.2.4. Leave the specimens (undisturbed) in the oven at this temperature for 72 h ± 1 h.

B.2.5. Remove the entire tray from the oven and place in front of a cooling fan at room temperature for at least 1 h.

B.2.6. If the specimens are not cooled in front of a fan, allow the specimens to cool at room temperature overnight.

B.2.7. Remove the specimens from the barrier.

B.2.8. After the specimens have cooled and the barrier has been removed, proceed to Section 11.

Appendix H: Technical Note Template for the Simplified Low-Temperature Semi-Circular Bend (SLT-SCB) Test

ote technical note technica

Standard Method of Test for Determining the Low Temperature Cracking Index of Asphalt Mixtures Using the Semi-Circular Bend Geometry (SCB)

Author name (if the report was authored only by the FAA)

Date

DOT/FAA/TC-TNxx/xx

This document is available to the U.S. public through the National Technical Information Services (NTIS), Springfield, Virginia 22161.

This document is also available from the Federal Aviation Administration William J. Hughes Technical Center at actlibrary.tc.faa.gov.

U.S. Department of Transportation
Federal Aviation Administration

NOTICE

Technical Report Documentation Page

1. Report No.	2. Government Accession No.	3. Recipient's Catalog No.
DOT/FAA/TC-TNxx/xx		

4. Title and Subtitle	5. Report Date
Standard Method of Test for Determining the Low Temperature Cracking Index of Asphalt Mixtures Using the Semi-Circular Bend Geometry (SCB)	APRIL 2025
	6. Performing Organization Code
7. Author(s)	8. Performing Organization Report No.
9. Performing Organization Name and Address	10. Work Unit No. (TRAIS)
	11. Contract or Grant No.
12. Sponsoring Agency Name and Address Sponsoring Agency name and address	13. Type of Report and Period Covered
	14. Sponsoring Agency Code

15. Supplementary Notes

The Federal Aviation Administration Aviation Research Division COR was

16. Abstract

17. Key Words	18. Distribution Statement
	This document is available to the U.S. public through the National Technical Information Service (NTIS), Springfield, Virginia 22161. This document is also available from the Federal Aviation Administration William J. Hughes Technical Center at actlibrary.tc.faa.gov.

19. Security Classif. (of this report)	20. Security Classif. (of this page)	21. No. of Pages	22. Price
Unclassified	Unclassified		

Form DOT F 1700.7 (8-72) Reproduction of completed page authorized

ACKNOWLEDGEMENTS

(Optional)

TABLE OF CONTENTS

LIST OF FIGURES

LIST OF TABLES

LIST OF ACRONYMS

FAA	Federal Aviation Administration
LCI	Low-temperature cracking index
LLD	Load line displacement
LVDT	Linear variable differential transducer
NMAS	Nominal maximum aggregate size
SCB	Semi-circular bend
SGC	Superpave gyratory compactor

EXECUTIVE SUMMARY

1. SCOPE

1.1. This test method covers the determination of the low-temperature pre-peak fracture energy ($G_{f\text{-}pre}$) and loading stiffness (S) of asphalt mixtures by means of the semi-circular bend (SCB) geometry (Modi et al., 2026). The SCB specimen is a half-disc with a notch in the center. The SCB test can be used to replicate mode I crack-opening and mixed-mode I and II cracking and shearing conditions (Lim et al., 1993). This standard addresses the mode I fracture condition only.

1.2. The procedures in this standard provide parameters that describe the fracture resistance of asphalt mixtures at low temperatures. These parameters and corresponding thresholds are recommended in the balanced mix design framework for airfield asphalt concrete mixes.

1.3. These procedures apply to test specimens having a maximum aggregate size of 19 mm or less. Specimens shall be 150 ± 1 mm in diameter and 50.0 mm ± 1 mm thick. These procedures are valid at a minimum temperature of either −12°C or 10°C above the lowest annual pavement temperature of the location with 50 % reliability, whichever is lower.

1.4. *This standard may involve hazardous materials, operations, and equipment. This standard does not purport to address all of the safety concerns associated with its use. It is the responsibility of the user of this procedure to establish appropriate safety and health practices and to determine the applicability of regulatory limitations prior to use.*

1.5. *The quality of the results produced by this standard is dependent on the competence of the personnel performing the procedure and the capability, calibration, and maintenance of the equipment used. Agencies that meet the criteria of AASHTO R 18 are generally considered capable of competent and objective testing/sampling/inspection/etc. Users of this standard are cautioned that compliance with R 18 alone does not completely assure reliable results. Reliable results depend on many factors; following the suggestions of R 18 or some similar acceptable guideline provides a means of evaluating and controlling some of those factors.*

2. REFERENCED DOCUMENTS

AASHTO STANDARDS

- M 320, Performance-Graded Asphalt Binder
- R 18, Establishing and Implementing a Quality Management System for Construction Materials Testing Laboratories
- R 30, Practice for Mixture Conditioning of Hot-Mix Asphalt (HMA)
- R 67, Standard Practice for Sampling Asphalt Mixtures after Compaction (Obtaining Cores)
- T 166, Bulk Specific Gravity (Gmb) of Compacted Asphalt Mixtures Using Saturated Surface-Dry Specimens
- T 269, Percent Air Voids in Compacted Dense and Open Asphalt Mixtures

- T 312, Preparing and Determining the Density of Asphalt Mixture Specimens by Means of the Superpave Gyratory Compactor
- T 394, Standard Method of Test for Determining the Fracture Energy of Asphalt Mixtures Using the Semicircular Bend Geometry (SCB)

ASTM STANDARDS

- D8, Terminology Relating to Materials for Roads and Pavements
- D3549/D3549M, Standard Test Method for Thickness or Height of Compacted Bituminous Paving Mixture Specimens
- D5045, Standard Test Methods for Plane-Strain Fracture Toughness and Strain Energy Release Rate of Plastic Materials
- D5361/D5361M, Standard Practice for Sampling Compacted Asphalt Mixtures for Laboratory Testing
- D6925 Test Method for Preparation and Determination of the Relative Density of Asphalt Mix Specimens by Means of the Superpave Gyratory Compactor
- D7643 Practice for Determining the Continuous Grading Temperatures and Continuous Grades for PG Graded Asphalt Binders
- E399, Standard Test Method for Linear-Elastic Plane-Strain Fracture Toughness of Metallic Materials
- E1823, Terminology Relating to Fatigue and Fracture Testing

3. TERMINOLOGY

3.1. *Definitions:*

3.1.1. *crack mouth*—portion of the notch that is on the flat bottom surface of the specimen, that is, opposite the notch tip.

3.1.2. *load line displacement (LLD)*—the displacement measured in the direction of the load application.

3.1.3. *linear variable differential transducer (LVDT)*—sensor device for measuring linear displacement.

3.1.4. *semi-circular bend (SCB) geometry*—a geometry that utilizes a semi-circular specimen.

3.1.5. *pre-peak fracture energy,* $G_{f\text{-}pre}$—the energy absorbed by asphalt concrete prior to reaching its peak strength, under conditions where the material exhibits linear viscoelastic behavior at a low temperature.

3.1.6. *loading stiffness, S*—the slope of the linear portion of the ascending load versus load line displacement curve.

3.1.7. *low temperature cracking index (LCI)*—index intended to characterize the resistance to crack initiation of asphalt mixtures at low temperature, calculated as the ratio of pre-peak fracture energy and loading stiffness.

4. SUMMARY OF TEST METHOD

4.1. A semi-circular asphalt mixture specimen is positioned with the flat side on two rollers that are covered with a friction-reducing material. A load is applied along the vertical diameter of the specimen, and the load and load line displacement are measured during the entire duration of the test. The load is applied to maintain a constant LLD rate of 0.15 mm/minute for the duration of the test.

4.2. Pre-peak fracture energy ($G_{f\text{-}pre}$), loading stiffness (S), and low-temperature cracking index (LCI) are calculated from the load and load line displacement results.

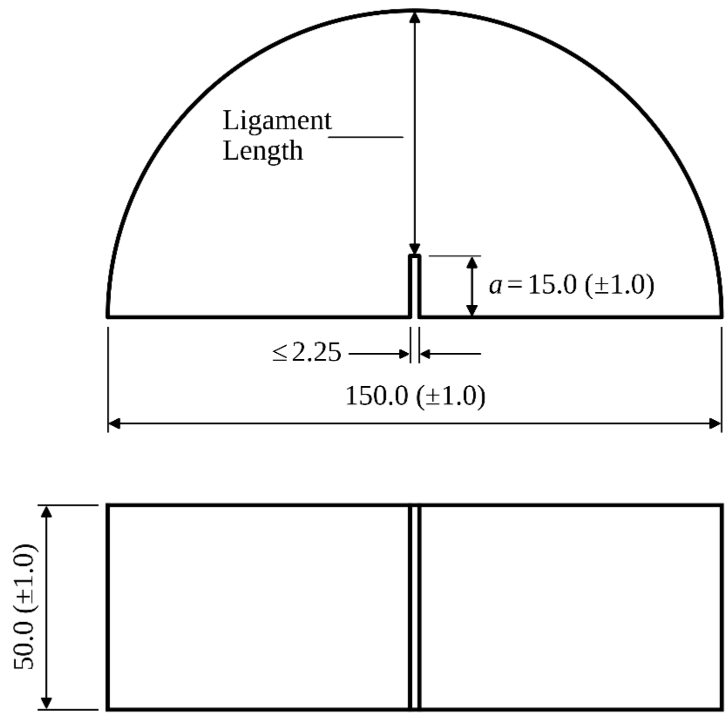

Figure 1: SGC Laboratory Compacted Specimen Configuration (dimensions in millimeters)

5. SIGNIFICANCE AND USE

5.1. The simplified SCB test is used to determine the pre-peak fracture energy and loading stiffness of asphalt mixtures. These parameters describe the fracture resistance of asphalt mixtures at low temperature. The ratio of pre-peak fracture energy and loading stiffness is used to calculate the low-temperature cracking index of an asphalt mix.

5.2. $G_{f\text{-}pre}$ can be used as an index to identify mixtures with increased crack initiation resistance. Crack initiation begins before reaching peak load; however, $G_{f\text{-}pre}$ can be used as an estimate for comparison and has been shown to effectively rank asphalt mixes. G_f can be used in more complex analyses based on a fictitious crack (cohesive zone) model.

5.3. *S* obtained with this test method can be related to the strain tolerance of asphalt mixtures before fracture at low temperatures. Previous research has shown that *S* relates to binder relaxation properties at low temperature (Bajaj et al., 2026).

5.4. LCI obtained with this test method indicates an asphalt mix's overall capacity to resist fracture at low temperature. The LCI should not be directly used in structural design and analysis of pavements. LCI values obtained using this procedure are used in ranking the cracking resistance of alternative mixtures for a given layer in a structural design. The range for an acceptable LCI will vary according to local environmental conditions, application of mixture, nominal maximum aggregate size (NMAS), asphalt binder content, asphalt binder performance grade (PG), air voids, expectation of service life, etc.

5.5. The specimens can be easily cut from Superpave gyratory–compacted cylinders and from field cores with a diameter of 150 ± 1 mm.

5.6. Field cores are sampled following the AASHTO R 67 standard specification.

6. APPARATUS

6.1. *Semi-Circular Bend (SCB) Test System*—A semi-circular bend (SCB) test system consisting of a closed-loop axial loading device, a load measuring device, a bend test fixture, specimen deformation measurement devices, an environmental chamber, and a control and data acquisition system (see **Figure 2**).

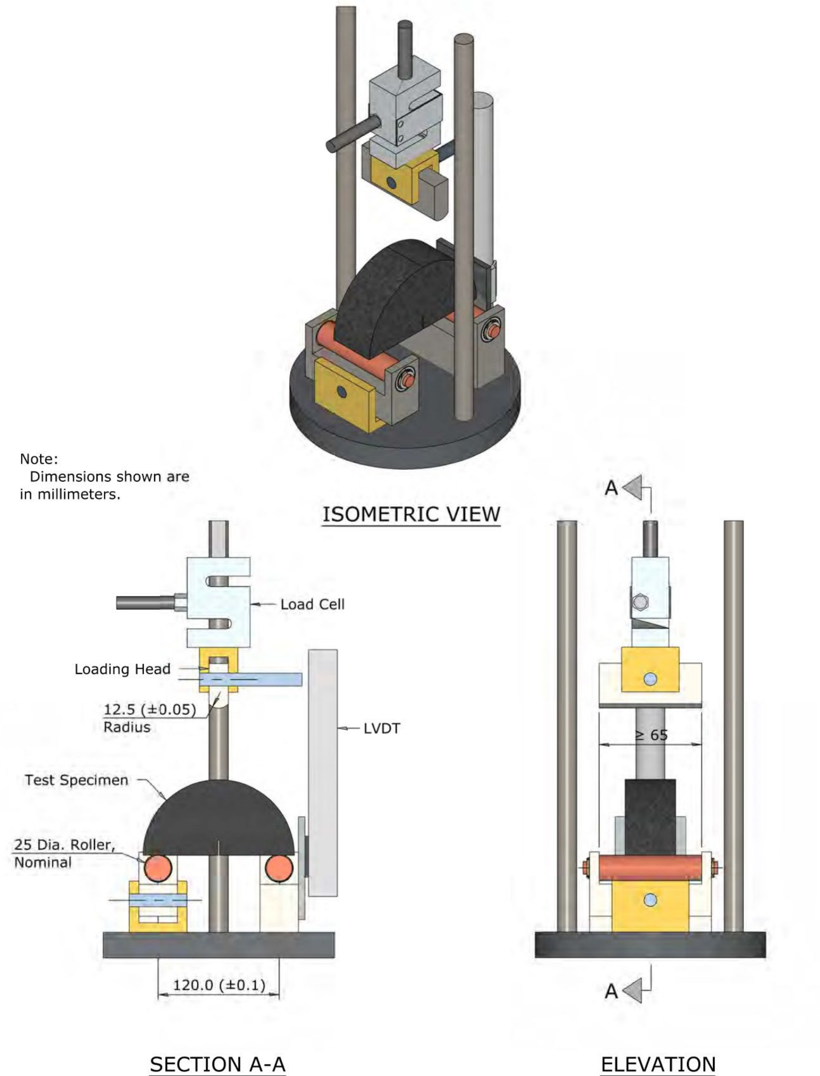

Figure 2: SCB Test Fixture

6.1.1. *Axial Loading Device*—The loading device shall be capable of delivering a minimum load of 15 kN in compression with a resolution of 20 N or better. The load apparatus shall be capable of maintaining a constant load line displacement within 1 percent of the target value throughout the test.

6.1.2. *Load Measuring Device*—The load measuring device shall consist of an electronic load cell, designed for placement between the loading platen and piston, with a minimum capacity of 15 kN and a sensitivity of 10 N or better.

6.1.3. *Bend Test Fixture*—The fixture is composed of a loading head, a steel base plate, and two steel rollers with a nominal diameter (D) of 25 mm. The tip of the loading head has a contact curvature with a radius of 12.5 ± 0.05 mm. The horizontal loading head shall pivot relative to the vertical loading axis to conform to slight specimen variations. The loading fixture is designed to minimize frictional effects through the use of rollers (as suggested by ASTM E399). The surface of the rollers can be covered with polytetrafluoroethylene (PTFE) strips to further reduce friction. The length of the two roller supports shall be a minimum of 65 mm with a nominal diameter of 25 mm. Typically, two steel rollers are mounted on bearings through their axis of rotation and attached to the steel base plate with brackets. One of the steel rollers may pivot on an axis perpendicular to the loading axis to accommodate slight specimen variations. Maintain a distance of 120 ± 0.1 mm between the two steel rollers throughout the test.

6.1.4. *Displacement Measuring Device*—The displacement measurement can be performed using the machine's stroke (position) transducer if the resolution of the stroke is sufficient (0.1 mm or lower). The fracture test displacement data may be corrected for system compliance, loading-pin penetration, and specimen compression by calibrating the testing system. If an internal displacement measuring device does not exist or has insufficient precision, an externally applied displacement measurement device such as a linear variable differential transducer (LVDT) accurate to 0.1 mm can be used.

6.1.5. *(Optional) Crack Mouth Opening Measuring Devices*—An optional CMOD gauge, with a range of at least 1 mm and a resolution of 0.0005 mm or better, can be used to track crack growth during the test. The data acquisition sampling rate must be maintained at a minimum of 50 Hz. The CMOD gauge is attached to the two gauge points glued to the bottom of the SCB specimen via knife edges (see **Figure 3**).

6.1.6. *Environmental Chamber*—The environmental chamber should be equipped with a temperature conditioner and controls capable of generating a test temperature between –40°C and 0°C inside the chamber and maintaining the desired test temperature to within ±0.5°C. The internal dimensions of the environmental chamber should be capable of holding a minimum of three test specimens for a period of at least 2 ± 0.5 h or until specimens reach the test temperature, whichever is longer, prior to testing.

6.1.7. *Control and Data Acquisition System*—Specimen behavior during the semi-circular bend test is evaluated from time records of applied load and LLD (using an external and/or internal displacement measurement device). The applied load is controlled via a closed loop by keeping the LLD rate constant during the test. A minimum sampling frequency of 50 Hz is required in order to obtain a smooth load–LLD curve.

6.1.8. *Measuring Device*—A caliper or ruler accurate to ± 0.1 mm shall be used for specimen thickness and area measurement.

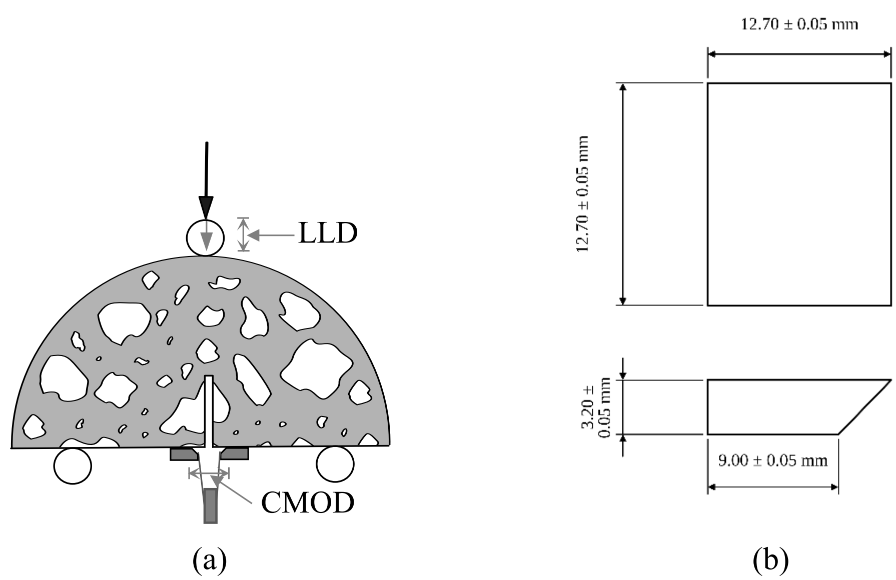

Figure 3: Optional CMOD Gauge (a) location and (b) dimensions

7. HAZARDS

7.1. Observe standard laboratory safety precautions when preparing and testing HMA specimens and when using a saw for cutting specimens.

8. STANDARDIZATION

8.1. The testing system should be calibrated prior to initial use and at least once a year thereafter.

8.1.1. Verify the capability of the environmental chamber to maintain the required temperature within the specified accuracy.

8.1.2. Verify the calibration of all measurement components (such as load cells and LVDTs) of the testing system.

8.1.3. If any of the verifications yield data that do not comply with the accuracy specified, correct the problem prior to proceeding with testing. Appropriate action may include maintenance of system components, calibration of system components (using an independent calibration agency, service by the manufacturer, or in-house resources), or replacement of the system components.

9. SAMPLING

9.1. *Laboratory-Molded Specimen*—Prepare three replicate laboratory-molded specimens, as a minimum for each test temperature, in accordance with AASHTO T 312.

9.2. *Roadway Specimen*—Obtain roadway specimens from the pavement in accordance with ASTM D5361/D5361M. Prepare cores with smooth and parallel surfaces that conform to the height and diameter requirements specified in Section 10.2. Prepare three replicate cores for each test temperature.

10. SPECIMEN PREPARATION AND PRELIMINARY DETERMINATIONS

10.1. *Specimen Size*—For mixtures with maximum aggregate size of 19 mm or less, prepare specimens having smooth parallel faces with a thickness of 50.0 ± 1 mm and a diameter of 150 ± 1 mm (see **Figure 1**).

10.2. *SGC Specimens*—Prepare one laboratory SGC specimen according to T 312 in the SGC with the compaction height a minimum of 160 ± 1 mm. From the middle of each 160 ± 1 mm-tall specimen, obtain two cylindrical 50 ± 1 mm-thick discs with smooth, parallel faces by saw cutting (see **Figure 4**). For laboratory-compacted specimens, the bulk specific gravity and the air voids shall be determined for each of the two circular discs according to T 269. Cut each disc into two dimensionally equivalent halves, resulting in four individual specimens. A minimum of three individual test specimens is required for one result.

Note 1—For coarse-graded 19-mm NMAS asphalt mixtures, a height of 180 ± 1 mm for SGC is recommended. If a lab does not have the capability to compact 160 ± 1 mm- or 180 ± 1 mm-tall gyratory specimens, then two 115 ± 1 mm-tall gyratory specimens may be compacted and used instead. A 50 ± 1 mm-thick disc will be cut from the middle of each gyratory specimen, which will result in four individual specimens (see **Figure 4**).

10.3. *Field Cores*—Field cores can also be used to fabricate the specimens. Obtain pavement cores in accordance with R 67. The target thickness for specimens obtained from field cores should be 50.0 ± 1 mm. The top and bottom of the core shall be cut to ensure that the test specimen has parallel faces. If multiple slices are cut from taller cores, the lift thickness shall be considered to obtain representative samples.

10.4. *Determining Specimen Dimensions*—Measure and record the diameter and thickness of each specimen in accordance with ASTM D3549/D3549M, and determine individual measurements to the nearest 1 mm. Measure the notch length on both faces of the specimen and record the average value to the nearest 0.5 mm.

10.5. *Determining the Bulk Specific Gravity and Air Voids*—Determine the bulk specific gravity directly on each disc obtained from pavement cores according to AASHTO T 166. The air void contents of each disc shall be determined according to T 269. Pavement cores will not be subject to air void content tolerances.

10.6. *Specimen Drying*—If specimens were immersed directly into water, after determining the bulk specific gravity, allow each specimen to dry at room temperature to a constant mass.

10.7. *Cutting Semi-circular Test Specimens*—Cut each cylindrical disc in half to produce two dimensionally equivalent semi-circular test specimens.

10.8. *Notch Cutting*—Cut a notch along the axis of symmetry of each individual semi-circular specimen to a depth of 15 ± 1 mm and ≤ 2.25 mm in width (see **Figure 1**).

Note 2—A tile saw is recommended for cutting the 15 ± 1 mm-notch into individual specimens. Diamond-impregnated cutting faces and water-cooling are recommended to minimize damage to the specimen. If the notch terminates in an aggregate particle 9.5 mm or larger on both faces of the specimen, the specimen shall be discarded.

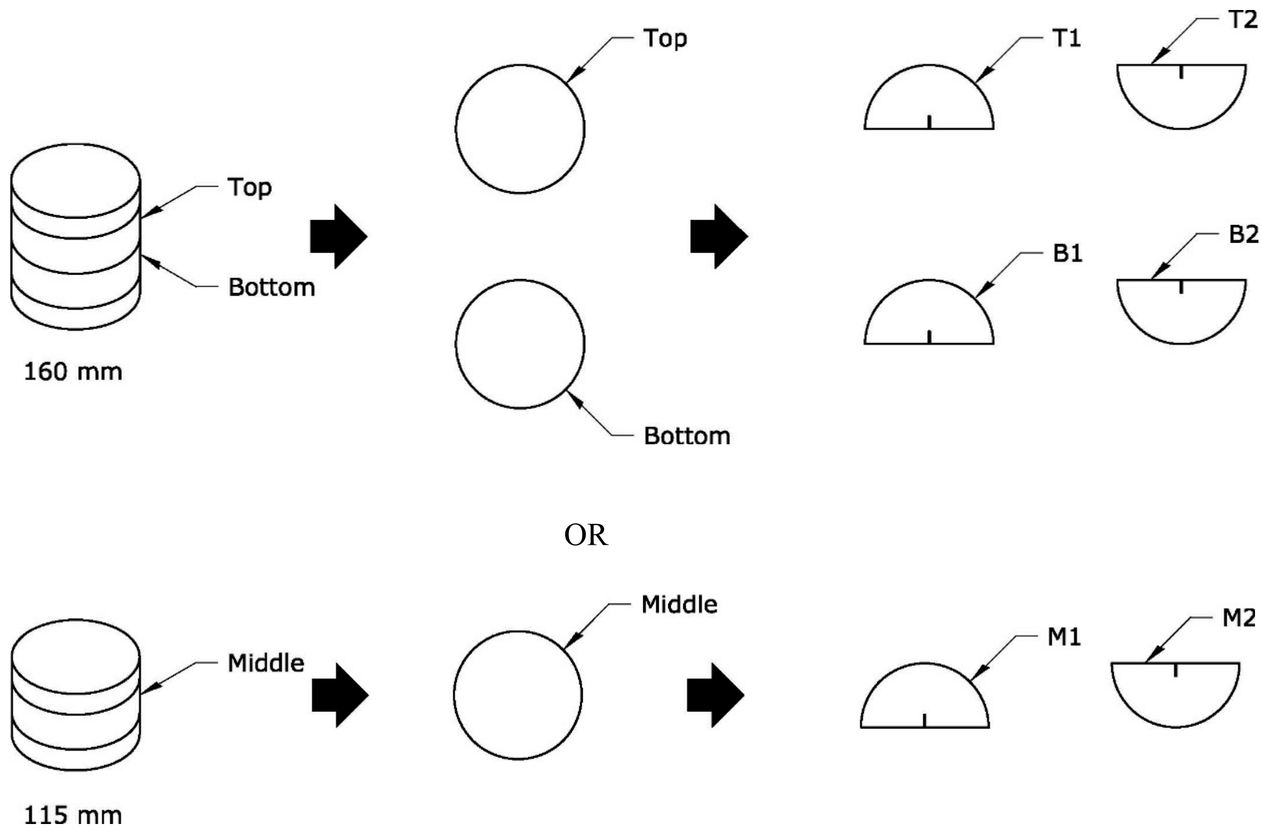

Figure 4: Sample Preparation

10.9. *Determining Specimen Dimensions*—Measure the notch depth on both faces of the specimen and record the average value to the nearest 0.5 mm. Measure and record the ligament length and thickness of each specimen. The ligament length may be measured *directly* on both faces of the specimen with the average value recorded, or the ligament length may be measured *indirectly* by subtracting the notch depth from the entire width (radius) of the specimen on both faces of the specimen and averaging the two measurements. Measure the specimen thickness approximately 19.0 mm on either side of the notch and on the curved edge directly across from the notch. Average the three measurements and record as the average thickness to the nearest 0.1 mm.

10.10. *(Optional) Mounting Deformation Measuring Devices*—Superglue the two CMOD gauge points on the specimen as shown in **Figure 3**.

11. TEST PROCEDURE

11.1. *Conditioning*—The specimens shall be placed in a temperature-controlled chamber at the desired test temperature for at least 4 ± 0.5 h. The temperature shall be maintained within 0.5°C of the desired test temperature throughout the conditioning and testing periods. The recommended test temperature is the minimum of either −12°C or 10°C above the lowest annual pavement temperature of the location with 50 % reliability. The chamber shall be large enough to accommodate the specimen to be tested plus a "dummy" cylindrical specimen with a temperature sensor mounted in the center for temperature verification.

11.2. *Position Specimen*—After temperature conditioning, the specimen shall be placed on the test fixture so that it is centered in both the "x" and "y" directions and so that the vertical axis of loading is aligned to pass from the center of the top radius of the specimen through the middle of the notch.

11.3. *Seating Load*—A seating load up to 0.5 ± 0.02 kN is applied in stroke control with an LLD rate of 0.02 mm/s. Record the seating load to ensure it is achieved.

11.4. *Loading*—After the contact load is reached, the test is executed at a constant LLD rate of 0.15 mm/min. The test stops when the load drops below 0.5 kN.

Note 3—Pre-peak fracture energy and loading stiffness are obtained from the initial ascending portion of the test. For practical purposes, the test may be terminated after peak load if the measured load has decreased by at least 25 % from the maximum, provided that the necessary data from the initial loading portion has been obtained.

12. PRE-PEAK FRACTURE ENERGY $G_{f\text{-}pre}$

12.1. *Determining Pre-Peak Work of Fracture ($W_{pre\text{-}peak}$)*—The pre-peak work of fracture is calculated as the area enclosed under the load versus load line displacement curve up to the peak load (see Figure 5). The pre-peak work of fracture is calculated using the same principle outlined in Section 12.2.1.

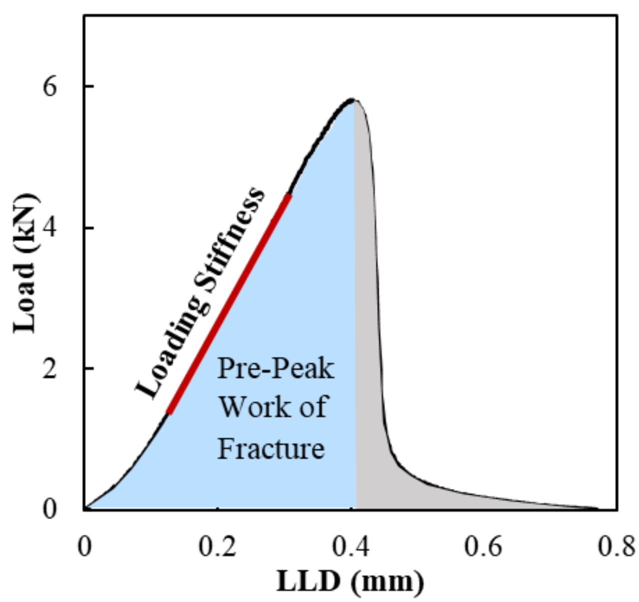

Figure 5: Typical Load versus Average Load Line Displacement Curve

12.2. *Pre-peak Fracture Energy ($G_{f\text{-}pre}$)*—The pre-peak fracture energy $G_{f\text{-}pre}$ is determined by dividing the pre-peak work of fracture by the ligament area (the product of the ligament length and the thickness of the specimen) of the SCB specimen prior to testing.

$$G_{f-pre} = \frac{W_{pre-peak}}{A_{lig}} \tag{1}$$

where:

G_{f-pre}	=	fracture energy to reach the peak load (J/m^2),
$W_{pre-peak}$	=	work of fracture to reach the peak load (J),
A_{lig}	=	ligament area (m^2), where
A_{lig}	=	$(r-a) \times t$
r	=	specimen radius (m);
a	=	notch length (m); and
t	=	specimen thickness (m).

12.2.1. *Determining Pre-peak Work of Fracture (W_{f-pre})*—The work of pre-peak fracture, W_{f-pre}, under the experimental curve can be computed using the trapezoidal technique:

$$\mathrm{W_{f-pre}} = \sum_{i=1}^{n}(u_{i+1} - u_i) \times P_i + \frac{1}{2} \times (u_{i+1} - u_i) \times (P_{i+1} - P_i) \tag{2}$$

where:

P_i	=	applied load (N) at the ith load step application;
P_{i+1}	=	applied load (N) at the ith+1 load step application;
u_i	=	load line displacement (m) at the ith load step application;
u_{i+1}	=	load line displacement (m) at the ith+1 load step application; and
n	=	peak load step application.

13. LOADING STIFFNESS

13.1. *Loading Stiffness (S)*—The loading stiffness, S, shall be defined as the slope of the linear portion of the ascending load versus average load line displacement curve prior to the peak load (Modi et al., 2026).

13.2. *Determination of Linear Region*—

13.2.1. A moving analysis window having a length equal to 15 % of the pre-peak portion of the load versus average load line displacement curve shall be translated along the ascending branch of the curve.

13.2.2. For each window position, a linear regression (least-squares fit) shall be performed to obtain the goodness-of-fit statistic, ${R_{raw}}^2$.

13.2.3. A penalty term shall be applied to favor windows located near the midpoint of the pre-peak region. The distance of the window center from the mid-pre-peak region shall be calculated as:

$$l_m = \frac{P_{avg}}{P_{max}} - 0.5 \tag{3}$$

where:

P_{avg} = Average load in the reduced window (optimized at 15%);
P_{max} = Peak load (kN); and
l_m = Distance of center of the reduced window to midpoint.

13.2.4. The penalized coefficient of determination shall be computed with a penalty term of 0.05 as

$$R_{penalized}{}^2 = R_{raw}{}^2 - \alpha l_m{}^2 \quad (4)$$

where:
α = penalty term (0.05);
$R_{raw}{}^2$ = raw/ uncorrected coefficient of determination; and
$R_{penalized}{}^2$ = corrected coefficient of determination.

13.2.5. The window that yields the maximum value of $R_{penalized}{}^2$ shall be taken as the linear region used to compute the loading stiffness, S. An example is shown in **Figure 6**.

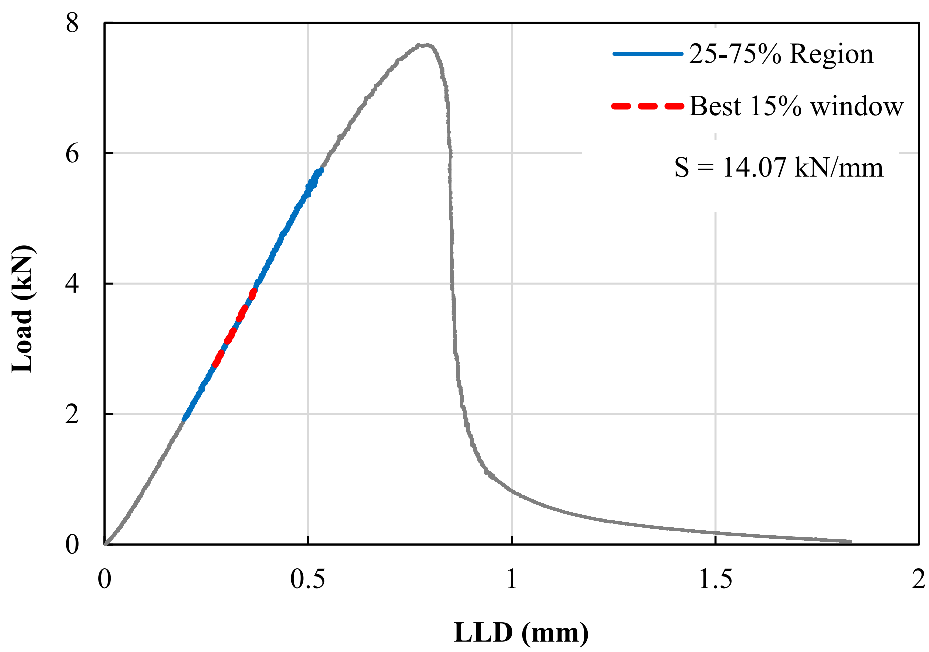

Figure 6: Example of Stiffness Determination

13.3. *Unit*—The unit of measure for loading stiffness (*S*) is kN/mm.

14. LOW-TEMPERATURE CRACKING INDEX

14.1. *Low temperature cracking index (LCI)*—The LCI can be calculated from the pre-peak fracture energy ($G_{f\text{-}pre}$) and loading stiffness (S) as shown in Equation 5.

$$LCI = \frac{G_{f-pre}}{S} \quad (5)$$

where:

LCI	=	low-temperature cracking index;
G_{f-pre}	=	pre-peak fracture energy (J/m^2); and
S	=	loading stiffness (kN/mm).

15. REPORT

15.1. *Report the following information*:
15.1.1. Bulk specific gravity of each specimen tested, to the nearest 0.001;
15.1.2. Maximum specific gravity of asphalt concrete mixture, to the nearest 0.001;
15.1.3. Air voids of each specimen, to the nearest 0.1 %;
15.1.4. Thickness *t* and radius *r* of each specimen tested, to the nearest 0.5 mm;
15.1.5. Test temperature, to the nearest 0.1°C;
15.1.6. Initial notch length *a*, to the nearest 0.5 mm;
15.1.7. Peak load, to the nearest 0.1 kN;
15.1.8. Time at peak load, to the nearest 0.1 s;
15.1.9. Pre-peak fracture energy G_{f-pre}, to the nearest 1 J/m^2;
15.1.10. Loading stiffness S, to the nearest 0.1 kN/mm;
15.1.11. Low-temperature cracking index (LCI), to the nearest 0.1.

16. PRECISION AND BIAS

16.1. *Precision*—The research required to develop precision estimates has not been conducted.
16.2. *Bias*—The research required to establish the bias of this method has not been conducted.

17. KEYWORDS

17.1. Pre-peak fracture energy; loading stiffness; low-temperature cracking index; semi-circular bend (SCB); LLD control.

18. REFERENCES

18.1. Modi, S. H., Bajaj, A., Dave, E. V., Sias, J. E., Al-Qadi, I. L., Lambros, J., & Tormos, S. (2026). Development of a simplified low-temperature SCB test protocol to characterise cracking potential of airfield mixtures. *International Journal of Pavement Engineering, 27*(1). https://doi.org/10.1080/10298436.2026.2698794
18.2. Bajaj, A., Modi, S. H., Al-Qadi, I. L., Dave, E. V., Lambros, J., & Sias, J. E. (2026). Lab and field validation of simplified low-temperature SCB test for airfield asphalt mixtures. *Journal of Transportation Engineering, Part B: Pavements*, *In Production*.

18.3. Li, X., & Marasteanu, M. (2004). Evaluation of the low temperature fracture resistance of asphalt mixtures using the semicircular bend test. *Asphalt Paving Technology: Association of Asphalt Paving Technologists—Proceedings of the Technical Sessions*, *73*, 401–426.

18.4. Li, X., & Marasteanu, M. O. (2006). Investigation of low temperature cracking in asphalt mixtures by acoustic emission. *Road Materials and Pavement Design, 7*(4), 491–512. https://doi.org/10.1080/14680629.2006.9690048.

18.5. Lim, I. L., Johnston, I. W., & Choi, S. K. (1993). Stress intensity factors for semi-circular specimens under three-point bending. *Engineering Fracture Mechanics, 44*(3), 363–382. https://doi.org/10.1016/0013-7944(93)90030-V

18.6. RILEM Technical Committee 50-FMC. (1985). Determination of the fracture energy of mortar and concrete by means of three-point bend tests on notched beams. *Materials and Structures*, *18*(4), 287–290. https://doi.org/10.1007/BF02472918.